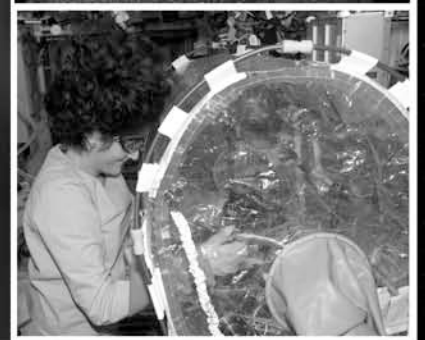


2007

Research & Technology



National Aeronautics and Space Administration
NASA/TM—2008-215054

ABOUT THE COVER:

Left: Artist's concept of Ares I on launch pad. NASA Glenn is designing and testing key subsystems of the upper stage for the Ares I Crew Launch Vehicle and is developing and manufacturing the Ares I-X Upper Stage Simulator test vehicle that will help prove the viability of the new rocket. Look for Research & Technology 2008 for updates on this work.

Top right: Full-scale NACA-23012 airfoil model in Office National d'Etudes et de Recherches Aeronautiques (ONERA) F1 wind tunnel facility in Le Fauga-Mauzac, France. The airfoil was fitted with ice shapes made from molds of ice accreted on a similar airfoil model in Glenn's Icing Research Tunnel then subjected to a wide range of aerodynamic conditions in order to determine, at full-scale, the effects of ice accretions on airfoil aerodynamic performance (p. 16).

Second from top right: Glenn's Vacuum Facility 12 with the compact flash evaporator system test rig. This spray-cooling concept is being developed as an alternative heat sink technology for future spacecraft thermal control architectures (pp. 87-88).

Third from top right: The Scarab lunar rover will obtain and analyze core samples from the Moon's surface to look for hydrogen, water, and other chemicals that could eventually be mined to support lunar outposts. Glenn developed the Smart Power System for the rover. This system will supply the general power needs of the rover as well as provide a programmable power supply that can be adjusted by the rover for any voltage between 24 and 48 V (pp. 110-111).

Bottom right: Astronaut Suni Williams performs the Soldering in Reduced Gravity Experiment (SoRGE) in the *International Space Station*. The soldered boards were returned to Earth and are being evaluated at Glenn. SoRGE was the first of a set of experiments designed by Glenn's Component Level Electronic Assembly Repair team to demonstrate methods for astronauts to conduct board-level electronic repairs within a spacecraft (pp. 84-86).

RESEARCH & TECHNOLOGY 2007



National Aeronautics and
Space Administration

Glenn Research Center
Cleveland, Ohio 44135-3191

NASA/TM—2008-215054

Trade names or manufacturers' names are used in this report for identification only. This usage does not constitute an official endorsement, either expressed or implied, by the National Aeronautics and Space Administration.

Notice for Copyrighted Information

This document contains material copyrighted by the parties submitting it to NASA—see the copyright notices on pages 26, 68, 71, 115, and 116. The figures referred to may be reproduced, used to prepare derivative works, displayed, or distributed only by or on behalf of the Government and not for private purposes. All other rights are reserved under the copyright law.

Available from

NASA Center for Aerospace Information
7115 Standard Drive
Hanover, MD 21076-1320

National Technical Information Service
5285 Port Royal Road
Springfield, VA 22100

Available electronically at <http://www.grc.nasa.gov/WWW/RT/>

Introduction



The NASA Glenn Research Center is pushing the envelope of research and technology to enable NASA missions in Aeronautics Research, Space Exploration, Science, and Space Operations. We excel in aeropropulsion, structures and materials, and instrumentation and control research, enabling next-generation transportation systems that are faster, more environmentally friendly, more fuel efficient, and safer. We develop critical space flight systems enabled by advanced power, propulsion, communications, and human health systems to advance the exploration of our solar system.

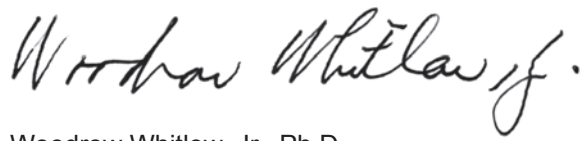
Our work is critical to making the Nation's vision for future space exploration a reality. For human space-flight systems, we are leading the development of the Service Module of the *Orion* Crew Exploration Vehicle, which will provide *Orion* with maneuvering capability (via the propulsion system), generate its power (via solar arrays), and keep it cool (via heat rejection radiators). We are designing and testing key subsystems of the upper stage for the Ares I Crew Launch Vehicle, and we are developing and manufacturing the test vehicle that will prove the viability of the upper-stage rocket. For the Ares V heavy-lift vehicle, we are leading efforts on the thrust vector control systems that will keep the vehicle under control during ascent, providing the electrical power systems, and developing the world's largest payload shroud to protect the lunar lander. We have key roles in providing propulsion, power, and testing for the lunar lander, and we will supply power and communications for lunar surface systems such as rovers, spacesuits, and the lunar base.

Our world-class research, technology, and capability development efforts also are critical for our Nation to maintain global leadership in aeronautics. We contribute to economic growth and national security by developing technology for safe, superior, and environmentally compatible U.S. aircraft propulsion systems. Several examples of our aeronautic success were demonstrated in 2007. Our advanced materials development was recognized for enabling the GENx engine (GE Aviation), which was certified by the Federal Aviation Administration and will power the New Boeing 787 Dreamliner; our alternative fuel research resulted in the successful completion of the first-ever alternative fuel test in an ultra-high-bypass-ratio engine, which demonstrated the feasibility of adopting alternative aviation fuel; and our instrumentation research achieved a world record for high-temperature silicon carbide integrated-circuit operation at 500 °C for over 5000 hours, in comparison to less than 10 hours of operation previously demonstrated.

Our recent accomplishments in electric propulsion and radioisotope power systems are noteworthy. We designed, built, tested, and delivered to the Department of Energy/Lockheed Martin three advanced Stirling convertors that have demonstrated an improvement of specific power six times greater than the current state of the art for radioisotope power systems. The NASA Science Mission Directorate has since identified the use of a pair of advanced Stirling radioisotope generators for the Discovery 13 missions. Also, NASA's Evolutionary Xenon Thruster (NEXT) long-duration test article exceeded the highest total impulse and most propellant throughput ever demonstrated by an ion thruster of the spare Deep Space-1 engine.

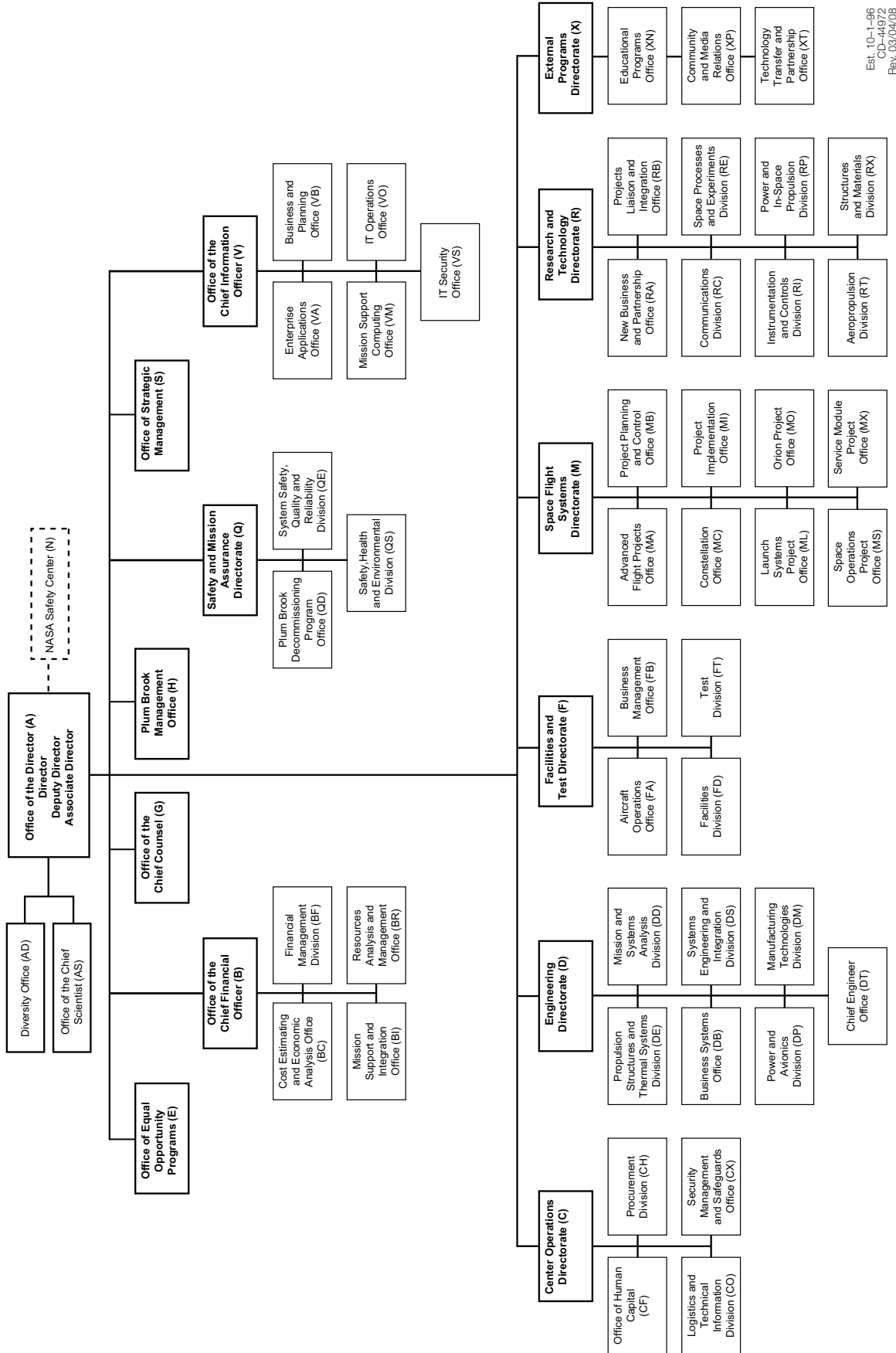
Glenn has two locations. Our Cleveland campus, located on 350 acres adjacent to the Cleveland Hopkins International Airport, has more than 140 buildings that include 24 major facilities and over 500 specialized research and test facilities. Plum Brook Station, located 50 miles west of Cleveland, offers four large, world-class facilities for space technology and capability development on 6400 acres. Our team consists of over 3000 dedicated civil service employees and support service contractor personnel. We aggressively strive for technical excellence through continuing education, increased diversity in our workforce, and continuous improvement in our management and business practices.

I hope that the information found in this technical accomplishments report is useful to you. If additional information is desired, you are encouraged to contact the researchers identified at the end of each article and to visit our Web site at <http://www.nasa.gov/glenn>. Thank you for your interest in and continued support of the NASA Glenn Research Center.

A handwritten signature in black ink that reads "Woodrow Whitlow, Jr." The signature is written in a cursive style with a prominent initial 'W' and a trailing flourish.

Woodrow Whitlow, Jr., Ph.D.
Director

NASA Glenn Research Center at Lewis Field



Est. 10-1-96
 CD-44972
 Rev. 03/04/06

NASA Glenn Research Center Senior Management



CONTENTS

Aeropropulsion

Aeroacoustics Theory of Slowly Diverging Supersonic Jets Developed and Compared With Experimental Data . . .	2
New Automated Data-Post-Processing Program Created for Statistical Analysis of Multiscalar, Single-Shot Raman-Scattering Measurements in Turbulent Flames	4
Outer Planet Mining Atmospheric Cruiser Systems Analyzed	6
Alternative Fuels Research Laboratory Construction Completed	8
Noise-Reducing Offset Fan Stream Nozzles Simulated by Computational Fluid Dynamics	9
Wind-US Code Improved for Hypersonic Flow Simulations	13
Small-Scale Inlet Mode Transition Model Tested in Glenn's 1- by 1-Foot Supersonic Wind Tunnel	14
Full-Scale Iced Airfoil Aerodynamic Performance Evaluated	16
Web-Based Icing Remote Sensing Product Developed	17
Novel Antivortex Turbine Film-Cooling Hole Concept Conceived and Developed	18
Ultra-high-Bypass-Ratio Propulsion Systems Studied	20

Power and Space Propulsion

First Phase of Advanced Feed System Development for Electric Propulsion Completed	22
Initial Prototype of Ares I Upper Stage Thrust Vector Control and Associated One-Axis Test Rig Developed	23
Electric Propulsion Breakthrough Demonstrated	24
Advanced Propellant Management System of NASA's Evolutionary Xenon Thruster Qualified for Electric Propulsion	25
NASA's Evolutionary Xenon Thruster Broke World Record and Successfully Completed Environmental Qualification Testing	27
Cryogenic Propellant Boiloff Reduction System Investigated	28
Liquid-Oxygen/Methane Ignition Tested for Application in the Main Engines of the Lunar Surface Access Module	29
Low-Gravity Pressure-Volume-Temperature Gauging Concept Demonstrated With Liquid Oxygen	31
Radiofrequency Tank Modes Tested at NASA Glenn To Gauge Liquid Oxygen and Liquid Methane	32
New Lithium-Ion Batteries With Enhanced Safety and Power Density Evaluated for Future NASA and Aerospace Missions	34
Lithium-Ion Battery Demonstrated for NASA Desert Research and Technology Studies	35
Passive Cooling Plates Studied for Fuel Cells	36
Passive Water Separator Developed for Fuel Cells	37
Battery Systems for Extravehicular Activities Studied	38
Lithium-Based Battery Performance Evaluated for NASA's Exploration Missions	39
<i>International Space Station</i> and Constellation Lithium-Ion Battery Commonality Trade Study Performed	41
Masterless Charge-Control Scheme Developed and Validated for a Modular Lithium-Ion Battery	43
Approach Developed for Optimizing Stirling Gas Bearing Performance	44
Carbon-Carbon Heat Pipe With Integral Fins and Potassium Working Fluid Designed, Fabricated, and Tested	46
Progress Made in Power-Conversion Technologies for Fission Surface Power	47
Advanced Stirling Convertors Began Extended Operation	49
Advanced Stirling Convertor Engineering Units Completed and Delivered	50
Heat-Rejection Systems Utilizing Composites and Heat Pipes Evaluated	52
Simple Mars Propellant Manufacture Investigated That Will Reduce Mass Required for Mars Sample Return	53
Hybrid Power Management Program: Prototype Grid-Tie Photovoltaic Power System Has Been in Successful Operation for Over 1 Year at NASA Glenn and Is Serving as the Basis for Future Expansion	54
Materials International Space Station Experiment 2 (MISSE 2) Polymer Erosion and Contamination Experiment (PEACE) Polymers Analyzed	56

Lunar Dust Abrasion Simulation Capability Completed	58
Stickiness of Silicone Elastomer Seal Material Reduced by Using Atomic Oxygen Treatment	59

Communications

Very High Frequency Antenna Developed for Sensor and Short-Range Communication Applications	62
Novel Nanoionics-Based Radiofrequency Switch Developed and Demonstrated	64
NASA Space Telecommunications Radio System Architecture Updated	66
Lunar Reconnaissance Orbiter Traveling-Wave Tube Completed	68
Simulation Study Conducted for a Wide-Band, Low-Loss, Short-Slot Coupler-Based Power Combiner	69
Terahertz Amplifier Design Improved With Metamaterial	70
High-Power Traveling-Wave Tube Space Qualified at Record Power Levels	71
Glenn’s Network Emulation Laboratory Established as a Networking Research and Emulation Environment for NASA	72

Space Processes and Experiments

Magnetic Stirrer Tested for a System To Produce Intravenous Fluid During Exploration Missions	76
Lunar Dust Toxicology Studied In Vitro at the Cellular Level	78
Three-Dimensional Monte Carlo Model Developed for Optical Mass Gauging	79
Microvascular Pathologies in Human Retinal Disease Analyzed by VESGEN Software	81
In Situ Resource Utilization Reactor Developed To Characterize Lunar Soil	83
Component-Level Electronics Repair in Space: Soldering Tested in Reduced Gravity—An Update	84
Compact Flash Evaporator System Developed	87
Capillary Flow Experiments Performed on the <i>International Space Station</i>	88
Vapor Phase Catalytic Ammonia Removal Tested in Reduced Gravity on NASA C–9 Aircraft	90

Instrumentation and Controls

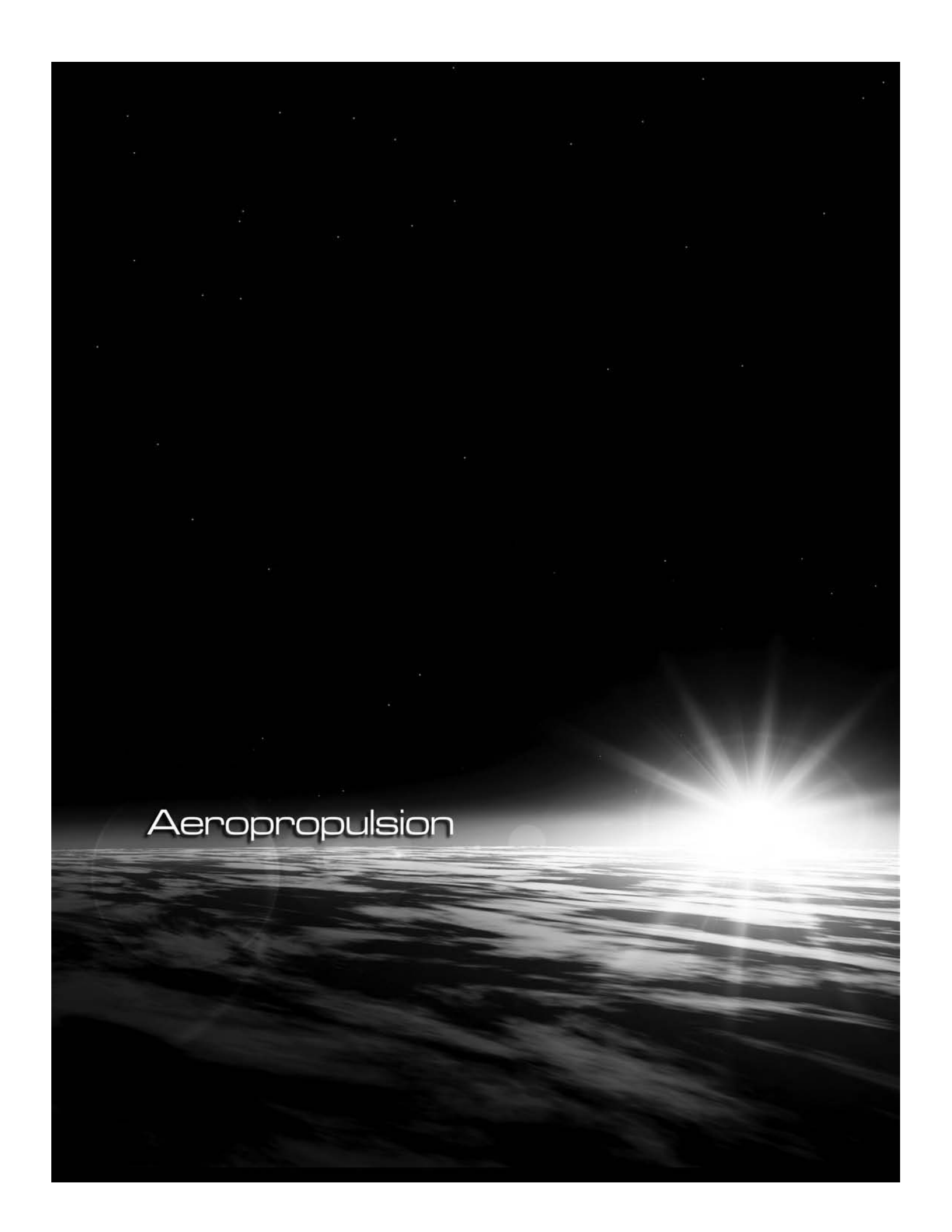
Simulation Developed That Captures the Thermoacoustic Instability Behavior of Advanced, Low-Emissions Combustor Prototype	94
Integrated Online and Offline Diagnostic Approach Demonstrated for Aircraft Engine Application	96
Loop-Shaping Design Approach With Practical Considerations Developed for Feedback Control Systems	97
Singular-Value Decomposition-Based Approach Developed for Thrust Estimation Over the Flight Envelope	99
Transient Simulation of Large Commercial Turbofan Engine Developed To Enable Advanced Controls and Diagnostics Research	100
Operability of a Gas Turbine With Pressure-Gain Combustion Investigated	102
Light-Driven Actuators Based on Polymer Films Developed and Demonstrated	104
Use of Sensors on a Bladed Rotating Disk Evaluated for Health Monitoring and Crack Detection	105
Development of Analytical Criteria for Crack Deflection and Penetration in Coated Ceramics Initiated	107
Microwave Turbine-Tip-Clearance Sensor Tested in Relevant Combustion Environment	109
Smart Power System Developed for Scarab Lunar Rover	110
N-Channel Junction-Field-Effect-Transistor-Based Digital Logic Gate Structure Using Resistive Level Shifters and Configurable From High-Temperature Silicon Carbide Electronics Developed	112
Great Lakes Environmental Aerial Monitoring Team Developed and Tested Second-Generation Hyperspectral Instrument Suite on NASA Glenn’s Learjet 25	114
Instrument Developed for Indicating the Severity of Aircraft Icing and for Providing Cloud-Physics Measurements for Research	115
Particle Image Velocimetry Capability Installed and Checked Out in NASA Glenn’s 10- by 10-Foot Supersonic Wind Tunnel	117

Multiparameter Fire-Detection System Miniaturized and Tested for Possible Use on Crew Exploration Vehicle . . .	118
Silicon Carbide Integrated Circuit Fabricated and Electrically Operated for 2000 hr at 500 °C	120
Reliability of Silicon Carbide Pressure Transducers Evaluated at 600 °C	122
Temperature Sensor Developed for a Wide Range of Applications From Hot Jet Engine Environments to Cryogenic Space Missions	124
Microelectromechanical Systems Packaging Technique and Chip Fabrication Method Developed for High-Temperature, Harsh-Environment Silicon-Carbide Pressure Sensors	126

Structures and Materials

Notch Fatigue Strength of a Powder Metallurgy Disk Superalloy Evaluated	130
Flexible Cross-Linked Aerogels Developed	131
Manufacturing Process for Polymer Cross-Linked Aerogel Composites Developed	133
Physical Properties of Exfoliated Graphite Nanocomposites Tailored by Variation of Graphite Surface Functionality	134
Fluorescent Dye Developed for the Detection of Nitroaromatic Compounds	136
Electrical Resistance Tested as a Nondestructive Evaluation Technique for Silicon Carbide/Silicon Carbide Composites	137
Technology for Integrating Ultra-High-Temperature Ceramic Composites With Metallic Systems Developed	138
Joining of Carbon-Carbon Composites to Metals Demonstrated for Thermal Management Applications	140
Nickel-Titanium-Platinum High-Temperature Shape-Memory-Alloy Viability Established Through Wind Tunnel Testing of a High-Speed Adaptive Inlet	141
High-Temperature Piezoelectric Material Developed	143
Glenn-Developed Copper-Chromium-Aluminum Coatings Evaluated for Reusable Launch Vehicles	145
Nanocomposite Environmental Barrier Coatings Evaluated for High-Temperature Combustion Environment Stability	146
Stress Rupture Life Models and Reliability Measures Established for Composite Overwrapped Pressure Vessels	149
Probabilistic Simulation for Nanocomposite Characterization Developed and Included in the Computer Code ICAN/JAVA	150
Formal Methodology Developed for Probabilistically Evaluating the Design of Composite Structures	153
Bauschinger Effect on Mechanical Response of Composite Overwrapped Pressure Vessels Investigated	156
Micromechanics Model Developed for External Tank Spray-On Foam Insulation	158
Structural Benchmark Testing Completed for Ares I-X Upper Stage Simulator Segment Joints	160
Effects of Cracks and Residual Stresses at the Toe of the Ares I-X Upper Stage Simulator Shell-to-Flange Weld Quantified Using Probabilistic Approaches and the NASGRO Crack-Growth Code	162
Pressure Measured in Ballistic Impact Testing of Simulated Birds	164
Probabilistic Analysis Conducted of Space Shuttle Body Flap Actuator Ball Bearings	165
Fatigue Crack Growth Behavior Evaluated for Grainex Mar-M 247 Used in NASA's High-Temperature, High-Speed Turbine Seal Test Rig	167
High-Temperature Seals Evaluated for Hypersonic Airframe Applications	168
Low-Noise Formate Spiral-Bevel Gears Evaluated	170
Design, Fabrication, and Performance of Open-Source Foil Bearings Demonstrated	172
Full-Rotor Aeroelastic Analysis Capability Developed and Tested	173
Ultra-High-Power, Lightweight Cryogenic Motor Developed and Operated in Liquid Nitrogen	175
Simulated Lunar Operations Facility Designed and Built for Lunar Vehicle Research	176

Appendix—Index of Authors and Contacts	179
--	-----

A black and white photograph of a bright sun or star on the horizon of a planet, with the word 'Aeropropulsion' overlaid in white text. The sun is positioned on the right side of the horizon, creating a lens flare effect. The horizon line is slightly curved, suggesting a spherical body. The sky is dark with some faint stars visible. The overall composition is dramatic and evocative of space exploration.

Aeropropulsion

Aeroacoustics Theory of Slowly Diverging Supersonic Jets Developed and Compared With Experimental Data

Noise remains one of the principal environmental barriers to expansion of the present air transportation system. Increasingly stringent noise regulations will require new technologies that reduce noise without sacrificing performance. Jet noise makes up a significant portion of the noise produced by aircraft and, although progress has been made over the last 50 years toward understanding and predicting this noise component, currently available jet noise prediction models do not provide the accuracy required to guide technological development for high-speed jets. In particular, they are unable to predict the high levels of peak noise produced by supersonic jets. In research carried out in-house at the NASA Glenn Research Center, in collaboration with the Ohio Aerospace Institute (OAI), a rigorous theory based on an acoustic analogy was developed and compared with experimental data. The results clearly demonstrate that the theory can predict jet noise accurately at both supersonic and subsonic Mach numbers.

In an acoustic analogy approach to predicting aerodynamically generated noise, the governing Navier-Stokes equations are rearranged to obtain a formally linear system of inhomogeneous equations, with the nonlinear terms considered to be the nominal source terms. In the present work, the implied linearization is about the actual mean flow in the jet. The strength of the resulting sound source is then completely characterized by a single, purely fluctuating, stress tensor—which greatly simplifies the analysis.

Supersonic jet noise is influenced by two important effects that were inadequately addressed in previous models: mean-flow amplification and source noncompactness. The first of these was dealt with by introducing a new non-parallel flow analysis, which eliminates a singularity that occurs at the so-called critical layer in the previous work. The second was dealt with by introducing a highly refined source model that accurately represents the experimentally observed anisotropy and nonnormality of the turbulence statistics in order to properly account for time variations in the sound emitted from different source locations.

A computer code was developed to implement the general theory for the important special case of a round jet. The required input about the mean flow and turbulence statistics were obtained by using the Glenn WIND code. Computations were run for subsonic to moderately supersonic, unheated jets with acoustic Mach numbers M_J covering the range of practical interest: that is, $0.9 \leq M_J \leq 1.4$. The graphs on the next page compare the normalized computed acoustic spectrum I_ω with experimental data taken at Glenn's Small Hot Jet Acoustic Rig at two polar angles θ measured from the downstream jet axis. The reference pressure p_{ref} is 2×10^{-5} Pa, and the frequency ω is normalized with the jet exit velocity U_J and exit diameter D . This work is ongoing, with plans for testing improved source models to increase the accuracy of the predictions and extend the method to additional flow conditions.

Bibliography

Goldstein, M.E.; and Leib, S.J.: The Aeroacoustics of Slowly Diverging Supersonic Jets. *J. Fluid Mechanics*, vol. 600, 2008, pp. 291–337.

Glenn Contact:

Dr. Marvin E. Goldstein, 216–433–5825,
Marvin.E.Goldstein@nasa.gov

Ohio Aerospace Institute Contact:

Dr. Stewart J. Leib, 216–433–8639,
Stewart.J.Leib@nasa.gov

Authors:

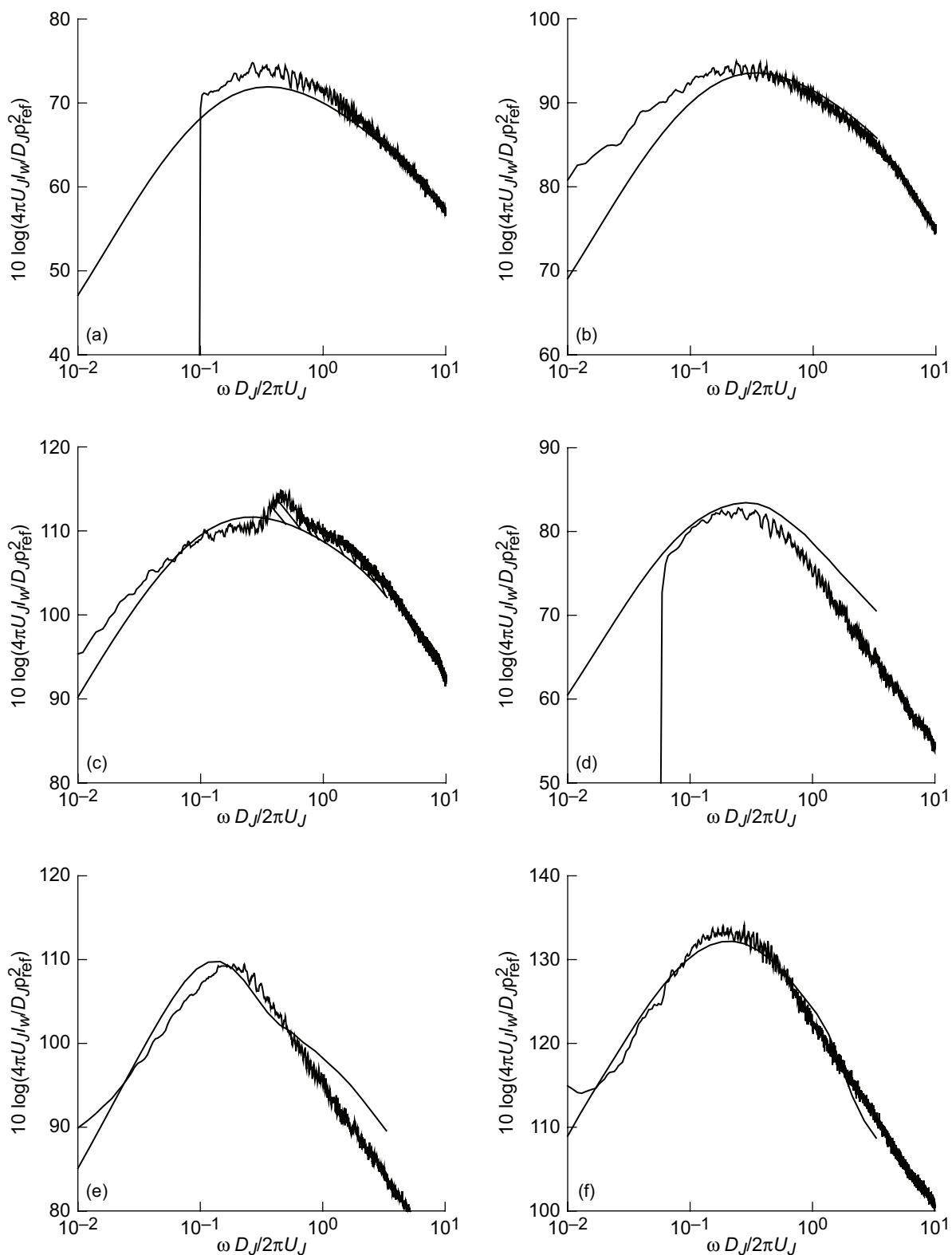
Dr. Marvin E. Goldstein and
Dr. Stewart J. Leib

Headquarters Program Office:

Aeronautics Research Mission Directorate

Programs/Projects:

Glenn Independent Research and
Development, Supersonics Project



Comparison of theoretical predictions with experimental data. (a) $M_J = 0.5$, $\theta = 90^\circ$; (b) $M_J = 0.9$, $\theta = 90^\circ$; (c) $M_J = 1.4$, $\theta = 90^\circ$; (d) $M_J = 0.5$, $\theta = 30^\circ$; (e) $M_J = 0.9$, $\theta = 30^\circ$; (f) $M_J = 1.4$, $\theta = 30^\circ$.

New Automated Data-Post-Processing Program Created for Statistical Analysis of Multiscalar, Single-Shot Raman-Scattering Measurements in Turbulent Flames

Experimental validation of predictive computer codes that simulate the combustion process inside aircraft gas turbine engines is critically important in ensuring sufficient code fidelity and robustness. The code-validation process is an important step in developing computer simulations that can enable the design and construction of advanced, low-emissions, fuel-efficient, clean-burning aircraft engines that have minimal impact on local air quality and global climate and resources. In pursuing this goal, a team of researchers from NASA Glenn Research Center's Combustion Branch and the Ohio Aerospace Institute (OAI) made significant progress by providing a preliminary set of quantitative multiscalar data for a high-pressure swirl-stabilized gaseous combustion using a time-resolved laser Raman diagnostic technique developed at Glenn over the past 6 years (refs. 1 to 6).

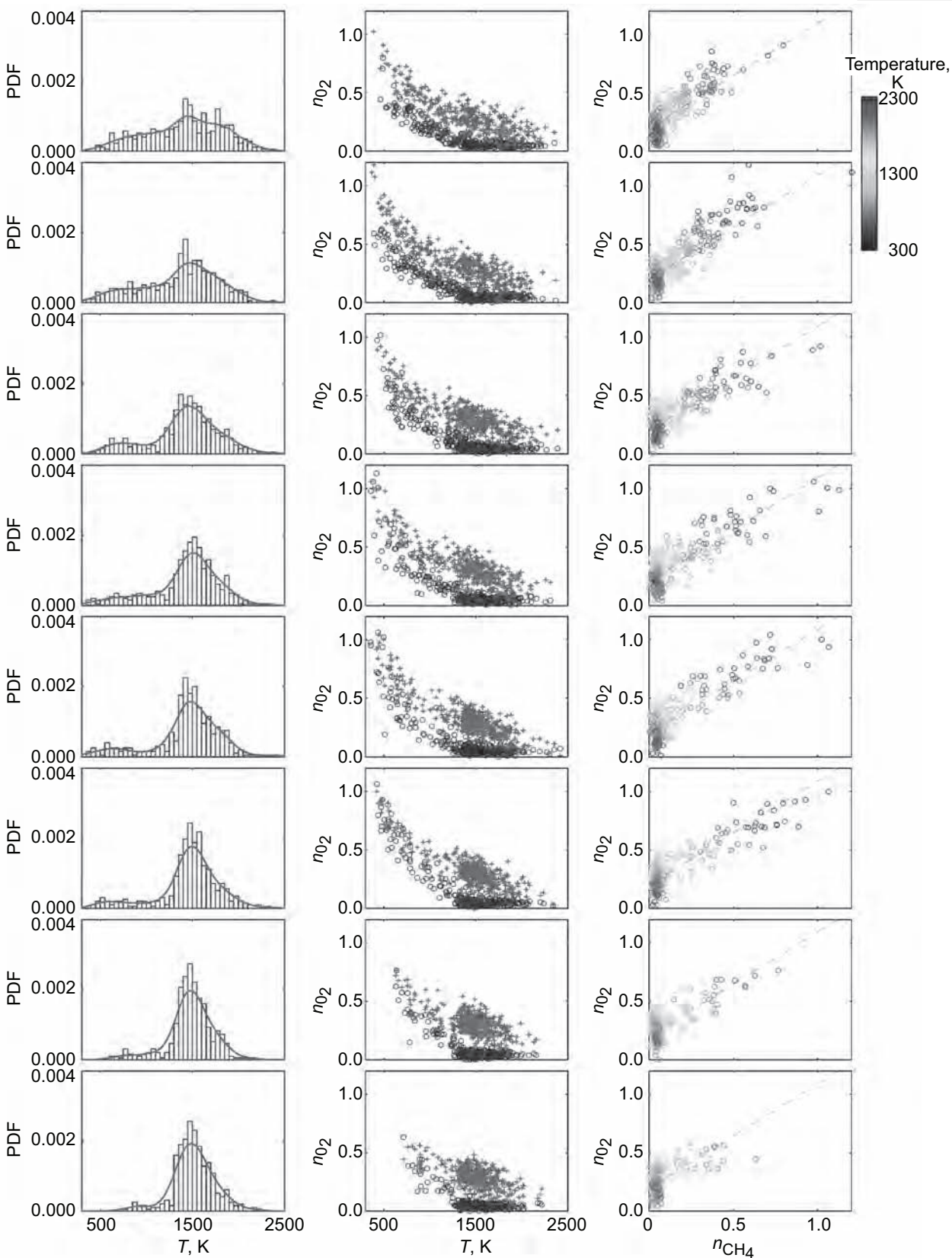
Recently, the team improved the efficiency of the data-post-processing algorithms, improving data quality and throughput, by developing a comprehensive computer program written in the MATLAB language (The MathWorks, Inc.). This program utilizes the latest developments in both theoretical and quantitative molecular spectroscopy, and it includes advanced statistical analysis routines. It has enabled new insights into the turbulent combustion process in swirl-stabilized high-pressure flames by using time-series Raman-scattering data obtained with the quantitative Raman spectroscopy apparatus in Glenn's High Pressure Gaseous Burner facility. Through the current computer program, combustion temperatures and concentration (or number density) of the major molecules, along with their statistical properties in combustion gases, can be deduced rapidly. The new program can automatically process hundreds or even thousands of Raman spectra simultaneously, and it can quickly generate graphical representations of the n -dimensional multiscalar data in two- or three-dimensional formats for researchers to analyze.

As an example of the statistical multiscalar analysis provided by the new program, the figure on the next page shows plots generated by the program from data obtained in a 5-atm swirl-stabilized methane- (CH_4 -) air flame. This direct-output graphic from the new MATLAB-based program shows three different kinds of analyses: (1) probability density functions (PDFs) of instantaneous temperature, determined by the newly developed, low-resolution rotational Raman bandwidth technique (ref. 7); (2) direct correlations between temperature and CH_4 or oxygen (O_2) concentrations; and (3) oxidizer-fuel-temperature correlations. The temperature PDFs, which were measured in turbulent regions showing large variations from 300 to 2300 K, are indicative of incomplete turbulent mixing. Scatter plots of the two- and three-parameter correlations clearly indicate the profound effect of unsteadiness on combustion. In particular, low-temperature points with higher fuel (CH_4) and oxidizer (O_2) concentrations indicate a significant amount of incomplete combustion.

These are the first-ever quantitative multiscalar measurements that show details of turbulent mixing and its impact on chemical reactions in a realistic lean-direct-injection flame at elevated pressures. These measurements will serve as the experimental code validation of state-of-the-art reacting-flow computational fluid dynamics codes such as NASA's National Combustion Code (NCC, ref. 8).

References

1. Kojima, J.; and Nguyen, Q.V.: Disclosure of New Invention and Technology (Software): Laser-Raman Spectral Analysis Software for Combustion Diagnostics. LEW-17769-1, 2004.
2. Kojima, Jun; and Nguyen, Quang-Viet: Quantitative Analysis of Spectral Interference of Spontaneous Raman Scattering in High-Pressure Fuel-Rich, Hydrogen-Air Combustion. *J. Quant. Spectrosc. Radiat. Transf.*, vol. 94, issues 3-4, 2005, pp. 439-466.
3. Nguyen, Quang-Viet: Spontaneous Raman Scattering (SRS) System for Calibrating High-Pressure Flames Became Operational. *Research & Technology 2002*, NASA/TM-2003-211990, 2003, pp. 118-120. <http://www.grc.nasa.gov/WWW/RT2002/5000/5830nguyen2.html>
4. Kojima, J.; and Nguyen, Quang-Viet: Measurement and Simulation of Spontaneous Raman Scattering in High-Pressure Fuel-Rich H_2 -Air Flames. *Meas. Sci. Technol.*, vol. 15, no. 3, 2004, pp. 565-580.
5. Nguyen, Quang-Viet; and Kojima, Jun: Transferable Calibration Standard Developed for Quantitative Raman Scattering Diagnostics in High-Pressure Flames. *Research & Technology 2004*, NASA/TM-2005-213419, 2005, pp. 170-172. <http://www.grc.nasa.gov/WWW/RT/2004/RT/RTB-nguyen.html>
6. Kojima, Jun; and Nguyen, Quang-Viet: Strategy for Multiscalar Raman Diagnostics in High-Pressure Hydrogen Flames. *New Developments in Combustion Research*, William J. Carey, ed., NOVA Science Publishers, New York, NY, 2006, pp. 227-256.
7. Nguyen, Quang-Viet; and Kojima, Jun N.: Alternative Rotational Raman Thermometry Developed for Turbulent Combustion. *Research & Technology 2006*, NASA/TM-2007-214479, 2007, pp. 149-151. <http://www.grc.nasa.gov/WWW/RT2006/RT/RTB-nguyen1.html>



Thermochemical multiscalar analysis at different radial locations ($x = 9$ mm). Left column: Histogram and PDF of temperature. Middle column: Scatter plots of temperature, T , and species concentration, n . Right column: Direct oxidizer–fuel–temperature (data triplet) correlation, with temperature in color scale. The dashed line indicates an equivalence ratio of 0.56. This figure is shown in color in the online version of this article (<http://www.grc.nasa.gov/WWW/RT/2007/Aerprop/02-RTB-nguyen.html>).

8. Iannetti, Anthony C.: National Combustion Code Validated Against Lean Direct Injection Flow Field Data. Research & Technology 2002, NASA/TM—2003-211990, 2003, pp. 114–116. <http://www.grc.nasa.gov/WWW/RT2002/5000/5830iannetti.html>

Authors:
Dr. Quang-Viet Nguyen and Dr. Jun Kojima

LEW Number:
LEW-17769-1

Headquarters Program Office:
Aeronautics Research Mission Directorate

Programs/Projects:
Fundamental Aeronautics Program,
Subsonic Fixed Wing Project,
Supersonics Project

Find out more about the research of Glenn’s Combustion Branch:
<http://www.grc.nasa.gov/WWW/combustion/zDiag.html>

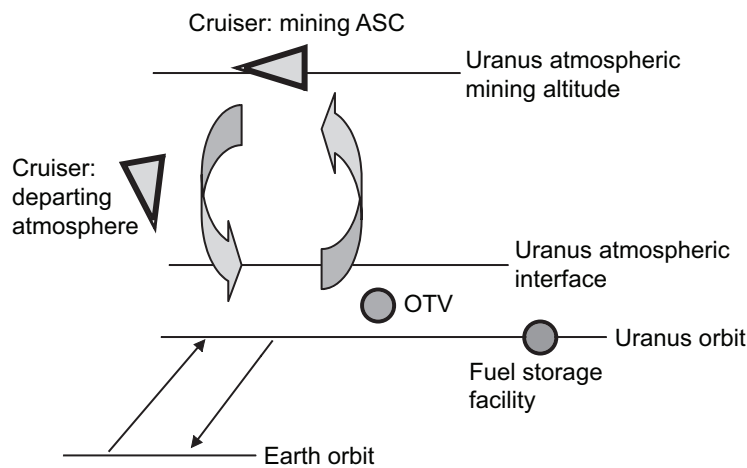
Glenn Contact:
Dr. Quang-Viet Nguyen, 216-433-3574, Quang-Viet.Nguyen-1@nasa.gov

Ohio Aerospace Institute (OAI) Contact:
Dr. Jun Kojima, 440-962-3095, Jun.N.Kojima@nasa.gov

Outer Planet Mining Atmospheric Cruiser Systems Analyzed

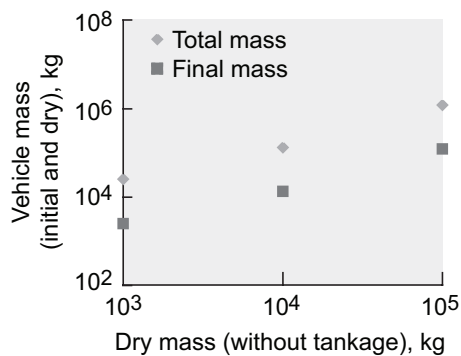
Mission scenarios were developed at the NASA Glenn Research Center for atmospheric mining in the outer solar system by both balloons and cruisers, and preliminary maneuver summaries and maps were developed for future mission planning. Balloon-borne factories would process the atmospheres of Uranus and Neptune, creating helium 3 and hydrogen (H₂) for fuel. Cruisers would fly the outer planet atmospheres, also creating helium 3 and H₂. A large set of spacecraft and spacecraft maneuvers would be required for delivering the vehicles to the atmosphere, wresting the fuels from the gravity wells of the planet, and returning these fuels to Earth. From the standpoint of lifetime and flexibility of operations, cruisers were the most attractive for mining the outer planets. The relatively short lifetimes of traditional balloons made them the second mining candidate. Atmospheric scoopers, the third candidate, have relatively high complexity, and the potentially short lifetime of their hot, hypersonic, aerodynamic structures may make them difficult to implement. The following diagram illustrates the cruiser scenario for atmospheric mining.

The cruiser is a combined miner and aerospacecraft (ASC). The cruiser would fly at subsonic speed in the planet’s atmosphere like aircraft do in Earth’s atmosphere. Once mining was complete, the cruiser would return to orbit outside the planet’s atmosphere and rendezvous and dock with an orbital transfer vehicle (OTV). The fuel would be transferred to the OTV, which would carry the fuel to the orbital storage facility. The cruiser would then return to the atmosphere to resume mining operations. The ASC would be powered by a nuclear “air-breathing” engine, similar to a nuclear thermal rocket. The nuclear engine would consume the planet’s atmosphere as fuel and would create a high-specific-impulse exhaust allowing the cruiser to enter the atmosphere and fly on station while mining. It also would be used as a rocket engine to return to orbit to transfer the fuel to the OTV.

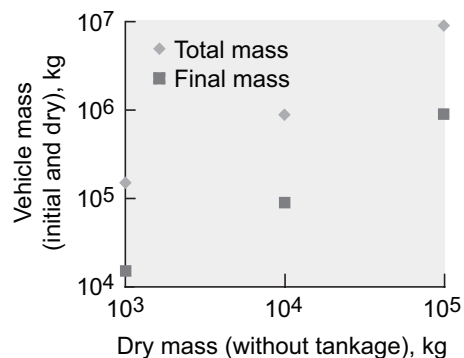


Cruiser mining scenario—combined miner and ASC.

The left graph on the next page shows the estimated range of fixed dry masses for the cruiser: 1000 to 100,000 kg. This reflects the range of masses for the atmospheric mining equipment. The



Cruiser mass with 2-percent tankage mass fraction and 900-sec specific impulse. This should be increased to a 10-percent mass fraction M_p (total propellant mass) for H_2 (only 2-percent now).



Cruiser mass with 10-percent tankage mass fraction for a H_2 -nuclear ASC with 900-sec specific impulse and 20-km/sec Delta-V.

specific impulse of the nuclear-powered ASC would be 900 sec. The total change in velocity (Delta-V) delivered by the ASC would be 20 km/sec. The graph on the left shows the results for a 2-percent tankage mass fraction (where the mass of the tankage is 2 percent of the total propellant mass on the ASC).

The graph on the right depicts the vehicle mass for a tankage mass fraction of 10 percent. Because the actual mass of the atmospheric mining equipment is unknown, a parametric analysis was conducted. These variations were chosen to cover the possible range of masses for the cruiser, covering the varying complexity of mining systems. With minimum mass assumptions, the total mass of the cruiser would be 25,513 kg (2-percent tankage mass fraction and 1000-kg fixed dry mass). The most massive case shown in this graph would be 8,901,000 kg (10-percent tankage mass fraction and 100,000-kg fixed dry mass).

With such a wide variation, it is clear that more focus must be placed on the lowest mass mining systems. The baseline cruiser selected for initial analyses had a 10,000-kg fixed dry mass and a 2-percent tankage mass fraction—a total mass of 133,453 kg. Overall analyses of the balloon, cruiser, and scooper atmospheric mining systems showed that a cruiser would require the lowest mass delivered from Earth orbit, making it the most economical mining system.

References

1. Palaszewski, B.: Atmospheric Mining In The Outer Solar System: Mission Scenarios and Options for In-Situ Resource Utilization. AIAA-2007-5598, 2007.
2. Palaszewski, B.: Atmospheric Mining In The Outer Solar System: Vehicle Sizing Issues. AIAA-2006-5222, 2006.
3. Palaszewski, B.: Atmospheric Mining in the Outer Solar System. NASA/TM-2006-214122 (AIAA-2005-4319), 2006. <http://gltrs.grc.nasa.gov>

Find out more about this research:

<http://sbir.grc.nasa.gov/launch/foctopsb.htm>

Glenn Contact:

Bryan A. Palaszewski, 216-977-7493,
Bryan.A.Palaszewski@nasa.gov

Author:

Bryan A. Palaszewski

Headquarters Program Office:

Aeronautics Research Mission Directorate

Programs/Projects:

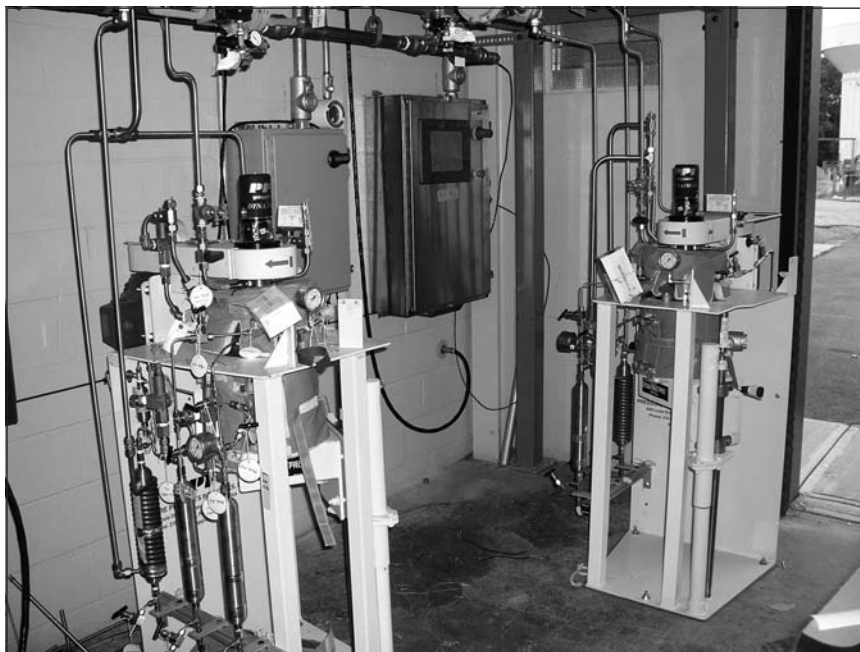
Supersonics Project

Alternative Fuels Research Laboratory Construction Completed

This year, the NASA Glenn Research Center completed the renovation of a building at its Cleveland campus for use as an alternative jet fuels test facility (see the top photograph). Glenn has invested over \$1,520,000 in facilities



Glenn's Alternative Fuels Research Laboratory.



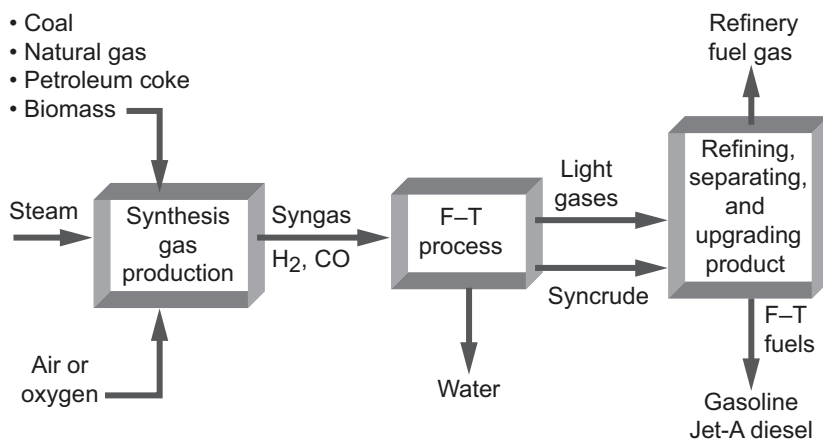
Fischer-Tropsch continuous stirred tank reactor installation.

engineering, construction for upgrading the infrastructure, and new research equipment installed inside the laboratory. Facility and research systems design and long-lead procurements began in November 2006. Construction of the laboratory was finished in December 2007.

Three Fischer-Tropsch (F-T) reactors supplied by Pressure Products Industries and the University of Kentucky were acquired by the program for testing purposes. The three high-pressure, 1-liter-capacity, continuous-stirred tank F-T reactors (see the bottom photograph) cost \$132,000. The reactor design setups included three parallel bench-scale F-T synthesis reactors; gaseous hydrogen (H_2), carbon monoxide (CO), and argon feed systems; reaction byproducts separation and handling; and hydrocarbon product composition analysis by gas chromatograph.

The University of Kentucky's Center for Applied Energy Research (CAER) has specialized in testing the F-T process for over 15 years. A research collaboration and technology exchange agreement was established with CAER, and collaboration with other entities, including the Department of Energy, the Department of Defense, and Boeing continued.

Glenn is focusing on refining the coal-to-liquids conversion and reducing or capturing the carbon dioxide generated by the conversion. The chief of Glenn's Combustion Branch, Dr. Chi-Ming Lee, is leading the research team exploring various alternatives to petroleum-based aviation fuel. Synthetic fuels derived from coal, natural gas, and other non-petroleum resources, in addition to biofuels from renewable sources (see the diagram on the next page), are being assessed by the research group.



Natural gas, coal, and biomass converted to liquids via the Fischer-Tropsch (F-T) process.

Glenn's research effort is concentrating primarily on using alternative fuels to improve combustion performance and reduce emissions in advanced jet engine designs. In addition, plans call for developing a set of predictive tools related to alternative fuel composition and combustor performance. Another goal is to reduce capital costs associated with synthetic jet-fuel production from nonconventional sources.

Reactor testing and kinetic studies at the Alternative Fuels Research Laboratory are scheduled to begin during the second quarter of 2008 following completion of integrated checkout tests of the new facility systems. F-T catalyst performance evaluation and kinetic mechanism studies will be conducted here with advanced catalyst materials from several sources including CAER and industrial suppliers.

Find out more about the research of Glenn's Combustion Branch:
<http://www.grc.nasa.gov/WWW/combustion/>

Glenn Contacts:

Dr. Chi-Ming Lee, 216-433-3413,
 Chi-Ming.Lee-1@nasa.gov
 Thomas M. Tomsik, 216-977-7519,
 Thomas.M.Tomsik@nasa.gov
 Angela D. Surgenor, 216-433-3251,
 Angela.D.Surgenor@nasa.gov

University of Toledo Contact:

(Judy) Chia Yen, 216-433-3626,
 Chia.H.Yen@nasa.gov

Author:

Thomas M. Tomsik

Headquarters Program Office:

Aeronautics Research Mission Directorate

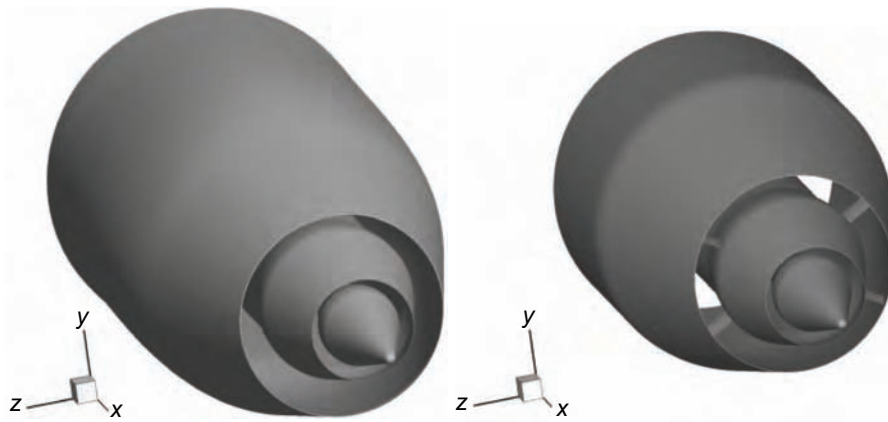
Programs/Projects:

Fundamental Aeronautics Program,
 Subsonic Fixed Wing Project, Supersonic
 Fixed Wing Project

Noise-Reducing Offset Fan Stream Nozzles Simulated by Computational Fluid Dynamics

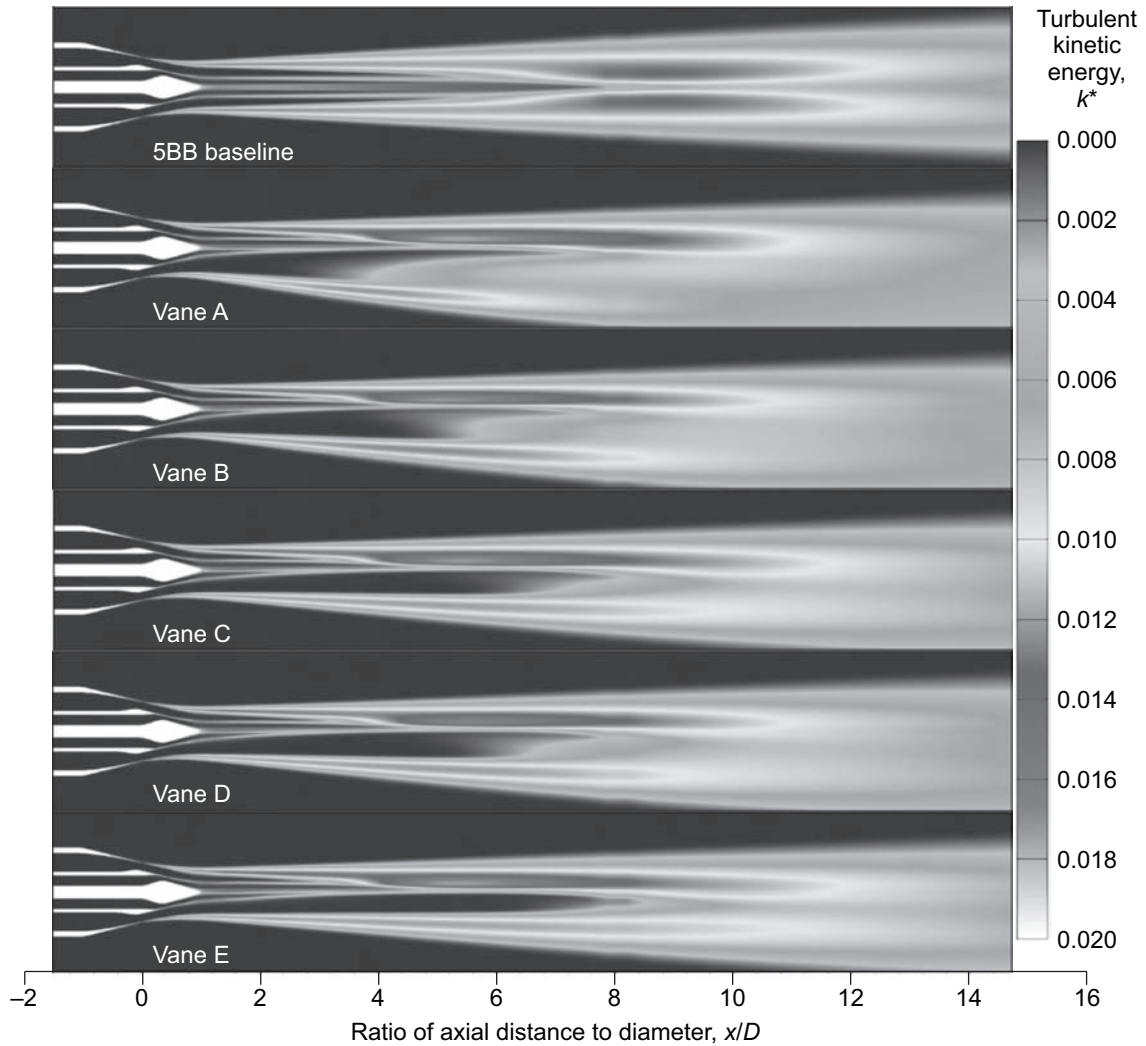
Airport noise reduction continues to be a major challenge for the aerospace community. Offset Stream Technology (OST) nozzles offset the bypass stream of a conventional dual-flow jet engine to create a thick, low-speed layer on the lower side of the jet plume, which has been shown to reduce noise. The bypass stream can be offset using vanes, wedges, or an S-duct in the bypass stream. The effort discussed here used the Wind computational fluid dynamics (CFD) code to assist in the development of various OST nozzle configurations, predict the OST nozzle performance, and observe the OST jet flow field. This effort used a dual-stream nozzle with a bypass ratio of 8 as the baseline and investigated the effects of S-ducts and vanes. CFD analyses were performed for the offset stream nozzles at simulated takeoff and cruise flow conditions.

Two S-duct nozzles were simulated. The first configuration offset the bypass stream 9.3-percent D (where D is the bypass stream diameter) toward the lower side of the nozzle; the second configuration offset the bypass stream 4.5-percent D toward the lower side of the nozzle. Five takeoff vane nozzle configurations were tested, each with two pairs of vanes using NACA 0012 airfoils with angles of attack between 5° and 15° . Two cruise

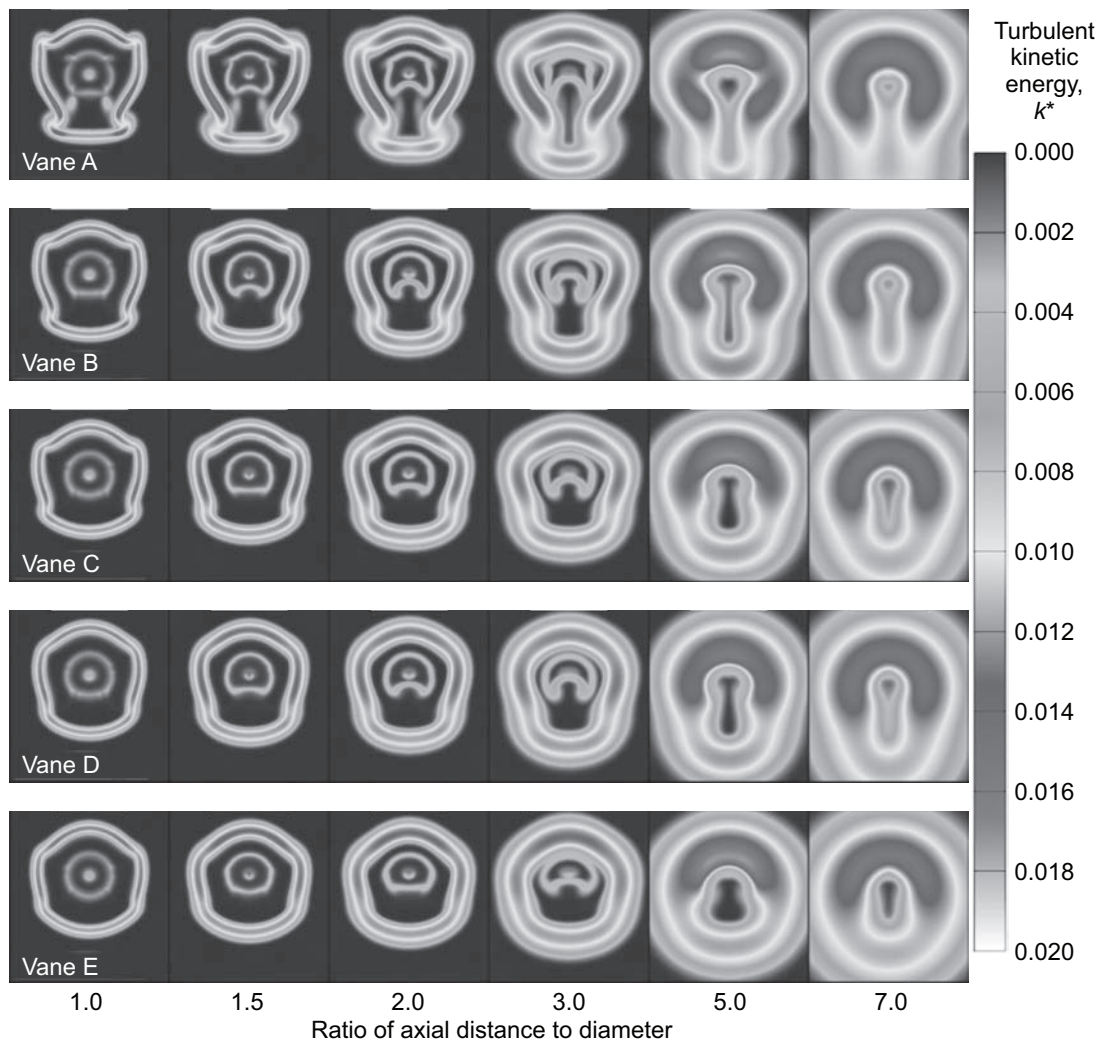


vane nozzle configurations were also tested, with the pairs of vanes set at 0° angle of attack. All but one of the S-duct and vane OST nozzles showed less than 0.7-percent reduction in mass flow and thrust from the baseline at takeoff conditions. The vane configuration that had the larger thrust and mass flow penalty showed severely separated flow from its 15° angle-of-attack vanes. The takeoff S-duct and vane nozzle configurations all successfully offset the bypass stream toward the lower side of the jet plume.

Left: S-duct nozzle. Right: Vane nozzle, with all vanes at 7.5°.



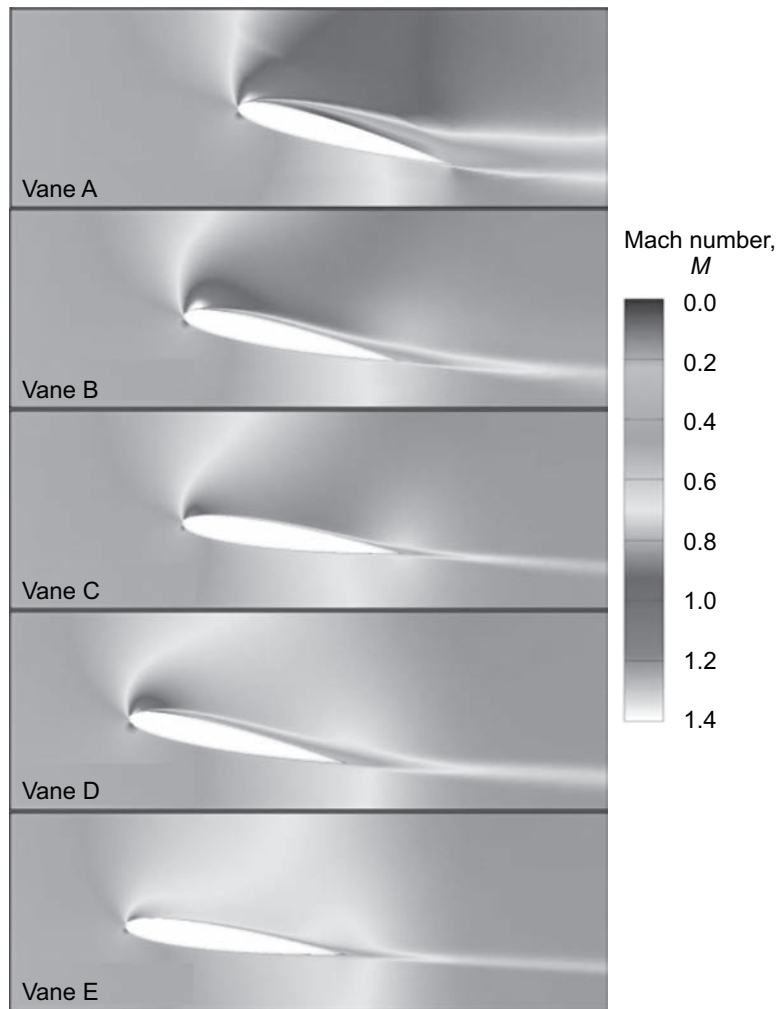
Contours of turbulent kinetic energy, k^* , along the symmetry plane for the vane OST nozzle with all vanes at 7.5° at takeoff conditions. Turbulent kinetic energy is nondimensionalized by the square of the area-averaged velocity of the primary jet: $k^* = k/u_{jet}^2$. This figure is shown in color in the online version of this article (<http://www.grc.nasa.gov/WWW/RT/2007/Aeroprop/05-RTE-dippold.html>).



Contours of turbulent kinetic energy at plume cross sections for the vane OST nozzle with all vanes at 7.5° at takeoff conditions. Turbulent kinetic energy is nondimensionalized by the square of the area-averaged velocity of the primary jet: $k^* = k/u_{jet}^2$. This figure is shown in color in the online version of this article (<http://www.grc.nasa.gov/WWW/RT/2007/Aeroprop/05-RTE-dippold.html>).

The turbulent kinetic energy in the plume was examined because it is directly related to the amount of noise produced by the jet. As expected, the turbulent kinetic energy was reduced from the baseline levels on the lower side of the plume for each OST nozzle. At cruise conditions, the 9.3-percent- D offset S-duct nozzle suffered 0.3-percent mass flow and 0.4-percent thrust penalties, whereas the smaller offset S-duct nozzle saw less than a 0.1-percent thrust loss and negligible mass flow loss from the baseline. The cruise-configured vane nozzles, with vanes rotated to 0° angle of attack, each suffered about 0.2-percent or less reduction in mass flow loss because of the blockage caused by the vanes in the bypass stream.

The results of this CFD study helped guide the OST jet noise experiments, showing which configurations performed well and which configurations performed poorly, including producing excessive amounts of turbulent kinetic energy and noise. Using CFD in the development of the test matrix ensured that the jet noise experiments were relevant in terms of performance and not wasteful in terms of noise.



Contours of Mach number, M , at the midplane of vanes. This figure is shown in color in the online version of this article (<http://www.grc.nasa.gov/WWW/RT/2007/Aeroprop/05-RTE-dippold.html>).

Glenn Contacts:

Vance F. Dippold III, 216-433-8365,
Vance.F.Dippold@nasa.gov

Mary Jo Long-Davis, 216-433-8708,
Mary.J.Long-Davis@nasa.gov

Author:

Vance F. Dippold III

Headquarters Program Office:

Aeronautics Research Mission Directorate

Programs/Projects:

Fundamental Aeronautics Program,
Subsonic Fixed Wing Project

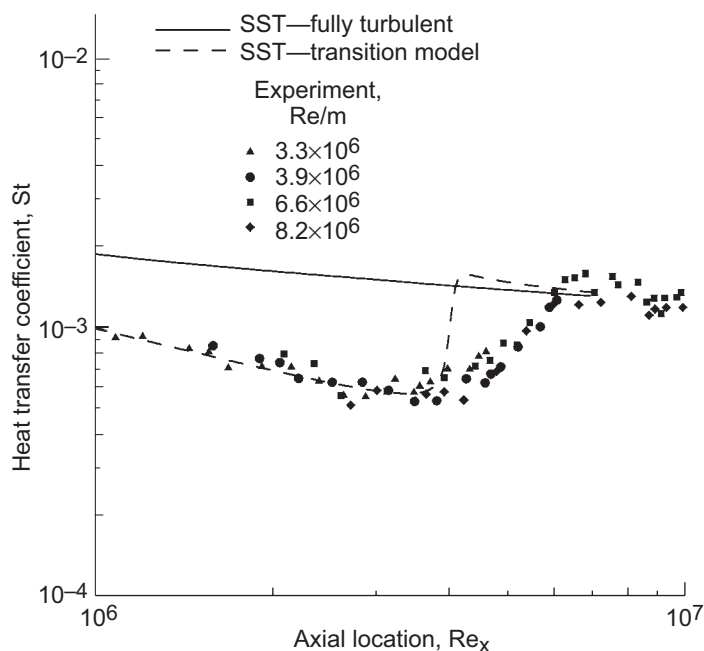
References

1. Papamoschou, Dimitri: Fan Flow Deflection in Simulated Turbofan Exhaust. AIAA J., vol. 44, no. 12, 2006, pp. 3088-3097.
2. Henderson, B.; Norum, T.; and Bridges, J.: An MDOE Assessment of Nozzle Vanes for High Bypass Ratio Jet Noise Reduction. AIAA-2006-2543, 2006.
3. Brown, Clifford A.; and Bridges, James E.: Offset Stream Technologies Test—Summary of Results. AIAA-2007-3664 (NASA/TM-2007-214992), 2007. <http://gltrs.grc.nasa.gov>
4. Dippold, V.; Foster, L.; and Wiese, M.: Computational Analyses of Offset Stream Nozzles for Noise Reduction. AIAA-2007-3598, 2007.
5. DeBonis, J.R.: RANS Analyses of Turbofan Nozzles with Wedge Deflectors for Noise Reduction. AIAA-2008-41, 2007. <http://ntrs.nasa.gov>

Wind-US Code Improved for Hypersonic Flow Simulations

The Wind-US computational fluid dynamics (CFD) computer code has been improved for hypersonic propulsion system and vehicle analyses. This work is jointly sponsored by the NASA Fundamental Aeronautics Program's Hypersonics Project and by the Defense Test Resource Management Center's Test and Evaluation/Science and Technology Program. NASA Glenn Research Center is the lead organization in this effort, which includes three partners: the U.S. Air Force Arnold Engineering Development Center (AEDC), Innovative Technologies Applications Company, and Embry-Riddle Aeronautical University. Wind-US is the flow solver of the National Program for Application-Oriented Research in CFD (NPARC) Alliance.

This Wind-US effort consists of physical modeling improvements, enhancements to the structured and unstructured solvers for chemically reacting flows, validation, and demonstration of the code for tip-to-tail hypersonic vehicle and propulsion system configurations. Initial work has concentrated on physical modeling improvements in the areas of laminar-to-turbulent transition modeling, conjugate heat transfer, and the high-speed combustion solver.



Heat transfer along cone in Mach 7.9 wind tunnel flow. St , Stanton number; Re , Reynold's number.

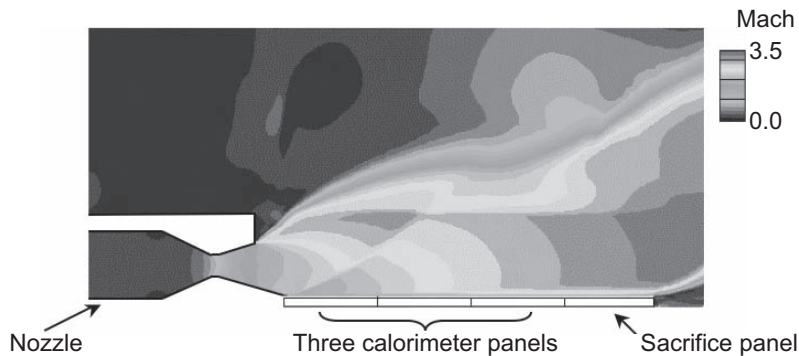
A laminar-to-turbulent transition model, based on the Menter Shear Stress Transport (SST) turbulence model, was added to Wind-US; and validation was conducted for flows ranging from incompressible to hypersonic boundary layers. The preceding graph compares a solution obtained with the Menter SST model in fully turbulent mode, a solution obtained with the transition model added here, and experimental data obtained in the AEDC Tunnel B for a Mach-7.9 flow over a hypersonic cone.

With the high temperatures associated with hypersonic vehicles, heat transfer has significant effects on internal and external aerodynamics, combustion

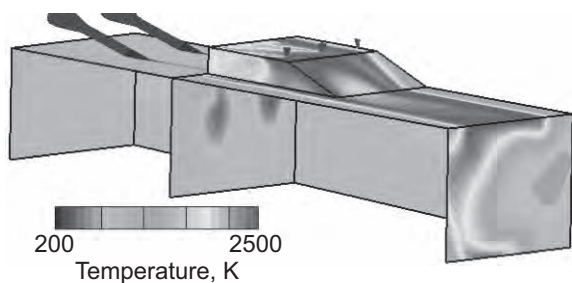
behavior, and structural integrity. As a result, a conjugate heat-transfer capability was added to Wind-US that couples Wind-US with a conduction heat-transfer solver for both the solid surfaces bounding the CFD solution and potentially a fluid path on the other side of a solid surface. The top figure on the next page shows a solution obtained with Wind-US and this conjugate heat transfer method for a case where a hydrogen-oxygen rocket produced an exhaust over calorimeter panels where the heat transfer to coolant water on the other side of the panels was measured. The coupled Wind-US/conjugate heat-transfer solution indicated total heat flux to within 10 percent of the experimental measurements.

Enhancements to the chemically reacting solver have also been completed to improve the solver accuracy and robustness. Previously, Wind-US had been used successfully to analyze a broad range of subsonic and supersonic flow problems free of chemical reactions and was not generally applicable to high-speed reacting flows. However, significant improvements to Wind-US made in this work now enable analysis of complex propulsion system cases with reacting flows. The bottom figure on the next page shows the flow inside a reference scramjet combustor where ethylene fuel is injected and ignited. The figure shows a closeup of the combustor region with the calculation also including an isolator upstream of the combustor and nozzle downstream of the combustor not shown in the figure.

Future efforts in physical modeling will be concentrated on adding advanced turbulence modeling capabilities, turbulent transport models for heat and mass fluxes, and more sophisticated combustion data sets. In addition, improvements to the structured and unstructured solvers will be made to enable more efficient calculations of time-varying flows.



Mach number contours for rocket exhaust in cooled panel experiments. This figure is shown in color in the online version of this article (<http://www.grc.nasa.gov/WWW/RT/2007/Aeroprop/06-RTE-georgiadis.html>).



Temperature contours in scramjet combustor with ethylene fuel injection. This figure is shown in color in the online version of this article (<http://www.grc.nasa.gov/WWW/RT/2007/Aeroprop/06-RTE-georgiadis.html>).

Find out more about this research:

Glenn's Inlet and Nozzle Branch:

<http://www.grc.nasa.gov/WWW/RT/>

NPARC Alliance:

<http://web.arnold.af.mil/nparc/>

Wind-US Version 2.0 documentation:

<http://www.grc.nasa.gov/WWW/winddocs/>

Glenn Contacts:

Dr. Nicholas J. Georgiadis, 216-433-3958, Nicholas.J.Georgiadis@nasa.gov

Dr. Dennis A. Yoder, 216-433-8716, Dennis.A.Yoder@nasa.gov

Dr. Charles E. Towne, 216-433-5851, Charles.E.Towne@nasa.gov

Authors:

Dr. Nicholas J. Georgiadis, Dr. Dennis A. Yoder, Dr. Charles E. Towne, Nicholas A. Denissen, Dr. Chris Nelson, Dr. William Engblom, Dr. Dennis Lankford, Joo Suh, Dr. Greg Power, and Bonnie Heikkinen

Headquarters Program Office:

Aeronautics Research Mission Directorate

Programs/Projects:

Fundamental Aeronautics Program, Hypersonics Project

Bibliography

Engblom, W.A.; Fletcher, B.; and Georgiadis, N.: Validation of Conjugate Heat-Transfer Capability for Water-Cooled High-Speed Flows. AIAA-2007-4392, 2007.

Small-Scale Inlet Mode Transition Model Tested in Glenn's 1- by 1-Foot Supersonic Wind Tunnel

A screening test of an inlet mode transition model was completed for hypersonic propulsion. The test was conducted at Mach 4 to verify the design concept for high performance and smooth transition between a low-speed turbofan to a higher speed scramjet operation. This effort ties into a need to demonstrate acceleration through intermediate supersonic Mach numbers, 2 to 4.

For hypersonic flight, air-breathing propulsion can enable new efficiencies for quick space access and global reach. Various propulsion modes have been proposed for the range of Mach numbers encountered by an accelerating hypersonic vehicle. One possible propulsion scheme is the turbine-based combined cycle (TBCC), which uses a high-Mach-capable engine to accelerate

the vehicle to scramjet takeover speeds. Switching between the turbine (turbofan) cycle and the scramjet is termed mode transition. Typically, the two engines are placed one above the other and are fed by a common inlet and nozzles to save weight. The focus of this effort was to design and verify an inlet concept for TBCC that is termed the Inlet Mode Transition (IMX).

A major element of the IMX design was variable geometry based on sets of cowl and ramp contours. Hydraulic actuation, providing a smooth transition from turbofan to dual-mode ramjet operation, was used to vary the cowl geometry. The design balances high performance (low loss), engine flow demand, and mechanical feasibility. A splitter-contoured surface directs flow into the turbofan up to the transition Mach number 4 and then closes to provide added compression to improve the dual-mode ramjet operability and performance. For lower Mach number turbofan flow demands, a variable geometry ramp was also designed.

The conceptual design was conceived by TechLand Research, Inc. (North Olmsted, OH), which had received funding through NASA's Small Business Innovation Research program. The Hypersonics Project of NASA's Fundamental Aeronautics Program adopted the design and directed the high-speed flowpath design to Mach 7. The NASA Glenn Research Center in collaboration with TechLand carried this aerodynamic design through mechanical



IMX model mounted in Glenn's 1×1 SWT.

was tested during the summer of 2007 in Glenn's 1×1 SWT, covering design and off-design conditions. The model featured nine bleed compartments in the region in the low-speed flowpath. Each of these bleeds was found to contribute to the overall high performance of the low-speed inlet. The objectives of the test were met: high performance, stability, and smooth mode transition. The experimental data are being compared with the CFD analysis methods; an effort that will help develop CFD tools for future hypersonic inlet design.

Find out more about the research of Glenn's Inlet and Nozzle Branch:
<http://www.grc.nasa.gov/WWW/RTE/>

Glenn Contact:

John D. Saunders, 216-433-6278,
 John.D.Saunders@nasa.gov

TechLand Research, Inc., Contact:

Bobby W. Sanders, 440-716-9077,
 techland@stratos.net

Author:

John D. Saunders

Headquarters Program Office:

Aeronautics Research Mission Directorate

Programs/Projects:

Fundamental Aeronautics Program,
 Hypersonics Project

Special Recognition:

Glenn Craftsmanship Award

design and in-house fabrication of a screening model for testing in Glenn's 1- by 1-Foot Supersonic Wind Tunnel (1×1 SWT). Glenn researchers used computational fluid dynamics (CFD) tools for three-dimensional, turbulent flow analysis to further refine the aerodynamic design.

The inlet was sized near maximum blockage limits at Mach 2.5. Main remotely variable geometry included rotating cowl lips for both the high- and low-speed inlets and an exit flow-metering plug on the low-speed inlet. The main parametric aspects of the low-speed inlet included interchangeable components for ramp contours (Mach 4 and 3) as well as bleed patterns and amounts. The IMX model was fabricated and instrumented at Glenn, and it

Full-Scale Iced Airfoil Aerodynamic Performance Evaluated

Researchers and a technician from the NASA Glenn Research Center traveled to the Office National d'Etudes et de Recherches Aeronautiques (ONERA) F1 wind tunnel facility in Le Fauga-Mauzac, France, to conduct full-scale, flight Reynolds number aerodynamic wind tunnel tests of an ice-contaminated airfoil. The objectives of the tests were to provide a better understanding of the effects of ice accretions on airfoil aerodynamic performance and to provide a benchmark database for iced-airfoil computational fluid dynamics (CFD) development. This study was part of a larger joint NASA-ONERA international agreement (which included important technical contributions from the University of Illinois at Urbana Champaign) to investigate ice-contaminated airfoil aerodynamics using a flow-physics-based approach. This is the first-ever, fundamental-aerodynamics-based approach to investigating the effects of aircraft icing.

In the F1 tests, a full-scale NACA-23012 airfoil was fitted with ice shapes made from molds of ice accreted on a similar airfoil model in NASA's Icing Research Tunnel (IRT). The IRT model was subjected to conditions that might be experienced by a commuter aircraft flying in natural icing. The conditions were selected to generate ice accretions resulting in fundamentally different airfoil aerodynamics. The F1 wind tunnel is unique in that it is large enough to allow aerodynamic performance testing of a full-scale model over a large range of angles of attack, including stall, and in that it can be pressurized, allowing independent studies of Mach and Reynolds number effects.

Primarily because of concerns about aerodynamic scaling of ice-contaminated surfaces, questions have remained regarding aerodynamic performance results in smaller wind tunnels with subscale models. Results from the recently completed F1 aerodynamic performance tests largely verify previous results from

the smaller tunnels, showing decreases in maximum lift coefficient of as much as 70 percent, decreases in stall angle of as much as 12° angle of attack, and increases in drag coefficient of as much as 400 to 1000 percent. These data not only provide a better understanding of the aerodynamic effects of ice accretions and a benchmark database for CFD, but they will be used to verify and validate subscale iced-aerodynamic performance testing. Where subscale testing is lacking, these results can be used to develop new, valid methods of subscale iced-aerodynamic performance testing.

A second set of tests was conducted in the F1 tunnel in June 2007. During these tests, particle imaging velocimetry (PIV) measurements were made of the airflow around the model with one of the ice shapes installed. These measurements provided flowfield details leading to a better understanding of iced aerodynamics and supplied information needed for iced CFD validation and development, which could not be obtained during the aerodynamic performance tests. Remaining work in the program consists of CFD code development and validation exercises as well as subscale testing to validate and further refine the experimental methods developed.

Glenn Contacts:

Harold E. (Gene) Addy, Jr.,
216-977-7467, Gene.Addy@nasa.gov
Dr. Mark G. Potapczuk, 216-433-3919,
Mark.G.Potapczuk@nasa.gov

Authors:

Harold E. Addy, Jr., and
Dr. Mark G. Potapczuk

Headquarters Program Office:

Aeronautics Research Mission Directorate

Programs/Projects:

Aviation Safety Program, Fundamental
Aeronautics Program

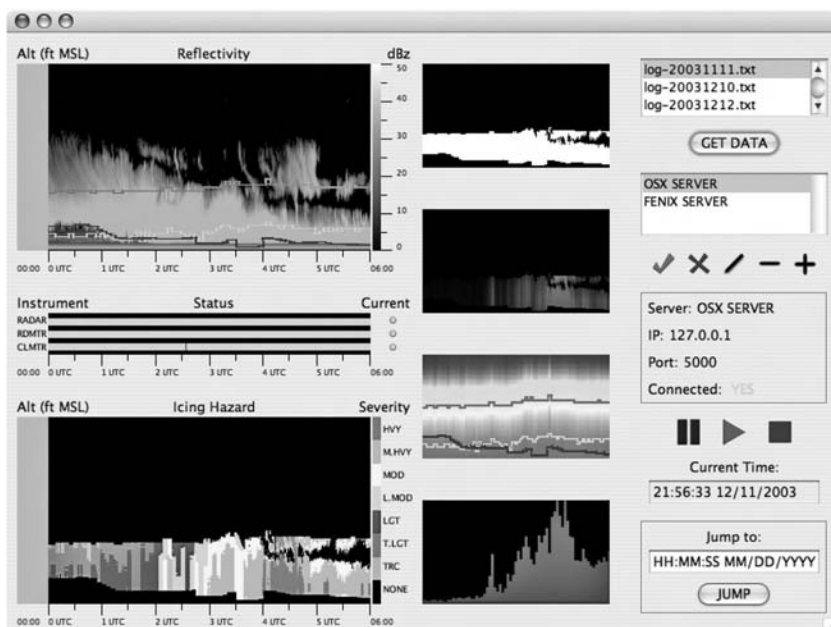


Full-scale NACA-23012 airfoil model in the ONERA F1 tunnel.

Web-Based Icing Remote Sensing Product Developed



Glenn's icing remote sensing ground site.



Graphic display for the Web-based Icing Remote Sensing Product. This figure is shown in color in the online version of this article (<http://www.grc.nasa.gov/WWW/RT/2007/Aeroprop/09-RTI-reehorst.html>).

The NASA Glenn Research Center's Icing Branch activated the initial version of its Web-based Icing Remote Sensing Product during 2007. Capable of describing the location and severity of icing hazards aloft, this is the first real-time output display based on the remote measurement of the icing environment. Although still an experimental system intended for use by the research community, it highlights the potential of Web-based products for disseminating icing hazard information to flight crews.

The Web-based Icing Remote Sensing Product is the final output of a processing system that starts with raw sensor data. The sensors currently used for the remote detection of icing conditions are a multifrequency microwave radiometer, a ceilometer, and an X-band radar. The radiometer makes passive measurements that provide a profile of air temperature above the instrument and the total liquid water content. The X-band radar defines the cloud boundaries, and the ceilometer further refines the lower cloud boundary.

The raw sensor data are gathered on individual personal computers and then transferred to a Linux-based computer. Software on the Linux machine processes the data through a series of algorithms to define cloud boundaries, map liquid water into the clouds, and determine altitudes with supercooled liquid water present. Finally, from the intensity of the calculated supercooled liquid water environment, the system determines the level of icing hazard at various altitudes using simplified aircraft icing performance degradation estimates. Good agreement has been achieved when comparing the algorithm output with data gathered during the Second Alliance Icing Research Study (AIRS II) field test program in 2003. Although the bulk of the work to date has occurred at Glenn, our research partners have completed

significant work effort in programming and algorithm development (National Center for Atmospheric Research) and in microwave radiometer development (Radiometrics Corporation).

References

1. Reehorst, Andrew, L., et al.: The NASA Icing Remote Sensing System. NASA/TM—2005-213591, 2005. <http://gltrs.grc.nasa.gov>
2. Reehorst, Andrew, L.; Brinker, David, J.; and Ratvasky, Thomas, P.: NASA Icing Remote Sensing System Comparisons from AIRS II. NASA/TM—2005-213592 (AIAA-2005-0253), 2005. <http://gltrs.grc.nasa.gov>
3. Reehorst, Andrew, et al.: Progress in the Development of Practical Remote Detection of Icing Conditions. NASA/TM—2006-214242, 2006. <http://gltrs.grc.nasa.gov>
4. Current Remote Sensing Data. Most current data from the instruments of the NASA Glenn Icing Remote Sensing project. <http://icebox-esn.grc.nasa.gov/RSDData/>

Find out more about the research of Glenn's Icing Branch:

<http://icebox.grc.nasa.gov>

Glenn Contacts:

Dr. David J. Brinker, 216-433-2236,
David.J.Brinker@nasa.gov

Andrew L. Reehorst, 216-433-3938,
Andrew.L.Reehorst@nasa.gov

Authors:

Dr. David J. Brinker and
Andrew L. Reehorst

Headquarters Program Office:

Aeronautics Research Mission Directorate

Programs/Projects:

Aviation Safety Program

Novel Antivortex Turbine Film-Cooling Hole Concept Conceived and Developed

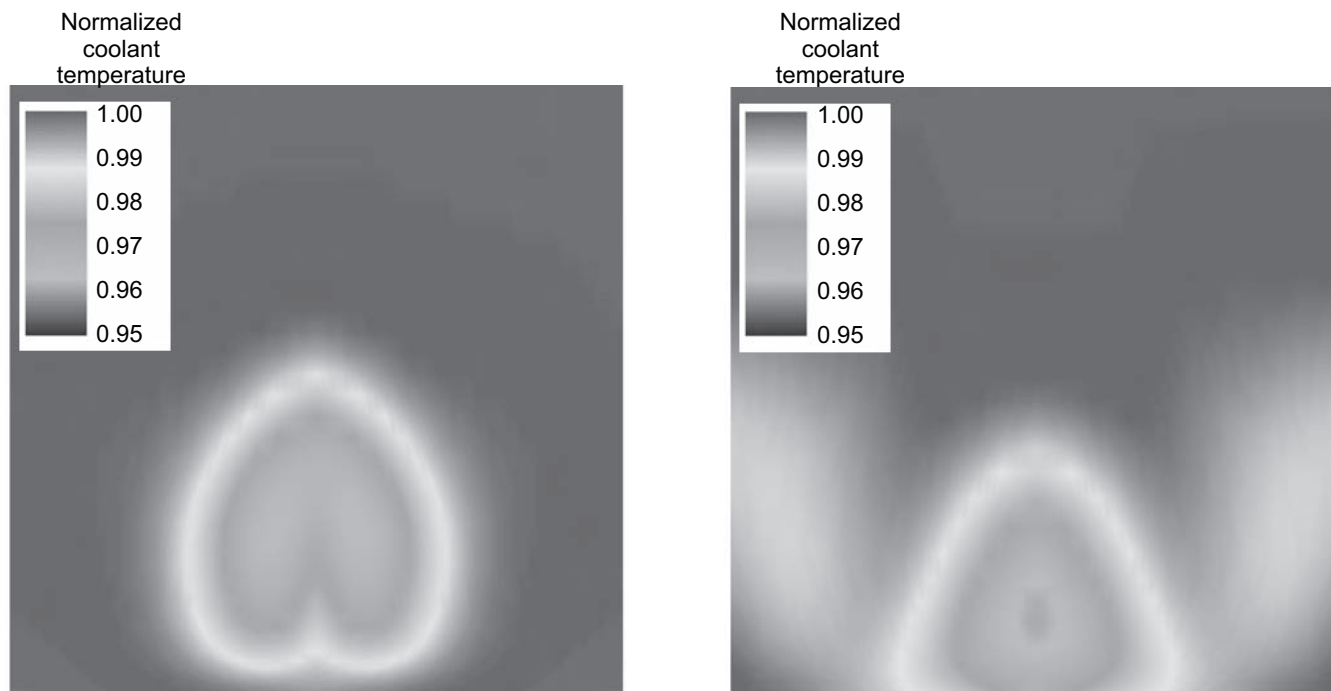
A new film-cooling design concept (ref. 1) has been conceived and developed at the NASA Glenn Research Center. This “antivortex” film-cooling concept is designed to mitigate the effects of the counterrotating vortex pair, which reduces the effectiveness of circular cross-section film-cooling holes at moderate to high blowing ratios. The design developed in the present study is shown in the following figures, although many parameters can be modified in an optimized design.

This film-cooling is a modification to a standard, single-row, round film-cooling hole arrangement with the holes angled at 30° to the surface and a spanwise pitch of three hole diameters. The concept is compared with the baseline data of reference 2. The holes are placed in a flat plate geometry, which can be thought of as representing a turbine blade suction- or pressure-side film-cooling hole. In the antivortex design, two side holes are drilled that intersect with the main hole and that are angled in the spanwise direction on either

side of each main hole. Since each main hole has a side hole on both sides, the flow from the side holes of two adjacent main holes interact with each other, producing a strong vortex. This vortex is opposite in sense to the detrimental vorticity produced by the main hole, and it is intended to force the coolant flow from the main hole to remain attached to the surface. Another way to view this expected benefit is that the side holes produce a strong upwash that must be balanced by a net downwash in the main-hole jet-centerline plane. An additional benefit from the side-hole jet inclining



Antivortex design. Left: Top view. Center: Side view. Right: Front view.



Coolant temperature profiles five hole-diameters downstream. Temperatures are normalized by the freestream temperature. The normalized coolant temperature is 0.95. Left: Baseline. Right: Antivortex. These figures are shown in color in the online version of this article (<http://www.grc.nasa.gov/WWW/RT/2007/Aeroprop/10-RTT-heidmann.html>).

away from the main jet in the spanwise direction is that this draws the coolant from the bottom of the main jet away from the jet centerline, effectively flattening the coolant jet. These plots show the computed temperature field downstream of the hole, illustrating the improved film coverage of the anti-vortex design.

The antivortex film-cooling design concept has been shown computationally to dramatically improve film cooling over that of a standard round hole for a blowing ratio of 1.0 on a flat plate model. An improvement in area-averaged film effectiveness of about 0.2 and in net heat-flux reduction of about 0.2 is predicted for the modified antivortex design versus the baseline round hole for density ratios of 1.0 and 2.0. The concept is easily manufactured because only round holes are used. A benefit has been shown relative to a standard single row of round holes at an angle of inclination of 30° and a pitch-to-diameter ratio of 3.0. This concept could be added as a retrofit process to existing round-hole geometries on turbine blades and vanes since the total mass flow rate through the new hole is relatively insensitive to the addition of the side holes.

References

1. Heidmann, James D.; and Ekkad, Srinath V.: A Novel Anti-Vortex Turbine Film Cooling Hole Concept. ASME Paper GT2007-27528, 2007. J. Turbomachinery, vol. 130, July 2008 (in press).
2. Dhungel, A., et al.: Film Cooling From a Row of Holes Supplemented With Anti Vortex Holes. ASME Paper GT2007-27419, 2007.

Find out more about the research of Glenn's Turbomachinery and Heat Transfer Branch:

<http://www.grc.nasa.gov/WWW/RTT/>

Glenn Contact:

Dr. James D. Heidmann, 216-433-3604,
James.D.Heidmann@nasa.gov

Author:

Dr. James D. Heidmann

LEW Number:

LEW-18125-1

Headquarters Program Office:

Aeronautics Research Mission Directorate

Programs/Projects:

Fundamental Aeronautics Program,
Subsonic Fixed Wing Project

Special Recognition:

The antivortex film-cooling design received an award from NASA's Invention and Contributions Board. Such gas turbine engine cycle improvements can lead to reduced fuel consumption and greenhouse gas production.

Ultrahigh-Bypass-Ratio Propulsion Systems Studied

To generate thrust, it is usually more efficient to accelerate a large mass of air by a small amount than to accelerate a small mass of air by a large amount. In a turbofan jet engine, the airflow rate that bypasses the engine core divided by the airflow rate that travels through the core is called the bypass ratio, or BPR. This ratio is one of the key indicators of turbofan engine efficiency. The desire for better fuel efficiency has resulted in the evolution of commercial aircraft gas turbine engines from early turbojets (BPR = 0), to low-bypass-ratio, first-generation turbofans (BPR = 1 to 2), to today's high-bypass-ratio turbofans (BPR = 5 to 10). Now, ultrahigh-bypass-ratio (UHB) turbofans (BPR = 10 to 20) are being designed for a next-generation, intracontinental commercial aircraft. This aircraft could enter service as early as 2015.

The Intercenter Systems Analysis Team, consisting of systems engineers from the NASA Glenn Research Center and the NASA Langley Research Center, conducted an analytical feasibility study of UHB turbofans for NASA's Fundamental Aeronautics Program. With a little math, it can be shown that fuel efficiency increases along with BPR. The engine core, however, has a limited supply of power available to propel the bypass airstream, so it can be difficult to increase BPR arbitrarily. One path to UHB engines and better efficiency is to reduce the fan's pressure ratio; this lowers the fan's power requirement and allows higher BPRs. The analysis team designed nine notional UHB propulsion systems for the new aircraft along a parametric design sweep of fan pressure ratio. Using advanced computational tools, these propulsion systems were analytically installed on the airframe and "flown" on missions to determine overall airplane system performance.

In addition to improving engine fuel efficiency, increasing bypass ratio also reduces engine noise because of the strong relationship between noise and the velocity of the air exiting the engine. The lower jet velocities associated with low fan pressure ratio can lead to substantial engine noise reduction. However, there is a practical limit to how much bypass ratio can be increased before significant penalties arise that quickly erode the benefits. UHB engines have relatively large, low-speed fans, which may require gearboxes and even variable-geometry exhaust nozzles in order to be practical. Engine weight and drag increase as well, making it more difficult to integrate the engines with the airframe.

Despite these difficulties, the NASA team's results indicate that UHB turbofans can be viable, low-noise alternatives to today's more conventional propulsion systems. The purpose of NASA's parallel, independent system studies is not to direct industry's designs, but rather to exchange data and ideas, and to provide industry with innovative NASA technologies and options.

Find out more about the research of Glenn's Propulsion Systems Analysis

Branch:

<http://www-psao.grc.nasa.gov>

Glenn Contacts:

William J. Haller, 216-977-7004,
William.J.Haller@nasa.gov

Jeffrey J. Berton, 216-977-7031,
Jeffrey.J.Berton@nasa.gov

Kenneth L. Fisher, 216-433-5655,
Kenneth.L.Fisher@nasa.gov

U.S. Army Research Laboratory at Glenn Contact:

Douglas R. Thurman, 216-433-6573,
Douglas.R.Thurman@nasa.gov

Authors:

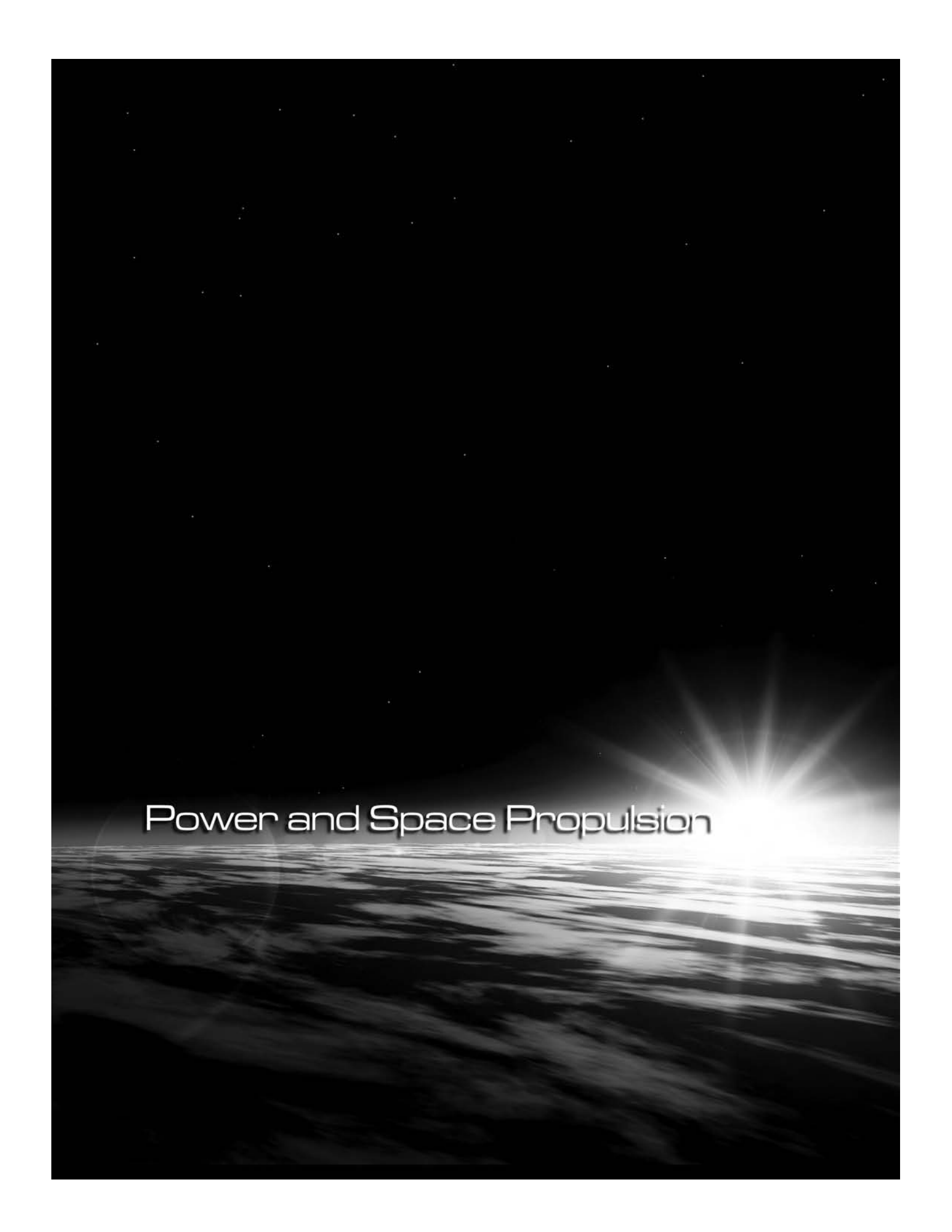
Jeffrey J. Berton and Mark D. Guynn

Headquarters Program Office:

Aeronautics Research Mission Directorate

Programs/Projects:

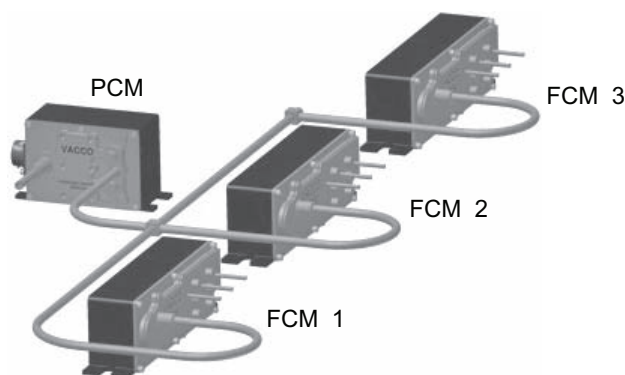
Fundamental Aeronautics Program,
Subsonic Fixed Wing Project

A black and white photograph of a bright sun or star on the horizon of a planet, with the text "Power and Space Propulsion" overlaid. The sun is positioned on the right side of the horizon, creating a lens flare effect. The horizon line is slightly curved, suggesting a view from space. The background is a dark, starry sky.

Power and Space Propulsion

First Phase of Advanced Feed System Development for Electric Propulsion Completed

VACCO Industries has successfully completed the first phase of a contract with NASA Glenn Research Center to design and develop an Advanced Xenon Feed System (AXFS). The objective was to reduce cost, size, and mass while increasing functionality and component reliability. These goals were accomplished using a simple, modular system architecture consisting of one pressure control module (PCM) per system and one flow control module (FCM) per thruster. This effort was funded by NASA's In-Space Propulsion Technology Project.



Advanced Xenon Feed System architecture.

To achieve reliability, each module is one-fault tolerant of any functional failure and one-fault tolerant of any leakage failure. The PCM contains a 5- μm (absolute) system filter, high-pressure transducers and temperature sensors, two high-pressure isolation valves, and two proportional pressure-control valves. The FCM features a 5- μm filter, pressure/temperature sensors, six isolation valves, and six proportional flow control valves arranged into three independent flow channels. These highly integrated modules were made possible by applying a novel manufacturing technology.

The AXFS program had several specific accomplishments over the past year:

- It is the first feed system design to be based on an extensive user requirements study. This study influenced the design requirements to include independent, throttleable control of the main, cathode, and neutralizer flow output and true one-fault tolerance.
- The manufacturing technology utilized diffusion-bonded titanium manifolds in both FCM 1 and 2. This proved that these manifolds can be produced reliably with external leakage characteristics consistent with all-welded assemblies.
- Six microlatching isolation valves were application-engineered, built, and integrated into each FCM. This unique titanium solenoid design is ideally suited for effective packaging into highly integrated modules.

- The user requirements study revealed a need for independent and throttleable control of flow to the thruster. Accordingly, a proportional flow control valve was application-engineered for this purpose. Six low-power flow control valves are used in each FCM.
- Through an extensive test program, the technology readiness level (TRL) of the FCM was elevated to TRL 6, so it is ready for flight applications.

The VACCO AXFS was required to be a substantial improvement over the benchmark—NASA's Evolutionary Xenon Thruster (NEXT) flight feed system. As a result, AXFS is 80-percent lighter, 93-percent smaller, and significantly more reliable than the NEXT feed system.

With a continuation of fiscal year 2007 funds, NASA awarded VACCO a contract to complete this technology product by designing, developing, and testing a PCM and an electronic controller. These will be combined with an existing FCM to form a complete AXFS. After benchmark testing, the resulting system will be extensively hot-fire tested with Hall and ion thrusters at Glenn.

Find out more about the research of Glenn's Science Division:

<http://www.grc.nasa.gov/WWW/Science/>

Glenn Contacts:

Eric J. Pencil, 216-977-7463,
Eric.J.Pencil@nasa.gov

Tibor Kremic, 216-433-5003,
Tibor.Kremic@nasa.gov



Flow control module.

Authors:

Eric J. Pencil, Dr. Michael R. LaPointe, and Joseph Cardin

Headquarters Program Office:

Science Mission Directorate

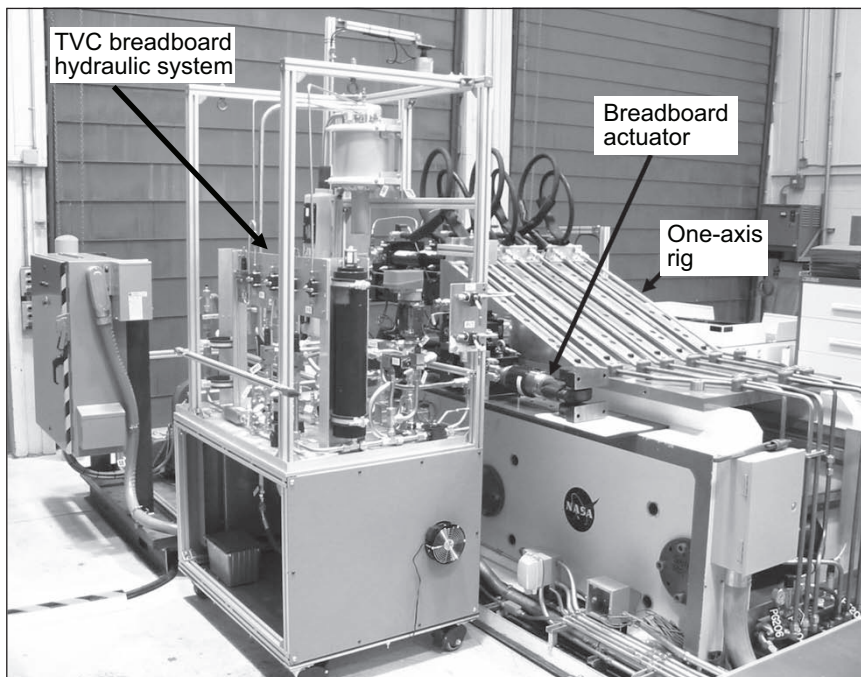
Programs/Projects:

NASA In-Space Propulsion
Technology Project

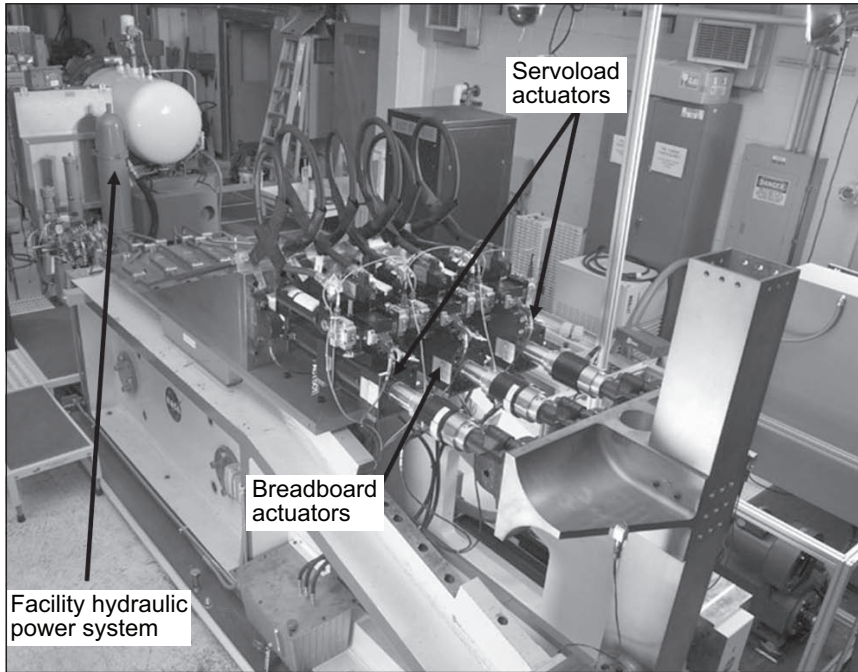
Initial Prototype of Ares I Upper Stage Thrust Vector Control and Associated One-Axis Test Rig Developed

Thrust Vector Control (TVC) provides a critical function in steering the Ares I Upper Stage (US) in the pitch and yaw direction during powered flight. An initial prototype of the Ares I US TVC and its associated one-axis test rig have been developed by the NASA Glenn Research Center TVC team.

The initial prototype is a TVC breadboard (see the photograph to the left) that represents a single TVC string with a hydraulic pump, hydraulic system, and an actuator. The TVC breadboard is built with off-the-shelf hardware. The one-axis test rig (see the photograph on the next page) was developed to simulate the gimbaling dynamics and rocket engine system characteristics including inertia, gimbal friction, thrust offset, moment arm, propellant feed line, and acceleration loads. The one-axis test rig includes a closed-loop rocket dynamic control algorithm that computes the required load. This load is applied to the TVC breadboard actuator using two servoload actuators, one on each side of the TVC breadboard actuator, connecting through a common beam. The test rig is supported by a facility hydraulic power system and control and data management systems. The TVC breadboard and one-axis test rig will be integrated and tested in early calendar year 2008. The objective of the TVC breadboard testing is to provide engineering data to support the preliminary design of the selected TVC architecture and to validate analysis models.



Ares I US TVC breadboard and one-axis test rig at Glenn.



One-axis test rig at Glenn.

Glenn leads the design and development of the Ares I US TVC. The TVC breadboard is the initial development hardware in the design, development, test, and evaluation phase. Following the breadboard phase, engineering-model TVC hardware along with a two-axis test rig will be developed and tested in the second quarter of calendar year 2009. Successful completion of engineering hardware and evaluation will support a key decision point leading to the start of the qualification and flight development phase.

Electric Propulsion Breakthrough Demonstrated

The NASA Glenn Research Center is developing Hall thruster technology for future cost-capped NASA science missions through the High Voltage Hall Accelerator (HIVHAC) task. The objective of this activity is to increase the lifetime of Hall thrusters sufficiently to enable deep-space science missions. To meet this objective, Glenn designed and fabricated a thruster with the following capabilities: operation at input powers ranging from 300 to 3500 W, specific impulses to 2800 sec, and a total propellant throughput capability of 300 kg of xenon.

Beginning in 2007, this thruster, designated the NASA-1003M.XL, was subjected to long-duration wear testing with thruster performance and propellant throughput being continuously monitored. As of September, this thruster

Find out more about the Launch Systems Project at Glenn:
<http://spaceflight systems.grc.nasa.gov/LaunchSystems/>

Glenn contacts:
 Nang Pham, 216-433-6165,
 Nang.T.Pham@nasa.gov
 David Frate, 216-433-8329,
 David.T.Frate@nasa.gov
 Scott Graham, 216-977-7123,
 Scott.R.Graham@nasa.gov
 Bob Tornabene, 216-433-3045,
 Robert.T.Tornabene@nasa.gov
 Jim Zakany, 216-433-5080,
 James.S.Zakany@nasa.gov
 Joe Zoeckler, 216-977-7411,
 Joseph.G.Zoeckler@nasa.gov

Authors:
 Nang T. Pham and Dave T. Frate

Headquarters Program Office:
 Exploration Systems Mission Directorate

Programs/Projects:
 Constellation Systems

had operated at full-power conditions of 700 V and 5 A, with a xenon flow rate of 60 mg/sec for over 3000 hr. As of October 1, 2007, the total demonstrated propellant throughput was 70 kg of xenon. Wear profiles also were measured during this test to provide data needed to validate numerical wear simulations. According to current projections from these simulations, the current thruster design will be able to meet the total propellant throughput objective of 300 kg of xenon.

This represents an approximately tenfold increase in the throughput capability of high-voltage Hall thrusters. Additional testing of this laboratory-model thruster is planned for next year as is the design and fabrication of an engineering-model version of this thruster.

Find out more about Glenn's electric propulsion research:

<http://www.grc.nasa.gov/WWW/ep/>

Glenn Contacts:

Dr. David H. Manzella, 216-977-7432, David.H.Manzella@nasa.gov

Dr. Hani Kamhawi, 216-977-7435, Hani.Kamhawi-1@nasa.gov

Author:

Dr. David H. Manzella

LEW Numbers:

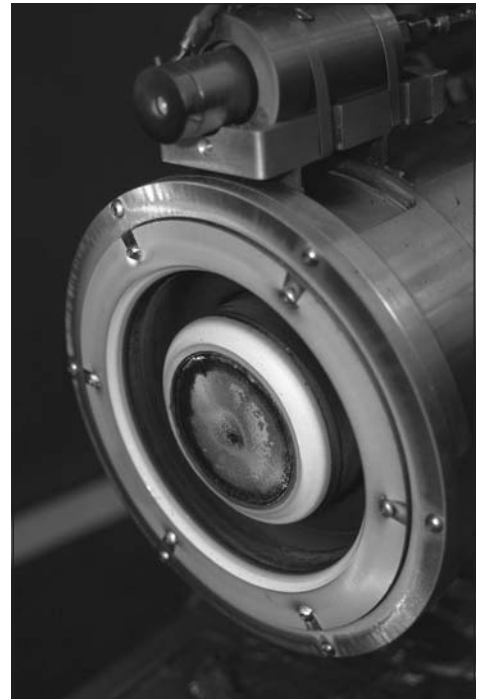
LEW-17678 and LEW-17932

Headquarters Program Office:

Science Mission Directorate

Programs/Projects:

In-Space Propulsion Technology Program



Glenn's 3.5-kW HIVHAC thruster removed from the wear test facility for erosion measurements.

Advanced Propellant Management System of NASA's Evolutionary Xenon Thruster Qualified for Electric Propulsion

The NASA Glenn Research Center is responsible for the development of NASA's Evolutionary Xenon Thruster (NEXT) ion-propulsion system. The objective of the NEXT project is to advance next-generation ion-propulsion technology to a high state of technical readiness. The NEXT ion-propulsion system consists of a high-performance ion thruster; a modular, high-efficiency power processor unit; a highly flexible advanced xenon propellant management system (PMS) consisting of one high-pressure assembly (HPA) for the system and one low-pressure assembly (LPA) per thruster; and other subsystem elements. This design approach was selected to provide future NASA science missions with the greatest value in mission performance at a low total development cost.

The xenon feed system (XFS) developed under the NASA Solar Electric Propulsion Technology Application Readiness (NSTAR) program for Deep Space 1 and implemented on the 2007 Dawn mission established the state of the art. Future missions, however, will require propellant management systems with lower mass and volume, as well as increased system flexibility.

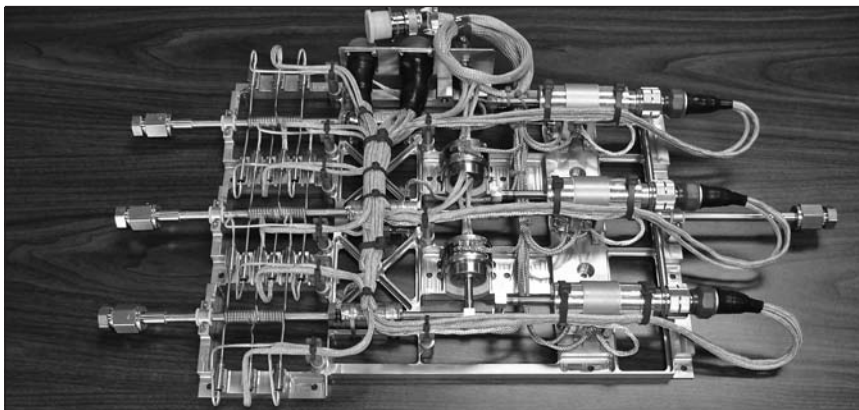
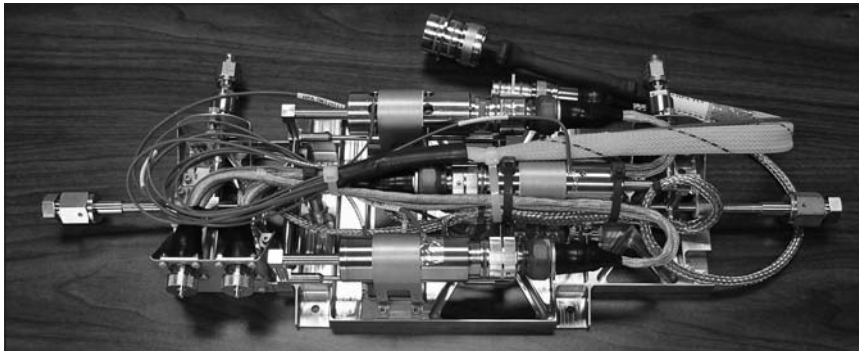
The NEXT PMS xenon flow rate control uses the combination of a thermal throttle flow control device and a proportional flow control valve (PFCV). The thermal throttle allows a repeatable flow rate for a given inlet pressure and operating temperature. It achieves precise, rapid throttling of flow rate by actively controlling the inlet pressure with the PFCV while controlling the operating temperature to a constant set-point. With this approach, the NEXT PMS exhibits significantly improved performance and lower mass in comparison to the NSTAR and Dawn mission feed systems. Because the bang-bang-operated solenoid valves were eliminated, both the plenum

Performance criteria	NEXT PMS	NSTAR XFS
Mass, kg	5.0	11.4
Volume, cm ³	11,775	27,300
Independent throttling of main, cathode, and neutralizer?	Yes	No
Throttle rate, min	<1	~45
Xenon residuals, percent	<1	<2.4
Plenum tanks required?	No	Yes

tank and saw-tooth pressure waveform could be eliminated. Through elimination of the plenum tanks, throttle rates—as well as system volume and end-of-life xenon residuals—were reduced dramatically. The table compares the NEXT PMS and the NSTAR XFS.

The NEXT PMS is segregated into one HPA for the system and one LPA for each thruster. The HPA is functionally a redundant, precision pressure regulator that regulates the xenon tank pressure from as much as 2700 psia typically to 50 psia for input to the LPAs. The LPAs control the three independent flow rates needed for a single thruster. The engineering model LPA design contains three independent PFCVs, providing fully independent flow ranges for each branch.

Following final assembly, two HPAs and three LPAs were subjected to an extensive test sequence at Aerojet that included functional, calibration, qualification-level random-vibration, and qualification-level thermal-vacuum testing. All tests have met their objectives with no findings. The assemblies have been delivered to Glenn and are being prepared for NEXT ion-propulsion system integration testing (see the photographs).



Aerojet's engineering model HPA and LPA. Copyright Aerojet; prepared under contract to NASA.

Bibliography

Patterson, M.; and Benson, S.: NEXT Ion Propulsion System Development Status and Performance. AIAA-2007-5199, 2007.

Hoskins, A., et al.: NEXT Ion Propulsion System Production Readiness. AIAA-2007-5856, 2007.

Find out more about this research:

NASA's In-Space Propulsion Technology Program:

<http://www.inspacepropulsion.com>

Ion propulsion research at Glenn:

<http://www.grc.nasa.gov/WWW/ion/>

Glenn Contacts:

Michael J. Patterson, 216-977-7481,
Michael.J.Patterson@nasa.gov

Scott W. Benson, 216-977-7085,
Scott.W.Benson@nasa.gov

Author:

Michael J. Patterson

Headquarters Program Office:

Science Mission Directorate

Programs/Projects:

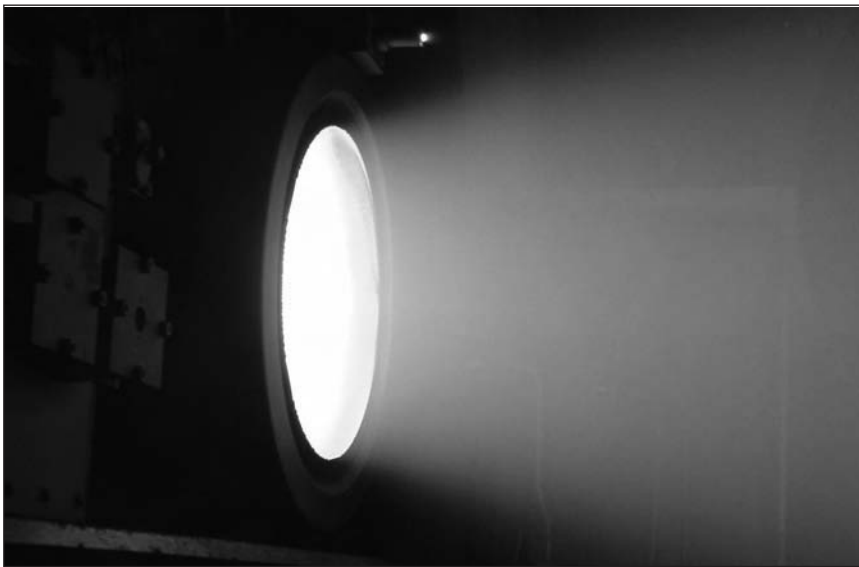
NASA's Evolutionary Xenon Thruster project

NASA's Evolutionary Xenon Thruster Broke World Record and Successfully Completed Environmental Qualification Testing

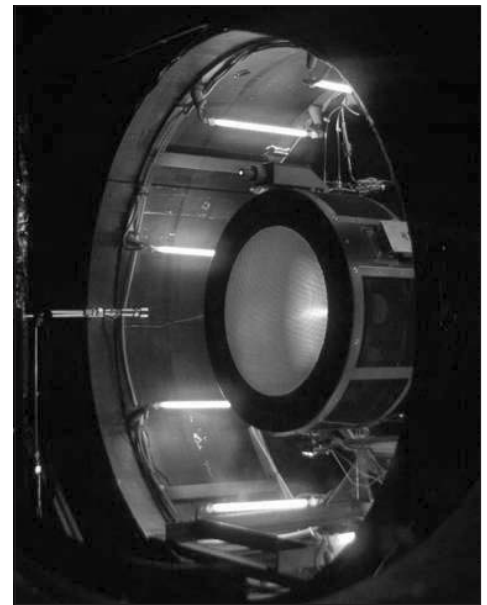
NASA's Evolutionary Xenon Thruster (NEXT) project is developing next-generation ion-propulsion technologies to provide future NASA science missions with enhanced mission performance at a low total development cost. The objective of the NEXT project is to advance next-generation ion-propulsion technology by producing engineering model system components, validating these through qualification-level and integrated system testing, and ensuring preparedness for transitioning to flight system development.

The NEXT system consists of a high-performance, 7-kW ion thruster; a modular, high-efficiency 7-kW power processor unit; a highly flexible advanced xenon propellant management system consisting of one high-pressure assembly per system and one low-pressure assembly per thruster; a lightweight engine gimbal; and key elements of a digital control interface unit including software algorithms. The NEXT thruster and other component technologies represent a significant advancement in technology beyond state-of-the-art NASA Solar Electric Propulsion Technology Application Readiness (NSTAR) thruster systems. NEXT performance exceeds single or multiple NSTAR thrusters over most of the thruster input power range. Higher efficiency and specific impulse and lower specific mass reduce the wet propulsion system mass and parts count. The NEXT thruster xenon propellant throughput is more than twice NSTAR's, so fewer thrusters are needed.

by an ion thruster in the history of space propulsion—exceeding the previous record demonstrated by the 30,000-hr life test of the Deep Space 1 spare flight thruster conducted at the Jet Propulsion Laboratory (JPL). The EM thruster performance has remained constant and nominal, and the wear rates of critical thruster components have been consistent with model predictions. The life test is scheduled to continue at full power until the 300-kg requirement is demonstrated, at which point the thruster will be power throttled to an intermediate level and continue operation. The xenon throughput requirement is 300 kg, with a 450-kg qualification level. The analysis-based capability of the thruster is estimated to be in excess of 730 kg.



NEXT EM thruster under life test at Glenn.



NEXT PM thruster undergoing thermal vacuum testing at JPL.

A NEXT engineering model (EM) thruster is undergoing long-duration life testing at the NASA Glenn Research Center at full power, having accumulated approximately 12,000 hr of operation and processing over 245 kg of xenon as of September 2007. In addition, the thruster had demonstrated over 10-million N-sec total impulse: the highest total impulse ever demonstrated

A NEXT prototype model (PM) thruster manufactured by Aerojet successfully completed acceptance testing at Glenn, and the performance was found to be consistent with that demonstrated from multiple EM thrusters. The PM thruster was subsequently subjected to a series of validation tests at JPL including thruster/gimbal functional tests, a thermal development test, and qualification-level environmental—vibration and thermal vacuum—tests. The thruster completed all qualification testing without issue, and the test results indicate that the thruster and gimbal designs will meet environmental requirements.

Bibliography

Patterson, M.; and Benson, S.: NEXT Ion Propulsion System Development Status and Performance. AIAA–2007–5199, 2007.

Hoskins, A., et al.: NEXT Ion Propulsion System Production Readiness. AIAA–2007–5856, 2007.

Find out more about this research:

NASA’s In-Space Propulsion Technology Program:

<http://www.inspacepropulsion.com>

Ion-propulsion research at Glenn:
<http://www.grc.nasa.gov/WWW/ion/>

Glenn Contacts:

Michael J. Patterson, 216–977–7481,
Michael.J.Patterson@nasa.gov

Scott W. Benson, 216–977–7085,
Scott.W.Benson@nasa.gov

Author:

Michael J. Patterson

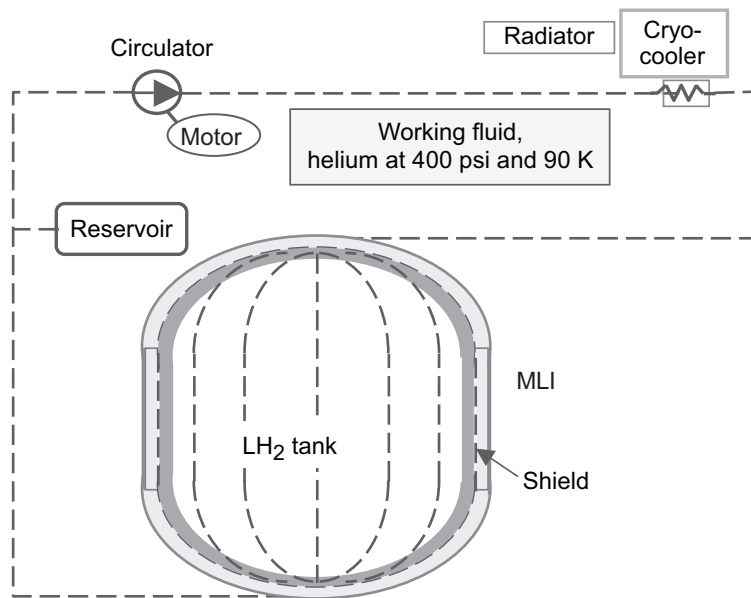
Headquarters Program Office:

Science Mission Directorate

Programs/Projects:

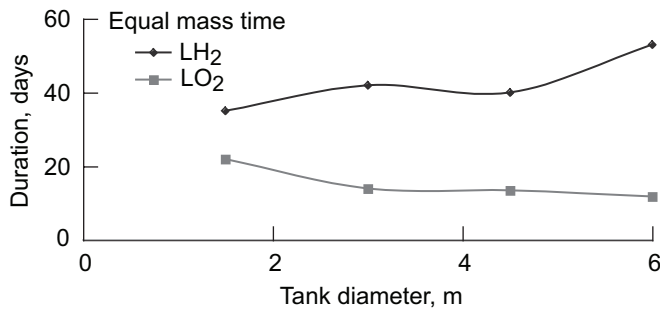
NASA’s Evolutionary Xenon Thruster project

Cryogenic Propellant Boiloff Reduction System Investigated



Cryogenic Boiloff Reduction System for a single LH₂ tank. The inner multilayer insulation (MLI) is shown with darker gray shading, and the MLI outside the shield is shown as the lighter gray shading outside of the darker gray. This figure is shown in color in the online version of this article (<http://www.grc.nasa.gov/WWW/RT/2007/PS-Prop/06-RPP-plachta.html>).

Lunar missions under consideration will benefit from incorporation of high-specific-impulse propellants such as liquid hydrogen and oxygen (LH₂ and LO₂), provided cryogenic propellant tank boiloff does not reduce payload excessively. Engineers at the NASA Glenn Research Center, with participation from colleagues at the NASA Ames Research Center, have investigated a method to reduce propellant tank boiloff on hydrogen tanks, using today’s technology, and eliminate boiloff on the LO₂ tank. This Cryogenic Boiloff Reduction System (CBRS) efficiently moves heat to the cryocooler over long distances via a compressed helium loop. The schematic shows that concept. The analyses and designs for this were incorporated into Glenn’s Cryogenic Analysis Tool. Parametric cases were developed for a range of tank diameters as a function of the days in storage. This analysis was done assuming a low-Earth-orbit environment. Analysis shows that, in



Estimate of the durations when projected passive and CBRS cryogenic storage mass are equal as a function of tank size. For durations longer than these, CBRS should be considered.

comparison to passive-only cryogenic storage, the boiloff reduction system begins to reduce system mass if durations are as low as 42 days for LH₂, and 14 days for LO₂. The graph shows curves for the equal mass times, when the passive and active system masses are projected to be equal.

In addition to mass savings, other important findings were discovered. The first is that the CBRS's cooling loops can be long and, as such, can cool all heat sources that enter the tank(s). This permits flexibility in locating the cryocoolers. The second significant development is that CBRS substantially reduces LH₂ boiloff and storage mass yet does not require flight LH₂ temperature cryocoolers, which have not been developed and would be expensive.

These research efforts are being done in support of the Cryogenic Fluid Management program in cooperation with the NASA Ames Research Center, NASA Marshall Space Flight Center, NASA Johnson Space Center, and NASA Goddard Space Flight Center.

Glenn Contacts:

Dave Plachta, 216-977-7126,
David.W.Plachta@nasa.gov

Sue Motil (manager of Cryogenic Fluid Management program), 216-433-8589,
Susan.M.Motil@nasa.gov

Author:

David W. Plachta

Headquarters Program Office:

Exploration Systems Mission Directorate

Programs/Projects:

Cryogenic Fluid Management program, lunar architectures, lunar lander descent and ascent modules, Earth Departure Stage, Mars mission architectures

Liquid-Oxygen/Methane Ignition Tested for Application in the Main Engines of the Lunar Surface Access Module



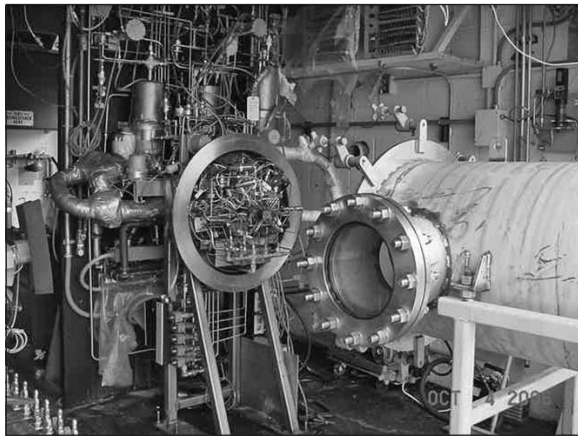
Successful test of LO₂/methane igniter at altitude in the ejector can.

The liquid-oxygen (LO₂)/methane propellant combination has been baselined for the Lunar Surface Access Module ascent engine main propulsion. The proposed switch from the hypergolic propellants used in the Apollo lunar ascent engine to LO₂/methane propellants requires the development of igniters capable of highly reliable performance in a lunar surface environment. A test program at the NASA Glenn Research Center utilized an in-house-designed LO₂/methane spark torch igniter (shown during an ignition test in this photograph).

The testing occurred in Glenn's Research Combustion Laboratory, utilizing its altitude simulation capability to simulate a space vacuum environment.

The next photograph shows the igniter installed on the altitude chamber bulkhead. The altitude was maintained by an air-driven ejector train capable of simulating 95,000 ft (10 torr, or 0.2 psia). A low-tension Unison spark plug (Unison Industries, LLC) was used to ignite the propellants. The spark plug was mounted in the center of the igniter and, for most tests, was flush with the top face of the igniter. A variable spark-energy (0.007 to 0.55 J) and spark-rate (to 196 sparks per second) Unison exciter was used to fire the spark-plug. Approximately 750 successful ignition tests were performed. Ignitions were obtained down to an igniter body temperature of approximately 260 °R with a 10-torr backpressure. Tests were performed to evaluate the effects of methane purity, igniter body temperature, spark energy level and frequency, mixture ratio, flow rate, and igniter geometry on the ability to obtain successful ignitions.

The data obtained from this ignition test program are also being used to anchor a computational-fluid-dynamics-based igniter model. The National Combustor Code (NCC, ref. 1)—a state-of-the-art computational tool that can solve time-dependent, Navier-Stokes equations with chemical reactions—was used to perform unsteady simulations of the ignition process in



Igniter mounted on the stand in Glenn's Research Combustion Laboratory with the ejector can pulled back.

Glenn's main engine igniter. The NCC is being developed primarily at Glenn to support combustion simulations for a wide range of applications and has been extensively validated and tested for low-speed chemically reacting flows. A finite-rate chemistry model was used to compute the species source-terms for Jet-A/air chemistry. The chemistry model incorporates nine species and seven chemical reaction steps. The model is based on the Sandia one-dimensional flame methane/air kinetics model, with the reactions involving nitrogen as a species removed. The results of three-dimensional, transient simulations of ignition and nonignition tests are shown in the contour plots.

Reference

1. Liu, Nan-Suey: Overview of the NCC. NASA/CP—2001-211141, 2001. Proceedings of the Tenth Thermal and Fluids Analysis Workshop, 2001. <http://ntrs.nasa.gov>

Glenn Contacts:

Kevin J. Breisacher, 216-977-7475,
Kevin.J.Breisacher@nasa.gov

ASRC Aerospace Corporation Contact:

Dr. Kumud Ajmani, 216-433-2671,
Kumud.Ajmani-1@nasa.gov

Authors:

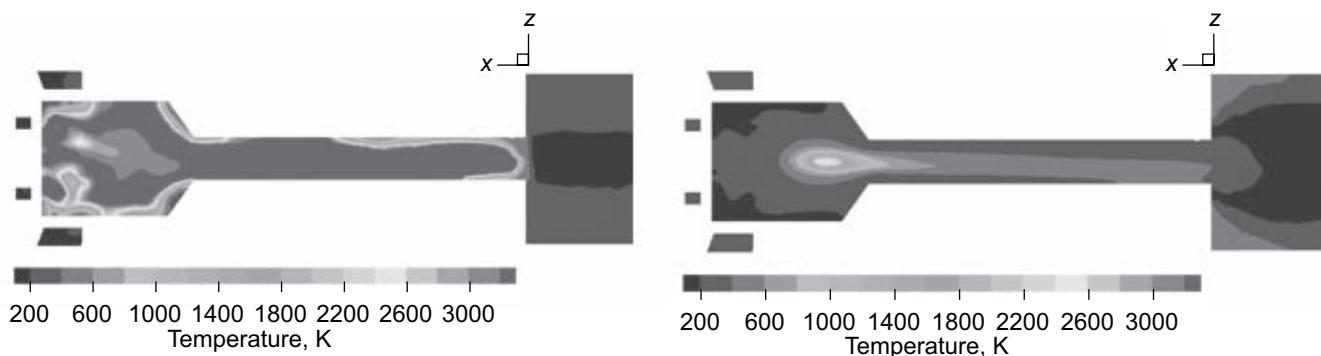
Kevin J. Breisacher and Dr. Kumud Ajmani

Headquarters Program Office:

Exploration Systems Mission Directorate

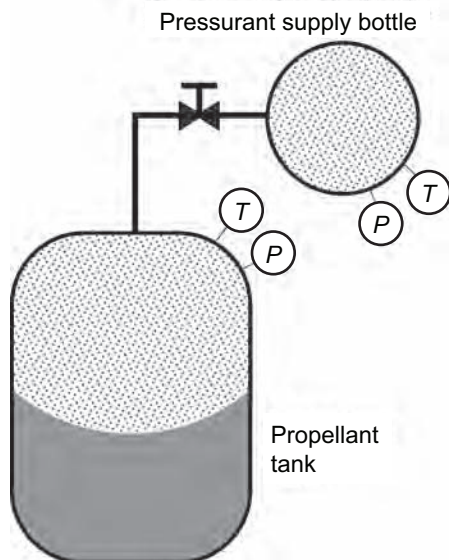
Programs/Projects:

Lunar Surface Ascent Module

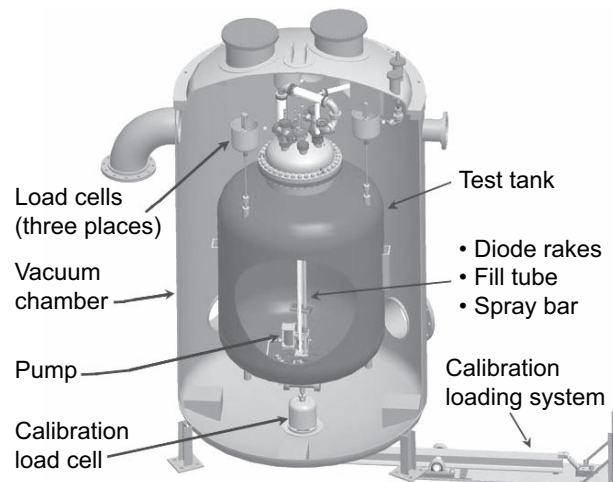


Temperature contour plots from computer modeling of ignition tests. A successful ignition test is on the left. This figure is shown in color in the online version of this article (<http://www.grc.nasa.gov/WWW/RT/2007/PS-Prop/07-RTB-breisacher.html>).

Low-Gravity Pressure-Volume-Temperature Gauging Concept Demonstrated With Liquid Oxygen



Basic PVT gauging hardware configuration with temperature, T, and pressure, P, instrumentation (liquid propellant is shown in a possible low-gravity orientation).



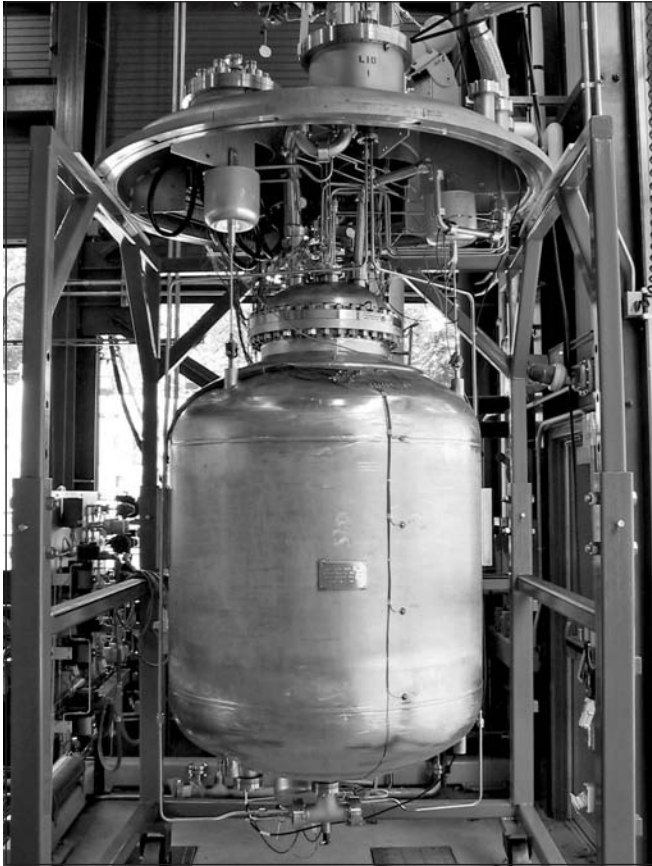
Cutaway of test tank suspended inside vacuum chamber.

The pressure-volume-temperature (PVT) method of liquid quantity gauging in low-gravity is based on calculations assuming conservation of pressurant gas within the propellant tank and the pressurant supply bottle (such as depicted in the diagram on the left). This method is currently used to gauge the remaining amounts of storable propellants onboard the space shuttle's orbital maneuvering system and on Earth-orbiting communications satellites. There is interest in applying this method to cryogenic propellant tanks since it requires minimal additional hardware or instrumentation. Consequently, a PVT gauging experiment with liquid oxygen was completed at the NASA Glenn Research Center using a large-scale cryogenic test tank with an attached cold, high-pressure helium supply bottle.

A noncondensable pressurant gas (helium) is required in order to use PVT with cryogenic fluids. With cryogenics, a significant amount of propellant vapor will be mixed with the pressurant gas in the tank ullage. This condition, along with a cryogenic propellant's high sensitivity of propellant vapor pressure to temperature, makes the PVT method susceptible to substantially greater measurement uncertainty than is the case with less volatile propellants. An uncertainty analysis applied to example cases of liquid oxygen tanks indicated that the PVT method will be feasible for liquid oxygen (ref. 1). A previous experiment with liquid nitrogen, which has properties similar to those of liquid oxygen, also demonstrated the feasibility of PVT gauging (ref. 2).

The liquid oxygen PVT gauging experiments were conducted with a 1.6-m³ liquid oxygen tank (shown in the diagram on the right and the photograph on

the next page) pressurized with helium in the normal-gravity environment. The helium supply tank was maintained at 160 °R with initial pressures up to 1650 psia. Gauging data were collected at tank fill levels from 90 to 10 percent and at nominal tank pressures of 0.3, 1.0, and 1.7 MPa. The test tank was equipped with a liquid pump and spray manifold to circulate and mix the fluid contents and therefore create near-isothermal conditions throughout the tank. Silicon diode sensors were distributed throughout the test tank and helium supply tank to monitor temperatures. The test tank was suspended from three load cells to obtain a high-accuracy reference measurement of liquid oxygen fill level. PVT gauging results agree with the reference load cell liquid-level measurements to within 2 percent. Further work is underway at Glenn to conduct similar PVT tests with liquid methane.



Liquid oxygen test tank suspended from vacuum chamber lid.

References

1. Van Dresar, Neil T.: An Uncertainty Analysis of the PVT Gauging Method Applied to Sub-Critical Cryogenic Propellant Tanks. *Cryog.*, vol. 44, 2004, pp. 515–523.
2. Van Dresar, Neil T.: PVT Gauging With Liquid Nitrogen. *Cryog.*, vol. 46, 2006, pp. 118–125.

Glenn Contacts:

Dr. Neil T. Van Dresar, 216–977–7533,
Neil.T.VanDresar@nasa.gov

Dr. Greg Zimmerli, 216–433–6577,
Greg.Zimmerli@nasa.gov

Michael L. Meyer, 216–977–7492,
Michael.L.Meyer@nasa.gov

Author:

Dr. Neil T. Van Dresar

Headquarters Program Office:

Exploration Systems Mission Directorate,
Exploration Technology Development
Program Office

Programs/Projects:

Exploration Technology Development
Program, Propulsion and Cryogenic
Advanced Development Program

Radiofrequency Tank Modes Tested at NASA Glenn To Gauge Liquid Oxygen and Liquid Methane

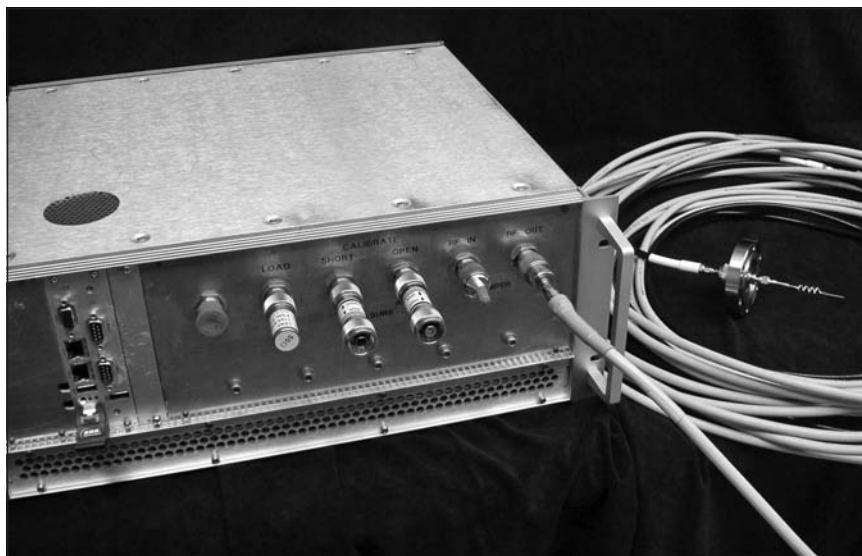
A novel method for gauging the amount of cryogenic propellant in a tank is being developed in-house at the NASA Glenn Research Center using radio-frequency (RF) waves. Metal tanks have resonant electromagnetic cavity modes that occur in the RF range (~100 MHz) for tanks approximately 1 m in diameter. When the tanks are loaded with a dielectric fluid (such as liquid oxygen, hydrogen, or methane), the resonant frequencies shift and the frequency shift can be used to gauge the amount of liquid in the tank (ref. 1). The technique has potential applications in gauging cryogenic propellant tanks for space exploration vehicles such as the Earth Departure Stage and the Lunar Surface Access Module. The RF-gauging method only requires an antenna internal to the tank, which is considerably smaller and lighter than other gauging hardware, such as capacitance probes. The RF-gauging technique also offers a potential solution to the problem of gauging propellants in low gravity, where the liquid configuration in the tank is unknown.

This past year, the technique was successfully tested in both liquid oxygen and liquid methane at Glenn's Creek Road Cryogenics Complex. The liquid methane tests were carried out using a small (6-ft³) tank, which rested upon a high-accuracy weight scale for reference measurements (see the illustration on the next page).

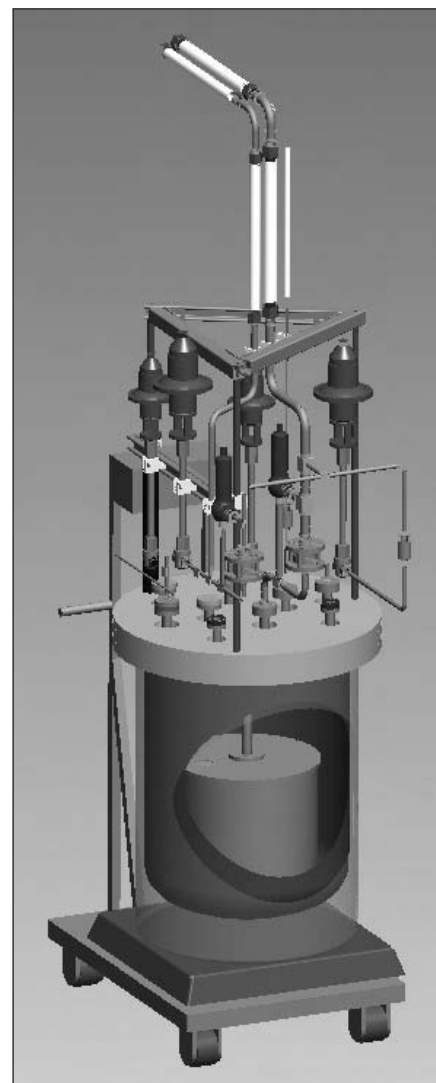
The methane testing also included RF-spectrum measurements in a 1.5-ft³ cylinder fully immersed in liquid methane. Measuring the cylinder spectrum when the cylinder was both empty and completely full of liquid methane allowed the dielectric constant of the fluid to be measured at various radio-frequencies, and this information was then used for computer simulations of the tank spectra at other fill levels.

The liquid methane tests utilized an RF engineering development unit (EDU) that was assembled in-house using commercial parts (see the photograph). The EDU was a first step toward producing a higher technology readiness level RF avionics unit, and it performed flawlessly during the methane test series.

Liquid oxygen testing of the RF mass gauge was conducted in a 58-ft³ test tank, in conjunction with another gauging technique known as the pressure-volume-temperature (PVT) method. This initial phase of RF tests in liquid oxygen was very successful, and after some calibration test runs were performed, the RF-gauging system demonstrated near-real-time gauging updates that typically agreed with the reference weighing system to within better than ± 1 -percent of the full-scale reading. We plan to develop the RF gauging technology further during the next year, with additional testing in liquid oxygen and liquid hydrogen.



RF-gauging EDU used for acquiring data during liquid methane testing. The EDU contains the RF-spectrum analyzer, a single-board computer, power supplies, and other RF electronics. Connected to the EDU is a long RF cable to which is attached a small antenna.



Cutaway view of the 6-ft³ tank used for RF-gauging tests in liquid methane. The tank lid had provisions for attaching a cylinder that could be completely immersed in the liquid methane to measure the index of refraction of the liquid at various RFs.

Authors:

Dr. Gregory A. Zimmerli, James D. Wagner, Michael D. Herlacher, Jeffrey C. Follo, and Karl R. Vaden

Headquarters Program Office:

Exploration Technology Development Program

Programs/Projects:

Propulsion and Cryogenic Advanced Development

Reference

1. Zimmerli, G.A., et al.: Radio Frequency Mass Gauging of Propellants. NASA/TM—2007-214907 (AIAA-2007-1198), 2007. <http://gltrs.grc.nasa.gov>

Glenn Contact:

Dr. Greg Zimmerli, 216-433-6577, Greg.Zimmerli@nasa.gov

New Lithium-Ion Batteries With Enhanced Safety and Power Density Evaluated for Future NASA and Aerospace Missions

Lithium-ion rechargeable battery technology is being developed by NASA to address future aerospace mission needs and requirements, with particular emphasis on inherent safety characteristics for crewed missions. In 2007, a NASA Innovative Partnership Program (IPP) seed fund provided the impetus to structure a unique relationship between two NASA centers and three industrial partners to develop and evaluate the performance of an alternative, high-rate, and inherently safe lithium-ion battery/cell chemistry and design and to assess its relevance for future NASA and commercial aerospace mission applications.

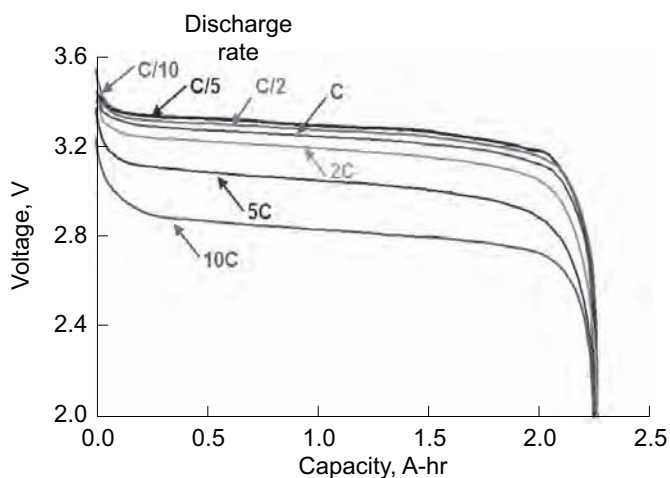
The ongoing IPP cost-shared project, which is supported by the NASA Exploration Systems Mission Directorate, is administered at the NASA Glenn Research Center. The five diverse team partners and stakeholders are providing unique expertise and facilities to address the technical tasks in a complementary manner. A123Systems (A123) is a manufacturer and provider of novel high-power battery/cell technology for the commercial marketplace. ABSL Space Products has pioneered the use of small, commercial-off-the-shelf (COTS) lithium-ion cells for space applications, and they have flight proven the use of such conventional cells in their modular battery design architecture. Northrop Grumman Space Technology is balancing the project team as a technology integrator and user of space systems products. Glenn and the Jet Propulsion Laboratory (JPL) are providing technical support and facilities for test and development tasks. The formal relationships between NASA and the industrial partners were implemented through Space Act Agreements.

The primary objectives of the project are to assess both the electrochemical and safety performance of the A123 COTS baseline cells in both generic and NASA mission-relevant test conditions, and to forecast the viability of such cells in space-qualified battery hardware. A123 provided their commercial cell hardware to all participants for baseline performance evaluations. The

A123 commercial batteries/cells employ an inherently safer and higher-power cell chemistry, which is based on a lithium iron phosphate cathode material, in contrast to most conventional, lithium-ion batteries, which contain oxide-based cathode materials. Also, the A123 cell design does not include inherent safety devices found in conventional batteries. ABSL Space Products is using their proven test methodologies to provide and assess data relevant to the future utilization of the high-power COTS cells in their flight-battery hardware. Northrop Grumman Space Technology is providing test data for and assessments of A123 cells relative to long-term satellite and other aerospace mission applications. Within the NASA framework, JPL and Glenn with support from the NASA Johnson Space Center are providing complementary battery/cell performance data, such as rate capabilities at various temperatures, fast recharge capability, cycle life stability, thermal characteristics, and abuse tolerance.

In addition to assessing the performance of baseline high-power cells and multicell modules, the NASA centers made performance enhancements to the A123 baseline cell chemistry with respect to low-temperature performance and high-temperature resilience for enhanced safety, and these enhancements continue to be assessed. Advanced cell electrolytes developed by JPL have been incorporated into the A123 cell design, and such cells are undergoing extensive characterization testing. The plot shows the performance of the A123 cells as a function of discharge rate.

The successful completion of the IPP effort will afford a higher level of technology readiness for utilizing high-power battery chemistries in aerospace missions, and it will impact energy storage



A123 cell discharge performance at 20 °C as a function of discharge rate.

technology selections for human-rated NASA Constellation Systems and other relevant missions. In addition, the program has successfully cultivated mutually beneficial relationships between the team's industrial partners, which will ultimately result in reduced systems-level cost and reduced times for technology maturation.

Find out more about the research of Glenn's Electrochemistry Branch:

<http://grc.nasa.gov/WWW/Electrochemistry/>

Glenn Contact:

Dr. Richard S. Baldwin, 216-433-6156, Richard.S.Baldwin@nasa.gov

JPL Contact:

Dr. Ratnakumar V. Bugga, 818-354-0110, Ratnakumar.V.Bugga@nasa.gov

Authors:

Dr. Richard S. Baldwin, William R. Bennett, Dr. Ratnakumar V. Bugga, Gary A. Horsham, Concha M. Reid, and Dr. Marshall C. Smart

Headquarters Program Offices:

Exploration Systems Mission Directorate, Innovative Partnership Program Office

Programs/Projects:

Exploration Technology Development Program, Energy Storage Project

Lithium-Ion Battery Demonstrated for NASA Desert Research and Technology Studies

Lithium-ion batteries have attractive performance characteristics that are well suited to a number of NASA applications. These rechargeable batteries produce compact, lightweight energy-storage systems with excellent cycle life, high charge/discharge efficiency, and low self-discharge rate. NASA Glenn Research Center's Electrochemistry Branch designed and produced five lithium-ion battery packs configured to power the liquid-air backpack (LAB) on spacesuit simulators. The demonstration batteries incorporated advanced, NASA-developed electrolytes with enhanced low-temperature performance characteristics. The objectives of this effort were to (1) demonstrate practical battery performance under field-test conditions and (2) supply laboratory performance data under controlled laboratory conditions. Advanced electrolyte development is being conducted under the Exploration Technology Development Program by the NASA Jet Propulsion Laboratory.

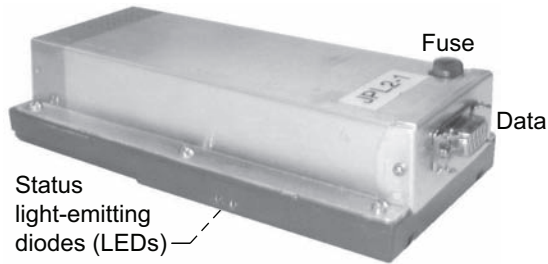
Field trials were completed at the 2007 NASA Desert Research and Technology Studies (Desert RATS) outings at Cinder Lake, Flagstaff, Arizona. Desert RATS is a NASA-led team of research partners involved in developing technologies applicable to the human exploration of a planetary surface (the Moon and Mars). Individual teams work throughout the year on promising new technologies that are candidates for demonstration at the outing. The demonstration batteries produced at Glenn powered the LAB cooling system as well as two secondary loads. The nominal power level was approximately 18 W, with a maximum of 31 W. In previous work, a commercial camcorder battery powered the LAB.

Demonstration batteries used four lightweight, 4.5-A-hr pouch cells, connected in series. The pouch cells, manufactured by Quallion LLC, were based on a product developed for the U.S. Army's Communications-Electronics Research, Development and Engineering Center under



NASA Desert RATS battery installed on a spacesuit LAB.

the Ultra Safe High Energy Density Rechargeable Soldier Battery Program (Contract No. W15P7T-05-C-P212). Cells were prepared using two NASA-developed electrolyte formulations. Control cells, prepared with Quallion electrolyte, were included as a control.



NASA demonstration lithium-ion battery.

The Desert RATS demonstration batteries were completed between May and September 2007. Design features included internal protection against over-current, over-discharge, and over-temperature. Controls for charging were external to the battery. Two prototype batteries were tested in Desert RATS dry-run activities at the Johnson Space Center from August 13 to 17, 2007. These trials verified fit and function with the Desert RATS spacesuits and helped identify areas of improvement for the batteries and support equipment. In laboratory testing at room temperature, the 500-gram Desert RATS batteries produced 66 W-hr, sustaining a constant power output of 38.6 W over 103 min of discharge time. This corresponds to a specific energy of 130 W-hr/kg, which represented a 24-percent improvement over the commercial camcorder battery.

Three field trials were successfully completed at Cinder Lake from September 10 to 12, 2007. Extravehicular activities of up to 1 hr and 50 min were supported, with residual battery capacity sufficient for 30 min of additional

run time. Additional laboratory testing of batteries and cells is underway at Glenn's Electrochemistry Branch.

Find out more about the research of Glenn's Electrochemistry Branch:

<http://www.grc.nasa.gov/WWW/Electrochemistry/>

ASRC Aerospace Corporation Contact:

William R. Bennett, 216-433-2486,
William.R.Bennett@nasa.gov

Glenn Contact:

Dr. Richard S. Baldwin, 216-433-6156,
Richard.S.Baldwin@nasa.gov

Authors:

William R. Bennett and
Dr. Richard S. Baldwin

Headquarters Program Office:

Exploration Systems Mission Directorate

Programs/Projects:

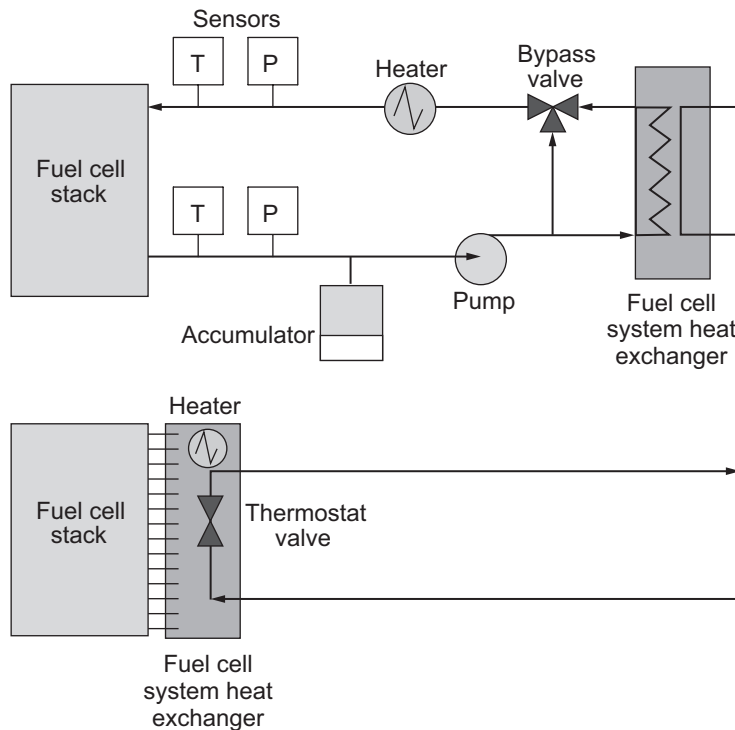
Exploration Technology Development
Program, Energy Storage Project

Passive Cooling Plates Studied for Fuel Cells

The required characteristics of passive cooling plates for fuel cells were analyzed at the NASA Glenn Research Center. Fuel cells are typically cooled using a liquid coolant that is circulated through coolant cavities that are adjacent to each cell in a fuel cell stack. These coolant cavities must be sealed to prevent leakage between the coolant cavities and the hydrogen and oxygen cavities, as well as any leakage external to the fuel cell stack. In addition to the components inside the fuel cell stack, this approach to fuel cell cooling requires valves, a coolant pump, and external plumbing to circulate the coolant; a coolant accumulator to account for the volumetric expansion and contraction of the coolant during operation; sensors to monitor and control the cooling process; and the associated electronics for both power and control. Ideally, if the fuel cell stack temperature and heat removal could be controlled passively by highly thermally conductive plates, there would be a significant reduction in overall fuel cell system mass and complexity. Without the need to seal a coolant inside the cell stack, the number of fluidic seals

could be substantially reduced, improving the reliability of the fuel cell stack fluidic integrity.

The cooling studies revealed that for small- to moderate-size fuel cells ($\leq 225 \text{ cm}^2$ in active area) cooling plates of less than a millimeter in thickness could be used if the thermal conductivity of the plates was 800 W/m/K or greater. Although this thermal conductivity is about twice that of copper, there are materials that have thermal conductivities greater than 1000 W/m/K that could potentially be used.



Top: Conventional fuel cell with pumped-loop thermal management.
Bottom: Fuel cell with passive thermal management.

Future work in this area is planned to test advanced thermally conductive materials for potential use as cooling plates inside fuel cell stacks and to construct sample cooling plates for incorporation into fuel cell stacks to demonstrate the feasibility of the new technology.

Glenn Contact:

Kenneth A. Burke, 216-433-8308,
Kenneth.A.Burke@nasa.gov

Analex Corporation Contact:

Tony Colozza, 216-433-5293,
Anthony.J.Colozza@nasa.gov

Authors:

Anthony J. Colozza and Kenneth A. Burke

Headquarters Program Office:

Exploration Technology Development
Program

Programs/Projects:

Lunar Lander, Lunar Rover, and other lunar
surface power systems

Passive Water Separator Developed for Fuel Cells

A separator that passively removes liquid water from a fuel cell flowing gas was developed at the NASA Glenn Research Center. Excess oxygen typically flows through a fuel cell and sweeps the water that is produced inside the fuel cell out of the fuel cell. The resultant oxygen/liquid-water mixture is typically separated into oxygen (which is recycled into the fuel cell) and liquid water (which is discharged from the fuel cell system to prevent the fuel cell from flooding). The passive water separator removes the water without the use of rotating components or other power-consuming components, and it can be easily incorporated into the fuel cell stack. The size of the passive water separator can be adjusted easily to match the gas-flow and water-removal requirements of the fuel cell.

Devices currently used to perform this type of water separation use electricity to power a rotating component that spins the denser water out of the lighter oxygen phase. These types of devices—besides consuming electrical power—are heavy, are susceptible to mechanical failure, and are not easily scaled in size to meet the requirements of different size fuel cells. Other devices use a cyclonic flow path to impart acceleration to the two-phase mixture, but these devices are limited because they require a minimum flow

velocity and are not easily scaled in size. Still other separator devices use porous media components that are flow restrictive either for the water penetrating through the porous media, or the oxygen flowing past the porous media, or both. These porous media devices also are not easily scaled in size to match the requirements of different size fuel cells.

The innovations of the passive water separator follow:

- (1) It uses a highly hydrophilic, polyether-sulfone membrane that is lightweight and easily transmits water through the membrane, yet has a high resistance to gas flow going through the thickness of the membrane.

- (2) It uses a highly absorbent, wicking material around the walls of the oxygen flow path that absorbs the water and assists in transmitting it to the surface of the separating membrane. This permits the oxygen flow path opening to be large, which results in a low overall oxygen flow resistance past the membrane.
- (3) It has the overall geometry of the cells within the fuel cell stack, which allows the water separator to be incorporated into the fuel cell stack as the “last cell.” Thus, the water separator can be very easily incorporated into the fuel cell system, and it can be easily scaled in size by stacking additional separators in parallel.
- (4) It uses no electricity or moving parts and, therefore, is highly reliable.

Glenn Contacts:

Kenneth A. Burke, 216–433–8308, Kenneth.A.Burke@nasa.gov
 Mark A. Hoberecht, 216–433–5362, Mark.A.Hoberecht@nasa.gov

Author:
 Kenneth A. Burke

LEW Number:
 LEW–18304–1

Headquarters Program Office:
 Exploration Technology Development Program

Programs/Projects:
 Lunar Lander, Lunar Rover, other lunar surface power systems

Battery Systems for Extravehicular Activities Studied

A new generation of spacesuits is needed to support extravehicular activities (EVAs) for future surface exploration missions. These new suits will require improved functionality and reliability, decreased mass and volume, and lower operating cost in comparison to current in-space suits. Although the power subsystem requirements are still being defined, tradeoff studies have shown that the next-generation surface suit will require more power than today’s suit. A significant component of the power system will be the battery, which will provide an energy source for life-support functions, communications, system health status, and other needs. The battery must be capable of operating safely in the harsh environments of space by tolerating radiation, dust, and large temperature variations.

The NASA Glenn Research Center is supporting the battery definition and development activity for the next-generation spacesuit under the Constellation Program’s EVA Systems Project, which is being led by the NASA Johnson Space Center. To date, a series of system studies have been completed to assess the feasibility of various operational scenarios using preliminary power requirements. The first of these studies evaluated the feasibility of using solar power to augment the energy-storage system on the suit. The study showed that while solar augmentation can provide a power system mass savings up to 10 percent for a lunar suit, significant issues would discourage its use, including terrain and mission site variations and complexity.

A second study evaluated the benefits of distributing the power system/energy storage throughout the suit to specific sites instead of centralizing the energy-storage system and distributing the power through the suit with cables. The study

concluded that only small total-power-system mass benefits (<11 percent) would be possible with localized power systems. A centralized power system/energy-storage system with power distribution cables was determined to be the best option for a combined metric of total power system mass, hand/foot volume and mass, and logistics.

Lastly, a study was conducted to identify power subsystem options that would minimize the mass of the lunar surface EVA suit Portable Life Support System (PLSS) and EVA PLSS support equipment. Options considered were the use of one 8-hr energy-storage system on the PLSS or the use of one 4-hr energy-storage system that would be recharged or replaced during the EVA. The results of this study suggest that, if possible, a single 8-hr energy-storage system would be the lightest mass option, followed by the replacement option, and finally the recharge option.

Future work will involve defining detailed power requirements and a power profile for a nominal EVA mission. Candidate battery technologies will be identified and evaluated against the specific mission requirements and technology development needs that have been identified. A baseline battery technology will be selected leading to the development of a conceptual battery design.

Find out more about the research of Glenn's Electrochemistry Branch:

<http://www.grc.nasa.gov/WWW/Electrochemistry/>

Glenn Contacts:

Lisa L. Kohout, 216-433-8004, Lisa.L.Kohout@nasa.gov

Michelle A. Manzo, 216-433-5261, Michelle.A.Manzo@nasa.gov

Authors:

Lisa L. Kohout and H. James Fincannon

Headquarters Program Office:

Exploration Systems Mission Directorate

Programs/Projects:

Extravehicular Activity Systems Project

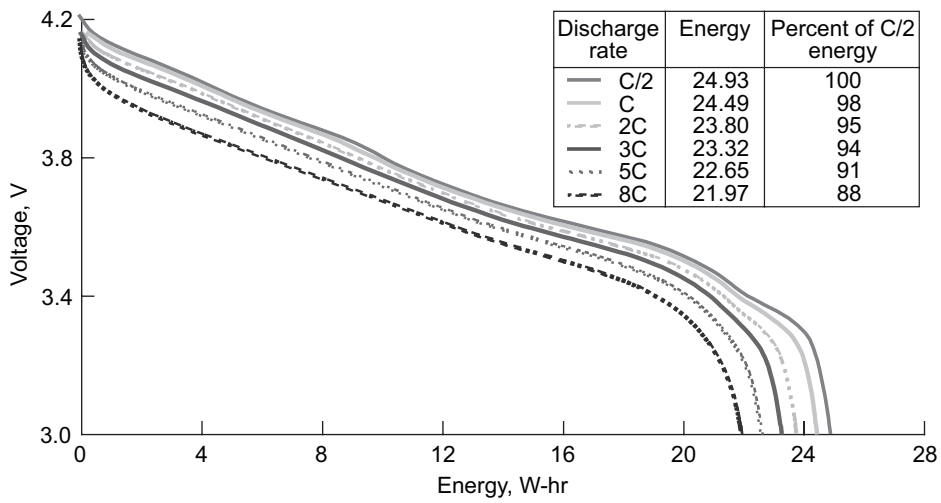
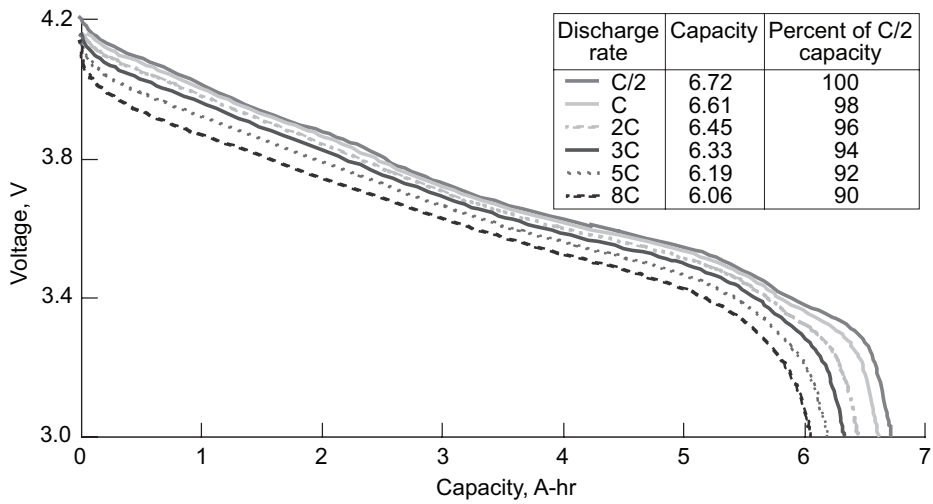
Lithium-Based Battery Performance Evaluated for NASA's Exploration Missions

NASA's upcoming space exploration missions will require safe, human-rated energy-storage systems that are optimized for operation in space and on the lunar and martian surfaces. Lithium-ion batteries are baselined for many of these missions because of the mass, volume, operating temperature, and ground operation advantages the chemistry offers over heritage aerospace battery chemistries. In fiscal year 2007, cell and battery performance evaluations were conducted at the NASA Glenn Research Center in support of future lunar surface operations addressed by the Exploration Technology Development Program (ETDP) Energy Storage Project (refs. 1 to 3) and the Ares I Crew Launch Vehicle electrical power system development.

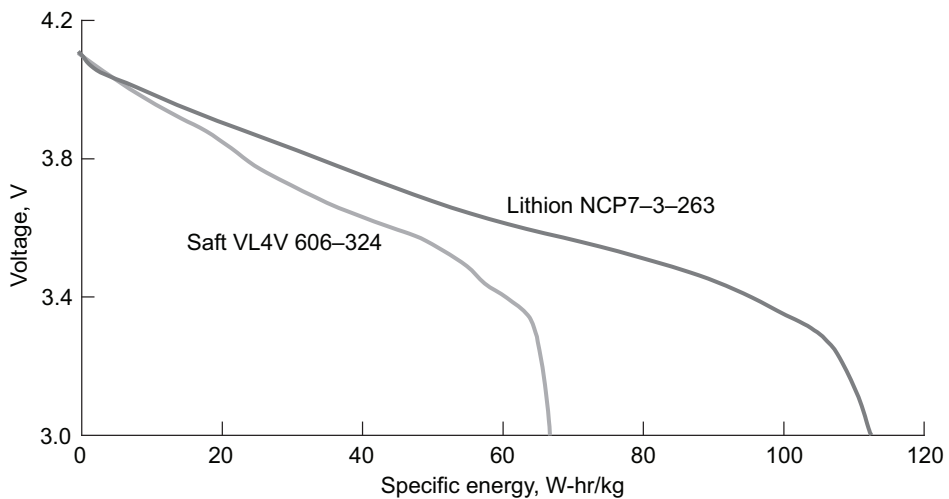
Future space exploration energy-storage needs span a wide range of requirements. Testing and demonstration of candidate cells provided an assessment of the state of current technologies to meet these varying requirements. A general performance characterization database for cells and batteries was generated at Glenn to quantify the performance of cells and batteries to specific mission profiles, assist in the development of requirements for mission battery systems and vehicle designs, evaluate and verify cell and battery technology developments made through internal NASA development projects (i.e., ETDP), and enable the determination of gaps in the ability of current technologies to meet future needs so that research investments are more focused.

Chemistries that were evaluated include lithium-ion cells with traditional mixed-metal cathodes; cells with newer, lithium iron phosphate cathodes; and lithium-sulfur cells, a developmental chemistry at a low technology readiness level. Each of these technologies demonstrated particular advantages that could address certain needs of customers—such as an ultralight system, a high-power system, a safer system, or an established aerospace design that provided good overall performance. Representative results of the testing performed on the Saft VL4V, 6-A-hr lithium-ion cell are shown in the top two graphs on the next page.

The Saft VL4V cell, optimized to provide high-rate capability, demonstrated excellent capability to discharge at high currents while delivering most of its rated capacity and energy. Greater than 90 percent of the C/2 capacity and greater than 88 percent of the C/2 energy were delivered at discharge rates as high as 8C. However, the specific energy of high-rate cells is typically sacrificed because of internal design features that are necessary to provide their high-rate capability. The bottom graph on the next page compares the specific energy of two cells, a Saft VL4V cell and a Lithion NCP7-3 7-A-hr nameplate cell, a cell that is optimized to deliver high specific energy. When operated at 20 °C at a C/5 discharge rate, the Saft cell delivered 67 W-hr/kg, whereas the Lithion cell delivered 113 W-hr/kg.



Capacity and energy at different discharge rates at 20 °C for Saft VL4V cell 606-28. Charged at C/2 to 4.2 V; taper limit, C/50; discharged to 3.0 V. Top: Capacity. Bottom: Energy.



Voltage versus specific energy at 20 °C for Saft and Lithion cells. Charged at C/8 to 4.1 V; taper limit, C/50; discharged at C/5 to 3.0 V.

References

1. Bennett, William R.; and Baldwin, Richard S.: Lithium-Ion Battery Demonstrated for NASA Desert Research and Technology Studies. Research & Technology 2007. NASA/TM—2007-215054, 2007, pp. 35–36. <http://www.grc.nasa.gov/WWW/RT/2007/PS-Prop/11-RPC-bennett.html>
2. Britton, Doris L.; Miller, Thomas B.; and Bennett, William R.: Thermal Characterization Study of Lithium-Ion Cells. 10th Electrochemical Power Sources Symposium, Williamsburg, VA, 2007. <http://ntrs.nasa.gov>
3. Reid, Concha M.: Lithium Iron Phosphate Cell Performance Evaluations for Lunar Extravehicular Activities. 10th Electrochemical Power Sources Symposium, Williamsburg, VA, 2007. <http://ntrs.nasa.gov>

Find out more about the research of Glenn's Electrochemistry Branch:
<http://www.grc.nasa.gov/WWW/Electrochemistry/>

Glenn Contacts:

Concha M. Reid, 216–433–8943,
 Concha.M.Reid@nasa.gov
 Thomas B. Miller, 216–433–6300,
 Thomas.B.Miller@nasa.gov

Author:

Concha M. Reid

Headquarters Program Office:

Exploration Systems Mission Directorate

Programs/Projects:

Exploration Technology Development
 Program, Crew Launch Vehicle Upper
 Stage Avionics

International Space Station and Constellation Lithium-Ion Battery Commonality Trade Study Performed

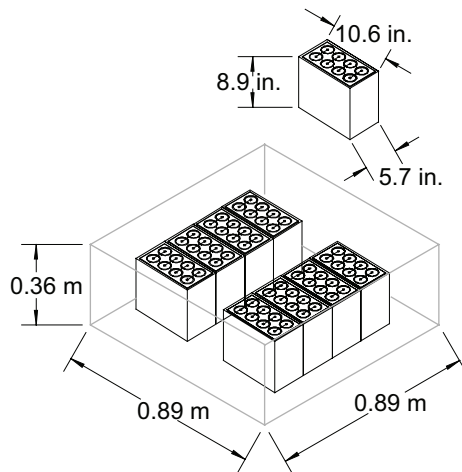
The *International Space Station* (ISS) presently uses nickel-hydrogen batteries to supply power during the eclipse (or dark) phase of its orbit. Once all four of the photovoltaic modules are deployed on-orbit in 2009, the ISS will have 24 batteries consisting of 48 battery Orbital Replacement Units (ORUs). The current program has enough spare nickel-hydrogen battery ORUs to last to the end of the mission in 2015. If the ISS mission is extended beyond 2015, additional spare batteries will be needed to replace those battery ORUs already on-orbit. Because of obsolescence concerns, any such future spares will contain lithium-ion cells instead of the current nickel-hydrogen cells.

In order to save on battery development costs, the ISS is looking to the Constellation Program for potential collaboration. The NASA Glenn Research Center was tasked by the ISS Program to perform a trade study to determine if a common ISS/Constellation lithium-ion battery module is feasible.

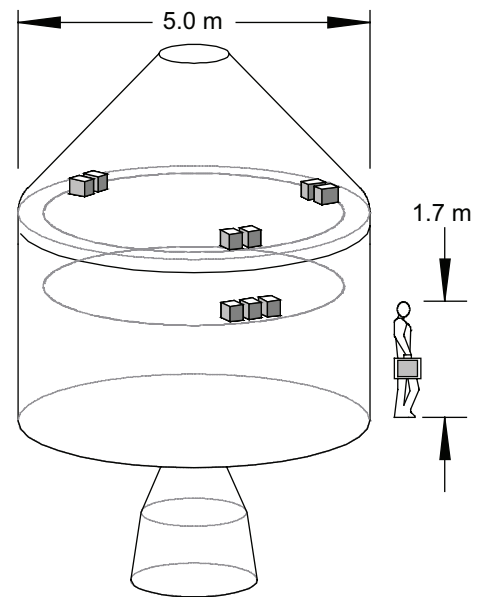
Since the ISS battery ORUs must interface with the existing electric power system, new lithium-ion battery ORUs will conform to the same physical size and power requirements. All of these requirements are well defined and were available for the trade study. At the time of the study, the Constellation battery requirements were not quite as firm, so the best estimates of the requirements were used in the study. After examining the requirements for the Crew Exploration Vehicle (CEV) and the Crew Launch Vehicle (CLV), we determined that the battery needed for the CLV was not common to either the CEV or ISS because of the lower energy and higher discharge rate requirements. Lander and rover batteries were not included in the study because their requirements were not known.

For the trade study, we examined battery requirements such as nominal battery voltage, discharge and charge times, total cycles, average power (watts), and delivered watt-hours for each orbit or mission phase. The ISS is in a low Earth orbit, whereas the CEV will have several mission phases—low Earth orbit, low lunar orbit, launch/orbit once around, and ISS docked—each with different power requirements. For each of these phases, battery depth of discharge, total energy (watt-hours), current (amperes), capacity (ampere-hours), and discharge rates were calculated from the requirements.

The CEV power bus will be designed to operate from 26 to 36 V. A lithium-ion cell operates from ~3.0 to 4.2 V, thus an eight-cell series string module for the CEV meets the voltage limits (24 to 32.8 V). The ISS battery charge/discharge unit can operate from 76 to 131 V, so four of the eight-series string modules are needed in series.



Conceptual CEV distributed battery with nine common modules.



Conceptual layout of ISS battery ORU using eight common lithium-ion battery modules.

The driver for the CEV battery capacity became the high depth of discharge—75 percent per total power (12.6 kW-hr)—needed during the launch/orbit once-around phase. The total capacity required is 451 A-hr. Since there are nine batteries in parallel on the CEV, an approximately 50-A-hr battery cell will be needed (see the figure on the left). The ISS would require 102 A-hr, or two of the CEV-size cells in parallel.

The ideal ISS lithium-ion battery would consist of a 30 series string of 102-A-hr lithium-ion cells. However, the lithium-ion cell has such a weight/size advantage over the current nickel-hydrogen technology, that even using four series, two parallel 28-V, 50-A-hr CEV modules would result in a battery that was half the size of the existing battery. Instead of two ORUs per battery, as is the case for the nickel-hydrogen, the new lithium-ion battery would provide the same watt-hours in one ORU box (see the figure on the right). The trade study concluded that the lithium-ion common module concept was highly feasible for the ISS and Constellation Programs.

Find out more about this research:

Glenn's Electrochemistry Branch: <http://www.grc.nasa.gov/WWW/Electrochemistry/>

Glenn Contacts:

Penni J. Dalton, 216-433-5223,
Penni.J.Dalton@nasa.gov

Michelle A. Manzo, 216-433-5261,
Michelle.A.Manzo@nasa.gov

Author:

Penni J. Dalton

Headquarters Program Office:

Space Operations Mission Directorate

Programs/Projects:

International Space Station

Masterless Charge-Control Scheme Developed and Validated for a Modular Lithium-Ion Battery

Lithium-ion battery chemistry is being considered seriously for unmanned and manned space missions in the near future. A primary reason for this consideration is the higher energy density lithium-ion batteries in comparison to other rechargeable batteries, such as nickel metal-hydride and silver zinc. The nominal voltage of a cobalt-based lithium-ion cell is 3.6 V, with a charge voltage limit of 4.2 V. Other lithium-ion chemistries, such as manganese-based or nickel-cobalt manganese-based, have similar voltage specifications. In 28-V bus applications (or higher), multiple cells must be stacked in series, and if all the cells in the stack are not closely matched, the cells must be balanced to obtain maximum performance from the battery.

The current state-of-the-art in digital cell balancing uses a single controller (e.g., Digital Signal Processor) for the entire battery stack. The obvious problem with this approach is that the cell balancing controller is not fault tolerant. This was addressed in this research and development effort at the NASA Glenn Research Center through a grant with Cleveland State University using individual digital charge controllers for each cell and “linking” the controllers to each other via a masterless communication bus. Each cell’s charge controller monitors critical parameters of the cell (e.g., voltage, temperature, and current), and some monitor the overall battery voltage, resulting in a redundant system. For cell balancing and state-of-charge estimation, relevant parameters are relayed to the other cells in a masterless fashion.

This masterless charge-control scheme was validated with a 28-V, 60-A-hr battery (see the photograph). All eight cells remained within a small programmed voltage range of each other. In this case, a dissipative cell-balancing approach was taken, but the scheme is equally applicable to nondissipative cell-balancing techniques.

Cleveland State University Contact:

Marcelo C. Gonzalez, 216-433-8408,
Marcelo.C.Gonzalez@nasa.gov

Glenn Contact:

Robert M. Button, 216-433-8010,
Robert.M.Button@nasa.gov

Authors:

Marcelo C. Gonzalez and Robert M. Button

LEW number:

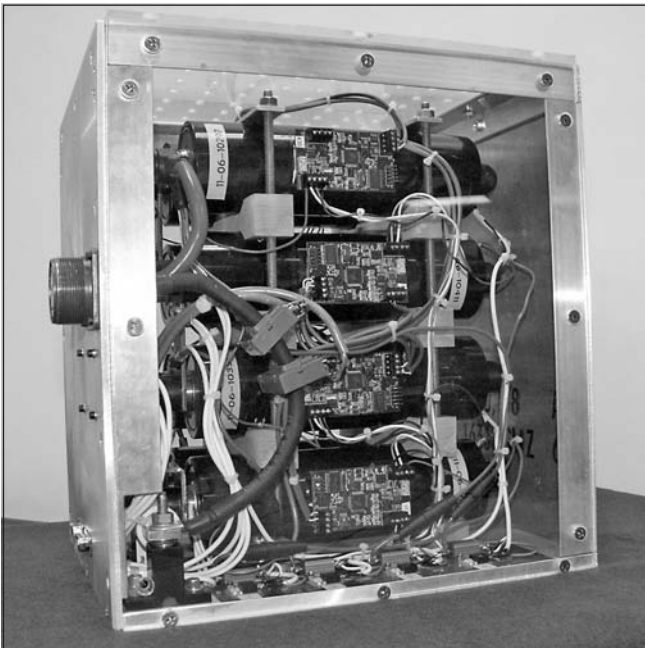
LEW-18297-1

Headquarters Program Office:

Exploration Systems Mission Directorate

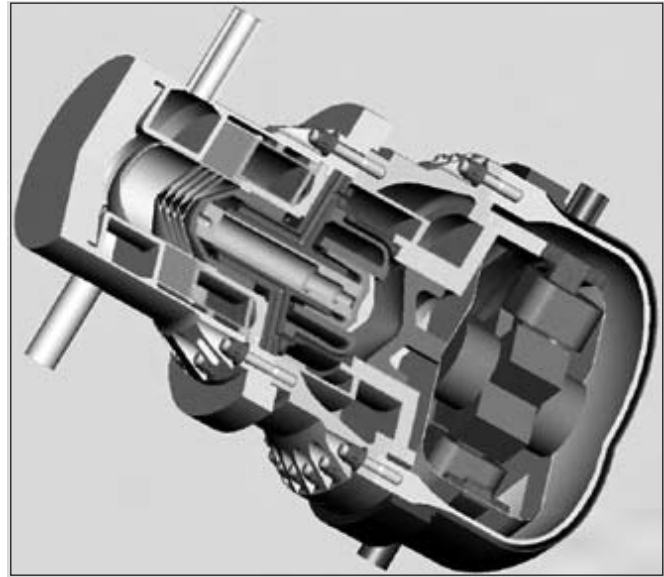
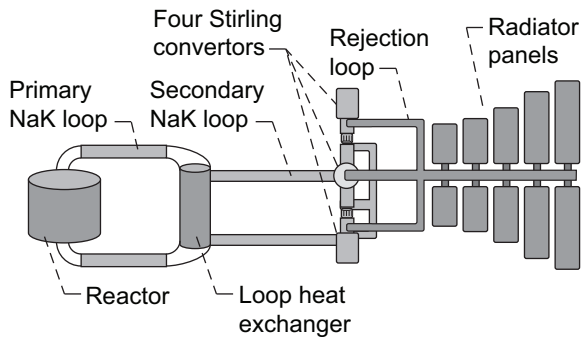
Programs/Projects:

Constellation Test and Verification,
Crew Exploration Vehicle



28-V, 60-A-hr lithium ion battery.

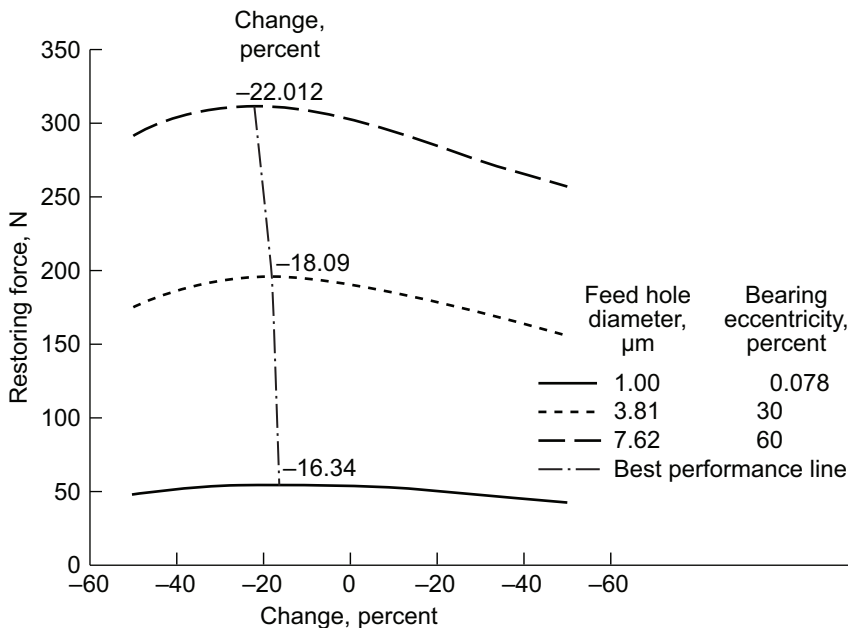
Approach Developed for Optimizing Stirling Gas Bearing Performance



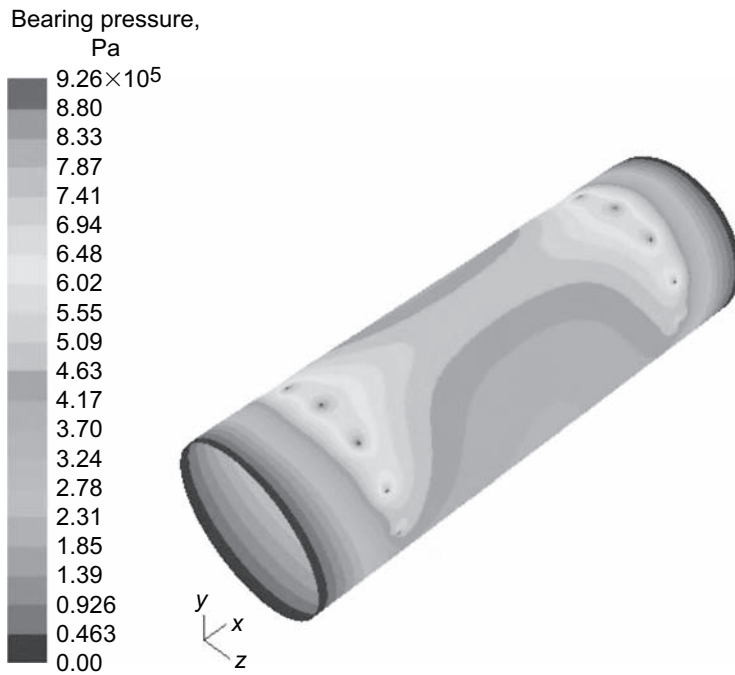
Left: Notional layout of sodium-potassium- (NaK-) heated Stirling converter. Right: Five-kilowatt Stirling converter closeup.

NASA researchers anticipate that future Moon and Mars surface missions will require a nuclear-reactor-heated high-power Stirling converter to provide reliable power for long-duration colony operations. The notional design layout (on the left) shows the Stirling converter being heated in space via a liquid-metal-cooled (NaK-cooled) reactor. A closeup of a proposed 5-kW Stirling converter is shown in the illustration on the right. The converter is designed to operate with a linearly oscillating aerostatic gas bearing to allow for non-contact, greaseless, long-term operation in space.

An approach was recently developed at the NASA Glenn Research Center for optimizing the design of these bearings, in which the ideal feeder channel holes are determined at various bearing eccentricities. In this case, a reduction approximating 20 percent produces the best performance over the entire range (see the graph and the figure on the next page). Analyses such as these reduce the risk associated with designing Stirling converters.



Optimal bearing design.



Linearly oscillating bearing pressure distribution. This figure is shown in color in the online version of this article (<http://www.grc.nasa.gov/WWW/RT/2007/PS-Prop/18-RPT-dyson.html>).

Find out more about the research of Glenn's Thermo-Mechanical Systems Branch:

<http://www.grc.nasa.gov/WWW/TECB/>

Glenn Contact:

Dr. Rodger Dyson, 216-433-9083,
Rodger.W.Dyson@nasa.gov

Author:

Dr. Rodger W. Dyson

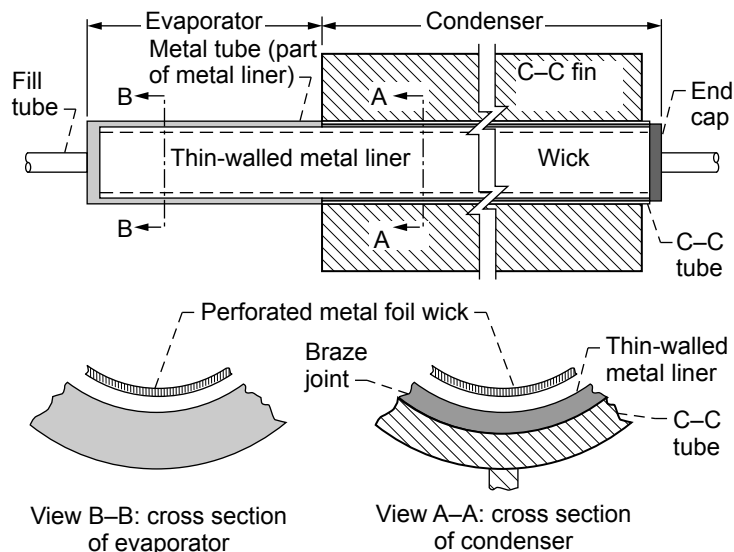
Headquarters Program Office:

Exploration Systems Mission Directorate

Programs/Projects:

Fission Surface Power Systems Project

Carbon-Carbon Heat Pipe With Integral Fins and Potassium Working Fluid Designed, Fabricated, and Tested



Longitudinal and transverse sections of carbon-carbon heat pipe. (Cross sections are not to scale.)

As shown in the diagrams, this elemental space radiator heat pipe, designed at the NASA Glenn Research Center and fabricated under contract to operate in the 700- to 875-K temperature range, consists of a carbon-carbon (C-C, graphite-fiber carbon-matrix composite) shell with integrally woven fins. It has a thin-walled (~0.002-in.) furnace-brazed high-temperature alloy (niobium 1-wt%-zirconium, referred to as “Nb-1Zr”) liner with end caps to contain the potassium working fluid. A short extension of this liner, at increased wall thickness beyond the C-C shell, forms the heat-pipe evaporator section. The evaporator section is in thermal contact with the power system heat-transport fluid, which needs to be cooled. The finned C-C condenser section completes the final heat-transfer step by thermal radiation to space.

The finned C-C shell condenser section was exposed to an atomic oxygen ion source during the fabrication process to increase the emissivity of the radiating surface. The total atomic oxygen fluence was 4×10^{20} atoms/cm², which raised the surface emissivity to between 0.85 and 0.90 at design operating temperature. The principal advantage of this device is its low mass per unit radiating area, resulting in a high thermal power-to-weight ratio. Its weight is between 20 and 33 percent of an all-metal heat pipe of equal heat-carrying capacity at the operating temperature.

When C-C is exposed to molten potassium, an intercalation reaction takes place, causing swelling and eventual erosion of the C-C heat pipe wall. To prevent this reaction and safely contain the potassium working fluid, fabricators lined the C-C tube (a shell with integrally woven fins) with a thin-walled metallic tube liner (Nb-1Zr alloy). This is an integral part of a hermetic metal subassembly that is furnace brazed to the inner surface of the C-C tube. The external section of this liner, which was formed by a “Uniscan” rolling process,

transitions to a larger wall thickness (0.020 in.). This section, which protrudes beyond the C-C shell (as shown in the figures), constitutes the evaporator part of the heat pipe, whereas the section inside the C-C shell constitutes the condenser part of the heat pipe.

The heat pipe was successfully tested at evaporator temperatures ranging from 850 to 875 K. Although this prototype heat pipe was designed to operate in the 700- to 875-K temperature range with potassium working fluid, the C-C shell with metal liner concept is applicable to a much greater range of operating temperatures, as long as the liner and wick metal are chosen to be compatible with the proper working fluid for the desired operating temperature range. Thus, for an operating temperature range of 300 to 500 K, the recommended working fluid would be purified water, and the containment material could be Monel metal (a copper-nickel alloy) or titanium. For lower temperatures (200 to 300 K), the recommended working fluid would be ammonia, which is compatible with aluminum.

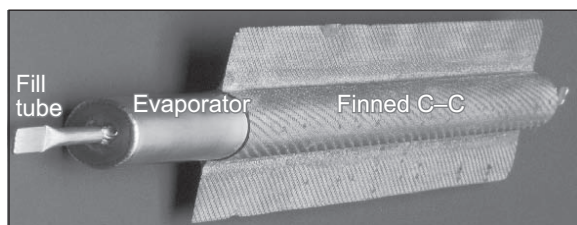
Bibliography

Juhasz, Albert J.: Design Considerations for Lightweight Space Radiators Based on Fabrication and Test Experience With a Carbon-Carbon Composite Prototype Heat Pipe. NASA/TP—1998-207427-REV1, 2002. <http://gltrs.grc.nasa.gov>

Juhasz, Albert J.: Heat Transfer Analysis of a Closed Brayton Cycle Space Radiator. NASA/TM—2007-215003, 2007. <http://gltrs.grc.nasa.gov>

Find out more about the research of Glenn’s Thermo-Mechanical Systems Branch

<http://www.grc.nasa.gov/WWW/TECB/>



Finned carbon-carbon heat pipe with Nb-1Zr evaporator liner.

Glenn Contact:

Dr. Albert J. Juhasz, 216-433-6134,
Albert.J.Juhasz@nasa.gov

Author:

Dr. Albert J. Juhasz

Headquarters Program Office:

Exploration Systems Mission Directorate

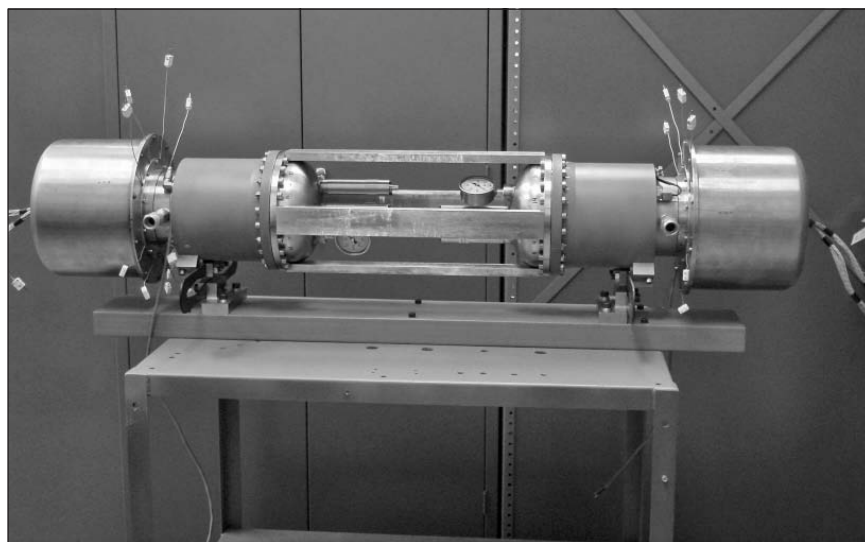
Programs/Projects:

Fission Surface Power Program

Progress Made in Power-Conversion Technologies for Fission Surface Power

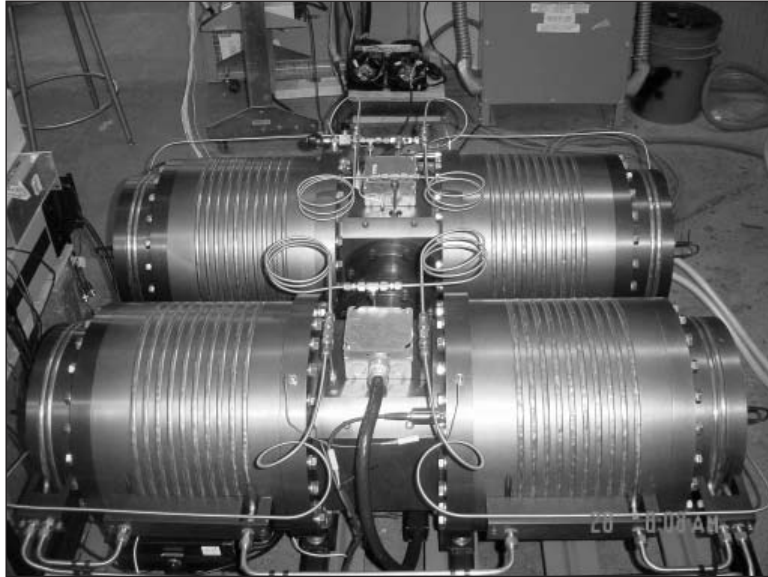
NASA has begun technology development of power-conversion systems for fission surface power (FSP). FSP provides a low-mass, long-life power option for Moon and Mars applications, especially for human outposts. These systems could be developed to satisfy power requirements from tens of kilowatts to hundreds of kilowatts. Risk and cost could be reduced if the fission reactor could utilize terrestrial-derived components and materials. A possible reactor configuration might include uranium dioxide fuel with stainless steel cladding and liquid metal coolant, permitting operating temperatures up to 900 K. A key technical challenge is the development of high-power, high-efficiency power-conversion technologies that are compatible with this heat source and operating temperature. The NASA Glenn Research Center is evaluating both free-piston Stirling and closed-Brayton-cycle options. Both technologies provide a feasible path to meet the power, efficiency, and lifetime goals for FSP.

For Stirling convertors, Glenn has three separate but coordinated efforts under FSP. For the first effort, Glenn has procured two 1-kW Stirling convertors from Sunpower, Inc. (see the photograph). These convertors will be modified for testing at the NASA Marshall Space Flight Center with a liquid-metal heating loop representative of a possible reactor interface. Glenn engineers are designing and fabricating a shell heat exchanger to be integrated with the Stirling heater head. The liquid-metal testing is planned to begin in late 2008.



Dual, opposed 1-kW Stirling convertors.

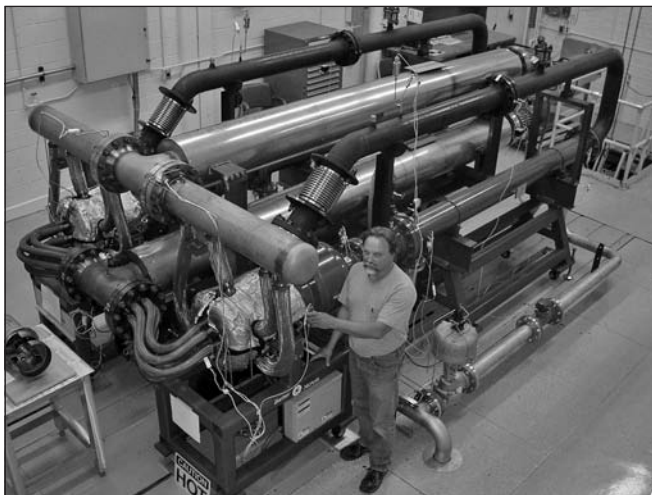
For the second effort, Glenn has procured a high-power linear alternator test rig from Clever Fellows Innovative Consortium, Inc. The test rig is composed of two opposed 5-kW linear alternators (see the top photograph on the next page) that are driven by pressure-wave generators to simulate the Stirling pneumatic interface. The rig will be used at Glenn to investigate power management and distribution options including alternating-current to direct-current conversion, alternator load control, and user load integration.



Dual, opposed 5-kW Stirling Alternator Test Rig.

The third effort is a collaboration between Auburn University, Foster-Miller, Inc., and Glenn to design and fabricate a 5-kW free-piston Stirling convertor. The new convertor design will be derived from high-power Stirling development work conducted during the 1980s and will be updated with current design techniques from the Advanced Stirling Radioisotope Generator project. A prototype is planned to be completed in spring 2008 and tested at Auburn later in the year.

For the Brayton convertors, there are two main FSP efforts at Glenn. The first is a high-power, dual closed Brayton test system (designed and built by Barber-Nichols Inc. and installed at Glenn) that uses a shared heat source and common nitrogen working fluid inventory. The system uses two commercial, recuperated turbine-generators coupled to an electrical resistance heater and water cooling system (see the final photograph). The



Thirty-kilowatt dual Brayton test system.

configuration, which is designed to produce about 30 kW, roughly represents a gas-cooled reactor concept with redundant Brayton units. Initial testing is planned for winter 2007.

The second effort is a joint activity with Marshall to test a space-configured 2-kW Brayton unit with a prototypic gas reactor simulator. Testing is expected to begin at Glenn in spring 2008. The objective is to demonstrate stable and controllable operation of the integrated system under conditions that closely approximate nuclear heating. Although both of these efforts are related to gas-cooled reactor concepts, Brayton technology could easily be applied to the liquid-metal reactor discussed previously.

Find out more about the research of Glenn's Thermo-Mechanical Systems Branch

<http://www.grc.nasa.gov/WWW/TECB/>

Glenn Contacts:

Lee S. Mason, 216-977-7106,
Lee.S.Mason@nasa.gov

Steven M. Geng, 216-433-6145,
Steven.M.Geng@nasa.gov

Author:

Lee S. Mason

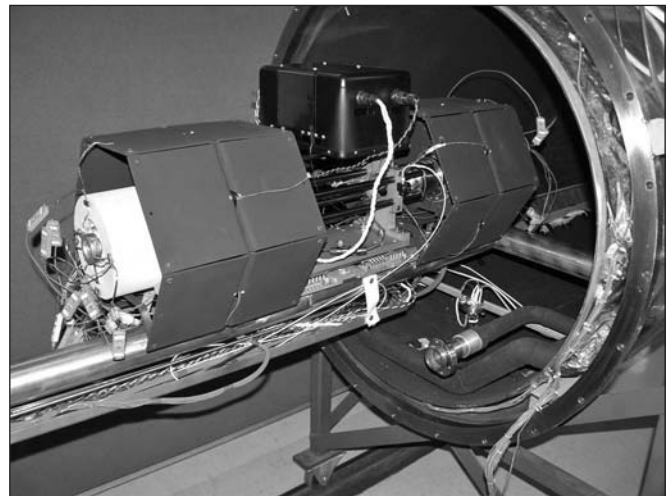
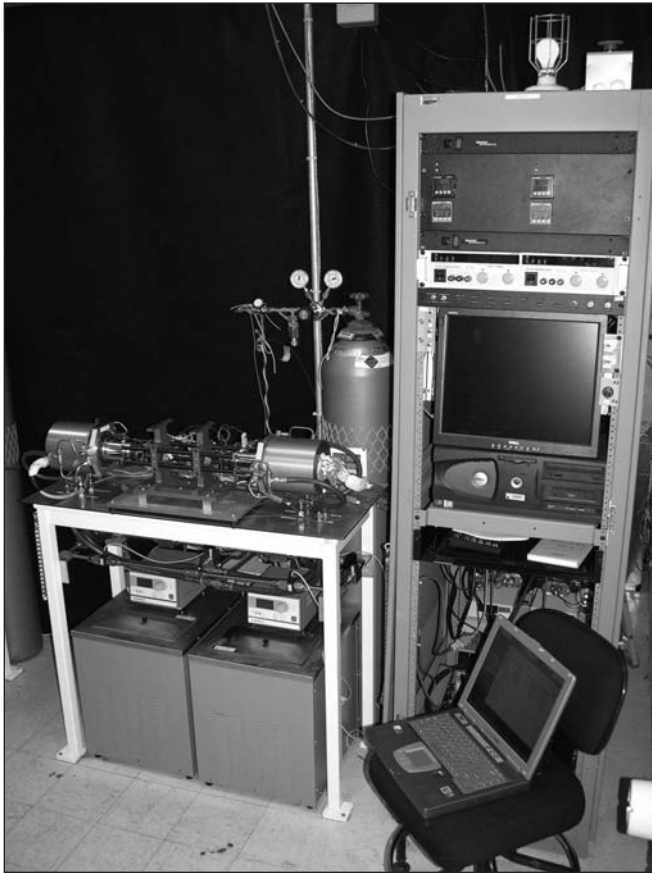
Headquarters Program Office:

Exploration Systems Mission Directorate

Programs/Projects:

Exploration Technology Development Program, Advanced Fission Based Power Systems

Advanced Stirling Convertors Began Extended Operation



Left: ASC-0 #1 and #2 configured for in-air operation. Right: ASC-0 #1 and #2 configured for thermal vacuum operation.

The NASA Glenn Research Center has been supporting development of the Advanced Stirling Radioisotope Generator (ASRG) for the Department of Energy; and Lockheed Martin Space Systems (Valley Forge, PA) has been assigned as system integrator under contract to the Department of Energy. The generator will utilize free-piston Stirling conversion technology to produce electrical power from a plutonium-238 heat source and will be able to operate in deep space or in gaseous atmospheres such as Mars. Free-piston convertor designs make use of noncontacting moving parts to eliminate wear mechanisms and enable the long life required by deep-space missions.

Glenn has been supporting Lockheed Martin Space Systems and the ASRG project by providing key data in the areas of performance enhancement and risk mitigation. Glenn tasks include extended-duration convertor testing, heater head life assessment, structural dynamics testing and analysis, organics assessment, and reliability analysis.

The purpose of the convertor testing effort is to provide independent validation and verification of the conversion technology as well as demonstrate its life and reliability. To accomplish this, Glenn researchers have put several convertors on extended, around-the-clock operation. The Stirling research

lab at Glenn comprises six test stations for in-air operation and one for thermal vacuum operation. Each station can maintain unattended, continuous operation of a pair of convertors. Five of the stations also can sample the convertor working fluid via a residual gas analyzer and ultra-high vacuum system. The gas analysis capability allows for detection of contaminants entering the convertor working fluid either through pressure boundary flange o-rings or outgassing of internal components.

Six prototype convertors, designated Advanced Stirling Convertors (ASCs), have operated for over 10,700 total hours with no failures. These units were designed and fabricated by Sunpower, Inc., and are earlier versions of the units

ASC OPERATION SUMMARY

ASC pair	Length of extended operation, hr
ASC-0 #1 and #2	4500
ASC-0 #3 and #4	79
ASC-1 #3 and #4	712

currently being integrated into the ASRG engineering unit. The first pair of these six convertors, ASC-0 #1 and #2, completed in-air checkout testing and was then transitioned to thermal vacuum operation. The other two pairs, ASC-0 #3 and #4, and ASC-1 #3 and #4, are being operated solely in air. During the first quarter of 2008, delivery of a fourth pair of convertors, ASC-1HS #1 and #2, is anticipated. This pair will undergo checkout testing and will then continue extended operation in thermal vacuum.

Two pairs of Infinia, Corp., Technology Demonstration Convertors (TDCs) also continued extended operation. TDCs #13 and #14 have operated for 32,200 hours, and TDCs #15 and #16 have operated for over 18,000 hours.

The end of fiscal year 2007 free-piston Stirling convertors have operated for over 138,000 hour at Glenn. This effort is supported by NASA's Science Mission Directorate, Radioisotope Power Systems.

Find out more about the research of Glenn's Thermo-Mechanical Systems Branch:

<http://www.grc.nasa.gov/WWW/TECB/>

Glenn Contact:

Jeffrey G. Schreiber, 216-433-6144, Jeffrey.G.Schreiber@nasa.gov

Author:

Salvatore M. Oriti

Headquarters Program Office:

Science Mission Directorate

Programs/Projects:

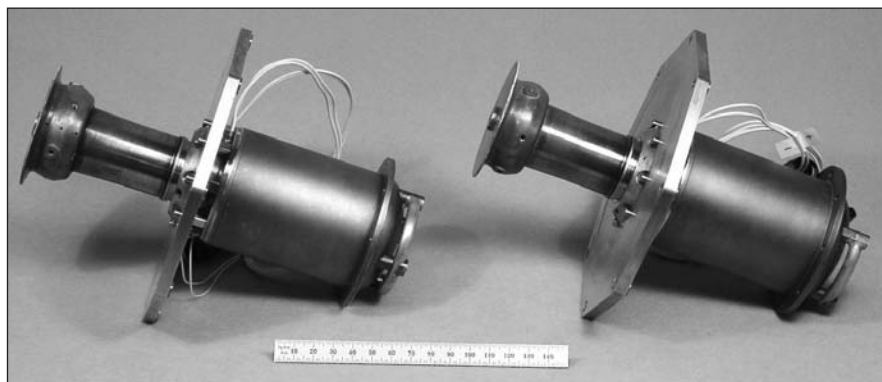
Radioisotope Power Systems, Advanced Radioisotope

Advanced Stirling Convertor Engineering Units Completed and Delivered

In fiscal year 2007, Advanced Stirling Convertor Engineering Units (ASC-Es) were completed and delivered by the NASA Glenn Research Center and Sunpower, Inc., team to Lockheed Martin Space Systems Company (LMSSC), the Department of Energy's (DOE) system integration contractor for the Advanced Stirling Radioisotope Generator Engineering Unit (ASRG EU). The ASC-Es were developed under a Glenn contract with Sunpower (Athens, OH) with Glenn technical support as low-mass, high-efficiency power convertors for the ASRG EU and were provided as Government-furnished property by Glenn to DOE and LMSSC. Each ASC-E produces 78-W alternating current (ac) at nominal operating conditions representing a beginning-of-mission 640 °C hot-end temperature and 60 °C rejection temperature with 224-W heat input, exceeding the 75-W ac requirement. The 35-percent power conversion efficiency of the free-piston ASC-E enables the ASRG EU to have a specific power of ~7.0 We/kg—a significant improvement over the ~3.5 We/kg of the previous Stirling Radioisotope Generator design (SRG110). Furthermore,

the high efficiency represents a factor of 4 reduction in the radioisotope fuel requirement in comparison to lower efficiency thermoelectric-based radioisotope power systems.

Sunpower began development of the ASC in 2003 under 1 of the 10 technology development and research contracts awarded as part of the 02-OSS-01 National Research Announcement entitled "Radioisotope Power Conversion Technology." After the ASC technology was demonstrated successfully during phase I and phase II of the contract on earlier



Advanced Stirling Converter Engineering Unit (ASC-E) pair.

Find out more about the research of Glenn's Thermo-Mechanical Systems Branch:

<http://www.grc.nasa.gov/WWW/TECB/>

Glenn Contacts:

Wayne A. Wong, 216-433-6318,
Wayne.A.Wong@nasa.gov

Richard K. Shaltens, 216-433-6138,
Richard.K.Shaltens@nasa.gov

Author:

Wayne A. Wong

Headquarters Program Office:

Science Mission Directorate

Programs/Projects:

Radioisotope Power Systems

developmental units, in March 2006 NASA directed the use of the ASC on the DOE/LMSSC SRG110 design, which was renamed ASRG. Glenn technology support was also redirected to the ASC and ASRG. Initial tradeoff studies were performed by Glenn, Sunpower, and LMSSC to assess features and design modifications that would be required to evolve the ASC from the previous technology development design to one suitable for integration onto the ASRG. The ASC-E final design review was completed in November 2006, and the ASRG EU final design review was completed in February 2007.

The ASC-E design modifications include two thermal and structural interfaces to the ASRG, a heat collector and a cold-side adapter flange, an additional structural interface on the pressure vessel, an internal piston position sensor, and feed-through electrical interfaces for power and for the piston position sensor. In addition to design modifications, the quality practices involved in producing the ASC-Es were required to be more rigorous than those for previous developmental builds. Configuration management, establishment of an ASC-E engineering review board to approve design modifications and nonconformances, and more detailed process documentation and test plans were instituted as part of the ASC-E build.

The ASC-E was assembled and operational by July 2007, providing full power during initial testing. Subsequent processing included extended burn-in tests, welding of the external structure, vacuum bakeout, and fill-and-purge cycling of the helium working gas. After the ASC-Es were hermetically sealed, they successfully completed 6.8-g workmanship-level vibration testing at Glenn followed by final performance testing at Sunpower. Two ASC-E converters were delivered on schedule to LMSSC on October 4, 2007, and will undergo acceptance testing prior to integration onto the ASRG EU. A third spare converter was also delivered on schedule on October 29, 2007.

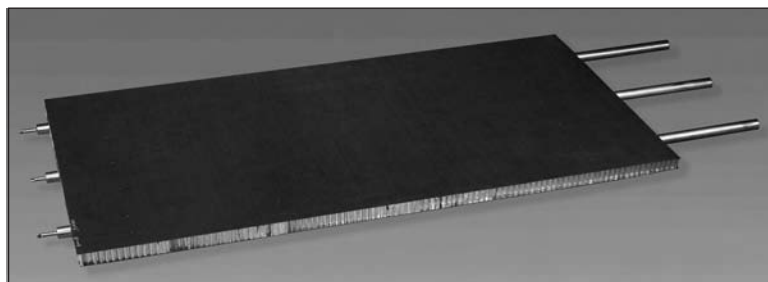
Heat-Rejection Systems Utilizing Composites and Heat Pipes Evaluated

Heat-rejection systems designed for long-term use need to be durable to the space environment. One threat to such systems is that of micrometeoroid impact on tubing with subsequent loss of coolant. To accommodate the inevitability of micrometeoroid impacts, system design is driven toward the use of individual heat pipes, where a micrometeoroid impact on a given heat pipe removes only a small portion of the total cooling capability (ref. 1). With this design philosophy in mind, development of heat-rejection systems utilizing heat pipes is of ongoing interest. Furthermore, heat-rejection systems for power-conversion systems utilizing a fission heat source need to reject heat at high temperatures, perhaps as high as 500 K.

One heat-pipe system under consideration for such temperature conditions is the titanium-water heat-pipe system. High-temperature titanium-water heat pipes show great promise (ref. 2). Titanium offers excellent strength and is easily machined into the needed heat-pipe cross-sectional geometry. For minimal mass and sufficient support for deployment, panels composed of aluminum honeycomb sandwiched between two composite face sheets are currently of interest. Composite face sheets composed of high-thermal-conductivity fibers offer improved efficiency.

A technology development effort was initiated at the NASA Glenn Research Center to develop heat-rejection systems utilizing titanium-water heat pipes. Several radiator demonstration units (RDUs) were designed, fabricated, and tested. The photograph shows the 0.5- by 1-m RDU panel. Three heat-pipe evaporators extend beyond the composite structure and were equipped with band heaters during testing.

Thermal performance was evaluated at steady state in a liquid-nitrogen-cooled thermal vacuum chamber. Thermal performance also was compared with analytical predictions based on a thermal model utilizing the physical properties of the RDU constituents. Maximum performance was found to be approximately 350 W per heat pipe at a temperature of 480 K. Graphite saddles directed heat from the condenser section of each heat pipe to the composite face sheets. POCO graphite (Poco Graphite, Inc.) was utilized for the graphite saddles to provide good thermal conduction and compliance to the differing coefficients of thermal expansion. The high-thermal-conductivity fibers used in the face sheets spread the heat successfully, independent of the polymer matrix utilized.



Completed RDU panel with heat pipe evaporators to the far right.

Off-nominal panel performance successfully simulated a micrometeoroid strike. With the loss of the center heat pipe, the temperature of the face sheet dropped by about 28 K in the vicinity of the still-working neighbors while it dropped by about 70 K in the region above the null heat pipe. Future work is planned to improve the thermal conductance between the heat pipe and face sheet. An upgrade to the thermal vacuum chamber is planned to vary sink temperatures to simulate lunar sunrise and sunset.

References

1. Mason, Lee S.: A Comparison of Fission Power System Options for Lunar and Mars Surface Applications. Space Technology and Applications International Forum—STAIF 2006, Mohamed S. El-Genk, ed., AIP Conf. Proc., vol. 813, 2006, pp. 270–280.
2. Sanzi, James L.: Thermal Performance of High Temperature Titanium—Water Heat Pipes by Multiple Heat Pipe Manufacturers. Space Technology and Applications International Forum—STAIF 2007, Mohamed S. El-Genk, ed., AIP Conf. Proc., vol. 880, 2007, pp. 681–691.

Find out more about the research of Glenn's Space Environmental Durability Branch:

<http://www.grc.nasa.gov/WWW/epbranch/ephome.htm>

Glenn Contacts:

Dr. Donald A. Jaworske, 216–433–2312,
Donald.A.Jaworske@nasa.gov

Duane E. Beach, 216–433–6285,
Duane.E.Beach@nasa.gov

SEST, Inc., Contact:

James L. Sanzi, 216–433–5036,
James.L.Sanzi@nasa.gov

Authors:

Dr. Donald A. Jaworske, Duane E. Beach,
and James L. Sanzi

Headquarters Program Office:

Exploration Technology Development
Program

Programs/Projects:

Fission Surface Power

Simple Mars Propellant Manufacture Investigated That Will Reduce Mass Required for Mars Sample Return

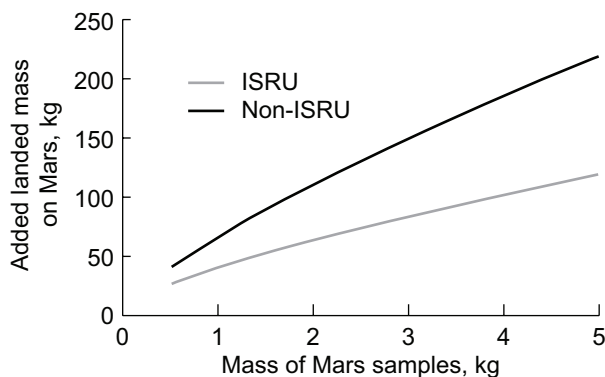
Returning samples from the surface of Mars (Mars sample return, or MSR) is a high priority for Mars science, but conventional approaches could return only a small sample at high cost. Producing rocket propellants from the resources of Mars (in situ resource utilization, or ISRU) could significantly reduce the amount of propellant needed to be transported to Mars.

Mars propellant production is an enabling technology for a human Mars mission, and safety requires that this technology be demonstrated on Mars well in advance of a human mission. By returning a sample, a Mars ISRU demonstration mission could serve an added scientific function.

Conventional sample-return mission architectures have very little margin, and high complexity and risk. Using ISRU propellant would increase the margin and reduce the complexity and the risk. To show that this is feasible, the NASA Glenn Research Center, in collaboration with the Satellite Engineering Class at MIT (Massachusetts Institute of Technology), compared an MSR using ISRU propellant, with an MSR using propellant brought from Earth (ref. 1). The study used a solid-oxide electrolysis (SOE) process to produce oxygen (O₂) from the Mars atmosphere (ref. 2) to use as an oxidizer with fuel brought from Earth.



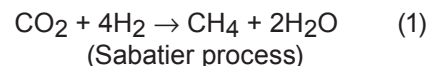
The SOE process was chosen because a flight unit had been built (ref. 2) for the 2001 Surveyor Lander (ref. 3). Although the mission was cancelled, the electrolysis unit was completed and flight qualified. The study used SOE cells identical to those built for Surveyor, with the number of individual cells increased to reach the required O₂ output. A hybrid rocket using Mars ISRU oxygen with a solid fuel brought from Earth was used for the ascent. The vehicle was sized to launch a 1-kg sample in a lightweight canister to rendezvous in Mars orbit with an Earth return vehicle.



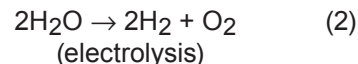
Required landed mass of the Mars ascent vehicle and propellant manufacturing as a function of the mass of sample launched (ref. 1). The mass benefit of ISRU increases with sample size.

The graph shows the calculated landed mass for the Mars ascent vehicle and propellant (with a 10-percent propellant margin) for the ISRU and non-ISRU missions. The total mass landed on Mars, including the power system, oxygen-generation system (OGS), and cryocooler to liquefy the propellant was considerably lower with ISRU propellant. The OGS was sized to produce 30 percent more liquid oxygen (LO₂) than required for the mission, and a 15-percent mass and power margin was used for the equipment. With ISRU, either a lower mass system could be used to launch a 1-kg sample into Mars orbit, or over twice the sample mass could be returned with the same landed mass.

An alternate technology, which has been proposed for a human mission, is the Sabatier production of methane (CH₄)/O₂ fuel by reacting hydrogen (H₂) with carbon dioxide (CO₂):



followed by electrolysis of the generated water:



The H₂ produced is returned to step (1). The process makes 18 kg of CH₄/O₂ rocket fuel per 1 kg of H₂ brought from Earth.

Bringing liquid hydrogen (LH₂) from Earth is challenging because LH₂ must be kept at cryogenic temperature. For the small amounts required for MSR, the overhead required for cryogenic storage would overwhelm any mass advantage. Hence, the proposed robotic MSR architecture brings water, which is easily stored, dense, noncorrosive, and noncryogenic. Although it does not achieve the 18:1 mass leverage

produced with H₂, it still yields 2.2 kg of propellant on Mars per 1 kg of reactant brought from Earth, without requiring added O₂ from SOE.

Alptekin et al. demonstrated a space-qualified low-temperature Sabatier reactor with a mass of 1.94 kg (ref. 4), based on a design by Strumpf et al. (ref. 5). Calculated results for the Sabatier/electrolysis process for Mars fuel production were very similar to those for the MIT study. The lower mass of propellant brought from Earth doubles the sample mass returned for the same landed mass on Mars.

The Glenn/MIT study shows that extremely simple, well-demonstrated propellant production technologies would enhance the science value of MSR missions.

Bibliography

Landis, Geoffrey A., et al.: Mars Sample Return With ISRU. Seventh International Conference on Mars, Abstract 3369, Pasadena, CA, 2007.

References

1. Cunio, P., et al.: Near-Term Mars Sample Return Using In-Situ Oxygen Generation. AIAA-2007-6064, 2007.
2. Sridhar, K.R.; Iacomini, Christine S.; and Finn, John E.: Combined H₂O/CO₂ Solid Oxide Electrolysis for Mars In Situ Resource Utilization. *J. Propul. P.*, vol. 20, no. 5, 2004, pp. 892-901.
3. Kaplan, David I., et al.: The 2001 Mars In-Situ-Propellant-Production Precursor (MIP) Flight Demonstration—Project Objectives and Qualification Test Results. AIAA-2000-5145, 2000.

4. Alptekin, Gökten, et al.: Prototype Demonstration of the Advanced CO₂ Removal and Reduction System. Presented at International Conference on Environmental Systems, 05ICES-31, Rome, Italy, July 2005. Available from Society of Automotive Engineers, Inc.
5. Strumpf, Hal J., et al.: Sabatier Carbon Dioxide Reduction System for Long-Duration Manned Space Application. SAE Paper 911541, 1991.

Glenn Contact:

Dr. Geoffrey A. Landis, 216-433-2238, Geoffrey.A.Landis@nasa.gov

Author:

Dr. Geoffrey A. Landis

Headquarters Program Office:

Office of Educational Programs

Programs/Projects:

Mars Sample Return, human Mars missions, Mars in situ resource utilization

Hybrid Power Management Program: Prototype Grid-Tie Photovoltaic Power System Has Been in Successful Operation for Over 1 Year at NASA Glenn and Is Serving as the Basis for Future Expansion

Present global energy concerns reinforce the need for the development of alternative energy systems. Modern photovoltaic (PV) panels and electronics have made grid-tie PV power systems safe, reliable, efficient, and economical with a life expectancy of at least 20 years. During fiscal year 2007, the NASA Glenn Research Center collected data from a state-of-the-art 2-kW grid-tie PV power system designed, developed, and installed at Glenn. These data will show how solar energy varies in Cleveland, Ohio, over the year. In the year since operation was initiated, the system has provided 2194 kW-hr of electrical power to Glenn's power grid for use by all. This work was performed by Glenn's Electrical, Electromagnetic, and Communications Systems Branch (of Glenn's Power and Avionics Division) for Glenn's Facilities Division.

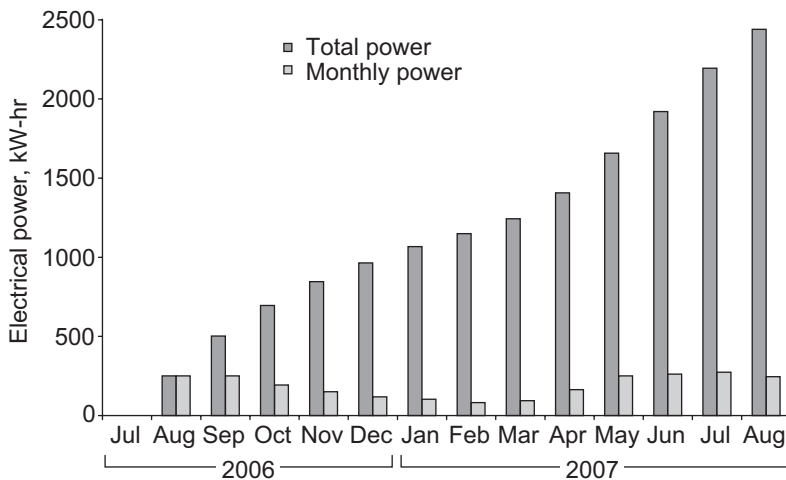
As a result of the significant success of the prototype photovoltaic power system, the Electrical, Electromagnetic, and Communications Systems Branch

proposed a significantly larger system to the Facilities Division:

- Design, install, and test a 12-kW grid-tie PV power system for the NASA Glenn Visitor Center.
- Connect the grid-tie system to the utility distribution grid.
- Make it possible to obtain facility power from the utility system as normal.
- Synchronize the PV system with the utility system.



The Hybrid Power Management (HPM) Program's NASA Glenn prototype grid-tie PV power system has been in successful operation for over 1 year.



Results for the 1-yr test of the Glenn prototype grid-tie PV power system exceeded expectations. Data were collected on the 10th of each month.

- Use the PV system to provide power for the facility, and sell excess power to the utility.
- Incorporate a Web-based interface to allow remote monitoring of the PV power system.
- Install a large display in the Visitor Center for local monitoring of the PV power system by the public.

The project transfers space technology to terrestrial use via nontraditional partners, and it provides power system data valuable for future aeronautics and space applications. In fiscal year 2007, all of the solar panels were installed on the Visitor Center roof. The system will be wired into the utility

system and is expected to be operational in fiscal year 2008.

The work on both power systems is being done under the Hybrid Power Management (HPM) Program, which is the innovative integration of diverse, state-of-the-art power devices in an optimal configuration for space and terrestrial applications. The Electrical, Electromagnetic, and Communications Systems Branch initiated the HPM Program for the Technology Transfer and Partnership Office. The appropriate application and control of the various power devices significantly improves overall system performance and efficiency. Applications include power generation, transportation systems, biotechnology systems, and space power systems.

There are many benefits to the grid-tie PV power system:

- Glenn personnel glean valuable experience with PV power systems that are directly applicable to various Exploration Mission power systems.
- Power generated by the PV system reduces Glenn's utility demand and aids the community.
- The power system provides valuable space program test data.

Not only did the success of the prototype 2-kW grid-tie PV power system lead to the development of the 12-kW Visitor Center grid-tie PV power system, but the 2-kW system is being considered for significant future expansion.

Glenn Contact:

Dennis J. Eichenberg, 216-433-8360,
Dennis.J.Eichenberg@nasa.gov

Author:

Dennis J. Eichenberg

Headquarters Program Office:

Technology Transfer and Partnership Office

Programs/Projects:

Facilities

Materials International Space Station Experiment 2 (MISSE 2) Polymer Erosion and Contamination Experiment (PEACE) Polymers Analyzed

As part of the Materials International Space Station Experiment 2 (MISSE 2), 41 different polymers—collectively called the Polymer Erosion and Contamination Experiment (PEACE) Polymers experiment—were exposed for approximately 4 years to the low-Earth-orbit (LEO) space environment. MISSE is a series of materials flight experiments consisting of trays (called Passive Experiment Carriers, PECs) that are exposed to the space environment on the exterior of the *International Space Station* (ISS). MISSE 2 was placed outside of the ISS during the STS-105 shuttle mission in August 2001 and was successfully retrieved during a space walk on July 30, 2005, during Discovery's STS-114 Return to Flight mission.

Polymers are commonly used as spacecraft materials because of their desirable properties such as good flexibility, low density, and certain electrical or optical properties. Two examples of the use of polymers on the exterior of spacecraft exposed to the space environment include metallized Teflon FEP (fluorinated ethylene propylene, DuPont) thermal control materials on the Hubble Space Telescope, and polyimide Kapton (DuPont) solar array blankets.

Atomic oxygen (AO) is the predominant species in LEO (between 180 and 650 km), and spacecraft surfaces, such as polymers, that literally ram into the resident oxygen atoms are oxidized. Because the oxidation product for most polymers is a gas, AO exposure results in erosion. Over time, the polymer can be completely lost if it is not properly protected. Therefore, the specific goal of the MISSE PEACE Polymers experiment is to accurately determine the AO erosion yield of a wide variety of polymeric materials.

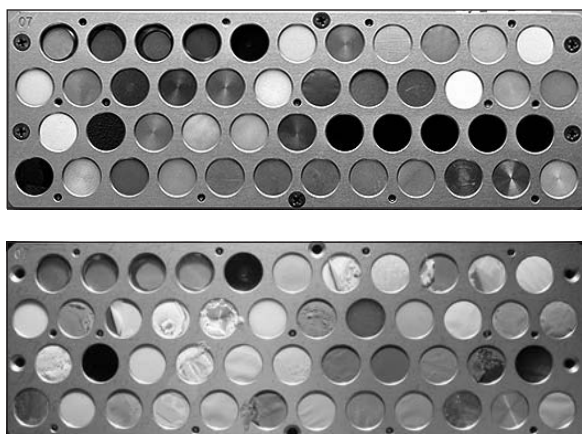
A very wide variety of polymers were flown, such as those commonly used for spacecraft applications. Polymers not desired for spacecraft applications also were included solely because of their chemical composition in order to verify existing, and/or to develop new, predictive models based on chemistry



MISSE 2 after installation on the space station Quest airlock in 2001. The MISSE PEACE Polymers experiment tray is the upper left tray.

for AO erosion yield determination of new and non-flown polymers. Having the erosion yield data for many different polymers that have been characterized and exposed to space under identical conditions, and having space data to compare with the predictive model will be very useful to spacecraft designers.

AO erosion yields have been determined for the MISSE 2 PEACE Polymers experiment on the basis of mass loss obtained from preflight and postflight vacuum-dehydrated samples. The average AO fluence for the experiment was determined from two Kapton H witness samples to be 8.43×10^{21} atoms/cm². There was partial or complete erosion through the entire sample thickness of 6 of the 41 flight samples, and hence the erosion yield values for these samples are greater than the value determined. Extensive error analyses were conducted and completed in 2007 determining the error in the erosion yield values for each of the MISSE 2 PEACE Polymers flight samples, completing data analyses for



MISSE 2 PEACE Polymers experiment. Top: Before flight. Bottom: After flight.

this experiment. Details on the specific polymers flown, flight sample fabrication, preflight and postflight characterization techniques, and AO fluence calculations are reported in reference 1 along with a summary of the AO erosion yield results.

The NASA Glenn Research Center invited high school students from Hathaway Brown School to collaborate on the Glenn MISSE 2 PEACE Polymers experiment. The MISSE 2 PEACE Polymers experiment is unique because it has the widest variety of polymers flown in LEO for a long duration under identical conditions, and it provides extremely valuable erosion yield data for spacecraft design and predictive model development.

Reference

1. de Groh, Kim K., et al.: MISSE PEACE Polymers Atomic Oxygen Erosion Results. NASA/TM—2006-214482, 2006. <http://gltrs.grc.nasa.gov>

Find out more about this research:

MISSE:

<http://misse1.larc.nasa.gov/>

Feature article—High School Students Team With NASA on Space Experiments:

http://www.nasa.gov/mission_pages/station/science/MISSE_PEACE_Feature.html

Feature article—The Wait Is Over: Space Station Project Returns:

http://www.nasa.gov/mission_pages/station/science/MISSE_returnstoGlenn_120505.html

Glenn's Space Environmental Durability Branch:

<http://www.grc.nasa.gov/WWW/epbranch/ephome.htm>

Glenn Contact:

Kim K. de Groh, 216-433-2297, Kim.K.deGroh@nasa.gov

Authors:

Kim K. de Groh, Bruce A. Banks, Catherine E. McCarthy, Rochelle N. Rucker, Lily M. Roberts, and Lauren A. Berger

Programs/Projects:

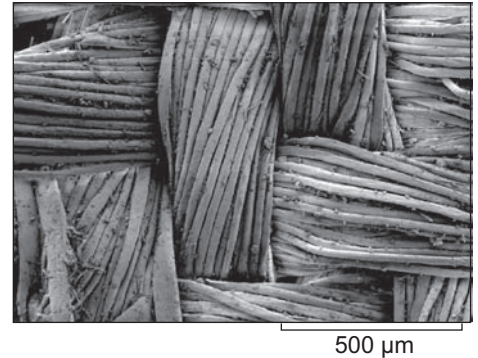
Glenn Independent Research and Development Program; low-Earth-orbit (LEO) spacecraft—International Space Station, Earth-observing systems, Hubble Space Telescope, and Commercial Orbital Transportation Services; spacecraft passing through LEO—Orion Crew Exploration Vehicle and Department of Defense spacecraft; Mars orbiters

Special Recognitions:

Best Branch Paper-of-the-Year Award, Space Environmental Durability Branch 2006 for reference 1. Siemens Foundation Performance Award to Kim de Groh for “being recognized as an outstanding mentor of 2006/2007 Siemens Competition in Math, Science & Technology winners.” Hathaway Brown School students Catherine McCarthy, Rochelle Rucker, and Lily Roberts won the Midwest Regional Competition at the University of Notre Dame in the 2006–07 Siemens Competition in Math, Science & Technology for their team research paper “International Space Station Experiment to Measure Effects of Atomic Oxygen on Spacecraft Materials.” As National Finalists, the students won over \$20,000 in scholarships and awards. The Siemens competition is the nation’s most prestigious science and mathematics research competition for high school students, and the PEACE team students are the first Ohio team to compete at the Siemens Competition National Finals.

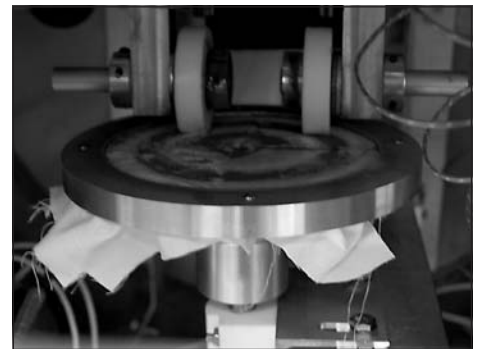
Lunar Dust Abrasion Simulation Capability Completed

NASA's Vision for Space Exploration calls for a return of humans to the Moon by no later than 2020. Reducing risk to astronaut safety and mission success will require technology development in a wide variety of areas, including the protection of astronauts and their equipment from the lunar environment. The exploration community is beginning to come to consensus with Apollo 17 astronaut Harrison Schmitt who recently declared, "Dust is the number one environmental problem on the Moon" (ref. 1). The Apollo record shows that dust caused a wide variety of problems for those missions, including vision obscuration, false instrument readings, equipment clogging, radiator degradation, seal degradation, abrasion, and respiratory and eye irritation (ref. 2). Abrasion of the fabric of the extravehicular activity (EVA) suits was much more extensive than anticipated. The electron micrograph to the right shows abrasive damage of a portion of Alan Bean's suit from Apollo 12. The Apollo 12 astronauts also reported, "The suit material just beneath the top of the lunar boots chafed sufficiently to wear through the outer suit layer in several spots" (ref. 3). This is of particular concern since the missions are being planned to last as long as 6 months, and the Apollo damage was incurred in less than 3 days.



Portion of the EVA suit worn by Alan Bean during Apollo 12. Lunar dust particles are embedded in the fabric, and abrasion can be observed on several of the individual fibers.

Although the abrasive damage was much worse than anticipated, exactly why has not been determined. Certainly a major factor is the nature of the lunar regolith—the upper part of the lunar crust, which is composed of pulverized rock, dirt, and dust. The lunar surface is weathered primarily by the impacts of meteoroids, which vary in size from mountains to microns. Impacts melt and weld regolith together at the impact point, and impact shock waves break regolith apart. This results in very sharp particles, some of which have irregular and protruding shapes. These particles tend to hook into fabric fibers and become difficult to dislodge. They work their way into the fabric and abrade it. In addition, the lunar environment is filled with radiation from the Sun, so these fabrics also are subjected to thermal extremes, energetic x-rays, ultraviolet light, solar wind protons and electrons, and cosmic rays. In addition to possibly embrittling the suit fabric in long-term use, these conditions make the surface of the regolith chemically active, which may change the adhesive and abrasive characteristics of the dust and dirt.



Abrasion fixture with four fabric samples installed in the LDAB at the conclusion of a test.

In fiscal year 2007, a fixture was designed and fabricated at the NASA Glenn Research Center for studying abrasion in a lunar-like environment—the Lunar Dust Adhesion Belljar (LDAB, see the photograph). The LDAB was designed to mimic the vacuum, thermal, illumination, and radiation environment of the lunar surface (ref. 4). The fixture was adapted from a standard abrasion test (ref. 5), but testing is being carried out under simulated lunar conditions. Preliminary tests were done with lunar simulants, such as JSC-1A, but later testing will be done with actual lunar regolith. Electron microscopy is being used to match the abrasive damage of samples with that experienced by the Apollo fabrics. This will enable ground test conditions to be developed that will result in realistic testing of fabric abrasion on the lunar surface.

References

1. Schmitt, Harrison: The Apollo Experience/Problems Encountered With Lunar Dust. Biological Effects of Lunar Dust Workshop, Sunnyvale, CA, 2005.
2. Gaier, James R.: The Effects of Lunar Dust on EVA Systems During the Apollo Missions. NASA/TM—2005-213610, 2005. <http://gltrs.grc.nasa.gov>
3. Apollo 12 Mission Report. NASA-TM-X-74200 (MSC-01855), section 9.10.9, 1970, p. 9-21.
4. Gaier, James R.; and Sechkar, Edward A.: Lunar Simulation in the Lunar Dust Adhesion Bell Jar. AIAA-2007-0963 (NASA/TM—2007-214704), 2007. <http://gltrs.grc.nasa.gov>
5. Standard Guide for Abrasion Resistance of Textile Fabrics (Rotary Platform Double-Head Method), ASTM D3884-01, 2001.

Glenn Contacts:

Dr. James R. Gaier, 216-433-6686, James.R.Gaier@nasa.gov
 Dr. Mary Ann Meador, 216-433-3221, MaryAnn.Meador@nasa.gov

Author:

Dr. James R. Gaier

Headquarters Program Office:

Advanced EVA Systems

Programs/Projects:

Lunar Surface Systems including Extravehicular Activity Systems, Lunar Surface Access Module, Lunar Habitat, and Dust Mitigation Project

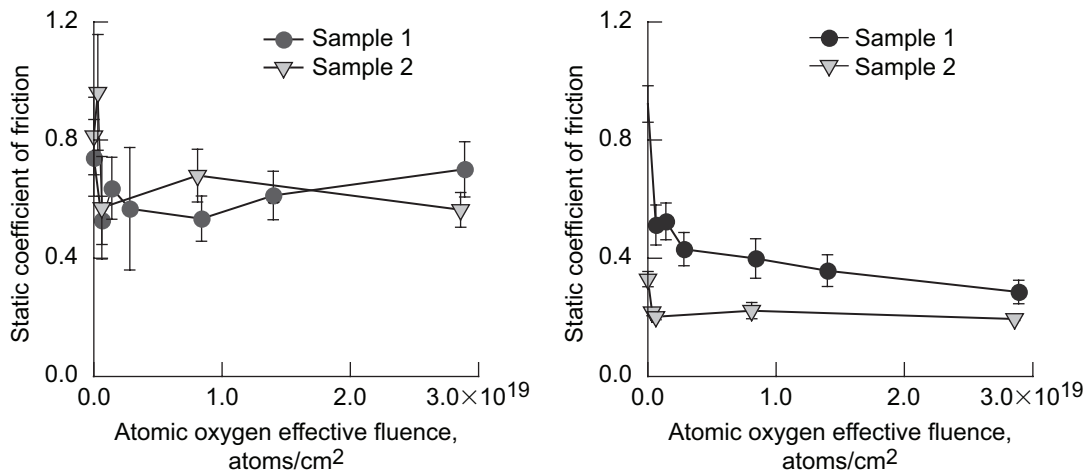
Stickiness of Silicone Elastomer Seal Material Reduced by Using Atomic Oxygen Treatment

Silicone elastomers, used in seals for airlocks or other sealing surfaces in space, are somewhat sticky in their as-received condition. Because of the sticking, a greater separation force is needed to enable the seal to release. This can lead to sudden unpredicted movement of the spacecraft, vibration, uneven release, and even pull out or pull off of the seal, resulting in a seal failure. This is especially of concern for androgynous seals, which have identical mating surfaces on both sides for interchangeability and redundancy. These seals typically have elastomer-on-elastomer sealing surfaces. To reduce sticking, one could use release agents such as powders and lubricants, but these can be easily removed and transferred to other surfaces, causing uneven sealing and contamination. Application of a more slippery coating that is integral with the surface would be more desirable.

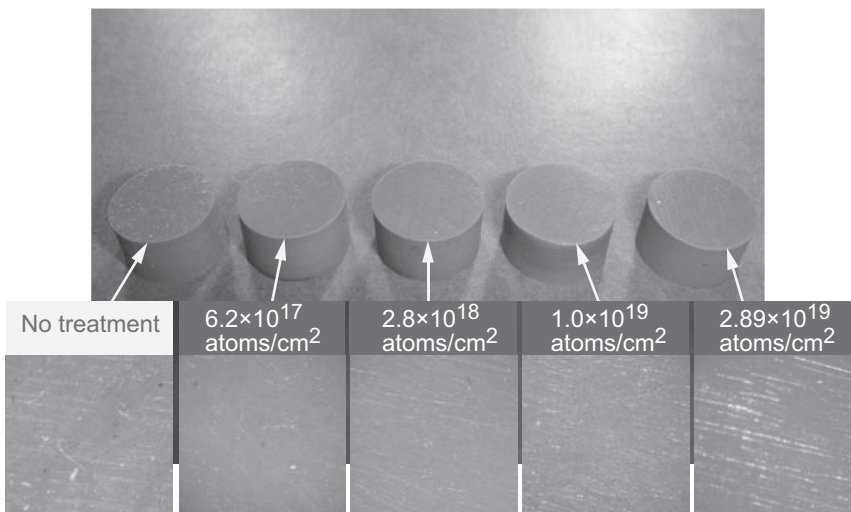
The most integral type of coating is a conversion of the surface of the silicone elastomer to a thin layer of silicon oxide. This conversion can be readily accomplished by oxidation using atomic oxygen (AO). The most predominant species in the low-Earth-orbit environment, AO is produced as ultraviolet radiation from the Sun splits oxygen molecules (O₂) in the atmosphere into two oxygen atoms (O). The atoms readily react with surfaces that they come in contact with to create an oxide. Even though AO can be used to convert a surface to an oxide, as the thickness of the oxide increases, the shrinkage on the surface due to this oxide formation leads to surface cracking. Too much cracking can cause the elastomer seal to leak, so the question to be answered was, "How much atomic oxygen exposure is needed to make an oxide layer thick enough to reduce surface sticking but not form deep surface cracks?"

To answer this, researchers at the NASA Glenn Research Center developed and conducted tests to expose several samples of a silicone elastomer to increasing durations of AO to determine the stickiness and level of surface cracking as a function of AO dose. The elastomer (Parker Hannifin S0383-70)

is a candidate for the Low-Impact Docking System on the Crew Exploration Vehicle. The testing was conducted in a ground-based AO exposure system consisting of a small vacuum chamber and a radiofrequency power supply to dissociate air. The samples were removed at selected intervals, examined under a microscope, and measured for stickiness. One nondestructive method for evaluating the extent of surface sticking is to measure the static coefficient of friction by determining the tangent of the angle of inclination at which the treated silicone elastomer just begins to slide when placed on another treated silicone elastomer (typical mating surface) or glass (to screen out changes due to oxidation of the mating surface). Results shown in the figures on the next page indicate that the exposure of silicone elastomers to low levels ($\sim 2.5 \times 10^{18}$ atoms/cm²) of AO can reduce surface sticking without causing extensive surface cracking.



Static coefficient of friction as a function of AO treatment dose. Left: Silicone elastomer on silicone elastomer. Right: Silicone elastomer on glass.



Microscope images of seal samples as a function of AO dose.

Find out more about the research of Glenn's Space Environmental Durability Branch:

<http://www.grc.nasa.gov/WWW/epbranch/ephome.htm>

Glenn Contact:

Sharon K. Miller, 216-433-2219,
Sharon.K.Miller@nasa.gov

Authors:

Sharon K. Miller and Bruce A. Banks

Headquarters Program Office:

Exploration Systems Mission Directorate

Programs/Projects:

Crew Exploration Vehicle, International Space Station, Hubble Space Telescope

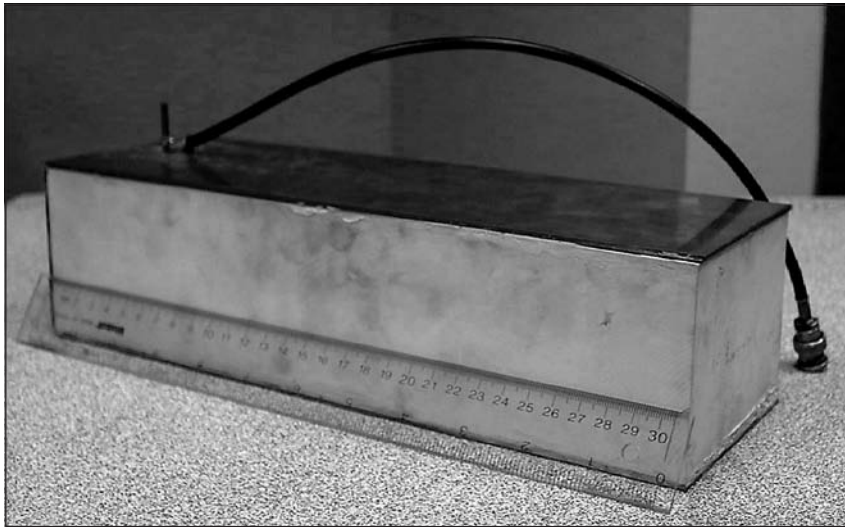
This represents less than a day's worth of exposure in low Earth orbit at the *International Space Station* altitude, or about 2 min of exposure in a typical ground-based AO plasma system. This level would reduce light contact sticking of seals. Reducing the sticking of seals that are compressed together would take a longer, but still acceptable, treatment time. The short treatment time and the benefit gained make the treatment of silicone elastomer seals with AO to reduce sticking both effective and practical.

A black and white photograph of a sunset or sunrise over a body of water. The sun is a bright, glowing orb on the right side of the horizon, creating a lens flare effect with multiple rays of light. The water in the foreground is dark and shows some ripples. The sky is a deep black, dotted with small white stars. The word "Communications" is written in a white, sans-serif font on the left side of the image, positioned just above the horizon line.

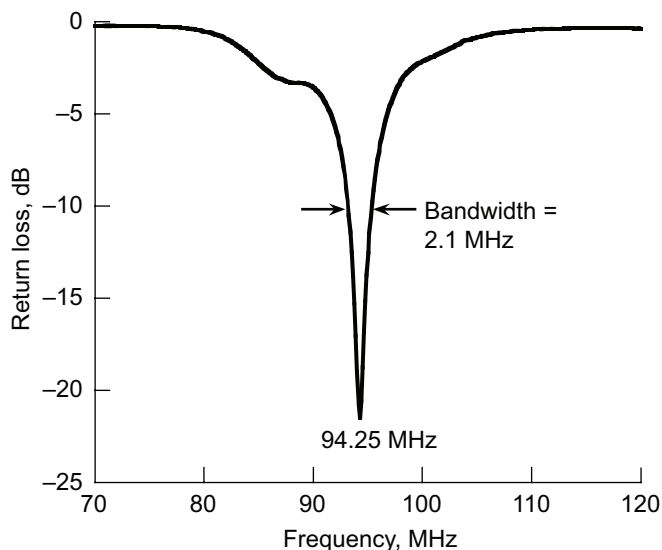
Communications

Very High Frequency Antenna Developed for Sensor and Short-Range Communication Applications

Very high frequency (VHF) communication systems operate between 30 and 300 MHz. This frequency range is useful for aerospace, naval, and ground applications that require robust, line-of-sight communication. Because VHF communication systems are not impacted by topographic impediments as much as higher frequency systems are, VHF is promising for use in lunar surface applications where ad hoc networks will be needed to create reliable links in a wide variety of challenging environments.



One-quarter-wavelength microstrip patch antenna. Radiofrequency power is radiated or received at the aperture defined by the width and thickness parameters.



Return loss (S_{11}) for patch antenna.

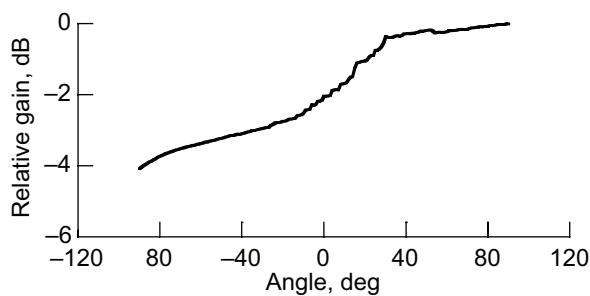
VHF antennas developed under this program are tailored for NASA applications. For most applications, the antenna is mounted so as to minimize interactions with nearby metallic structures, since these interactions degrade antenna performance. However, as the need for more closely networked communication and sensor systems grows, there is also a need to develop VHF antennas that are electrically small and operate in close proximity to metallic structures. At the NASA Glenn Research Center, we are developing microstrip patch antennas that can be mounted directly onto metallic structures. The basic design consists of a rectangular patch that is one-quarter-wavelength long in the resonant direction. The antenna size is minimized by filling the space between the upper and lower plates with a high dielectric constant ($\epsilon_r = 10$) material.

The photograph shows one of the patch antennas, which is 30.5 cm long, 10.2 cm wide, and 7.6 cm thick. The graph shows that the center frequency of the antenna is 94.2 MHz, as evidenced by the minimum return loss, and that the antenna operates over a bandwidth of 2.1 MHz. The 10-dB bandwidth denotes the bandwidth over which the return loss (S_{11}) is less than -10 dB, which is roughly equivalent to the specification that the voltage standing wave ratio (VSWR) be maintained at less than 2:1 over the bandwidth of the antenna. We have observed that the bandwidth can be adjusted by altering the input impedance of the antenna.

We have modeled the performance of one-quarter-wavelength patch antennas and experimentally measured the performance. The three-dimensional plot on the next page shows the simulated realized antenna gain of the patch antenna shown in the photograph. This figure of merit takes into account the efficiency of

the antenna as well as the directivity and, thus, provides a direct estimate of the overall antenna performance. The simulated data show that the antenna gain is maximal and almost constant in the plane where the electric field is polarized, parallel to the x-direction in the plot to the right. Antenna gain is much more directional in the plane where the magnetic field is polarized, parallel to the y-direction.

The experimental E-plane copolarization data are shown in the following graph. The measurements were taken by transmitting the VHF signal via a dipole antenna, and the patch antenna was used as the receive antenna. The E-field orientation of the patch antenna was scanned over the range -90° to 90° with respect to the E-field orientation of the dipole antenna (0° is broadside). The experimental data indicate less than 4-dB difference in received power over the entire scan. Concurrent scans taken at 93.2 and 95.2 MHz show less than a 2-dB difference in received power, in comparison to the 94.2-MHz data. This confirms that the antenna operates over a 2-MHz bandwidth, consistent with the return loss data.



Electric plane data from one-quarter-wavelength microstrip patch antenna. Frequency, 94.2 MHz.

Glenn Contacts:

James A. Nessel, 216-433-2546, James.A.Nessel@nasa.gov

Dr. Félix A. Miranda, 216-433-6589, Felix.A.Miranda@nasa.gov

Authors:

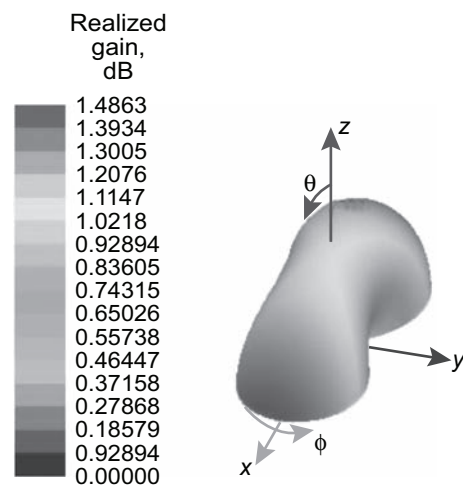
Dr. Carl H. Mueller, James A. Nessel, and Dr. Félix A. Miranda

Headquarters Program Office:

Exploration Systems Mission Directorate

Programs/Projects:

Exploration Missions



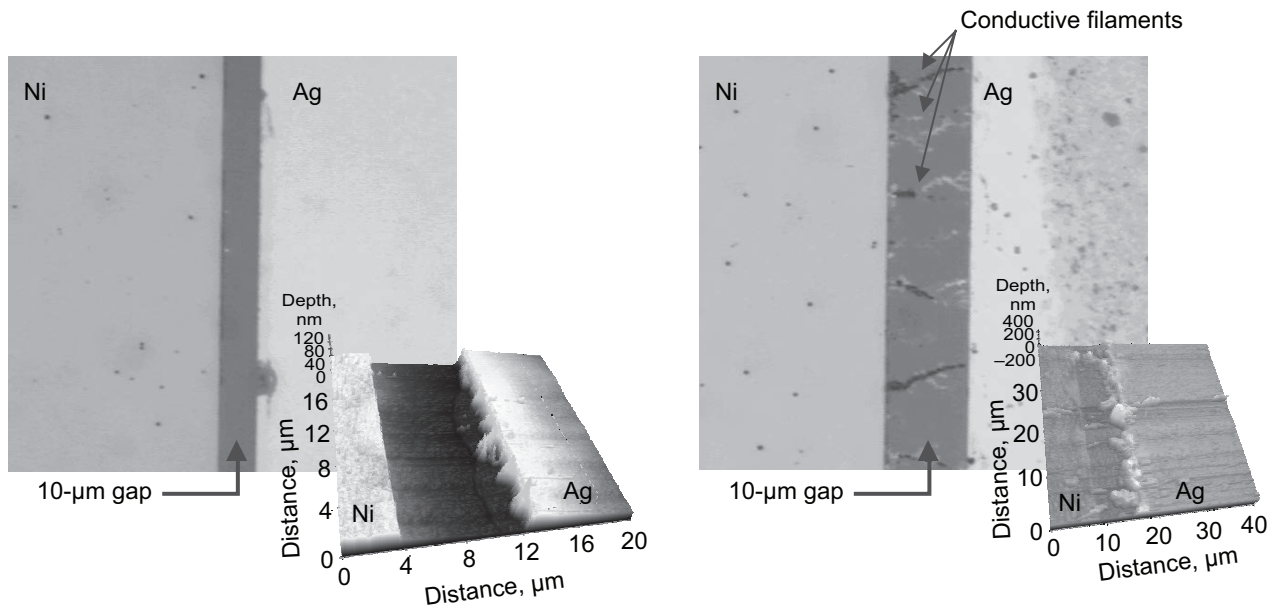
Simulated realized gain of one-quarter-wavelength microstrip patch antenna. The electric and magnetic fields are polarized parallel to the x- and y-directions, respectively. θ denotes the orientation between the patch antenna and the transmit antenna, with the E-fields of both antennas parallel to the x-direction. This figure is shown in color in the online version of this article (<http://www.grc.nasa.gov/WWW/RT/2007/Comm/01-RCA-mueller.html>).

Novel Nanoionics-Based Radiofrequency Switch Developed and Demonstrated

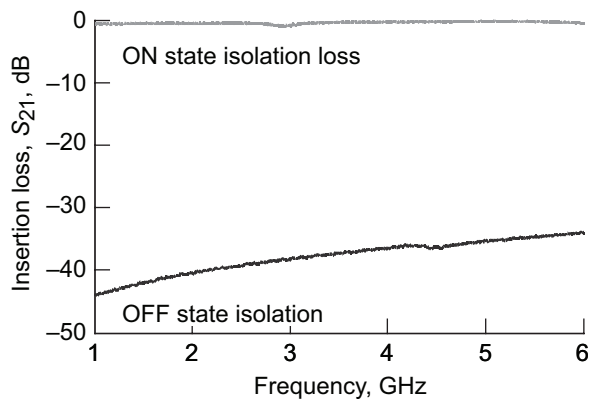
Radiofrequency (RF) switches, basic building blocks for communications and control systems, are used to multiplex signals for system reconfigurability and dynamic control. Applications include portable, mobile, and satellite communication systems, particularly where power is scarce (e.g., cell phones, personal digital assistants (PDAs), laptops, phased-array antennas, sensors, and transceivers). As these communications systems approach higher data rates (gigabits per second) and multifunctional operation, stringent requirements are being placed on RF switch performance. Individually, neither solid-state nor microelectromechanical systems (MEMS) -based switches are capable of meeting this demand. Therefore, a radically new approach based on integrated nanoionics was investigated to combine the superior RF performance and low power consumption of MEMS with the high-speed operation and low cost of solid-state devices.

Integrated nanoionics is an emerging field based on fast ion transport in solids. This technology makes use of a little-known feature of some amorphous materials, which can incorporate relatively large amounts of metal and behave as solid electrolytes. Under appropriate bias conditions (~1 V), metal ions in the solid electrolyte undergo reduction because of electron injection from the cathode to induce metallic growth between the two electrodes, as shown in the following image. Once a conductive pathway is formed, no further power is required to maintain the connection (nonvolatile). One can easily reverse the process by applying a reverse bias to recreate the insulating amorphous layer. This acts as an electrochemical switch that can, theoretically, be fabricated at nanoscale dimensions and operated at the nanosecond scale.

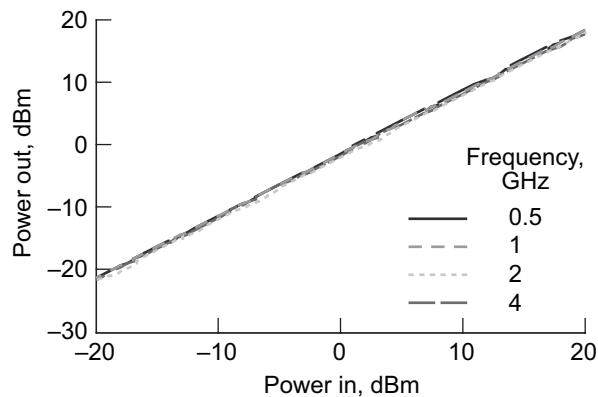
To demonstrate the concept, researchers at the NASA Glenn Research Center, in collaboration with Arizona State University through a NASA grant, designed and fabricated several electrochemical switches. The initial results (summarized in the figures and table on the next page) indicate that, with some further development, this technology could surpass both MEMS and solid-state switches in terms of overall performance and cost. After 1 year of development, nanoionic switches demonstrated performance comparable to that of MEMS (superior performance to solid state) in OFF-state isolation, power/energy consumption, and intermodulation distortion, and they demonstrated performance comparable to that of solid-state devices in ON-state insertion loss, power handling, and predicted cost. Furthermore, because of the ease of fabrication and basic operation of these switches, they could be used in novel device topologies that would be extremely difficult to realize with MEMS or solid-state switches (e.g., single-pole N-throw switches, vertical switches, and multilayer control circuitry).



Photomicrographs (larger images) and associated atomic force microscope images (smaller images at lower right) of nanoionics-based switch. Left: Switch in OFF state. Right: Switch in ON state.



Typical ON/OFF characteristics of a nanoionics-based switch. These measured results are comparable and/or superior to MEMS and solid-state RF switch performance in the same frequency range.



Power transfer curve (power in versus power out) of a typical nanoionics-based switch over its operating range for frequencies between 500 MHz and 4 GHz. No change is evident in the power transfer curve at different frequencies of operation, demonstrating the device's wide bandwidth operation capability.

COMPARISON OF PERFORMANCE OF MEMS-BASED, SOLID-STATE-BASED, AND NANOIONICS-BASED RF SWITCHES

Performance characteristics	MEMS	Solid state	Nanoionics
Frequency range, GHz	0 to 70	0 to 20	0 to 6
Average insertion loss, dB	0.1	0.5	0.5
Average isolation, dB	40	30	35
Actuation voltage, V	5 to 50	3 to 5	1
Power consumption	Microwatts	Milliwatts	Microwatts
Energy consumption	0.1 to 10 microjoules	Microjoules to millijoules	100 nanojoules
Power handling, W	1 to 20	1 to 10	0.5
Intermodulation distortion, dBm	80	70	75
Switching speed, μ sec	1 to 200	0.01 to 0.1	<1 to 10
Size	Square micrometers	Square nanometers to square micrometers	Square nanometers to square micrometers
Unit cost, \$	~\$5	~\$0.50	~\$0.50

Find out more about Glenn's Antenna, Microwave and Optical Systems Branch:

http://ctd.grc.nasa.gov/organization/branches/amosb/HOME/RCA_Home.htm

Glenn Contacts:

James A. Nessel, 216-433-2546, James.A.Nessel@nasa.gov

Dr. Richard Q. Lee, 216-433-3489, Richard.Q.Lee@nasa.gov

Authors:

James A. Nessel and Dr. Richard Q. Lee

LEW Number:

LEW-18313-1

Programs/Projects:

Space Communications and Navigation, Glenn Independent Research and Development

NASA Space Telecommunications Radio System Architecture Updated

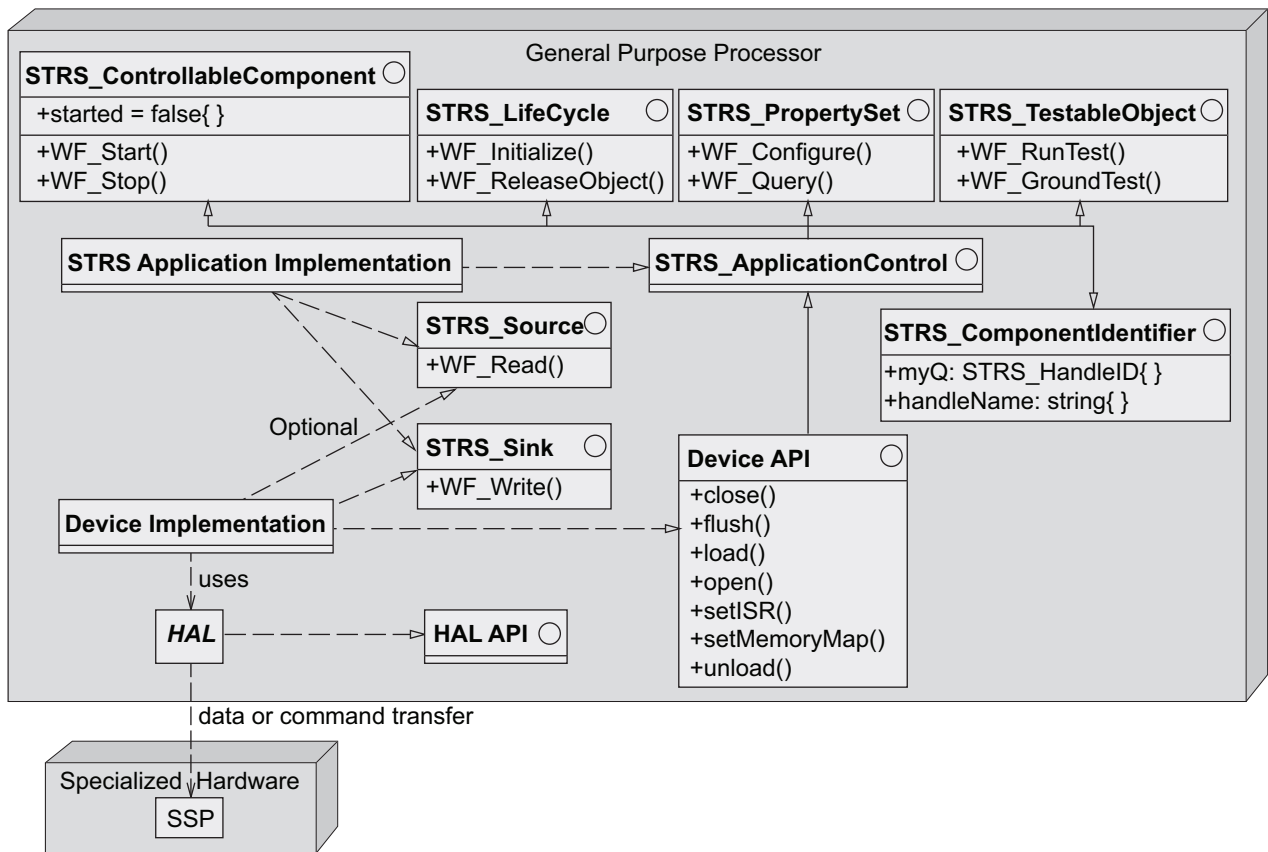
The NASA Glenn Research Center has updated the Space Telecommunications Radio System (STRS) architecture for NASA space-based radios on the basis of reviews by NASA missions, radio providers, and component vendors. Glenn recently released STRS Architecture Standard Version 1.01, which improved the software architecture and refined the STRS infrastructure, the STRS application programming interface (API), and the configuration files.

The STRS API is the well-defined set of interfaces used by the waveform applications to access radio functions or used by the infrastructure to control the waveform applications. The goal is waveform portability and reusability. The STRS infrastructure on the general purpose processor must implement the STRS API to support applications for execution within the radio platform.

The following diagram illustrates the inheritance between the classes and the corresponding implementation objects. It also depicts the hierarchy of include files. A waveform or service is an STRS application that must implement the STRS application control API, which comprises the STRS ComponentIdentifier, ControllableComponent, LifeCycle, PropertySet, and TestableObject APIs.

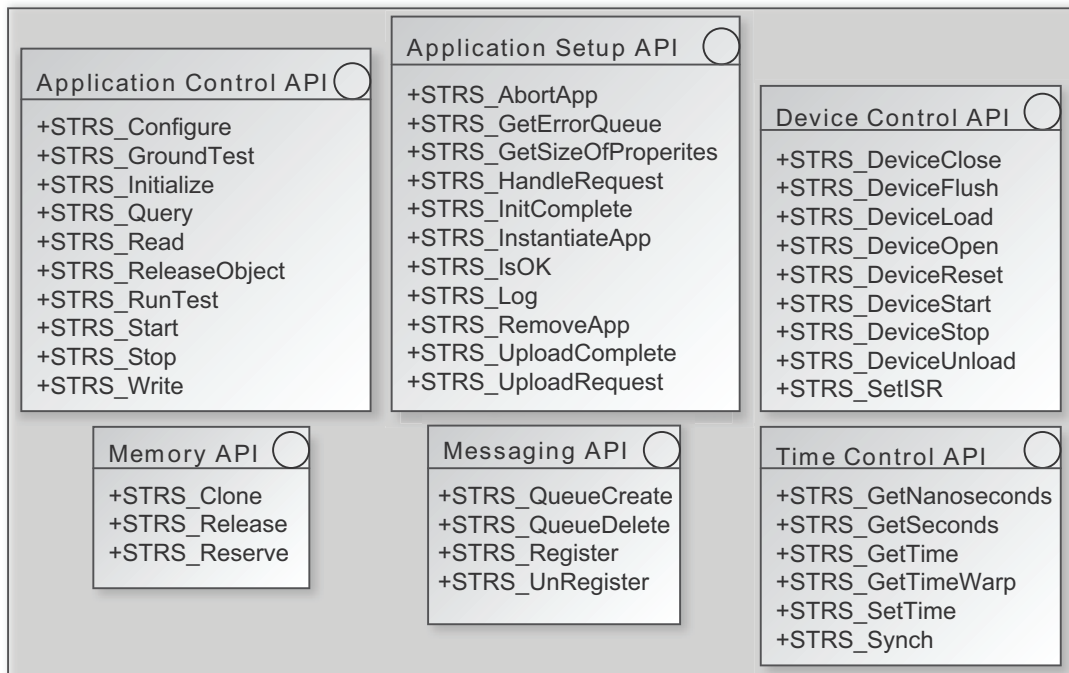
The infrastructure application control methods correspond exactly to the STRS application control API and are used to access those methods by any

STRS application or any portable part of the infrastructure. The infrastructure application control setup methods are used in general or to control one waveform from another. STRS devices are controlled with the STRS infrastructure device control API. An STRS device is an STRS application that can use the platform-specific hardware abstraction layer (HAL) to communicate with and control the specialized hardware. The infrastructure memory methods are used to isolate the memory manipulation to use the memory portably. The messaging methods allow STRS applications to use a single-target handle identification to send messages between applications or to multiple parts of the radio. The ability for waveforms to communicate with other STRS applications is crucial for the operation of radio services as well as for



STRS waveform/device structure. SSP, signal processing.

separating the receive and transmit functionality between two waveforms. The infrastructure messaging API is designed using the publish-subscribe design pattern. The infrastructure time control methods are used to access the hardware and software timers. The STRS infrastructure APIs are also shown in the following diagram.



STRS infrastructure APIs.

STRS configuration files contain platform- and waveform-specific information for the installation and customization of waveforms. The configuration files are used by the STRS infrastructure to determine what files, devices, waveforms, services, and hardware modules are used by the STRS radio. The name of the starting configuration file is specified on the command line when initializing the STRS infrastructure. Waveform configuration files contain information that allows STRS to instantiate and configure the application. The configuration files are defined in Extensible Markup Language (XML) using an XML Schema. The XML Schema definition language is an XML language for describing and constraining the content of XML documents. The XML can be preprocessed to optimize its footprint.

Minimum compliance requires publishing the hardware interface definition and HAL, employing configuration files defined in XML, using selected Portable Operating System Interface for UNIX (POSIX) subsets, and using the STRS API.

Glenn Contacts:

Richard C. Reinhart, 216-433-6588,
Richard.C.Reinhart@nasa.gov

Louis M. Handler, 216-433-8286,
Louis.M.Handler@nasa.gov

Authors:

Janette C. Briones, Louis M. Handler,
Thomas J. Kacpura, and Charles S. Hall

Headquarters Program Office:

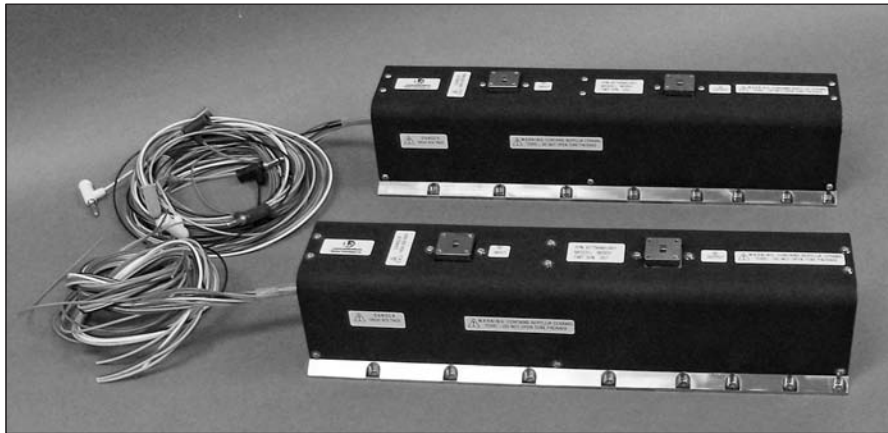
Space Operations Mission Directorate

Programs/Projects:

Space Communications & Data
Systems Project

Lunar Reconnaissance Orbiter Traveling-Wave Tube Completed

The Lunar Reconnaissance Orbiter (LRO) will be the first mission launched for NASA's Return to the Moon program. The traveling-wave tube (TWT), which will serve as the high-power microwave amplifier for the primary data channel back to Earth, is a mission critical item. Two TWTs have been completed, meeting all specifications, to provide the mission with a flight unit and a spare. They provide the 40 W of microwave power at 25.65 GHz needed to provide a 100-megabits-per-second (Mbps) Ka-band data link from lunar orbit to White Sands, New Mexico. The TWTs (shown in the photograph) have a 300-MHz bandwidth and use WR-34 waveguide for radiofrequency (RF) input and output because of the new frequency band.



LRO traveling-wave tubes. Copyright L-3 Communications Electron Technologies, Inc.; prepared under contract to NASA.

The TWTs were designed and manufactured by L-3 Communications Electron Technologies, Inc. (L-3 ETI) of Torrance, California. L-3 ETI is now building the electronic power conditioners (EPCs) that convert the spacecraft bus voltage to the voltages used in the TWT to power the TWT. After the EPCs are built, they will be mated with the TWTs to form traveling-wave-tube amplifiers (TWTAs). The TWT has an RF efficiency of 50 percent, weighs 1.5 kg (just over 3 lb), and measures 370 by 90 by 90 mm (almost 15 in. long). The TWT design has been baselined for use in the Communication Navigation and Networking Reconfigurable Testbed (CoNNeCT) project and on the Lunar Surface Communications Terminal.

The NASA Glenn Research Center is managing the contract for the LRO Project Office as a follow-on program to the 200-W, 32-GHz TWT development (ref. 1). Within Glenn, the Electron & Optical Device Branch of the Communications Technology Division is managing the contract under the supervision of the Advanced Capabilities Project Office. Glenn's Electron & Optical Device Branch has a long tradition of advancing the state of art of space TWTs for NASA missions, including performing design work on the TWT for the Mars Observer mission and providing the 32-GHz TWTA for the Cassini mission to Saturn. The LRO Project Office is managed by the NASA Goddard Space Flight Center.

Reference

1. Wilson, Jeffrey D.: High-Power Traveling-Wave Tube Space Qualified at Record Power Levels. Research & Technology 2007. NASA/TM—2008-215054, 2008. <http://www.grc.nasa.gov/WWW/RT/2007/Comm/07-RCE-wilson2.html>

Find out more about this research:

Glenn's Electron & Optical Device Branch:

<http://ctd.grc.nasa.gov/organization/branches/eodb/eodb.html>

Lunar Reconnaissance Orbiter (LRO):

<http://lunar.gsfc.nasa.gov>

L-3 Communications Electron Technologies, Inc. (outside URL):

<http://www.l-3com.com/eti/>

NASA Exploration Systems:

http://www.nasa.gov/mission_pages/exploration/main/

Glenn Contacts:

Dale A. Force, 216-433-3520,
Dale.A.Force@nasa.gov

Dr. Rainee N. Simons, 216-433-3462,
Rainee.N.Simons@nasa.gov

Author:

Dale A. Force

Headquarters Program Office:

Exploration Systems Mission Directorate

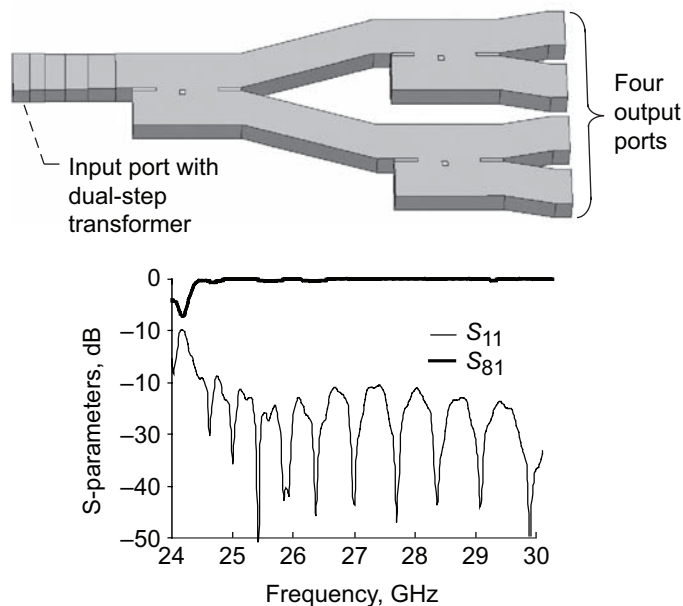
Programs/Projects:

Lunar Reconnaissance Orbiter

Simulation Study Conducted for a Wide-Band, Low-Loss, Short-Slot Coupler-Based Power Combiner

Under the Solid-State Power Amplifier activity at the NASA Glenn Research Center, a simulation study was performed to develop an extremely low loss and wide-band power combiner. The communications requirements for future space missions will necessitate much higher data flow rates, which ultimately require high-power microwave and millimeter-wave sources. The power available from the most promising solid-state devices, such as gallium nitride high electron mobility transistors is in the single digits of watts; however, most future missions will require power levels in the tens of watts. The power combining that will be needed is the motivation for this work.

Instead of the older, more established power combiners, we chose to use nonstandard waveguide short-slot couplers as the basic building block. We optimized the cross-sectional dimensions, slot-length, and tuning pin for a four-to-one combiner in the Ka band. The center frequency was 27.5 GHz. We obtained a total combining efficiency (with a back-to-back splitter and combiner) of greater than 86 percent over a 5-GHz bandwidth, using the best available experimental loss values reported for rectangular waveguides at these frequencies. Our predictions challenge the state of the art when both combining efficiency and bandwidth are considered. The nonstandard waveguide dimensions were transitioned into standard WR-42 dimensions with dual-step transformers. The figures show the 1:4 splitter and insertion/return losses for a back-to-back connection.



Top: Complete 1:4 power splitter composed of three short-slot couplers and a matching transformer at the input. Bottom: Return loss (S_{11}), and insertion loss (S_{81}) of the back-to-back combination of a 1:4 splitter-combiner tandem connection. The usable bandwidth (S_{11} below -20 dB) is over 5 GHz, and the insertion loss (upper trace) is excellent.

A four-to-one turnstile junction for power combining in this frequency band was also developed. It has the advantage of small size, low mass, and extremely low loss. The bandwidth is 2 GHz as it was developed in standard WR-42 waveguide. Although it has excellent electrical properties, it may not be suitable for low-cost manufacturing because of the orientation of tuning pins interior to the main turnstile junction.

A variation of the turnstile approach was developed to permit the combination of more than four devices. It is based on a distributed combining architecture and uses coupling apertures along a “main guide” that accumulates combined power as more “entering pipes” are encountered from the beginning to end of the combiner. This concept is currently under study. We have concluded that the conflicting requirements of low loss; wide bandwidth; a compact, small size; manufacturability; and compatibility with standard waveguide connections may be partially met using nonstandard cross-section coupling regions followed up with dual-step transformers. Advance simulations show that results for the new designs rival the best results reported in the literature.

Glenn Contacts:

Karl R. Vaden, 216-433-8831,
Karl.R.Vaden@nasa.gov

Edwin G. Wintucky, 216-433-3510,
Edwin.G.Wintucky@nasa.gov

Author:

Dr. Jon C. Freeman

Headquarters Program Offices:

Exploration Systems Mission Directorate

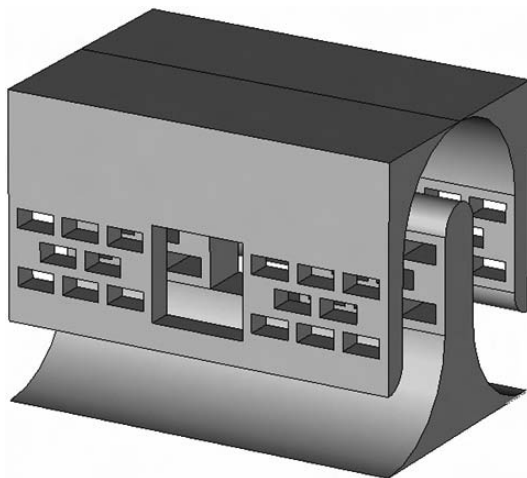
Programs/Projects:

Solid-State Power Amplifiers

Terahertz Amplifier Design Improved With Metamaterial

Terahertz waves are electromagnetic waves with frequencies higher than microwaves but lower than infrared radiation and visible light. They possess exciting potential advantages for radio astronomy spectroscopy; nondestructive testing of aircraft and spacecraft; non-ionizing medical imaging and tumor detection; high-resolution close-range radar; and security detection of chemicals, biological agents, and weapons. However, this frequency region (0.3 to 3.0×10^{12} Hz, or 0.3 to 3.0 THz) is largely underutilized and is referred to as the “terahertz gap” of the electromagnetic spectrum because compact moderate power amplifiers are not available.

In this in-house work at the NASA Glenn Research Center, we investigated the use of metamaterials—engineered materials with unique electromagnetic properties—to increase the power and efficiency of terahertz amplification in two types of vacuum electronics slow-wave circuits. The first type of circuit (refs. 1 to 3) has a folded waveguide geometry in which we investigated anisotropic dielectrics and holey metamaterials, which consist of arrays of subwavelength holes.



Section of a terahertz folded-waveguide traveling-wave tube circuit with hole arrays on walls.

The second type of circuit has a planar geometry with a meander transmission line to carry the electromagnetic wave and a metamaterial structure embedded in the substrate. Computational results are more promising with this circuit. Preliminary results suggest that the metamaterial structure is effective in decreasing the electric field magnitude in the substrate and increasing the magnitude in the region above the meander line, where it can interact with an electron sheet beam. In addition, the planar circuit is less difficult to fabricate and can enable a higher current. More work is needed to investigate other planar geometries, optimize the electric-field/electron-beam interaction, and design focusing magnet geometries for the sheet beam.



Terahertz planar traveling-wave tube circuit with metamaterial embedded in substrate.

References

1. Wilson, J.D.; and Chevalier, C.T.: Robust Optimization of High-Frequency Traveling-Wave Tube Slow-Wave Circuits. *IEEE Trans. Electron Devices*, vol. 54, issue 5, 2007.
2. Chevalier, Christine T.; Wilson, Jeffrey D.; and Kory, Carol L.: Comparing the Robustness of High-Frequency Traveling-Wave Tube Slow-Wave Circuits. NASA/TP—2007-214700, 2007. <http://gltrs.grc.nasa.gov>
3. Starinshak, David, P.; Wilson, Jeffrey, D.; and Chevalier, Christine, T.: Investigating Holey Metamaterial Effects in a Terahertz Traveling-Wave Tube Amplifier. NASA/TP—2007-214701, 2007. <http://gltrs.grc.nasa.gov>

Find out more about the research of Glenn's Electron & Optical Device Branch:

<http://ctd.grc.nasa.gov/organization/branches/eodb/eodb.html>

Glenn Contacts:

Dr. Jeffrey D. Wilson, 216-433-3513,
Jeffrey.D.Wilson@nasa.gov

Karl R. Vaden, 216-433-8131,
Karl.R.Vaden@nasa.gov

Authors:

Dr. Jeffrey D. Wilson, Karl R. Vaden,
Christine T. Chevalier, and
Dr. Carol L. Kory

Headquarters Program Offices:

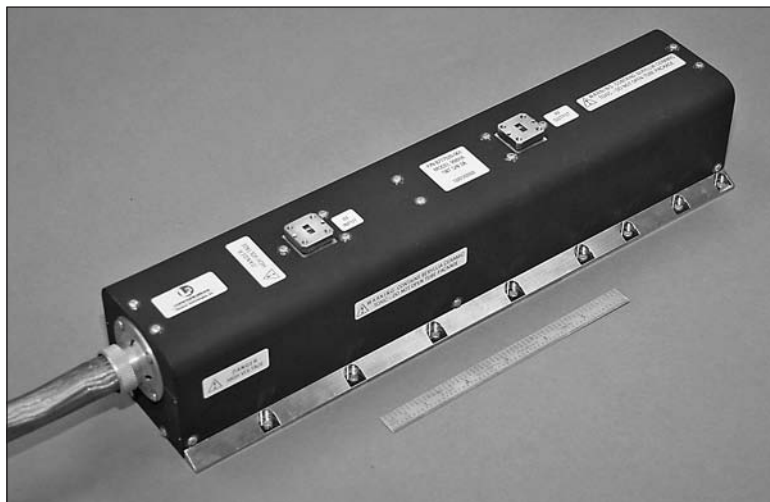
Science Mission Directorate, Exploration
Systems Mission Directorate

Programs/Projects:

Glenn's Independent Research and
Development Fund

High-Power Traveling-Wave Tube Space Qualified at Record Power Levels

The NASA Glenn Research Center, the Jet Propulsion Laboratory (JPL), and L-3 Communications Electron Technologies, Inc., (L-3 ETI) are pushing the limits on efficiently transmitting more data to the ground for NASA's space exploration missions. This year, L-3 ETI successfully completed building and space qualification testing of a 200-watt, high-efficiency Ka-band traveling-wave tube (TWT) under a Glenn-managed contract. The completion of this milestone marks the highest power Ka-band TWT ever space qualified. This TWT has been mated with an electronic power conditioner to produce a space-qualified traveling-wave-tube amplifier (TWTA) under a JPL-managed program.



The 200-watt Ka-band space-qualified traveling-wave tube manufactured by L-3 Communications ETI, Inc. Copyright L-3 Communications Electron Technologies, Inc.; prepared under contract to NASA.

The space qualification of the TWT consisted of

- (1) A 750-hr burn-in to confirm the stability of the cathode, focusing, power, and gain
- (2) A thermal vacuum test in which performance was monitored over eight thermal cycles from -35 to $+75$ °C at a vacuum pressure of less than 5×10^{-5} torr
- (3) A random vibration test
- (4) A pyrotechnic shock test

At each intermediate step and again after all testing was completed, the unit was exercised through a full functional and operational test regime. In all cases, the TWT performed flawlessly. A second TWT of this model was subjected to thermal vacuum cycles from -20 to $+95$ °C and also showed stable performance. These tests provide confidence in the reliability of the model. This is important because the lower power Ka-band L-3 ETI space TWTs that have been built for the Lunar Reconnaissance Orbiter and Kepler missions are based on this model with very similar electrical and mechanical designs.

This new TWTA model is 6 times more powerful than the previous highest power Ka-band space TWTA, and it is 20 times more powerful than the Cassini TWTA, which has been orbiting Saturn since July 2004. This increase in power capability directly translates into higher data transmission rates from greater distances, more flexibility, and more channels available for space communications.

This advance in TWTA technology will improve the speed and efficiency of data communications, enabling real-time, high-resolution video transmission from space. High-power TWTA's align with the U.S. President's vision for space exploration by increasing the science data rate-of-return for exploration missions by a factor of 6, enabling deeper, more sophisticated exploration of the solar system.

Find out more about the research of Glenn's Electron & Optical Device Branch:

<http://ctd.grc.nasa.gov/organization/branches/eodb/eodb.html>

Glenn Contacts:

Dr. Jeffrey D. Wilson, 216-433-3513,
Jeffrey.D.Wilson@nasa.gov

Dr. Rainee N. Simons, 216-433-3462,
Rainee.N.Simons@nasa.gov

L-3 Communications Electron Technologies, Inc., Contact:

Neal R. Robbins, 310-517-7548,
Neal.Robbins@L-3com.com

Author:

Dr. Jeffrey D. Wilson

LEW Number:

LEW-18220-1

Headquarters Program Office:

Exploration Systems Mission Directorate

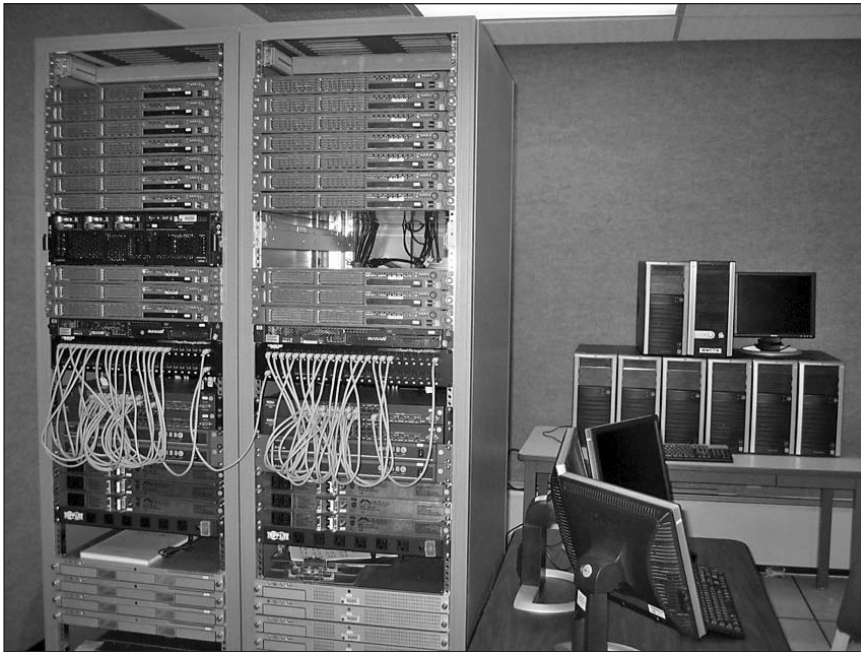
Programs/Projects:

Nuclear Technology and Demonstration

Special Recognition:

2006 R&D 100 Award, 2007 Space Act Award

Glenn's Network Emulation Laboratory Established as a Networking Research and Emulation Environment for NASA



Network Emulation Laboratory (NEL).

The Satellite Networks and Architecture Branch of the Communications Technology Division at the NASA Glenn Research Center has developed and established the Network Emulation Laboratory (NEL). NEL is a technology cross-cutting laboratory that provides the division with a reusable infrastructure focusing on network research and simulation/emulation services. Currently, the lab is composed of a heterogeneous 45-node cluster that includes

- Twenty-three HP DL-145 Servers running RedHat Linux
- Two IBM eServers running Debian Linux
- Eleven Apple X-Servers running Mac OS X
- Nine HP DL-110 Computers running MS Windows XP

In addition, the lab has connections to both Internet Protocol version 4 (IPv4) and IPv6 external networks.

Currently, NEL is supporting the following programs:

Channel Emulator development and support: The Channel Emulator (CE) is a realistic and flexible platform that emulates space-based links by providing delay, jitter, packet corruption, dynamic link configuration, and one-way communications. The CE functions as a level 2 link-layer 802.3 bridge that allows it to accommodate a number of protocols in addition to the IP. The CE also incorporates the 802.1q virtual interface, which permits the partitioning of a single physical networking interface into many interfaces that represent physical devices on a satellite. The current version is distributed on a Knoppix Live CD. More information can be obtained at <http://channel-emulator.grc.nasa.gov>.

Network Emulation Laboratory: NEL provides an end-to-end networking emulation that can be used throughout the mission lifecycle from requirements development and mission design through operational software testing. NEL executes all emulations on the basis of scenario parameters that contain the number of entities, data links, and the type of data traversing the links. It can determine throughput, source and destination, and a number of other user-defined parameters. Recently, NEL performed emulations to evaluate protocols as part of the Space Communications Testbed, which analyzed communications patterns for a *Crew Exploration Vehicle* mission on a trans-lunar injection orbit. NEL is planning to provide services for the Communication Navigation and Networking Reconfigurable Testbed (CoNNeCT) project, where an on-ground testbed will be created to evaluate potential experiments before they are uploaded to the *International Space Station*.

Delay-tolerant networking research: Delay-tolerant networking (DTN) is a recent technology that promises to be an effective solution for communicating in the harsh environments found in space exploration. NEL provided an environment to test current DTN specifications and software, which are still being finalized and developed by the research community. NEL was integral to research involving modifications and improvements to DTN, including efforts to develop functions necessary to reduce support costs in operational systems. NEL also provided a staging ground for deploying the first experimental DTN software to be used onboard an operational satellite in space. Finally, NEL provided members of the DTN research community with a means to reach active DTN nodes in order to test communications and enhancements over both IPv4 and IPv6 networks.

Find out more about this research:**Glenn's Satellite Networks and Architectures Branch:**

<http://ctd.grc.nasa.gov/capabilities/branches/snab/snab.html>

Channel Emulator:

<http://channel-emulator.grc.nasa.gov>

Glenn Contacts:

Richard A. Slywczak, 216-433-3493, Richard.A.Slywczak@nasa.gov

Joseph A. Ishac, 216-433-6587, Joseph.A.Ishac@nasa.gov

Authors:

Richard A. Slywczak and Joseph A. Ishac

Headquarters Program Office:

Exploration Systems Mission Directorate

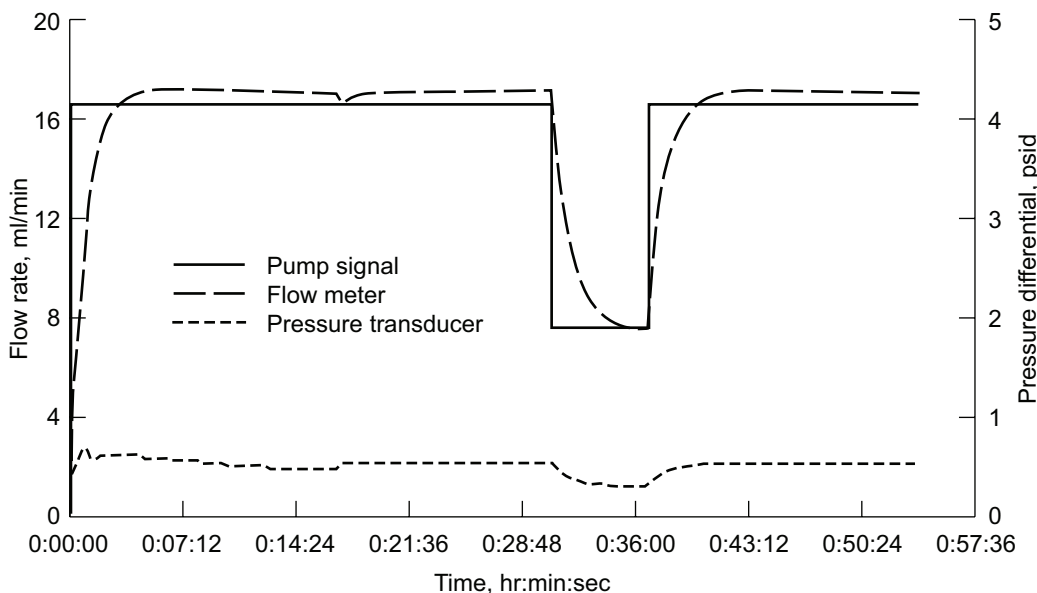
Programs/Projects:

Crew Exploration Vehicle; Communication, Navigation, Networking Reconfigurable Testbed; Satellite Missions; Command, Control, Communications, and Information

A black and white photograph of a sun rising over a horizon, with a starry sky above. The sun is a bright, multi-pointed starburst on the right side of the horizon. The horizon line is slightly curved, suggesting a view from space or a high-altitude perspective. The sky is dark with scattered stars. The foreground shows a dark, textured surface, possibly water or a planetary surface, with some light reflecting off it.

Space Processes and Experiments

Magnetic Stirrer Tested for a System To Produce Intravenous Fluid During Exploration Missions



Flow rate and pressure data during surge testing of a water filter.

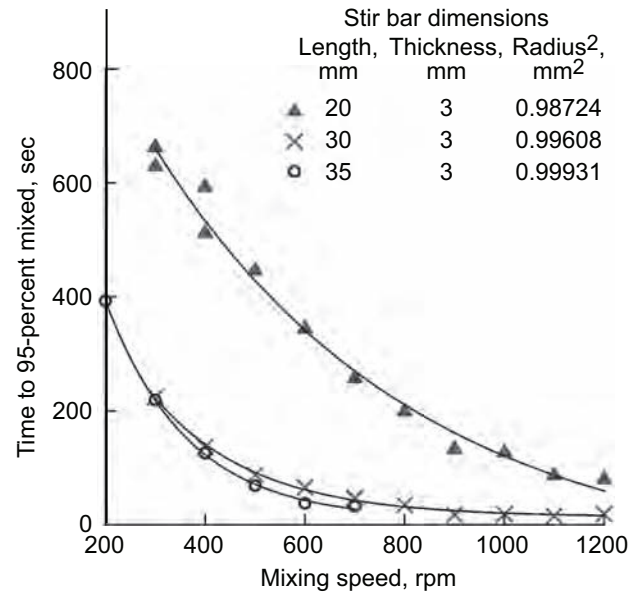
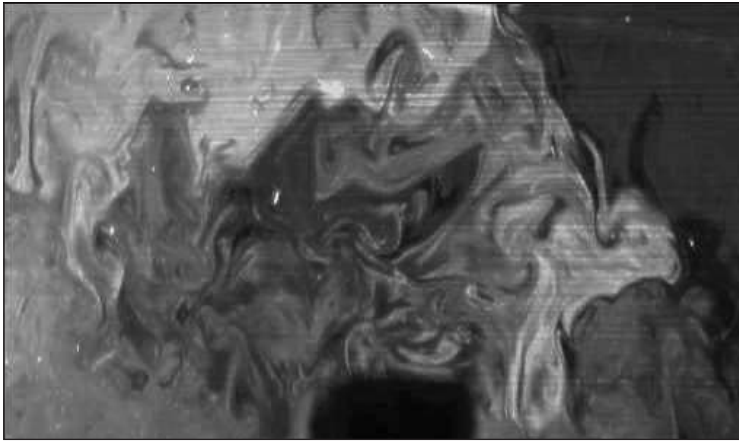
The longer duration crewed missions outlined in the Vision for Space Exploration increase the likelihood that intravenous (IV) fluids will be needed to treat a medical emergency. For example, severe burns may require up to 32 liters of IV fluid for proper treatment (ref. 1). Ready-to-use IV fluids have a relatively short shelf life, and the effects of radiation are uncertain. A system for generating medical-grade water from a potable water source and for mixing the sterile water with powders or concentrates to prepare IV fluids would reduce the storage requirements for IV fluids. The NASA Glenn Research Center analyzed several potential methods for doing this. The main parts of the system include a process to sterilize potable water and a technique to create a homogenous solution from drug concentrate and sterile water to generate the IV fluid on demand.

Several filtration technologies were considered for producing sterile water. Deionization, forward and reverse osmosis, and absorption were chosen for further evaluation to define the flow characteristics of the filters, predict performance in microgravity, and determine whether the filtrate passed U.S. Food and Drug Administration (FDA) specifications for Sterile Water for Injection. The preceding graph shows an example of data collected during flow surge testing, including pressure and flow rate over time.

A standard magnetic stirrer was selected from numerous other technologies as the mixing method because of its storage and power requirements and its high mixing efficiency. Ground experiments validated the amount of time to mix the fluid to within the concentration tolerances defined by the FDA. A

noninvasive optical diagnostic, planar laser-induced fluorescence (PLIF), was used to quantify these mixing times. In this optical technique, a laser source illuminates a plane in the flow field of interest. If the laser wavelength is resonant with the optical shift of a chemical species present in the sheet, a portion of the incident light is absorbed by the species and is emitted at a longer wavelength. This fluorescence is imaged, and the amount of light detected is proportional to the concentration of the species within the corresponding measurement volume and the local flow field conditions.

To mimic the production of normal saline—a standard IV fluid, researchers acquired PLIF image sequences of a salt solution containing fluorescent dye being mixed with distilled water (as shown in the sample PLIF image on the next page). Mixing times for different sized stir bars were determined by a histogram



Left: Example of an image obtained using PLIF. Right: Mixing times for three stir bar lengths at various speeds. The left image is shown in color in the online version of this article (<http://www.grc.nasa.gov/WWW/RT/2007/Proc-Exp/01-REB-barlow.html>).

analysis of the image sequence (as shown in the plot on the right). In fiscal year 2007, over 200 experiments were performed aboard NASA's reduced-gravity aircraft to rule out any complications that might arise with this mixing method in low gravity.

The information gathered throughout numerous ground experiments in normal and reduced gravity environments will help NASA's ongoing effort to design a system to generate IV fluids in the event of a medical emergency during exploration missions. A proof-of-concept apparatus will be tested aboard the International Space Station in 2010.

Reference

1. The Society of U.S. Naval Flight Surgeons: Boards of Flight Surgeons. United States Naval Flight Surgeon Handbook, 2nd edition, 1998.

Find out more about the IV fluid research at Glenn:

<http://exploration.grc.nasa.gov/Exploration/Advanced/Human/Fluids/>

Glenn Contacts:

Karen L. Barlow, 216-433-3543,
Karen.L.Barlow@nasa.gov

John B. McQuillen, 216-433-2876,
John.B.McQuillen@nasa.gov

Authors:

Karen L. Barlow and John B. McQuillen

Headquarters Program Office:

Human Research Program

Programs/Projects:

Exploration Medical Capability

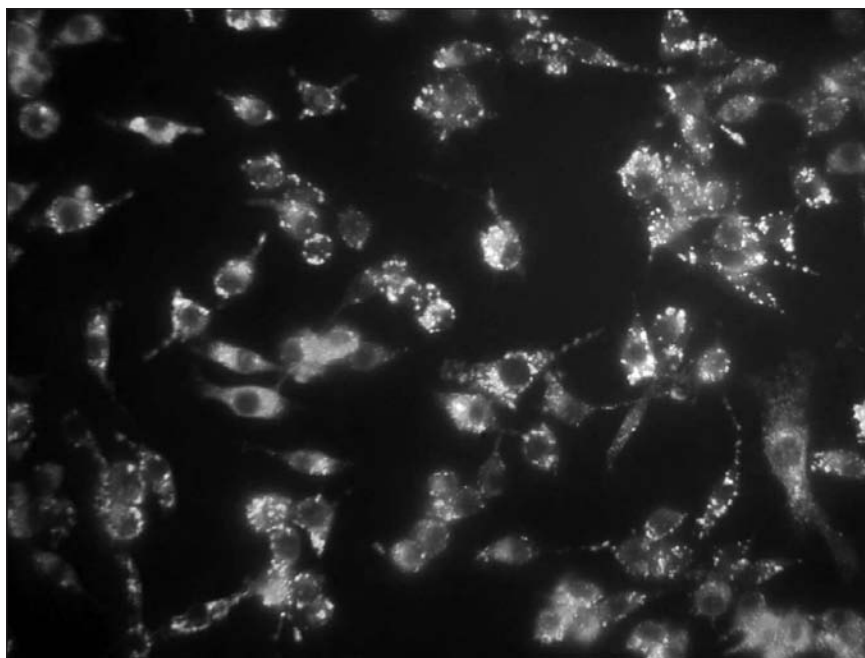
Lunar Dust Toxicology Studied In Vitro at the Cellular Level

NASA has near-term plans to return astronauts to the lunar surface. A major concern is astronaut exposure to the lunar dust. Numerous astronauts of the Apollo era complained of respiratory symptoms (e.g., irritation and swollen nasal cavities) following extravehicular activities. On Earth, ultrafine and fine airborne particles have been implicated in cardiovascular and pulmonary diseases such as atherosclerosis, strokes, chronic bronchitis, pneumoconiosis lung disease, and cancer. To date, however, the toxicity associated with the inhalation of lunar dust is undetermined. Through the Summer Faculty Fellowship program at the NASA Glenn Research Center, the in vitro cellular toxicity of lunar dust analogs was investigated.

Lunar dust is composed of a complex mixture of ultrafine ($<0.1 \mu\text{m}$) and fine ($<2.5 \mu\text{m}$) particles that contain silica (SiO_2), aluminum oxide (Al_2O_3), and iron oxide (FeO). Accordingly, macrophage and epithelial pulmonary cells were cultured and exposed to fine silica and aluminum oxide, as well as fine and ultrafine (dyed) polystyrene beads. The response was quantified as a function of particle type (size and composition) and exposure level (quantity and exposure time).

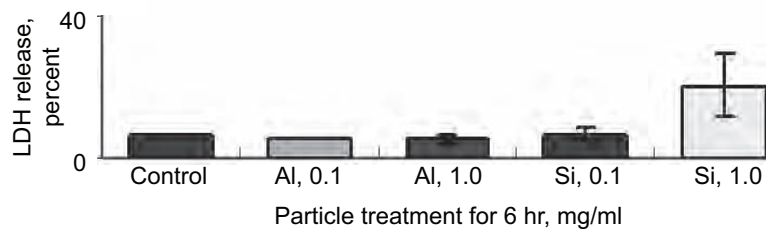
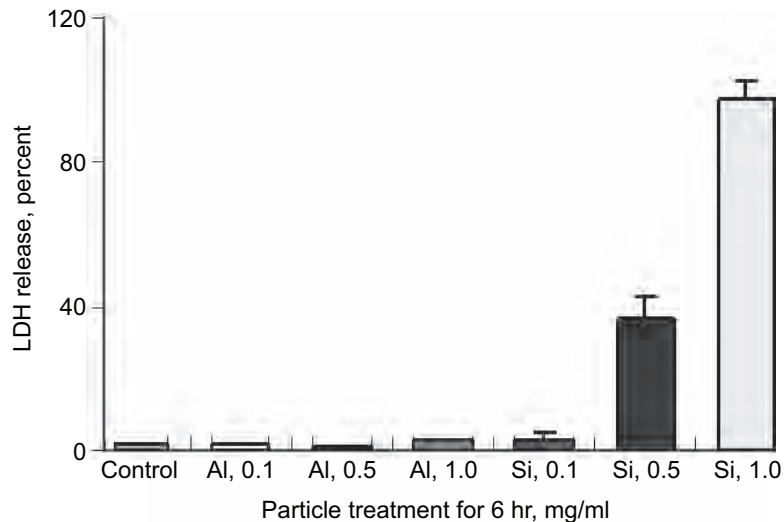
The phagocytic activity of the cells (i.e., their ability to ingest particles) was examined using both fluorescence and phase contrast microscopy. Phagocytosis by macrophage cells is important in the clearance of dust particles from the lungs. The macrophage cells were seen to be very efficient in

ingesting the polystyrene beads (see the photograph). Following a 6-hr exposure, macrophage cells had extended pseudopods and polystyrene beads were localized in the cytoplasmic region of these cells with few beads found in the nuclear regions. After 24 hr, the macrophage cells were round, clumping, and lacked pseudopods, indicating that phagocytosis was impaired. It is interesting that after 6 hr the epithelial cells did not contain polystyrene beads and that after 24 hr the majority of the polystyrene beads appeared to coat primarily the surface of the cells. Following 6-hr exposures to both fine SiO_2 and Al_2O_3 , the macrophage cells also possessed active pseudopods, indicating cell-particle interactions. After 24 hr, a significant number of the cells exposed to SiO_2 exhibited impaired phagocytic ability. Exposure to Al_2O_3 also reduced the number of phagocytic cells, but much less than for SiO_2 . For the epithelial cells, the metal oxide particles, as with the beads, were clustered on the surface.



Fluorescence image of macrophage cells after 6-hr exposure to 100-nm blue polystyrene beads. The cells are stained red. This photograph is shown in color in the online version of this article (<http://www.grc.nasa.gov/WWW/RT/2007/Proc-Exp/02-REB-fischer1.html>).

The direct cytotoxic ability of fine SiO_2 and Al_2O_3 was also examined using the release of lactate dehydrogenase (LDH). LDH is a stable cytoplasmic enzyme that is released into the cell culture supernatant upon damage of the cytoplasmic membrane. LDH assay results typically correlate well with the number of damaged cells. The macrophage cells exposed to 1.0 mg/ml SiO_2 for 6 hr had increased cellular damage, as measured by LDH release (see the graphs on the next page). The epithelial cells showed slight toxicity to SiO_2 at the same exposure time and dose. Only a higher dose (5.0 mg/ml) or a 24-hr exposure of epithelial cells to SiO_2 resulted in significant cytotoxicity. Importantly, both cell types showed minimal cytotoxic response following exposure to fine Al_2O_3 .



LDH release from cells after 6-hr exposure to different doses of silica and aluminum oxide. Top: Macrophage cells. Bottom: Epithelial pulmonary cells.

Glenn Contact:

Dr. David G. Fischer, 216-433-6379,
DGFischer@nasa.gov

Authors:

Prof. Jacqueline Jordan and
Dr. David G. Fischer

Headquarters Program Office:

Exploration Systems Mission
Directorate

Programs/Projects:

Human Research Program

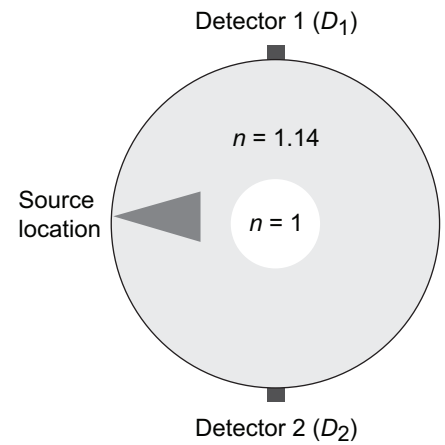
Three-Dimensional Monte Carlo Model Developed for Optical Mass Gauging

Accurate cryogenic propellant gauging is essential for space exploration. One candidate sensor for propellant gauging is the optical mass gauge (OMG), which is based on the premise that a propellant tank will act as an integrating sphere with respect to light that is introduced into its interior. It is assumed that light which is measured at a given tank port will be proportional to the fraction of the input light that is not absorbed (which is, in turn, related to the propellant mass or volume fraction). Furthermore, it is assumed that this will always be the case, independent of the location or size of any voids, the absorption characteristics of the propellant, or the characteristics of the tank walls. Unfortunately, the fundamental premise and in situ operation of an optical mass gauge cannot be tested in a realistic (i.e., zero gravity) environment. For this reason, a three-dimensional Monte Carlo model was developed to simulate the performance of an optical mass gauge in both 1g and 0g environments.

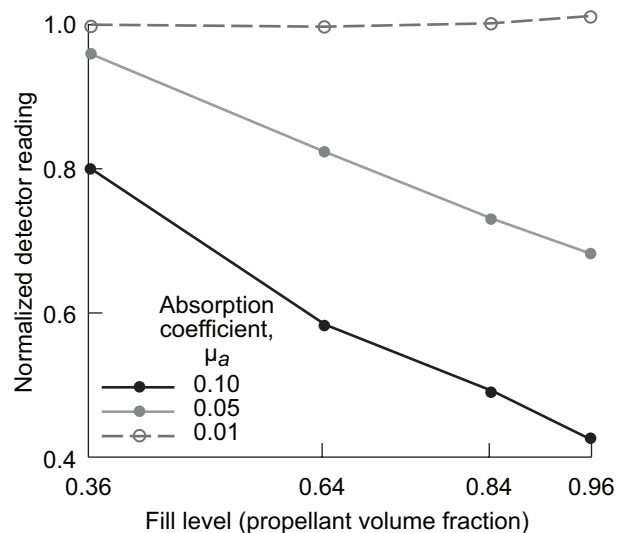
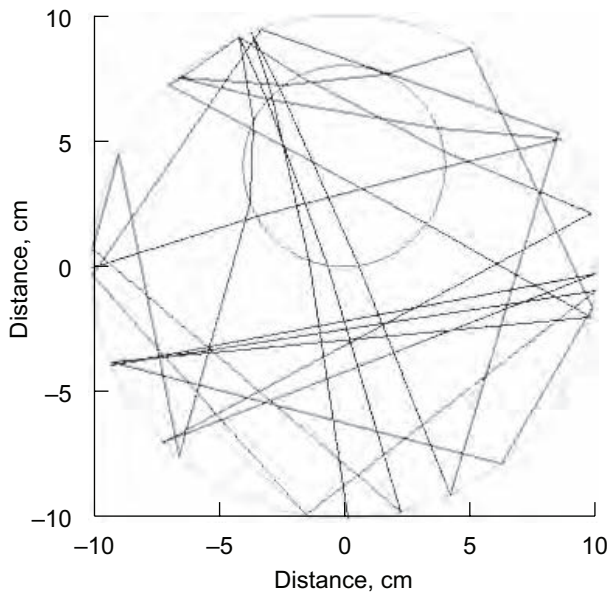
The Monte Carlo method is a numerical modeling technique based on repeated statistical sampling. In the context of optical mass gauging, it involves launching a photon into the tank. This photon is tracked until it is absorbed or registered at the detector. Interaction with the tank walls and tank interior are treated probabilistically based on the full electromagnetic theory. This process is then repeated for many photons (typically 10 million) to predict average system performance.

In the current model, the propellant tank and gas phase are taken to be spherical (see the diagram to the right). The total reflectivity R of the tank walls is varied, as well as the distribution of surface scatter (diffuse, specular, etc.). The absorption coefficient of the propellant (μ_a) is also varied. The propellant volume fraction and spatial distribution are varied by changing the size of the gas phase volume (i.e., the bubble) and its location, respectively. Finally, the spatial distribution of the injected photons is taken to be conical with a variable half-angle.

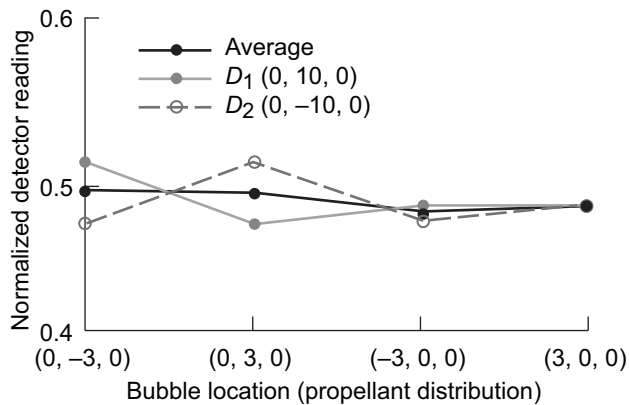
Two representative 0g simulation studies are presented next. The tank is taken to have a radius of 10 cm and perfectly diffuse walls. The half-angle of the injected light is 15° . The following figure on the left shows a typical photon trace. In the following figure on the right, the gauge (i.e., detector) reading is plotted as a function of propellant volume fraction for different values of propellant absorption. Gauging behavior is observed in the two cases with the largest absorption coefficients, but not in the third. This underscores the fact that propellant absorption must dominate wall absorption for gauging to be possible. In the figure on the next page, the gauge reading is plotted as a function of propellant distribution (i.e., bubble location), for different detector locations. In this case, the gauging variability between detectors is ± 10 percent. In general, gauging variability is largest for small propellant volume fractions, although averaging over multiple detectors can reduce its effects.



The 0g OMG model configuration; n is the index of refraction.



Left: Typical photon trace. Absorption coefficient of the propellant, μ_a , 0.1/cm; wall reflectivity, R , 0.97. Right: Optical mass gauge detector reading as a function of propellant volume fraction for different values of propellant absorption; wall reflectivity, R , 0.95.



OMG detector reading as a function of propellant spatial distribution. Wall reflectivity, R , 0.95; absorption coefficient of the propellant, μ_a , 0.1/cm; propellant volume fraction, 0.84.

Glenn Contacts:

Dr. David G. Fischer, 216-433-6379,
DGFischer@nasa.gov

Dr. Gregory A. Zimmerli, 216-433-6577,
Gregory.A.Zimmerli@nasa.gov

Author:

Dr. David G. Fischer

Headquarters Program Office:

Exploration Systems Mission Directorate

Programs/Projects:

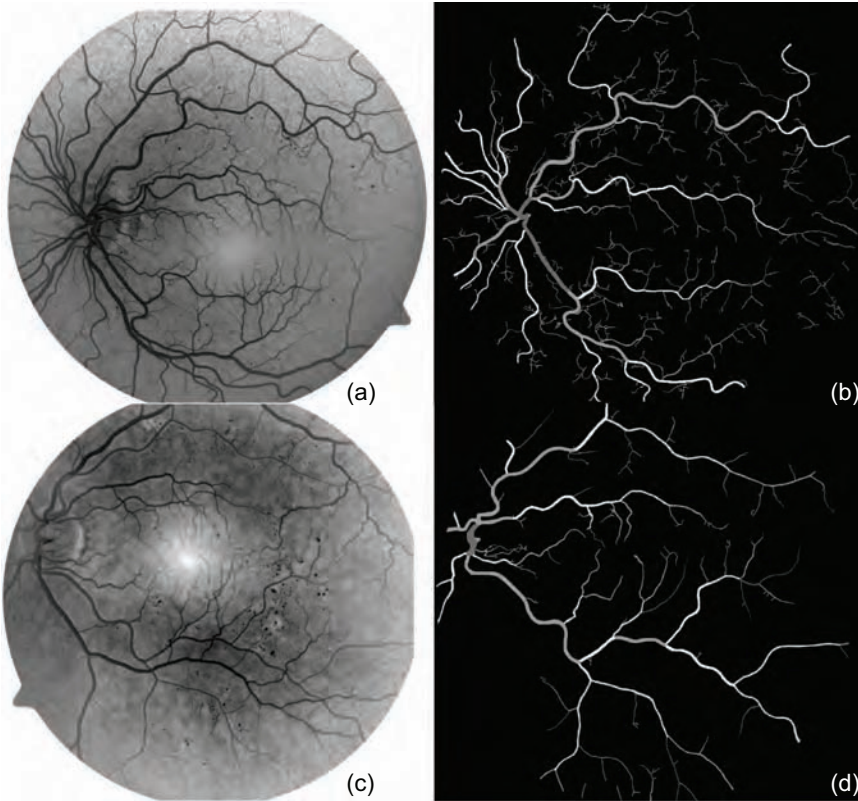
Propulsion and Cryogenic Advanced
Development Project

Microvascular Pathologies in Human Retinal Disease Analyzed by VESGEN Software

Microvascular remodeling is a critical hallmark of Earth-based diseases that include cancer, blindness in diabetes, heart disease, and other pathologies such as impaired wound healing. Long-term space travel in the microgravity environment exposes astronauts to major health risks that also appear to involve fundamental microvascular alterations. We are developing innovations for Earth-based microvascular pathologies using the software VESGEN (for generational analysis of vessel branching) that also will improve countermeasures for maintaining astronaut health. Every cell in the human body must reside in close proximity ($\leq 200 \mu\text{m}$) to a (microvascular) capillary blood vessel to accomplish necessary oxygen, metabolic, and fluid exchanges. Blood volume decreases up to 30 to 40 percent in microgravity, and 80 percent of astronauts can experience orthostatic intolerance after prolonged missions in space (ref. 1). Traveling to Mars is an example of a long-term microgravity mission, and most cardiovascular risks worsen as microgravity spaceflight is prolonged.

Current research goals at the NASA Glenn Research Center focus on application of the newly automated VESGEN to improve vascular diagnosis of human retinal disease during the progression of diabetic retinopathy, which can result in blindness (see the figure on the next page), and evaluating new therapeutics to regulate pathological vascular and lymphatic remodeling and fluid leakage, in collaboration with scientists and physicians at the Cole Eye Institute and Department of Cell Biology of the Lerner Research Institute at the Cleveland Clinic Foundation (CCF) and University Hospitals, Case Western Reserve University.

Microvascular remodeling is difficult to image and quantify, because the vascular system is a complex, three-dimensional, treelike structure embedded in opaque tissue. Imaging technologies such as magnetic resonance imaging and Doppler ultrasound are currently unable to visualize small blood vessels such as arterioles and capillaries. We use the optically accessible microvasculature of an avian model as a testbed to develop new methods for analyzing microvascular remodeling and blood flow (refs. 2 to 5). In 2007, methods for VESGEN analysis developed in our testbed model were extended to human retinal disease (see the figure on the next page and ref. 6) and the microvascular remodeling component of disease progression in genetically engineered laboratory mice (ref. 7).



VESGEN analysis of pathological remodeling in the human retina. Arterial branching trees are analyzed by VESGEN using ophthalmic clinical images of retinas diagnosed with diabetic retinopathy, in which the disease has progressed from mild nonproliferative diabetic retinopathy (NPDR, (a)) to severe NPDR (c). Note the loss of blood vessels throughout the arterial tree during NPDR progression. As quantified by VESGEN based on generational branching analysis (b), (d), vessel branch points decreased from 596 to 135, and the number of total vessel segments for nine generations of arterial branching decreased from 720 to 189. Our development of fractal-based techniques to quantify changes in blood vessel density (ref. 6) is now funded by the National Institutes of Health (NIH).

References

1. NASA Research Yields Insights Into Aging. NASA Space Research, Exploration Systems Mission Directorate, vol. 3, no. 4, Fall 2004, p. 6.
2. Parsons-Wingerter, P., et al.: The VEGF₁₆₅-Induced Phenotypic Switch From Increased Vessel Density to Increased Vessel Diameter and Increased Endothelial NOS Activity. *Microvasc. Res.*, vol. 72, no. 3, 2006, pp. 91–100.
3. Parsons-Wingerter, P., et al.: Lymphangiogenesis by Blind-Ended Vessel Sprouting Is Concurrent With Hemangiogenesis by Vascular Splitting. *Anat. Rec. A Discov. Mol. Cell Evol. Biol.*, vol. 288, no. 3, 2006, pp. 233–287.
4. Parsons-Wingerter, P., et al.: VEGF₁₆₅-Dependent Switch From Increased Vessel Density to Increased Vessel Diameter and Increased Endothelial NOS Activity. *FASEB J.*, vol. 20, no. 4, 2006, pp. A7087–A709.

5. Parsons-Wingerter, P.A.; McKay, T.L.; and DiCorleto, P.E.: VEGF-A Induces Reorganization of the Lymphatic Tree Into Homogeneous Vascular Networks. A Special Transatlantic Meeting of The Microcirculatory Society, Inc., and The British Microcirculation Society, Paper OC28, University of New Hampshire, Durham, NH, Sept. 2005.
6. Avakian, A., et al.: Fractal Analysis of Region-Based Vascular Change in the Normal and Non-Proliferative Diabetic Retina. *Curr. Eye Res.*, vol. 24, no. 4, 2002, pp. 274–280.
7. Parsons-Wingerter, P., et al.: Uniform Overexpression and Rapid Accessibility of $\alpha_5\beta_1$ Integrin on Blood Vessels in Tumors. *Am. J. Pathol.*, vol. 167, no. 1, 2005, pp. 193–211.

Glenn Contact:

Dr. Patricia Parsons-Wingerter,
216-433-8796,
Patricia.A.Parsons-wingerter@nasa.gov

Authors:

Dr. Patricia Parsons-Wingerter and
Mary B. Vickerman

LEW Number:

LEW-18277-1

Programs/Projects:

NASA Glenn Independent Research and Development, Human Research Program, National Eye Institute (NEI)/National Institutes of Health (NIH)

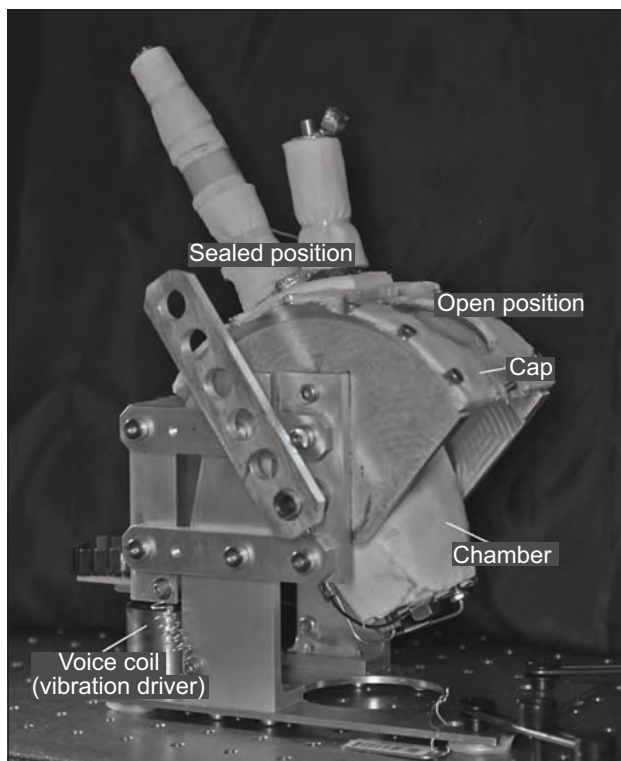
Special Recognition:

Development of a fully automated, user-interactive software version of VESGEN by Principal Innovator P. Parsons and Co-Innovators M. Vickerman and P. Keith was funded by Glenn's Independent Research and Development award 04-54 to Dr. Patricia Parsons (LEW-18277-1). An R01 Independent Principal Investigator grant entitled "Vascular Remodeling and Effects of Angiogenic Inhibition in Diabetic Retinopathy" was awarded to Dr. Patricia Parsons by the NEI and National Institute for Diabetes and Digestive and Kidney Diseases at the NIH to fund ongoing collaboration with the Cole Eye Institute of the CCF.

In Situ Resource Utilization Reactor Developed To Characterize Lunar Soil

The extraction and processing of planetary resources into useful products will have a profound impact on the future exploration of the Moon and Mars. Known as in situ resource utilization (ISRU), this idea of “living off the land” reduces dependence on Earth for mission consumables such as propellant and life-support oxygen and water, and it enables safer, cheaper, and longer-duration missions. The lunar soil is approximately 40-percent chemically bound oxygen, and volatile species such as hydrogen (and possibly water at the lunar poles) are present in smaller concentrations. The goal of the Regolith and Environment Science, Oxygen and Lunar Volatiles Extraction (RESOLVE) project is to quantify the resources that are available on the Moon and to demonstrate how to extract them.

The NASA Glenn Research Center designed, built, and tested a reactor for the volatile extraction aspects of the RESOLVE project (see the photograph). The reactor chamber holds approximately 100 g of soil, filling nearly half its volume. The chamber walls are heated, and water attached to the soil (e.g., in the form of ice) is released as steam. Other loosely bound volatiles, such as hydrogen or nitrogen may also be released during heating. The pressure in the chamber increases as gases are generated, reaching a maximum of 150 psia at 150 °C. The evolved gases are pressure fed to analysis modules elsewhere in the RESOLVE package.

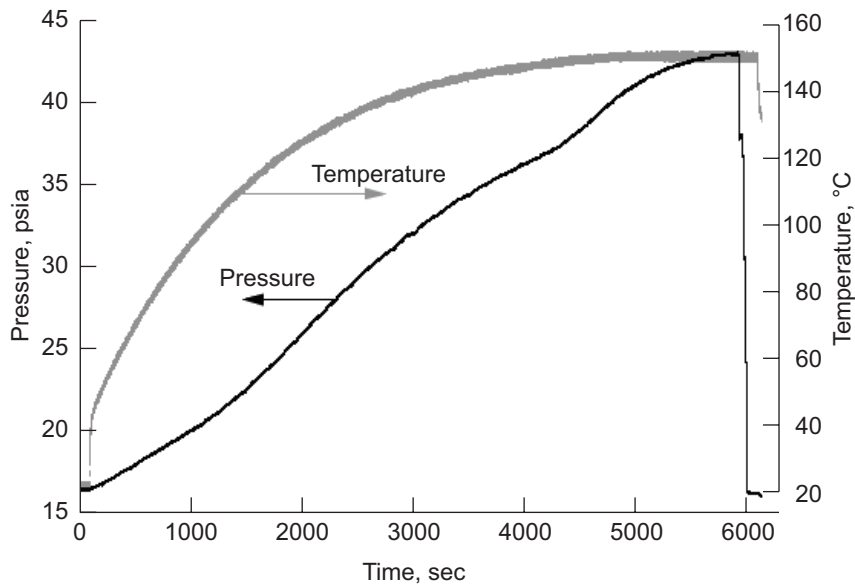


Glenn's reactor for the RESOLVE project.

The heating process is expedited using vibrational mixing, which is a low-power, efficient means of improving heat transfer in lunar soil. Alternative mixing schemes, such as a mechanical stirrer inside the chamber, could clog and would not endure well in the abrasive lunar soil. In addition, the vibration provides a means to shake loose small soil particles that may otherwise bind or clog the system.

In order to process multiple batches of lunar soil, the reactor can be rotated to accept fresh soil and dispose of processed soil. Similar to a ball valve, the chamber rotates beneath a curved cap between the open (soil-entry) and sealed (gas-evolution) positions. The chamber and cap assembly can be rotated to purge the soil sample. The rotational scheme allows the chamber to be filled and emptied using only one sealing surface, reducing the potential for leaks.

A series of engineering and scientific tests were performed to demonstrate the capabilities of this reactor before delivery to project partners at the NASA Kennedy Space Center. Since actual lunar soil is in short supply, a soil simulant, known as JSC-1, was used. Vibrational mixing of JSC-1 was characterized to find the optimal heat-transfer mode. To mimic water that may be present in the lunar soil, a hydrated mineral salt (borax) was added to the JSC-1. Water evolved from the soil was measured using pressure rise in the chamber (see the graph on the next page) until saturation pressure (100-percent relative humidity) was reached. Evolved water was collected in a condensing dewar and measured.



Data from a reactor test using JSC-1 soil simulant and 0.5 g of borax. Pressure (left axis) increases with temperature (right axis) as water is released from borax until either the saturation pressure is reached or all water is released.

Glenn's RESOLVE reactor demonstrated good soil mixing, uniform reactor heating, and successful gas evolution and recovery. The reactor is currently at Kennedy, where it is integrated into the water-detection (gas chromatograph) and collection (absorbent beds) portion of the system.

References

1. Nayagam, Vedha; and Sacksteder, Kurt A.: A Vibrofluidized Reactor for Resource Extraction From Lunar Regolith. AIP Conf. Proc., vol. 813, 2006, pp. 1101-1110.
2. Nayagam, V.; and Sacksteder, K.R.: Resonant Heat Transfer in a Vibrofluidized Reactor With Lunar Regolith Simulant. Presented at the Space Technology & Applications International Forum, Albuquerque, NM, Feb. 11-14, 2008.

Glenn Contact:

Dr. Kurt R. Sacksteder, 216-433-2857, Kurt.Sacksteder@nasa.gov

Case Western Reserve University

Contact:

Dr. Julie E. Kleinhenz, 216-433-5383, Julie.E.Kleinhenz@nasa.gov

Authors:

Dr. Julie E. Kleinhenz and
Dr. Kurt R. Sacksteder

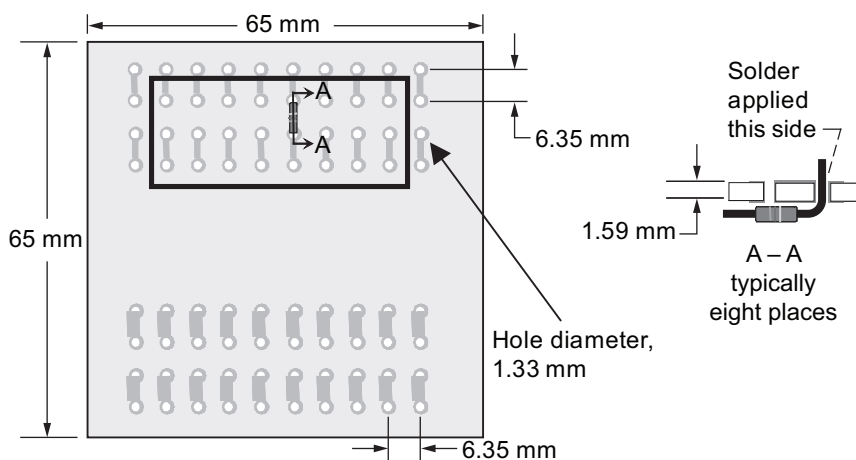
Headquarters Program Office:

Exploration Systems Mission Directorate

Programs/Projects:

In Situ Resource Utilization, Regolith and Environment Science, Oxygen and Lunar Volatiles Extraction

Component-Level Electronics Repair in Space: Soldering Tested in Reduced Gravity—An Update

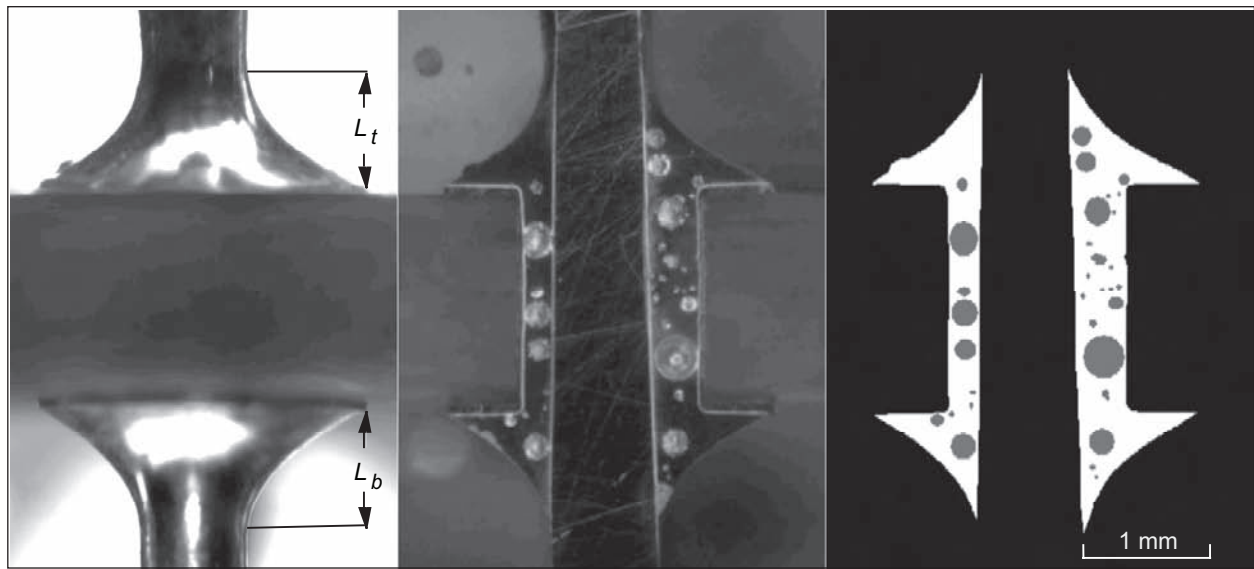


Plated-through-the-hole sample configuration used during reduced-gravity testing. Two resistor lead diameters were used—0.66 and 0.78 mm.

NASA Glenn Research Center's Component Level Electronic Assembly Repair (CLEAR) task is helping to enable future astronauts to repair electronics down to the component level (e.g., resistors, capacitors, and integrated circuits) in spacecraft or future habitats. CLEAR is a supporting task under a project called Supportability, which is part of NASA's Exploration Technology Development Program. Locally at Glenn, CLEAR is supported by the National Center for Space Exploration Research as well as the ASRC Aerospace Corporation.

Although CLEAR is looking at all aspects of repair, a key element of the repair process is soldering. From 2000 to 2005, a series of aircraft tests investigated how reduced gravity affected the soldering of small electrical components (see the diagram on the preceding page). This work showed that reduced gravity leads to a significant increase in voids, or porosity, in the joint (ref. 1). These voids (see the following images) come from entrapped vaporized flux, which is part of the soldering process, or water vapor in the circuit board. These gases form bubbles that are driven to the surface by buoyant forces in normal gravity. In reduced gravity they are slowed, becoming trapped and frozen in the final joint. A void in a solder joint can be detrimental to performance, but the use of an externally applied liquid flux and a solid-core solder showed promise as a potential void-mitigation technique (see the table).

Astronaut Suni Williams conducted a similar experiment—the Soldering in Reduced Gravity Experiment (SoRGE)—aboard the International Space Station (ISS), using the soldering kit available on orbit (see the top photograph on the next page). The soldered circuit boards were returned to Earth aboard the *Space Shuttle Endeavor* in August 2007 and are being analyzed at Glenn. SoRGE intends to verify the initial findings from



Solder was applied to the joint from the top of solder joint as oriented in the images. This joint shows significant sub-surface voids (18.8-percent voiding). Left: Joint after soldering in reduced gravity. Center: Joint after cross sectioning. Right: Joint after computer analysis.

MEAN POROSITY (PERCENT AREA OF VOIDS) FOR SAMPLES TESTED IN NORMAL- AND REDUCED-GRAVITY ENVIRONMENTS
[The larger data sets show the 95-percent confidence interval of the mean value.]

Test condition ^a	0g _E	0.10g _E	0.17g _E (Moon)	0.38g _E (Mars)	1g _E
Flux-core solder					
Area of voids, percent	11.0±2.38	9.27	7.75	5.41	3.21±1.17
Number of samples	77	11	16	18	102
Solid solder—liquid flux ^b					
Area of voids, percent	6.64±1.24	N/A	6.44	8.53	2.75±0.64
Number of samples	153		7	7	111

^aEarth gravity, $g_E = 9.8$ m/sec.

^bThe solid-solder—liquid-flux data represent a void-mitigation technique (ref. 1).

the aircraft studies and to examine several techniques that may mitigate the formation of voids in the solder joints. These results will be used to help guide repair strategies for future long-duration missions.

A follow-on experiment, Component Repair Experiment-1 (CRE-1), is under development by the CLEAR team to demonstrate methods for crewmembers to conduct board-level electronic repairs within a spacecraft. CRE-1 will focus on the physical processes of a manual electronics repair including (1) conformal coating removal, (2) component removal, (3) board cleaning, (4) component soldering, and (5) conformal coating reapplication on a modern circuit card (see the following photograph). Currently, NASA flight crews recover from electronic faults by replacing entire electronic assemblies,

or Orbital Replacement Units (ORUs). A faulty ORU is replaced with a spare, and the defective unit is returned to Earth for diagnosis and repair. Because an ORU strategy is more challenging for long-duration missions beyond Earth orbit, component-level repair may be required for future exploration missions.

Reference

1. Watson, J. Kevin, et al.: Experimental Investigation of Solder Joint Defect Formation and Mitigation in Reduced-Gravity Environments. *J. Spacecr. Rockets*, vol. 44, no. 1, 2007, pp. 174–182.

Find out more about this research:

CLEAR Project at Glenn:

<http://exploration.grc.nasa.gov/Exploration/Advanced/Capabilities/Clear/>

SoRGE:

<http://exploration.nasa.gov/programs/station/SoRGE.html>

Glenn Contact:

Peter M. Struk, 216–433–5948,
Peter.M.Struk@nasa.gov

National Center for Space Exploration Research (NCSER) Contact:

John W. Easton, 216–433–2643,
John.W.Easton@nasa.gov

ASRC Aerospace Corp. Contact:

Eric E. Anderson, 216–433–5389,
Eric.E.Anderson@nasa.gov

Author:

Dr. Peter M. Struk

Headquarters Program Office:

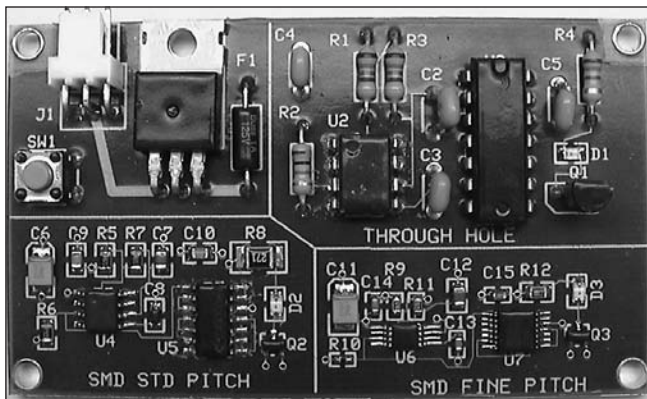
Exploration Systems Mission Directorate

Programs/Projects:

Exploration Technology Development Program Office, Constellation Program—Supportability



Suni Williams performs the SoRGE experiment in the ISS Maintenance Work Area during Expedition 14. The area will be configured similarly for CRE-1 operations.



Test card for the CRE-1 experiment on which crew members will attempt to remove and replace components (including conformal coating). The components include both through-the-hole and surface-mount device technology and both standard and fine-pitch lead spacing. The board is coated with silicone.

Compact Flash Evaporator System Developed

For future spacecraft thermal control architectures, an alternative heat sink technology is being developed at the NASA Glenn Research Center, a spray-cooling concept similar to the current space shuttle flash evaporator system (FES). In the compact FES (CFES) concept, the vehicle's primary heat transfer fluid flows inside a flat-plate heat exchanger while water is sprayed against the outside. The steam is then exhausted to space. Design, fabrication, and testing of the CFES have culminated in the successful delivery of the development unit.

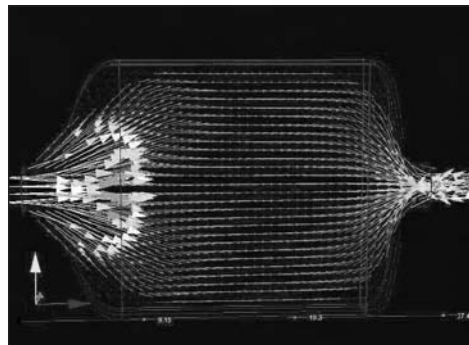
The space shuttle orbiter's FES cannot be scaled from its heat-rejection capability of 38 kW to the 4.5 kW required for the Orion Crew Exploration Vehicle (CEV) spacecraft. A completely new design is needed to meet the Orion's requirements. The CFES takes advantage of new spray nozzle designs and increased knowledge of spray cooling. An earlier CFES concept was based on the Cray X-1 supercomputer spray nozzle hardware made by Parker Hannifin Corporation's Gas Turbine Fuel Systems Division in Mentor, Ohio.

During mission phases when the CEV Service Module (SM) radiator is inadequate or unavailable (after SM and Crew Module separation), the CEV may use an open-loop evaporative cooling system to reject heat. The advantages of a spray concept are

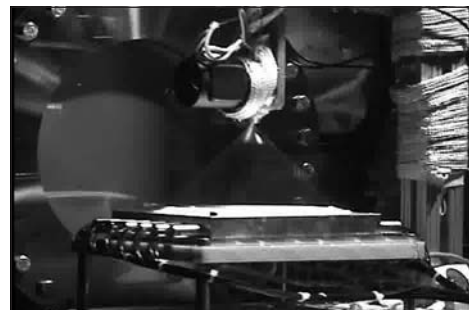
- Space shuttle flight heritage that has survived all anticipated mission phase environments including vibration
- Quick response for cooling needs with little required chilldown time
- Insensitivity to dissolved contaminants
- Simple control system

The principal disadvantage is that ice formation may occur for off-nominal conditions, such as changes in water feed pressure or sudden reductions in heat load that lead to the deposition of excess water onto the heat exchanger. This failure condition is unrecoverable in a short amount of time since it takes several minutes for the ice to melt after it has formed.

CFES hardware was developed using computational fluid dynamics (CFD) tools, standard computer-aided design (CAD) software (see the top figure), specialized control and diagnostics software, and experience gained from drop tower work. The electrical discharge machining (EDM) tools at Glenn were critical for fabrication of the unique minichannel high-heat-flux heat exchanger. Glenn's Vacuum Facility 12 was used in conditions beyond its design requirements: it was able to maintain vacuum, even with water being evaporated into the chamber (see the photographs on this page and the next page).

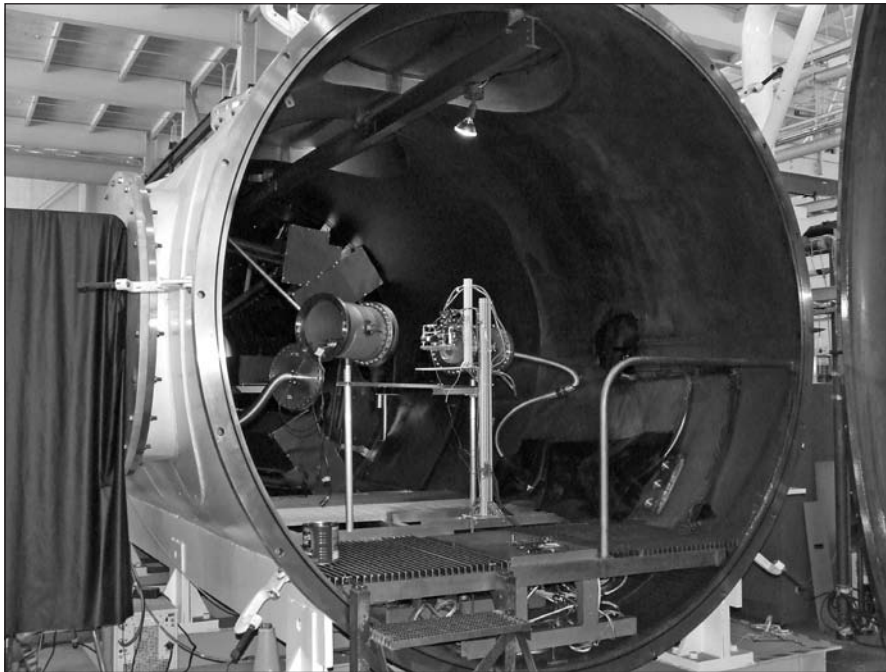


Heat exchanger CFD analysis. This figure is shown in color in the online version of this article (<http://www.grc.nasa.gov/WWW/RT/2007/Proc-Exp/07-RET-golliher.html>).



Single nozzle spray in a vacuum at 10^{-3} torr.

With the successful development of this hardware, quantifiable performance data under a realistic flightlike environment is now possible. Comparison of these data with similar data for the other two



Glenn's Vacuum Facility 12 with CFES test rig.

evaporative heat sinks will allow NASA to be better prepared in choosing options for future spacecraft thermal control architectures.

Bibliography

Golliher, Eric, et al.: Development of the Compact Flash Evaporator System for Exploration. SAE Technical Paper No. 2007-01-3204, 2007.

Golliher, Eric L.; Zivich, Chad P.; and Yao, S.C.: Exploration of Unsteady Spray Cooling for High Power Electronics at Microgravity Using NASA Glenn's Drop Tower. ASME Summer Heat Transfer Conference, HT2005-72123, 2005.

Glenn Contact:

Eric L. Golliher, 216-433-6575,
Eric.L.Golliher@nasa.gov

Author:

Eric L. Golliher

Headquarters Program Office:

Exploration Technology Development
Office

Programs/Projects:

Advanced Capabilities

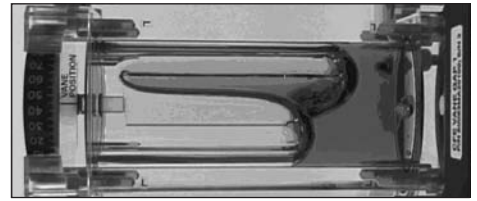
Capillary Flow Experiments Performed on the *International Space Station*

The Capillary Flow Experiments (CFEs) are a suite of fluid physics flight experiments that investigate capillary flows in low gravity. CFE data are crucial to the Space Exploration Initiative, particularly pertaining to fluid management systems including fuels and cryogen storage, thermal control, water recycling, and materials processing. NASA's exploration missions are planning to use larger liquid propellant masses than have ever flown before. Under low-gravity conditions, capillary forces can be exploited to control fluid orientation so that these mission-critical systems perform predictably.

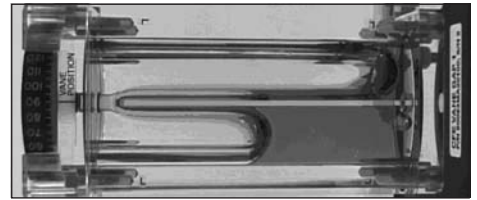
CFE is a simple fundamental scientific study that can yield quantitative results from safe, low-cost, short time-to-flight, handheld fluids experiments. The experiments should provide critical results to the capillary flow community that cannot be achieved in ground-based tests. For example, dynamic effects associated with a moving contact boundary condition, capillary-driven flow in interior corner networks, and critical wetting phenomena in complex geometries. The knowledge gained will help spacecraft fluid systems designers increase system reliability, decrease system mass, and reduce overall system complexity.

CFE is a set of NASA Glenn Research Center experiments developed under contract by ZIN Technologies, Inc. It includes the Interior Corner Flow (ICF), the Vane Gap (VG), and the Contact Line (CL) experiments. Each experiment has two unique experimental units. All units use similar fluid-injection hardware, have simple and similarly sized test chambers, and rely solely on video for highly quantitative data. Silicone oil, with different viscosities depending on the unit, is the test fluid for all the units. Other differences between units are wetting conditions and test cell cross-section. The experiment procedures are simple and intuitive.

- The ICF experiment investigates propellant management and passive capillary flow in tapered geometries for which boundary conditions are not well understood or modeled.
- The VG experiment scrutinizes the critical wetting condition when interior corners do not actually make contact, in particular the corner and gap formed by an interior vane and the interior wall of a propellant tank, or between the intersection of vanes in a complex vane network. The photographs to the right display the fluid response to two different vane gap critical angles.
- The CL experiment studies the impact of the dynamic contact line. The contact line controls the interface shape, stability, and dynamics of capillary systems in low gravity. These experiments provide a direct measure of expected behavior assuming either a free or pinned contact line condition. The two CL units are identical except for their respective wetting characteristics.



CFE Vane Gap-1 vessel at a 45° vane angle.



CFE Vane Gap-1 vessel at a 90° vane angle.

The CFE CL-2 unit was launched to the *International Space Station* on *Progress 13* in January 2004. The CL-1, ICF-1, ICF-2, VG-1, and VG-2 units were launched on STS-121 (space shuttle mission) in August 2006. Expedition 15 flight engineer, Sunita Williams, is shown in the following photograph performing one of the nine CFE operational runs that she completed. All units have been operated, and CL-2, VG-2, ICF-1, and ICF-2 were returned on STS-118 in August 2007. CL-1 and VG-1 each have one remaining operation.



Expedition 15 flight engineer, Sunita Williams, performs a filling operation on the CFE Vane Gap-2 unit.

Find out more about this research:

Capillary Flow Experiments (CFEs) at Glenn:

<http://spaceflightsystems.grc.nasa.gov/Advanced/ISSResearch/MWA/CFE/>

How to Manage Floating Fluids in Space:

http://www.nasa.gov/mission_pages/station/science/capillary_flow.html

Principal Investigator's web page:

<http://web.cecs.pdx.edu/~mmw/>

Glenn Contacts:

Robert D. Green, 216-433-5402,
Robert.D.Green@nasa.gov

Donna Y. Bohman, 216-433-8860,
Donna.Y.Bohman@nasa.gov

ZIN Technologies, Inc., Contact:

Charles T. Bunnell, 216-625-2280,
bunnellc@zin-tech.com

Author:

Robert D. Green

Headquarters Program Office:

Exploration Systems Mission Directorate

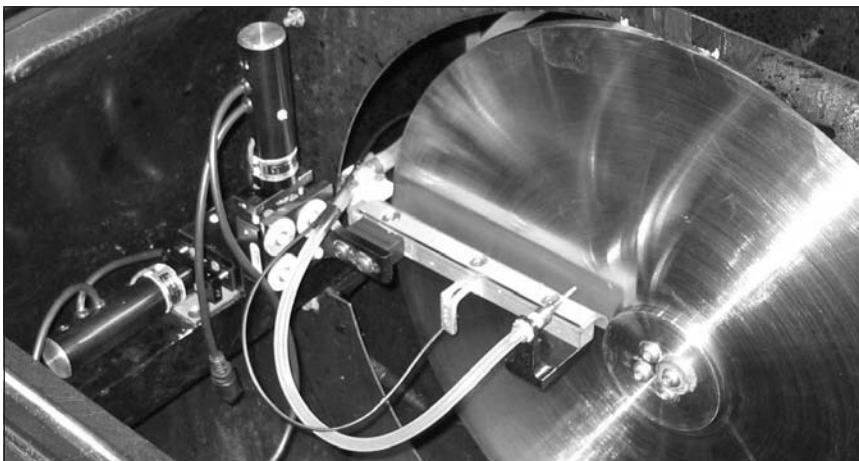
Programs/Projects:

Constellation Systems, Crew Exploration Vehicle, Crew Launch Vehicle

Vapor Phase Catalytic Ammonia Removal Tested in Reduced Gravity on NASA C-9 Aircraft



Front view of the VPCAR rig.



Rotating disk and wiper inside housing with translation stage.

The Vapor Phase Catalytic Ammonia Removal (VPCAR) project is candidate water-processing technology for a closed-loop water-recycling system applicable to long-duration missions including the Lunar Outpost. VPCAR utilizes a wiped-film rotating-disk (WFRD) evaporator that retains an evaporating film of wastewater on one side of a rotating flat disk and a condensing film of clean water on the other. A temperature difference is maintained across

the disk from the condensing side to the evaporating side so that the heat flows across the disk. This allows the WFRD to recycle the latent heat of vaporization. The NASA Glenn Research Center built and is currently evaluating the rotating disk unit of the WFRD and water delivery system to determine its reduced-gravity operation and performance (see the top photograph). The rotating disk can produce rotation rates from 100 to 600 rpm, and the fluid flow rate can be varied from 25 to 400 ml/min. Three reduced-gravity campaigns, under both lunar and microgravity conditions, have been conducted on NASA's C-9B Reduced Gravity Aircraft.

For the first round of aircraft testing (Feb. 2006), the rotation rates were 100, 200, 300, 400, 500, and 600 rpm, and the fluid flow rates were 25, 50, 100, 200, and 400 ml/min. Results from these tests indicated that the VPCAR wiper did not produce a uniform thin film. The film was thicker near the axis of rotation where centrifugal forces are small. This film thickening has a potential negative effect on the heat transfer coefficient of the evaporator and could result in higher than expected specific power consumption during microgravity operation.

During the second round of microgravity tests (Oct. 2006), a possible solution to this problem was tested. The wiper mechanism was mounted on a translation stage (see the bottom photograph) that varied the distance between the wiper and the disk axis relative to the disk centerline. In addition, the height of the wiper above the axis of rotation of the disk could be adjusted. Disk speeds were 200, 300, and 450 rpm, and fluid flow rates were 50 and 100 mL/min. The wiper assembly was translated horizontally (toward and away from the disk) at distances of 5, 7.5, and 10 mm, and vertically (above the disk axis)

at settings of 0, 5, 10, 15, and 20 mm. These tests demonstrated that mounting the feed wiper slightly higher than the axis of rotation of the WFRD disk produced a uniform thin film.

The third round of C9 testing (Sept. 2007, see the final photograph) included both lunar and microgravity trajectories to expand the test matrix. Some of the test points performed on the first two flights were repeated. Data from these tests are being analyzed.

Glenn Contacts:

Nancy Rabel Hall, 216-433-5643, Nancy.R.Hall@nasa.gov

Dr. Charles E. Niederhaus, 216-433-5461, Charles.E.Niederhaus@nasa.gov

Jeffrey R. Mackey, 440-343-4249, Jeffrey.R.Mackey@nasa.gov

Author:

Nancy Rabel Hall

Headquarters Program Office:

Exploration Systems Mission Directorate

Programs/Projects:

Constellation Systems, Crew Exploration Vehicle



C9 Flight Flyers in September 2006. From left to right: Eric J. Litwiller, NASA Ames Research Center; Ioan I. Feier, Nancy Rabel Hall, and Rochelle L. May, NASA Glenn; and Susan Rulis, NASA Johnson Space Center.



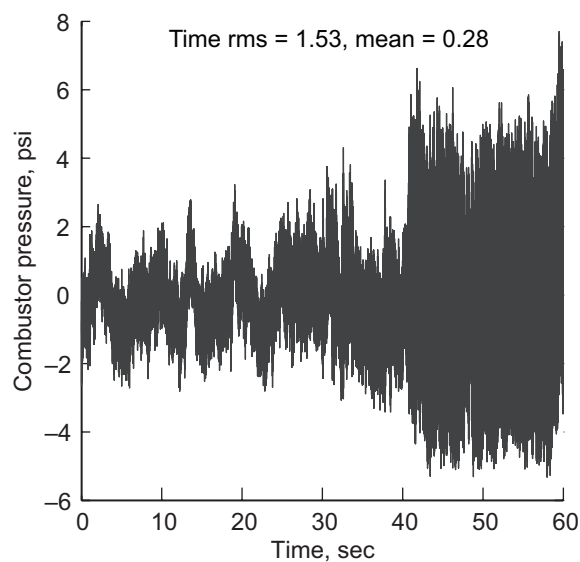
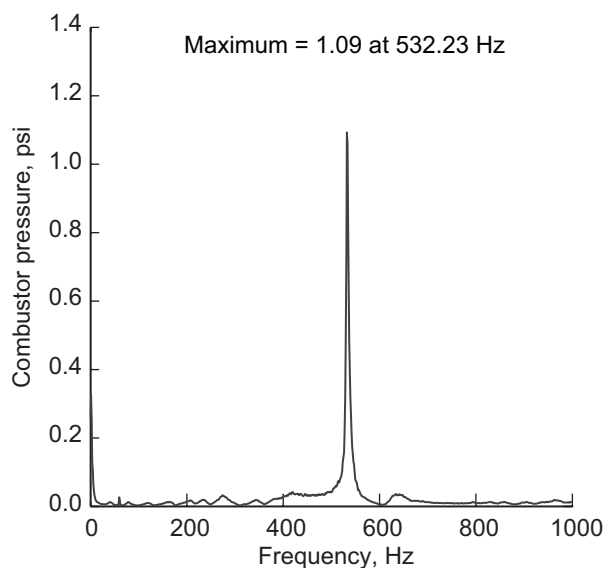
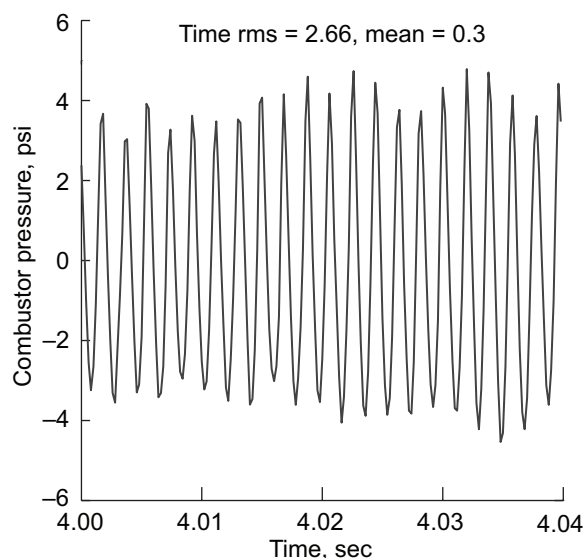
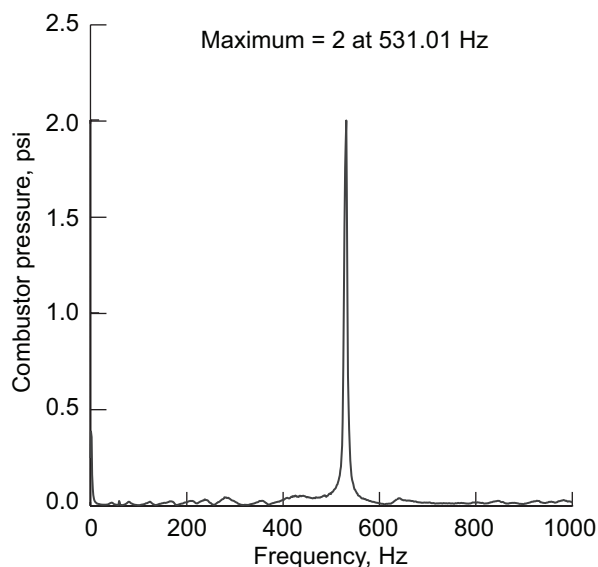
Instrumentation and Controls

Simulation Developed That Captures the Thermoacoustic Instability Behavior of Advanced, Low-Emissions Combustor Prototype

To reduce the environmental impact of aerospace propulsion systems, extensive research is being done in the development of lean-burning (low fuel-to-air ratio) combustors that can reduce emissions throughout the mission cycle. However, these combustors have an increased susceptibility to thermoacoustic instabilities, or high-pressure oscillations much like sound waves, that can cause severe high-frequency vibrations in the combustor. These pressure waves can fatigue the combustor components and even the downstream

turbine blades, significantly decreasing the safe operating life of the combustor and turbine.

This type of instability was recently observed in an advanced, low-emissions combustor prototype installed in a

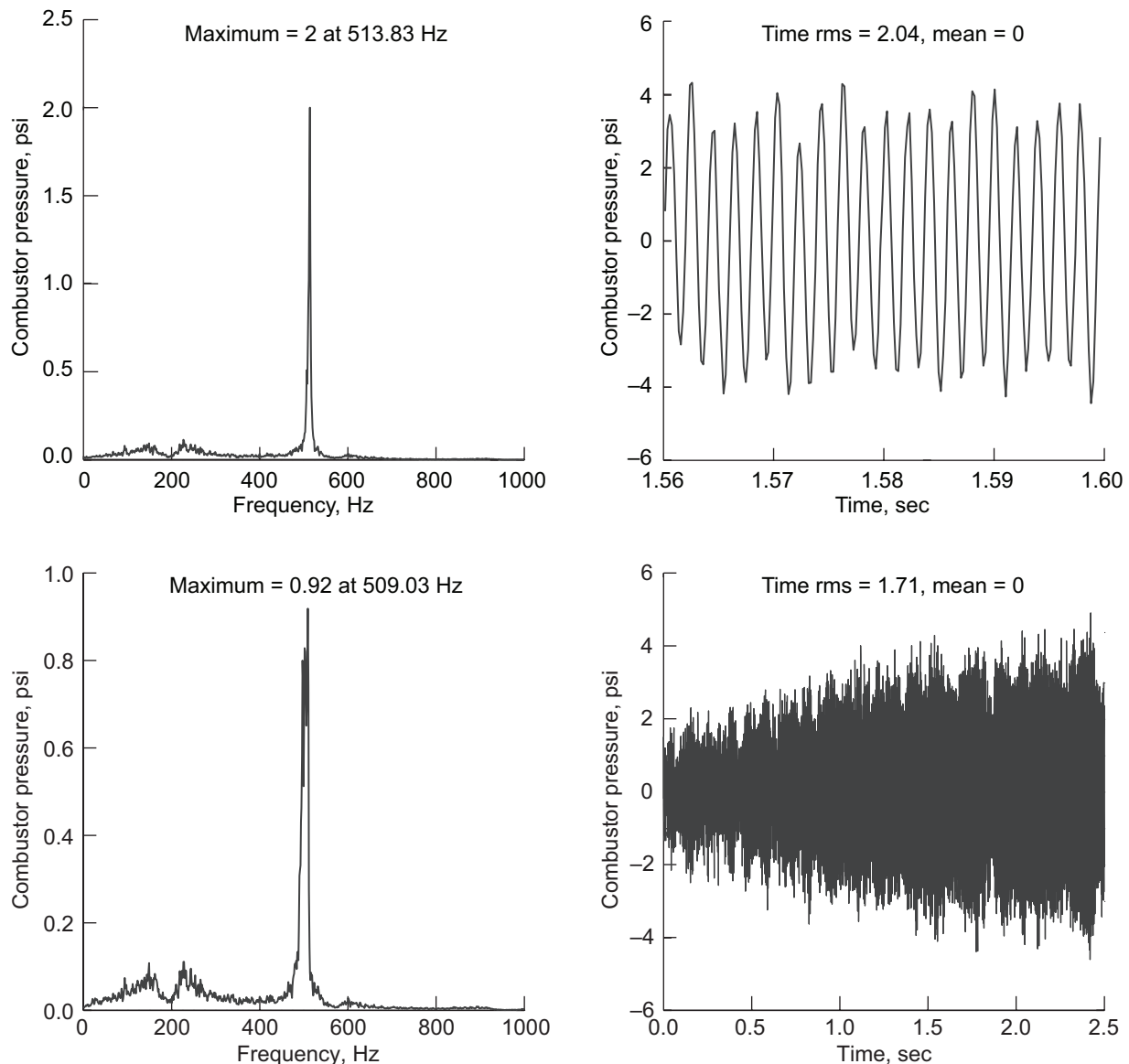


Combustor rig experimental data showing the combustion thermoacoustic instability. Left plots: Amplitude spectrum of the combustor pressure, indicating the instability frequency. Right plots: Time history of combustor pressure, indicating the instability amplitude and shape. Top plots: Steady fuel-to-air ratio of 0.03. Bottom plots: Increase in fuel-to-air ratio from 0.028 to 0.03.

NASA Glenn Research Center combustion test stand. The instability behavior was characterized by operating the combustor at engine pressures, temperatures, and fuel flows representative of operation within an aircraft gas turbine engine. As shown in the figure on the preceding page, the instability produces large pressure oscillations in the combustor. In addition, the pressure oscillations grow with increasing fuel-to-air ratio. Unfortunately, this instability growth prevents the combustor from reaching full power operation. Suppression of the thermoacoustic instability through active control, then, can enable this and other advanced combustors to achieve their full range of operation while maintaining low emissions.

can effectively suppress combustion instabilities in aircraft gas turbine engine combustors (see ref. 1). We desire to extend these active control methods to advanced low-emissions combustors such as that being prototyped. The ability to develop such active control designs successfully is greatly enhanced by accurate modeling and simulation of the thermoacoustic instability behavior of the combustor under investigation.

Previous work at Glenn has shown that active combustion control utilizing advanced algorithms and working through high-frequency fuel actuation



Simulation data showing that the simulation successfully captures the combustor instability frequency, amplitude, and shape for a fixed fuel flow and that, for a changing fuel-to-air ratio, the simulation successfully follows the experimentally observed trend. Top: Fixed fuel-to-air ratio of 0.03. Bottom: Linear fuel flow increase corresponding to a fuel-to-air ratio change from 0.025 to 0.03.

A simulation developed at Glenn captures the experimentally observed instability behavior of the low-emissions combustor prototype described earlier, and the layout of the simulation captures the relevant physical features of the combustor and test rig. The physics-based simulation uses a sectored one-dimensional approach, includes simplified reaction equations, and provides time-accurate results. A computationally efficient method is used for area transitions (see ref. 2). This decreases run times and allows the simulation to be used for parametric studies including control method investigations.

Simulation results show that the simulation exhibits self-starting, self-sustained combustion instability (see the figure on the preceding page). The instability is based strictly on the physics of the combustor and the coupling between heat addition and acoustics; that is, no forcing is required to cause the instability to appear. The simulated combustion instability closely matches the combustor for steady fuel flow, and it replicates the growth in instability amplitude as the fuel-to-air ratio is increased. This latter result is especially useful for developing controls that predict the onset of instability and mitigate its effects before the instability is fully developed. Future plans are to use the simulation to investigate active control strategies to suppress combustion instabilities in advanced low-emissions combustors.

References

1. DeLaat, John C.; and Chang, Clarence T.: Active Control of High Frequency Combustion Instability in Aircraft Gas-Turbine Engines. NASA/TM—2003-212611 (ISABE—2003—1054), 2003. <http://gltrs.grc.nasa.gov>

2. Paxson, Daniel E.: A Sectored-One-Dimensional Model for Simulating Combustion Instabilities in Premix Combustors, NASA/TM—1999-209771 (AIAA—2000—0313), 1999. <http://gltrs.grc.nasa.gov>

Find out more about Glenn's active combustion control research:

<http://www.grc.nasa.gov/WWW/cdtb/projects/combustor/>

Glenn Contacts:

John C. DeLaat, 216-433-3744, JDeLaat@nasa.gov

Dr. Daniel E. Paxson, 216-433-8334, Daniel.E.Paxson@nasa.gov

Author:

John C. DeLaat

Headquarters Program Office:

Aeronautics Research Mission Directorate

Programs/Projects:

Fundamental Aeronautics Program, Supersonics Project, High Altitude Emissions

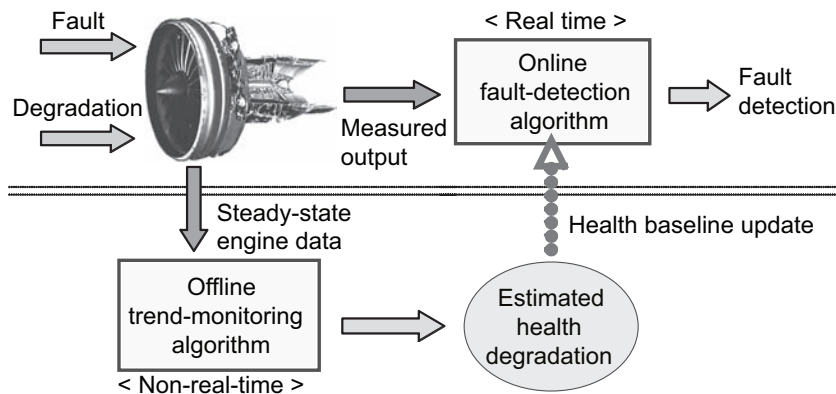
Integrated Online and Offline Diagnostic Approach Demonstrated for Aircraft Engine Application

Early detection of component and subsystem faults can help improve the safe and reliable operation of aircraft gas turbine engines. Such a capability requires an online fault-detection algorithm that is designed to operate on an onboard engine computer in real time. Since faults cause the measured engine output data to deviate from nominal condition values, the online algorithm continuously monitors engine output for anomalous signatures induced by faults. The online algorithm, however, has difficulty in achieving reliable diagnostic performance because the measured engine output data are influenced not only by faults but also by engine health degradation. Engine health degradation is a normal aging process that all aircraft engines will experience because of usage and, therefore, is not considered to be a fault (which is an abnormal, unexpected event). Without a capability to discern the difference between fault- and degradation-induced measurement shifts, the online algorithm eventually loses its diagnostic effectiveness as the engine degrades over time.

To address this challenge, researchers at the NASA Glenn Research Center developed a concept of integrating the online algorithm with an offline trend-monitoring algorithm (see the figure on the next page). The objective

of the offline algorithm is to track engine health degradation over the lifetime of an engine. It estimates the engine's health condition on the basis of steady-state engine output data recorded during flight. Since health degradation is a gradual process, the offline algorithm updates its estimate at a relatively low frequency, such as once per a number of flights or hours of operation.

The periodically updated knowledge of engine health degradation is used to update the design health condition, or the health baseline, of the online algorithm. Through the health baseline update, the online algorithm can account for the influence of health degradation



Concept of an integrated online and offline diagnostic approach.

and maintain its focus on detecting fault-induced engine output shifts. This approach allows the online algorithm to maintain its effectiveness while the engine's health condition changes with time.

The integrated online and offline diagnostic approach was demonstrated in a simulation environment using a nonlinear gas turbine engine model. The online algorithm avoided incorrectly diagnosing engine health degradation as a fault, and it detected sensor biases at consistent levels regardless of the severity of the engine health degradation. The demonstration study revealed that the integrated approach is essential to maintaining reliable performance of the online fault-detection algorithm over the lifetime of an engine.

Bibliography

Kobayashi, Takahisa; and Simon, Donald L.: Integration of On-Line and Off-Line Diagnostic Algorithms for Aircraft Engine Health Management. ASME Paper GT2007-27518 (NASA/TM-2007-214980 and ARL-TR-4090), 2007. <http://gltrs.grc.nasa.gov>

Find out more about the research of Glenn's Controls & Dynamics Branch:
<http://www.grc.nasa.gov/WWW/cdtb/>

ASRC Aerospace Corporation Contact:
Takahisa Kobayashi, 216-433-3739,
Takahisa.Kobayashi-1@nasa.gov

Glenn Contact:

Donald L. Simon, 216-433-3740,
Donald.L.Simon@nasa.gov

Authors:

Takahisa Kobayashi and Donald L. Simon

Headquarters Program Office:

Aeronautics Research Mission Directorate

Programs/Projects:

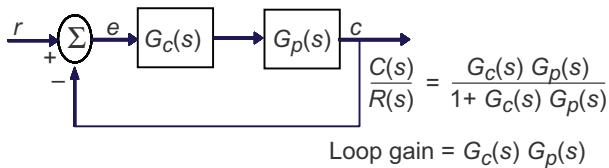
Aviation Safety Program, Integrated Vehicle Health Management Program

Loop-Shaping Design Approach With Practical Considerations Developed for Feedback Control Systems

A design approach has been developed at the NASA Glenn Research Center for feedback control systems where disturbance attenuation becomes an important criterion in the design process, such as in propulsion systems for supersonic vehicles. This approach directly ties requirements for disturbance attenuation, transient response, and stability into the plant dynamics and the actuation system limitation. The challenge in supersonic vehicle propulsion systems is to control the shock wave at a certain position inside the supersonic inlet in order to maximize performance, prevent inlet unstarts, and preserve aircraft ride quality and stability, while attenuating upstream flow-field disturbances, such as atmospheric wind gusts, aeroservoelastic disturbances coming from the vehicle structural modes, yaw and angle of attack disturbances, and disturbances coming from the engine itself. These objectives have to be met within the physical limitations of the actuators such as position and rate limits. Although this technique was developed under the Supersonics Project in NASA's Fundamental Aeronautics Program, it is applicable to any

classical feedback control system where the plant transfer function is known.

The technique is based on frequency-domain feedback control system design, where a desired loop gain is shaped in a step-by-step fashion to meet the requirements for disturbance attenuation, response time, and stability in terms of phase and gain margin, within the limitations of the actuation system. Once the desired system loop gain is shaped, and with knowledge of the plant transfer function, the technique shows how to systematically calculate the controller



Feedback control diagram, where r is the reference input, e is the error, G_C is the controller transfer function, G_P is the process transfer function, c is the output, and C and R are frequency domain variables associated with the time domain variables r and c .

second-order transfer functions representing the plant and actuator dynamics. The objective is to design a controller that achieves good command tracking with additional stringent specifications: actuation rate < 1000 units/sec; phase margin, $\phi M \geq 45^\circ$; gain margin, $GM \geq 10$ dB; one-time constant response ≤ 0.02 sec; settling time to 2-percent error ≤ 0.1 sec; midfrequency (≤ 100 rad/sec) disturbance attenuation, $DA = 20$ dB.

transfer function to arrive at the desired loop gain and meet the requirements. As such, the technique demonstrates what the limits of the control system design are based on the actuation system rates, so that the system will not be overdriven—avoiding possible damage to the hardware or driving the control system into saturation and nonlinear operation.

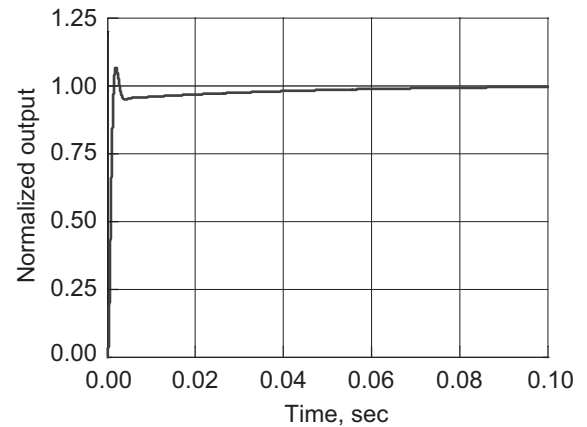
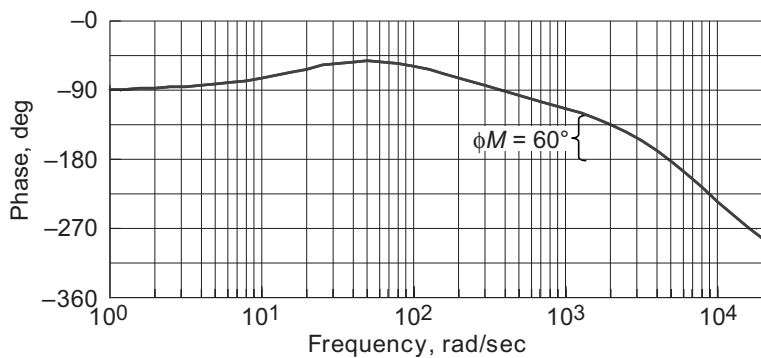
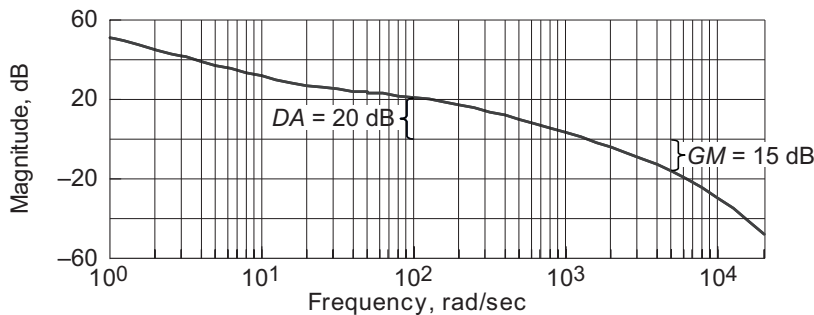
Understanding the limits of the control system design also allows for an in-depth understanding of how to evaluate system requirements and contrast them with the limits of design hardware. The technique includes lead-lag control compensation design to calculate the controller transfer function and arrive at the desired loop gain. Comparisons of this approach with more traditional feedback control designs, like proportional integral or proportional integral derivative control, demonstrate the advantages of this technique.

The diagram shows a traditional feedback control system with the closed-loop transfer function. In this design demonstration, the plant consists of two

The graphs on the left show the design of the loop gain to meet the specifications, and the right graph shows the time response of the system, with good tracking, one-time constant response (63 percent of steady state) well within 0.02 sec, and a settling time of < 0.1 sec. This design achieves the disturbance attenuation objectives in the time domain (as expected from the frequency domain in the left graphs), and the control deflections for the desired performance were within the actuator rate limit.

Bibliography

Kopasakis, George: Feedback Control Systems Loop Shaping Design With Practical Considerations. NASA/TM—2007-215007, 2007. <http://gltrs.grc.nasa.gov>



Left: Control loop gain design to meet requirements. Right: Designed closed-loop step response.

Glenn Contact:

George Kopasakis, 216-433-5327, GKopasakis@nasa.gov

Author:

George Kopasakis

Headquarters Program Office:

Aeronautics Research Mission Directorate

Programs/Projects:Fundamental Aeronautics Program,
Supersonics Project

Singular-Value Decomposition-Based Approach Developed for Thrust Estimation Over the Flight Envelope

In-flight estimation of unmeasurable turbofan engine output variables, such as thrust, is difficult because the values depend on the degradation level of the engine, which is often not known accurately. Degradation is generally defined in terms of parameters such as efficiency related to each major engine component. Variations in these parameters tend to cause shifts in the engine output. Standard estimation techniques can be used to determine the parameter values that result in the output deviations, and these estimated values can be used to reconstruct unmeasured output variables, such as thrust, using known relationships between variables. However, in standard engine installations there are too few sensors to make an accurate estimation of the deterioration level. Thus, the problem of reconstructing unmeasured output variables was addressed at the NASA Glenn Research Center by defining a reduced set of parameters that can be estimated and that have a similar effect on the unmeasured outputs.

At an operating point, the engine's behavior can be captured well by the linear model

$$\begin{aligned}\dot{x} &= Ax + Bu + Lp + e \\ y &= Cx + Du + Mp + w \\ z &= Ex + Fu + Np\end{aligned}$$

where x is the vector of state variables, u is the vector of control inputs, y is the vector of measured outputs, and z is the vector of unmeasurable outputs, such as thrust. The vector p represents parameters such as component efficiencies, which induce shifts in other variables as they move away from their nominal values. The vectors e and w represent uncertainty. The matrices A , B , C , D , E , F , L , M , and N are of appropriate dimension.

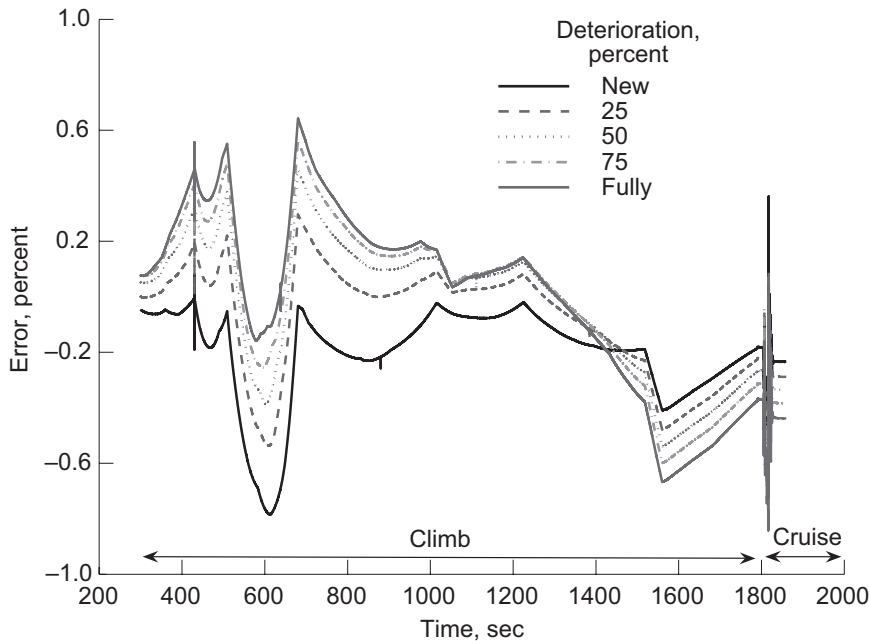
With an insufficient number of sensors to estimate p , the elements of z cannot be determined accurately. An existing approach is to estimate a subset of the parameters in p , the size of which corresponds to the number of measurements in y . The difficulty with this approach is deciding which subset to estimate while ensuring the best-possible estimate of the unmeasured output data. To address this problem, Glenn researchers developed a new design procedure. It utilizes singular value decomposition to help to create a linear model that contains the best representation of the deterioration-induced shifts in the

engine output variables using a nearly equivalent lower dimensional representation of degradation. This enables the user to determine a new vector q , of lower dimension than p , and corresponding matrices U_L , U_M , and U_N such that

$$\begin{bmatrix} U_L \\ U_M \\ U_N \end{bmatrix} q \approx \begin{bmatrix} L \\ M \\ N \end{bmatrix} p$$

This new representation is optimal in a least-squares sense, and because q can be estimated, the unmeasured output variables can be reconstructed using the linear model.

For evaluation, a complex nonlinear engine model was used to simulate thrust along a climb/cruise trajectory. A piecewise linear engine model, modified through the singular value decomposition design methodology, was used to track the thrust under various levels of engine deterioration. As seen in the figure on the next page, the thrust estimation error does not exceed 0.8 percent of the true value for any level of deterioration throughout the portion of the transient shown, and in the steady-state cruise portion, the worst case error is below 0.5 percent. This study demonstrates that this new approach can accurately estimate thrust over the flight envelope.



Percent thrust estimation error over the climb/cruise trajectory for various levels of engine deterioration, from new to fully deteriorated (ready for overhaul).

Find out more about the research of Glenn's Controls & Dynamics Branch:
<http://www.grc.nasa.gov/WWW/cdtb/>

Glenn Contact:
 Jonathan S. Litt, 216-433-3748,
 Jonathan.S.Litt@nasa.gov

Analex Corporation Contact:
 T. Shane Sowers, 216-433-3405,
 Thomas.S.Sowers@nasa.gov

Author:
 Jonathan S. Litt

LEW Number:
 LEW-18,093-1

Headquarters Program Office:
 Aeronautics Research Mission Directorate

Programs/Projects:
 Aviation Safety Program, Integrated Resilient Aircraft Control Project

Special Recognition:
 Best paper, Control, Diagnostics, and Instrumentation Track, ASME Turbo Expo 2005; Space Act Award 2007

Reference

1. Litt, Jonathan S.: An Optimal Orthogonal Decomposition Method for Kalman Filter-Based Turbofan Engine Thrust Estimation. NASA/TM-2005-213864 (ARL-TR-3487 and ASME Paper GT2005-68808), 2005. <http://gltrs.grc.nasa.gov>

Transient Simulation of Large Commercial Turbofan Engine Developed To Enable Advanced Controls and Diagnostics Research

There is great interest in the development of advanced control and diagnostic algorithms for turbofan engines to meet challenging performance and safety goals. However, an appropriate development platform such as a nonproprietary realistic transient simulation of a commercial, high-bypass engine with a representative Full Authority Digital Engine Control (FADEC) -like controller has been lacking. This has been a barrier to progress, especially in regard to collaboration between NASA researchers and their counterparts in academia and small businesses who wish to develop and evaluate their control and diagnostic algorithms on a realistic testbed.

To address this, the NASA Glenn Research Center has spearheaded the development of the Commercial Modular Aero-Propulsion System Simulation (C-MAPSS) software, in collaboration with ASRC Aerospace

Corporation, Saratoga Control Systems, Inc., and N&R Engineering researchers. C-MAPSS provides a transient simulation of a large commercial turbofan engine (up to 90,000-lb thrust) with a realistic engine control system. The software provides the user easy access to health, control, and engine parameters through a graphical user interface (GUI), and it operates several times faster than real time. In addition, the simulation can be deployed (all or in part) as machine code for hardware-in-the-loop applications

such as flight simulators and real-time controller/diagnostic system validation. The key function of C-MAPSS is to provide the user with a graphical turbofan engine simulation environment in which advanced algorithms can be implemented and tested. C-MAPSS can run user-specified transient simulations, and it can generate state-space linear models of the nonlinear engine model at an operating point.

The code is written in MATLAB/Simulink (The Mathworks, Natick, MA), with a number of GUI screens that allow point-and-click operation and have editable fields for user-specified input (see the figure). The software includes an atmospheric model that allows simulation of engine operation at altitudes from sea level to 40,000 ft, Mach numbers from 0 to 0.90, and ambient temperatures from -60 to 103 °F. The package also includes a power-management system that allows the engine to be operated over a wide range of thrust levels throughout the full range of flight conditions. This comprehensive control system consists of (1) a fan-speed controller; (2) three high-limit regulators that prevent the engine from exceeding its design limits for core speed, engine-pressure ratio, and high-pressure turbine exit temperature; (3) a fourth limit regulator that prevents the static pressure at the high-pressure compressor exit from going too low; (4) acceleration and deceleration limiters for the core speed; and (5) a comprehensive logic structure that integrates these control-system components in a manner similar to that used in real engine controllers such that integrator-windup problems are avoided.

Bibliography

Frederick, Dean K.; DeCastro, Jonathan A.; and Litt, Jonathan S.: User's Guide for the Commercial Modular Aero-Propulsion System Simulation (C-MAPSS). NASA/TM—2007-215026, 2007. <http://gltrs.grc.nasa.gov>

Find out more about MAPSS:

<http://www.grc.nasa.gov/WWW/cdtb/facilities/mapss.html>

Request MAPSS:

http://technology.grc.nasa.gov/software/SWInfo_form.asp?cat=all¢er=all&SwareKey=97

Glenn Contact:

Jonathan S. Litt, 216-433-3748,
Jonathan.S.Litt@nasa.gov

ASRC Corporation Contact:

Jonathan A. DeCastro, 216-433-3946,
Jonathan.A.Decastro@nasa.gov

Authors:

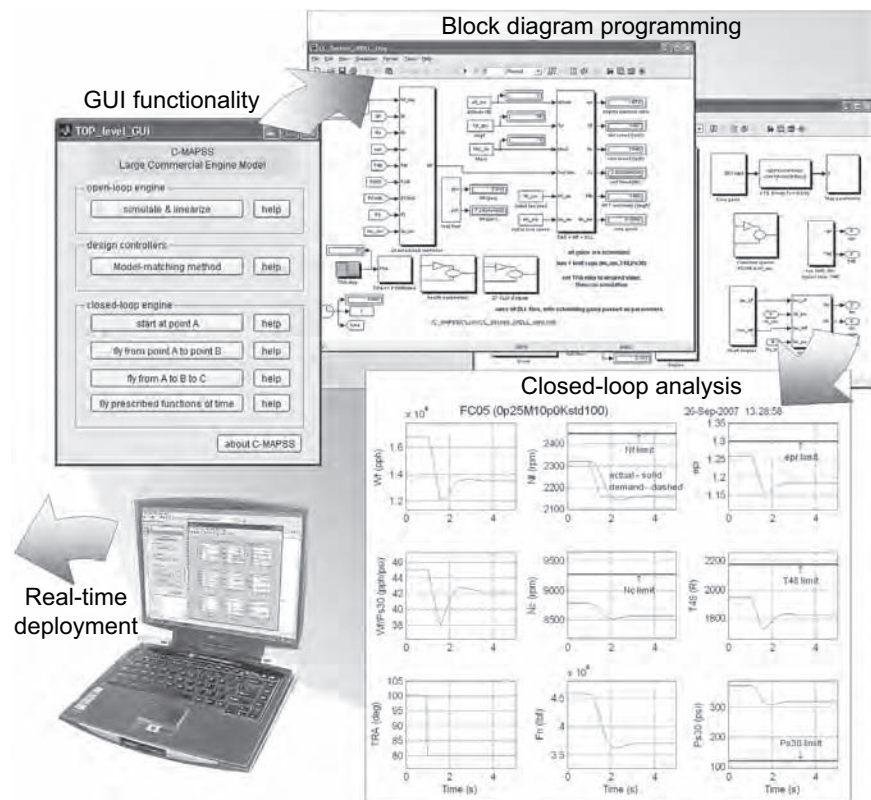
Jonathan S. Litt and Jonathan A. DeCastro

Headquarters Program Office:

Aeronautics Research Mission Directorate

Programs/Projects:

Aviation Safety Program, Integrated Resilient Aircraft Control Project



C-MAPSS is a transportable, modular, block-diagram-based code for GUI-driven engine simulation and analysis.

Operability of a Gas Turbine With Pressure-Gain Combustion Investigated

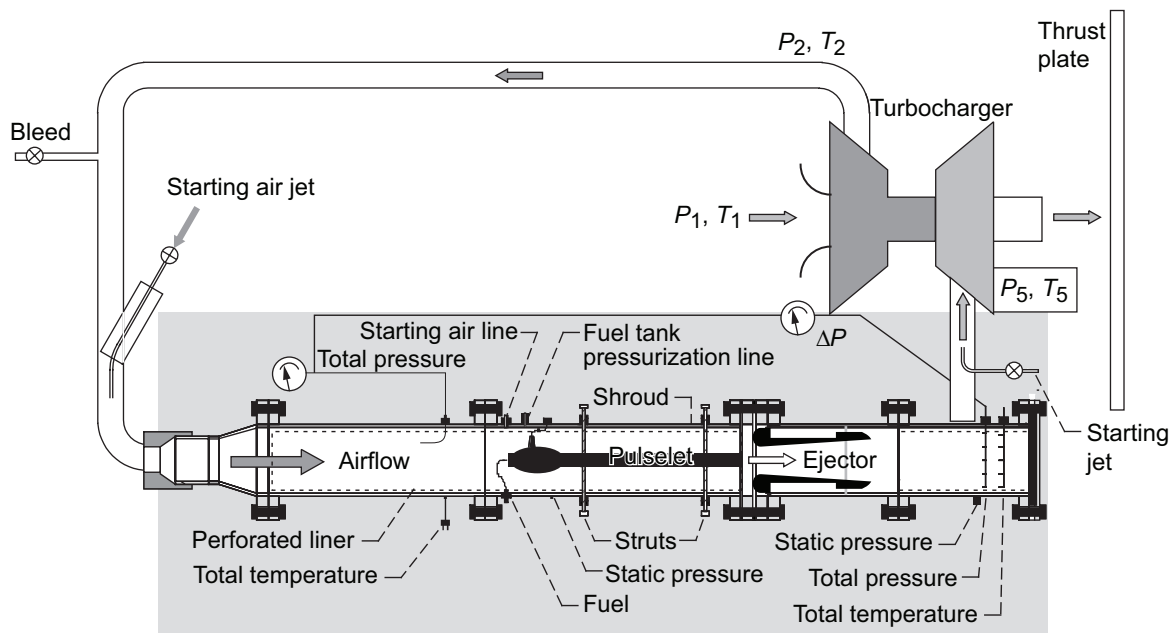
Gas turbine engines with conventional combustors suffer a loss in total pressure as the working fluid is heated. Typical combustor losses range from 4 to 8 percent of the total pressure from the upstream compressor. This loss yields lower work potential for the gas entering the downstream turbine. If the pressure loss can be reduced, or better still, if a modest pressure rise can be achieved across the combustor, significant improvements in specific fuel consumption are possible.

The benefits of pressure-gain combustion have been the impetus for numerous investigations. Each of these achieves pressure gain through some form of periodic, unsteady reaction. This, in turn, yields a combustor exit flow that is unsteady to one degree or another. Since unsteadiness is regarded as detrimental to the performance of downstream turbomachinery, its presence tends to detract from the thermodynamic benefits of the pressure gain. Therefore, it is desirable in any periodic combustion process to minimize unsteadiness in the exhaust path. Furthermore, the pulsed combustor effluent is generally far too hot to be sent directly into a turbine. Some form of bypass is necessary.

In 2005, an ejector-enhanced, pressure-gain combustor experiment was fabricated and tested at the NASA Glenn Research Center. The unit consists of a valved pulsejet and an optimized ejector, housed within a shroud. The shaded region of the schematic diagram shows the assembled rig. The combination forms a combustor across which there is a 3- to 4-percent total pressure rise. Associated with the unsteady combustion mode are total pressure fluctuations with root-mean-square (rms) levels measuring 4 to 5 percent of the mean. The rig was operated using a facility air supply, with no provision for heating the

inlet air to temperatures commensurate with a compressor exit. Furthermore, the combustor exhaust was simply vented to the ambient atmosphere. Thus, the impact of the pressure rise and unsteadiness on turbomachinery could not be assessed.

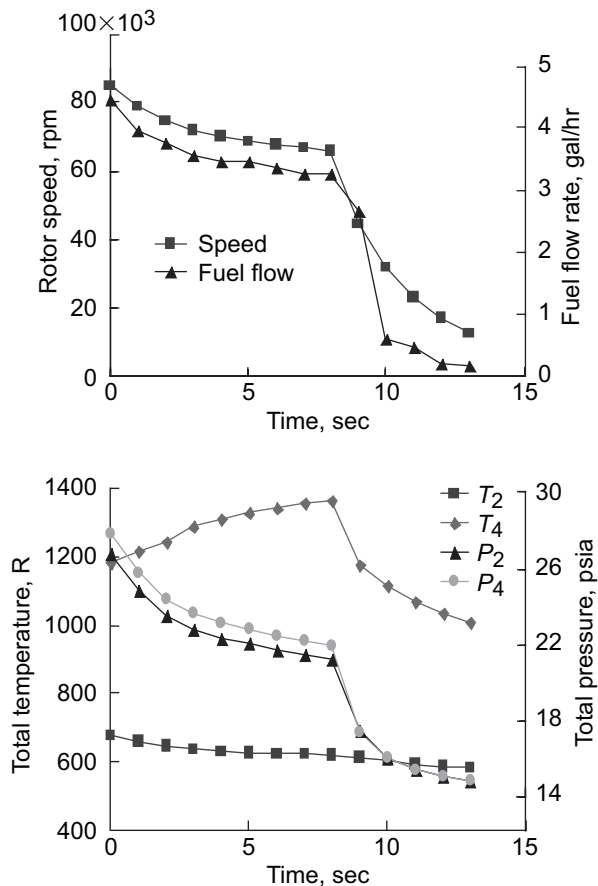
Recently, the rig was modified by the addition of a small automotive turbocharger sized for the combustor airflow rate, as shown in the unshaded portion of the diagram. The combustor exhaust gases are directed to the turbine inlet manifold of the turbocharger. The turbine exhaust is directed toward a thrust-measuring plate. The turbocharger compressor outlet is ducted to the inlet of the combustor. The combined turbocharger and combustor constitute a closed, functional gas turbine with pressure-gain combustion. The steady-state compressor and turbine performance maps are available, and the rig is sufficiently instrumented such that the impact of combustor-generated



Experimental pressure-gain combustor and associated turbomachinery. Pressure, P ; temperature, T .

unsteadiness on turbine operation can be assessed. Noise levels can be measured, and because the compressor discharges air at elevated temperature (thereby raising the speed of sound), resonant operability issues can be assessed.

The assembled rig has run successfully, achieving a steady rotor speed and generating thrust over the typical 15-sec test period. Several new instrumentation issues must be resolved before sufficient data can be acquired for complete, quantitative analyses. The graphs show select measured parameters as a function of time during a typical test run. There is a pressure rise across the combustor ($P_4 > P_3$) throughout the run duration.



Selected measurements obtained during operation.

Glenn Contact:

Dr. Daniel E. Paxson, 216-433-8334,
Daniel.E.Paxson@nasa.gov

ASRC Corporation Contact:

Kevin T. Dougherty, 216-433-3546,
Kevin.T.Dougherty@nasa.gov

Author:

Dr. Daniel E. Paxson

LEW Number:

LEW-18096-1

Headquarters Program Office:

Aeronautics Research Mission Directorate

Programs/Projects:

Fundamental Aeronautics Program,
Subsonic Fixed Wing Project

Special recognition:

A NASA Tech Brief about this research, "Ejector-Enhanced, Pulsed, Pressure-Gain Combustor," resulted in a Nominal Space Act Award from the Invention and Contribution Board.

Bibliography

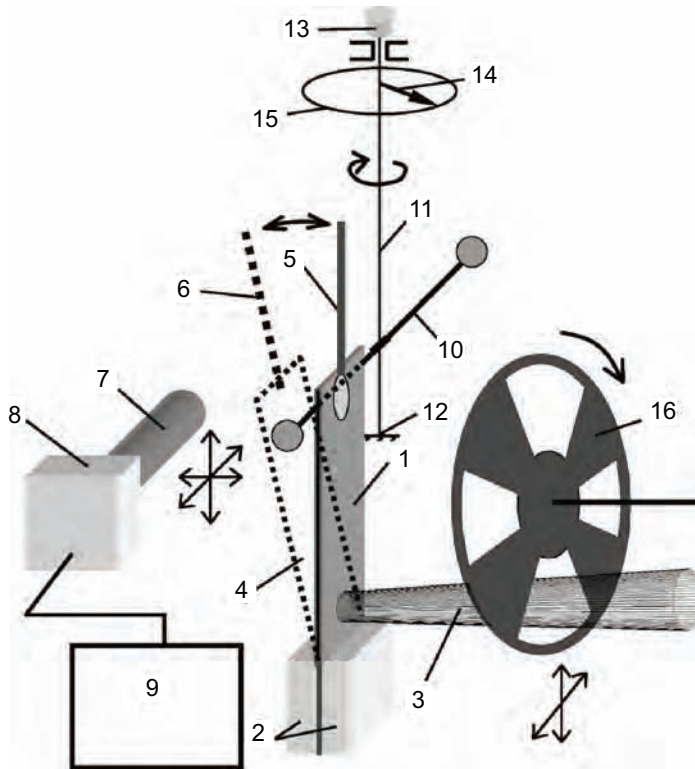
Paxson, Daniel E.; and Dougherty, Kevin T.: Ejector Enhanced Pulsejet Based Pressure-Gain Combustors: An Old Idea With A New Twist. NASA/TM-2005-213854 (AIAA-2005-4216), 2005. <http://gltrs.grc.nasa.gov>

Paxson, Daniel E.; and Perkins, H. Douglas: Thermal Load Considerations for Detonative Combustion-Based Gas Turbine Engines. NASA/TM-2004-213190 (AIAA-2004-3396), 2004. Available from the Center for AeroSpace Information.

Light-Driven Actuators Based on Polymer Films Developed and Demonstrated

A novel light-driven actuator technology based on films of polymer polyvinylidene fluoride, known as PVDF, was developed and demonstrated by the NASA Glenn Research Center and the Alabama A&M University. The actuation principle is in the mechanical bending of a polymer film caused by low-power (10-mW and less) laser radiation. The technology is based on a photomechanical effect that combines various physical mechanisms, such as thermal expansion, the converse piezoelectric mechanism, and photovoltaic and pyroelectric mechanisms, where thermal expansion is dominant.

The force applied by the actuators to external objects is measured with a torsion balance. It was found to be proportional to the power of the laser beam and could be as high as 10^{-4} N for a 50- μ m film illuminated with a 10-mW laser beam.



Experimental setup for investigating the photomechanical effect.

The schematic shows a strip of metal-coated PVDF film (1) clamped between two glass slides (2). After being illuminated with a laser beam (3) that can be moved laterally in the vertical and horizontal direction with respect to the strip, the strip bends and takes new position (4). A segment of optical fiber (5) is glued to the top free end of the strip. When the strip bends, the fiber takes position (6). A telescopic microscope (7) on a mount with three translational degrees of freedom monitors the displacement of the free end of the fiber with an attached charge-coupled device (CCD) camera (8) that is connected to a television monitor (9). The force generated by the bending strip

is measured with a torsion balance that consists of a rod (10) suspended on a string (11). The lower end of the string is fixed at point (12). The upper end is connected to a knob (13). By turning the knob, researchers can change the angular position of a pointer (14) attached to the string. The angular position of the pointer is read on a dial (15). A mechanical chopper (16) was used in the experiments on the vibrations of the PVDF strip, which were initiated by the pulsed laser light.

The force applied by the actuators to external objects was found to be proportional to the power of the laser beam and could be as high as 10^{-4} N for a 50- μ m film illuminated with a 10-mW laser beam. We demonstrated mechanical vibrations of a 1- by 7-mm strip actuator at a frequency of 0.3 kHz.

As examples of possible applications, a photonic switch and an actuator with a closed-loop motion that could drive the inner workings of a conventional mechanical clock were demonstrated. The proposed actuators also could be used as the propulsion components of future light-driven microsystems and nanosystems.

This work was done through a Partnership Award to Glenn and Alabama A&M that started in 1999. The university's involvement was supported by grant NCC3-736 from NASA Headquarters.

Bibliography

Sarkisov, S.S., et al.: Light-Driven Actuators Based on Polymer Films. *Opt. Eng.*, vol. 45, no. 3, 2006, p. 034302.

Bimorphic Polymeric Photomechanical Actuator, U.S. Patent 6,999,221 (LEW-17473-1).

Glenn Contact:

Dr. Grigory Adamovsky, 216-433-3736, Grigory.Adamovsky-1@nasa.gov

SSS Optical Technologies, LLC, Contact:

Dr. Sergey S. Sarkisov, 256-489-0081, mazillo@hotmail.com

Authors:

Dr. Grigory Adamovsky and Dr. Sergey S. Sarkisov

LEW Number:

LEW-17473-1

Headquarters Program Office:

Office of Equal Opportunity Programs

Programs/Projects:

Future light-driven microsystems and nanosystems

Special Recognition:

The paper in the bibliography was recognized as the most noteworthy original paper on the theoretical or experimental aspects of optical engineering published in 2006 in SPIE's Optical Engineering journal. On the basis of this work, the authors were awarded the 2006 Rudolph Kingslake Medal and Prize for original development of new light-driven actuators based on PVDF thin films with potential microscale and nanoscale applications.

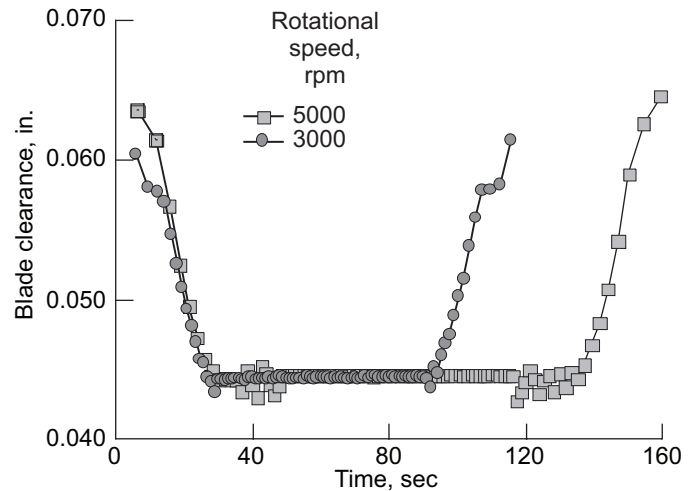
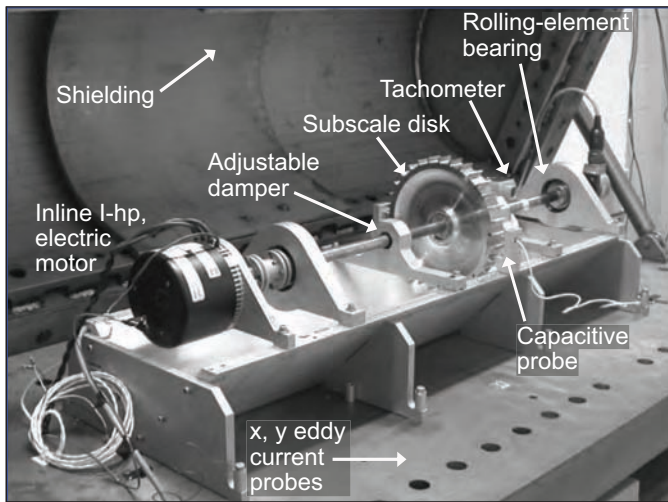
Use of Sensors on a Bladed Rotating Disk Evaluated for Health Monitoring and Crack Detection

Developing health management and ultrasafe engine technologies are the primary goals of NASA's Aviation Safety Program. In addition to improving safety, health monitoring can reduce maintenance costs. Typically, this involves a sensor system that can sustain normal operation in a harsh engine environment. The system should also be able to broadcast a signal if a crack detected in the component is greater than a prespecified length but below a critical length that would lead to failure. Furthermore, the system should have a neutral effect on overall engine system performance and should not interfere with engine maintenance operations. Currently, many different non-destructive evaluation (NDE) techniques are used to detect cracks to prevent catastrophic failure, but the effectiveness and reliability of these techniques vary substantially depending on the inspection conditions (ref. 1). Therefore, more reliable diagnostic tools and high-level techniques for detecting damage and monitoring the health of rotating components are needed to maintain engine safety and reliability and to assess life. As a result, the NDE Group at the NASA Glenn Research Center assembled a unique disk spin simulation system to verify and study a crack-detection technique that senses center-of-mass changes of the rotor system.

The study is under NASA's Aviation Safety Integrated Vehicle Health Management program, which is developing and demonstrating technologies that lead to safer aviation and to fewer injuries and fatal aviation accidents (ref. 2). Glenn's NDE Group is developing combined experimental-analytical capabilities to test the ability of health-monitoring technologies to detect rotor

damage in situ prior to a catastrophic event (refs. 3 and 4). The system can evaluate crack-detection techniques systematically through highly controlled crack-initiation and crack-growth tests on subscale rotors up to 46-cm (18-in.) diameter spinning at up to 10 000 rpm.

This year, spin tests were conducted at spin-up/cruise/spin-down and spin-up/spin-down states. Displacement data were recorded with noncontact sensors for blade-tip-clearance measurements. The sensor used was a capacitive-type system. The data were analyzed using a LabVIEW-based (National Instruments Corporation) front-end module customized to meet testing and data-collection requirements. Maximum rotational speeds were between 5000 and 6200 rpm, and acceleration and deceleration rates were between 25 and 50 rpm/sec.

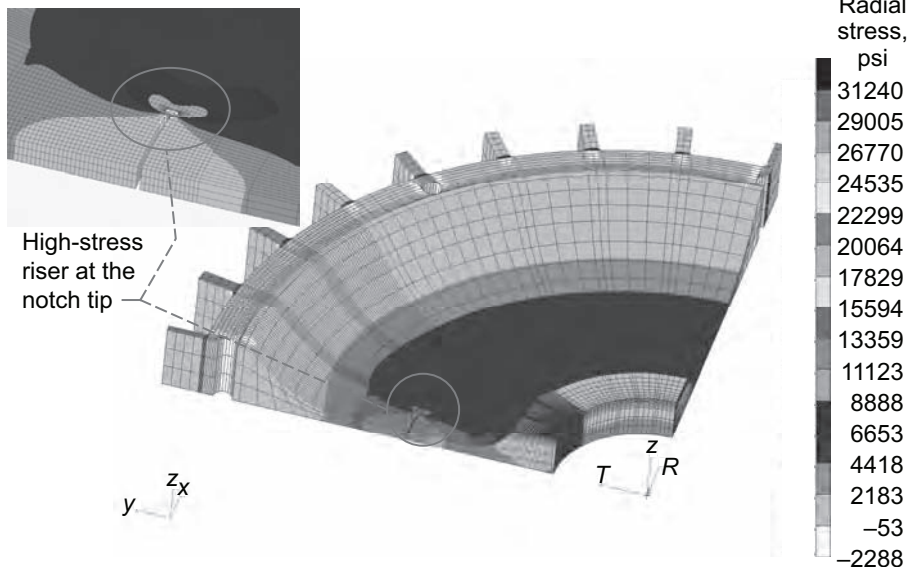


Left: Spin lab test rig. Right: Blade clearance as a function of time for a notch size of 3.05 cm (1.2 in.) for two different rotational speeds.

The photograph shows the spin test rig assembly and equipment, including the 25.4-cm- (10-in.-) diameter turbine-like disk test article used to evaluate the crack-detection techniques. The graph shows the experimental data collected, including the blade gap for a notched disk due to rotational speeds of 3000 and 5000 rpm for a spin-up/cruise/spin-down test. The data show that the blade gap is lower at cruise and that changes with respect to speed are minimal in comparison to those recorded at both spin up and spin down. The results indicate the success of the spin system in simulating a typical rotor-dynamic environment and demonstrate its ability to test and improve crack-detection systems. Parallel analytical work also is being conducted. The following figure represents the stress state of the rotor at a set speed of 8000 rpm. The high-stress riser at the notch tip indicates a possible crack-propagation site. We plan to give more details about these findings in future reports.

References

1. Abdul-Aziz, Ali; Trudell, Jeffrey J.; and Baaklini, George Y.: Finite Element Design Study of a Bladed, Flat Rotating Disk to Simulate Cracking in a Typical Turbine Disk. Proc. SPIE Int. Soc. Opt. Eng., vol. 5767, 2005, pp. 298–307.
2. Aviation Safety Program—Integrated Vehicle Health Management, Technical Plan Summary. National Aeronautics and Space Administration. http://www.aeronautics.nasa.gov/nra_pdf/ivhm_tech_plan_c1.pdf
3. Gyekenyesi, Andrew L.; Sawicki, Jerzy T.; and Baaklini, George Y.: Application of Vibration Monitoring Techniques for Damage Detection in Rotating Disks. Proceedings of the 9th International Symposium on Transport Phenomena and Dynamics of Rotating Machinery, Honolulu, HI, Feb. 2002.
4. Drumm, M.: Non-Destructive, Real-Time Measurement of Cracks in Jet Engine Rotors. White Paper—Test Devices, Inc., Hudson, MA, 1998.



Radial stresses at a speed of 8000 rpm. T, tangential; R, radial. This figure is shown in color in the online version of this article (<http://www.grc.nasa.gov/WWW/RT/2007/Inst-Cnt/08-RIO-aziz1.html>).

Glenn Contacts:

Dr. Ali Abdul-Aziz, 216-433-6729,
Ali.Abdul-aziz-1@nasa.gov

John D. Lekki, 216-433-5650,
John.D.Lekki@nasa.gov

Dr. Andrew L. Gyekenyesi, 216-433-8155, Andrew.L.Gyekenyesi@nasa.gov

Dr. George Y. Baaklini, 216-433-6016, George.Y.Baaklini@nasa.gov

Authors:

Dr. Ali Abdul-Aziz, John D. Lekki,
Dr. Andrew L. Gyekenyesi, and
Dr. George Y. Baaklini

Headquarters Program Office:

Aeronautics Research Mission Directorate

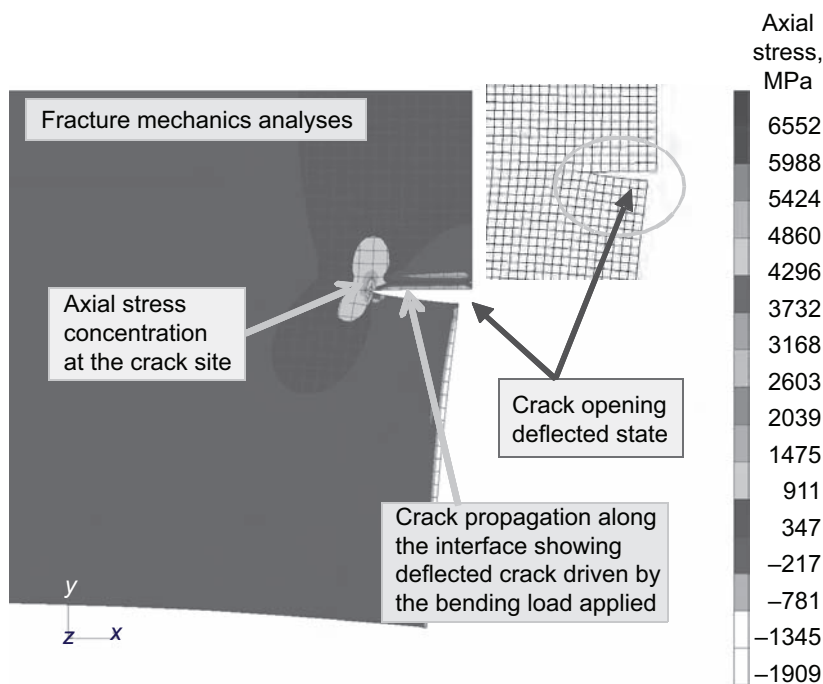
Programs/Projects:

Integrated Vehicle Health Management
Program

Development of Analytical Criteria for Crack Deflection and Penetration in Coated Ceramics Initiated

Silicon nitride (Si_3N_4) layered ceramics with weak boron nitride (BN) interphases have been manufactured in a conventional two-dimensional layered structure (ref. 1) as well as in a novel layered structure known as fibrous monolithic ceramic (ref. 2). Notable properties were reported for both structures with high strength and workout fracture (ref. 3). In some of these layered materials, delamination cracks bow out of the interface after propagating on the interface only a short distance (refs. 4 to 6). Such crack bowing occurs

because not much energy is absorbed when these materials fracture. Therefore, an understanding of the factors that control crack deflection and propagation along interfaces is needed to maximize the energy dissipation capabilities of layered ceramics.

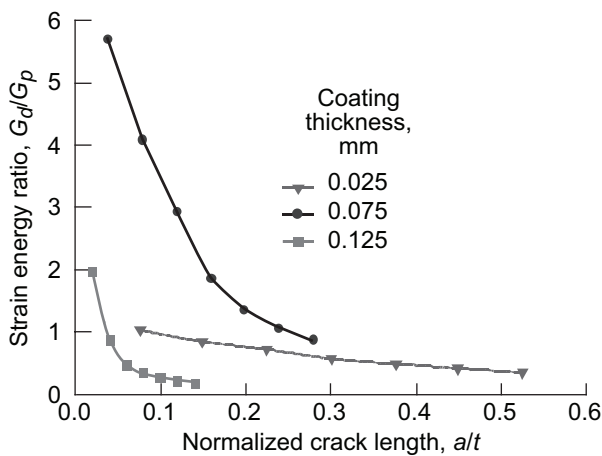


The proposed technical approach is to evaluate crack behavior analytically at the interface of an environmental barrier coating (EBC) with a monolithic ceramic. This establishes correlations that help to determine when the crack is arrested or advanced by either penetrating the interface or deflecting into the interface. Critical parameters determining penetration and deflection conditions in relation to the EBC's physical characteristics, such as porosity level, will be determined for single-layer and multilayered coatings, and will coordinate the interactions between the EBCs (mullite, mullite mixture, porous yttrium-stabilized zirconia (YSZ), etc.) and the substrate structure.

In 2007 and in support of the analytical activities proposed under the NASA Glenn Research Center grant entitled "Strain-Tolerant Self-Sensing Environmental Barrier Coatings for SiC/SiC Ceramic Matrix Composites and Si_3N_4

Fracture mechanic analyses showing an advanced crack parallel to the coating/substrate interface. This figure is shown in color in the online version of this article (<http://www.grc.nasa.gov/WWW/RT/2007/Inst-Cnt/09-RIO-aziz2.html>).

Ceramics,” numerical modeling of thermal-cycling-induced crack nucleation and propagation was initiated to assist the microstructural design of various layers in the EBC architecture. Relevant conditions that cover the effects of thermal cycling, resistance to bending, oxidation, high temperature, burner flame, and cooling are being considered. The diagram on the preceding page shows a contour for a crack propagating parallel to the coating/substrate interface. This represents a finite element model of a bend bar specimen under four-point loading conditions and the results of fracture mechanic analyses employing crack advancement in two directions: parallel and perpendicular to the coating/substrate interface. The analyses assumed that the combined residual stress effects and mechanical loading were due to both the coating application procedure and bending. The energy release rate for the deflected crack was compared with the maximum energy release rate for the penetrating crack. A range of interface toughness relative to bulk material toughness will be determined from the results. The graph represents the analytical findings for the crack surface deflection case. It shows the strain energy variation for three different coating thicknesses being considered, where G_d and G_p are, respectively, the strain energy release rates for the deflection and penetration conditions, and the normalized crack length is the ratio of the crack size a and the coating thickness t .



Normalized crack length as a function of the strain energy ratio for different coating thicknesses.

These data are expected to guide the optimization of the EBC system to deflect the crack away from the substrate and contain it mainly along the interface of the top layer or layers. The results presented are only for one layer of coating; however, work including multilayer coating conditions is planned, and experimental tests complementing these analytical studies are ongoing.

References

1. Chen, Dai-Heng: Crack Normal to and Terminating at a Bimaterial Interface. *Eng. Fract. Mech.*, vol. 49, no. 4, 1994, pp. 517–532.
2. Zak, A.R.; and Williams, M.L.: Crack Point Stress Singularities at a Bi-Material Interface. *J. Appl. Mech.*, vol. 30, series E, no. 1, 1963, pp. 142–143.

3. Dundurs, J.: Effect of Elastic Constants on Stress in a Composite Under Plane Deformation. *J. Compos. Mater.*, vol. 1, no. 3, 1967, pp. 310–322.
4. He, Ming-Yuan; and Hutchinson, John W.: Crack Deflection at an Interface Between Dissimilar Elastic Materials. *Int. J. Solids Struct.*, vol. 25, no. 9, 1989, pp. 1053–1067.
5. He, Ming-Yuan; Evans, Anthony G.; and Hutchinson, John W.: Crack Deflection at an Interface Between Dissimilar Elastic Materials: Role of Residual Stresses. *Int. J. Solids Struct.* vol. 31, no. 24, 1994, pp. 3443–3455.
6. Martinez, Doris; and Gupta, Vijay: Energy Criterion for Crack Deflection at an Interface Between Two Orthotropic Media. *J. Mech. Phys. Solids*, vol. 42, no. 8, 1994, pp. 1247–1271.

Cleveland State University Contacts:

Dr. Ali Abdul-Aziz, 216–433–6729,
Ali.Abdul-aziz-1@nasa.gov

Dr. Surendra N. Tewari, 216–523–7342,
S.TEWARI@csuohio.edu

U.S. Army Research Laboratory at Glenn Contact:

Dr. Ramakrishna T. Bhatt, 216–433–5513,
Ramakrishna.T.Bhatt@nasa.gov

Authors:

Dr. Ali Abdul-Aziz,
Dr. Ramakrishna T. Bhatt, and
Dr. Surendra N. Tewari

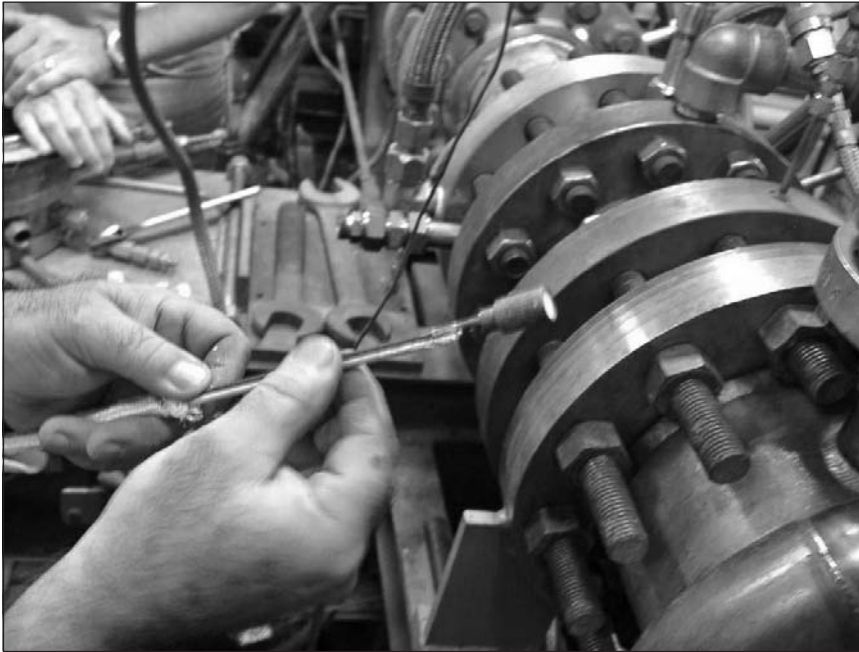
Headquarters Program Office:

NASA Grant NNX07AC76A

Programs/Projects:

Research Opportunity in Aeronautics—2006

Microwave Turbine-Tip-Clearance Sensor Tested in Relevant Combustion Environment



Microwave tip-clearance sensor being removed from the High Pressure Burner Rig upon completion of testing.

A microwave turbine-tip-clearance sensor was tested in a relevant combustion environment at temperatures exceeding 1000 °C in NASA Glenn Research Center's High Pressure Burner Rig. This sensor is an integral component in the development of active control of the gap between the rotating turbine blade and the stationary case of jet engines. Studies have shown that minimizing this gap to 0.25 mm could reduce fuel consumption by approximately 1 percent and significantly lower the emissions of nitrogen oxides, carbon monoxide, and carbon dioxide while lowering the exhaust gas temperature by 10 °C. Additional benefits include decreased operating and maintenance costs while increasing range and payload capabilities.

Microwave clearance probes work by emitting a radiowave from a sensor that actually is both a transmitting and receiving antenna. The signal is reflected off of a metal object and received back by the sensor. The difference between these sensors and traditional radar is that radar is used on distance scales of miles and microwave sensors measure fractions of a millimeter. Like radar, these sensors can "see" through nonmetallic materials and are unaffected by contaminants from combustion in jet engines. The sensor system was developed and purchased under NASA's Small Business Innovation Research program from Radatec, Inc. (currently Vibro-Meter S.A.).

The microwave tip-clearance probe was successfully tested at Glenn at temperatures exceeding 1000 °C for 45 min at conditions that were more extreme than a typical mounting in a turbine engine. The sensor would typically

be mounted in the engine casing, where only the probe face would be exposed to the extreme combustion temperatures internal to the jet engine while the probe sensor shell and cable would be exposed to lower temperatures (approximately 700 °C). This test exposed the entire probe and several inches of cable to the higher temperatures because of the test fixtures available. The test comprised a series of burner start transients and dwells at temperature followed by a shut-down to evaluate the probe for turbine environment survivability. As shown in the photograph, the sensor was discolored but functional upon removal from the mounting hardware after testing. Microwave tip-clearance sensor technology is currently being studied in turbine blade health-monitoring applications where the structural health of the internal rotating components can be assessed through analysis of the signal acquired from the clearance sensor.

Find out more about the research of Glenn's Optical Instrumentation & NDE Branch:

<http://www.grc.nasa.gov/WWW/OptInstr/>

Glenn Contacts:

Timothy J. Bencic, 216-433-5690,
Timothy.J.Bencic@nasa.gov

Mark R. Woike, 216-433-5701,
Mark.R.Woike@nasa.gov

Author:

Timothy J. Bencic

Headquarters Program Office:

Aeronautics Research Mission Directorate

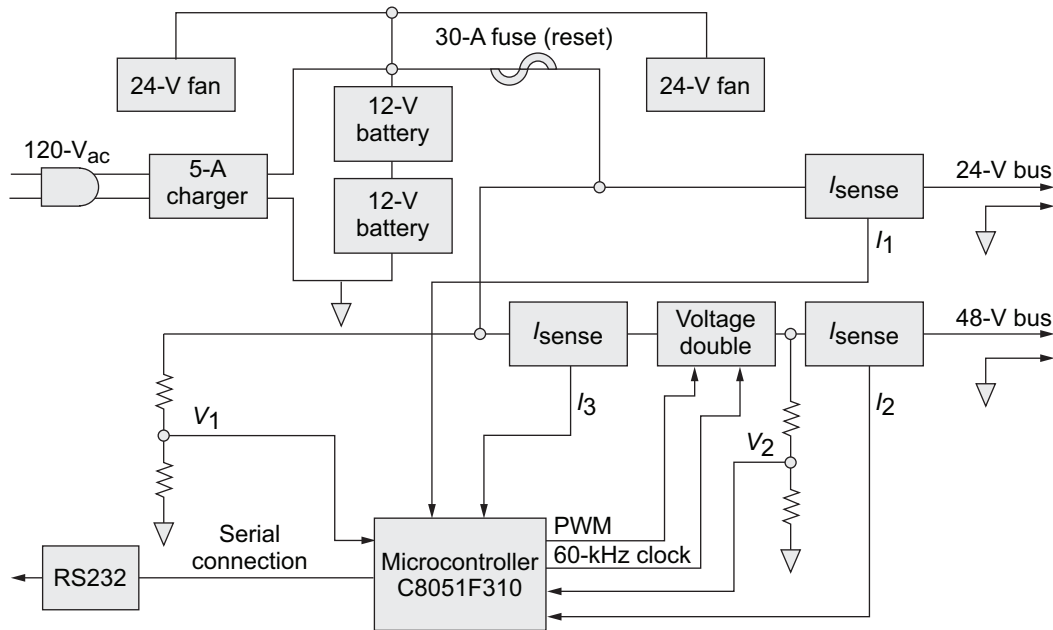
Programs/Projects:

Fundamental Aeronautics Program,
Supersonics Project, Aviation Safety
Program, Integrated Vehicle Health
Management Program, Small Business
Innovation Research

Smart Power System Developed for Scarab Lunar Rover

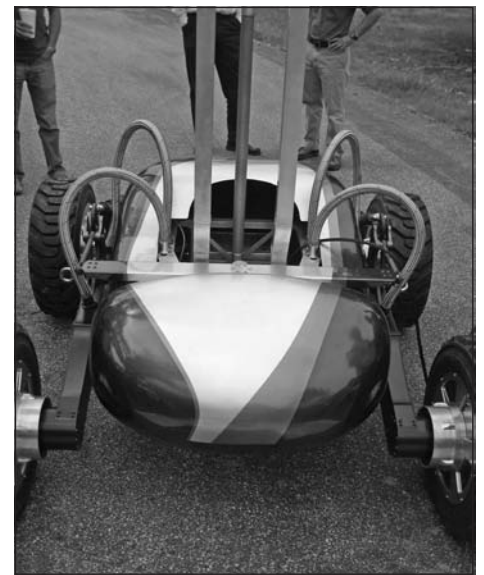
NASA Glenn Research Center's Optical Instrumentation and Nondestructive Evaluation (NDE) Branch delivered its Smart Power System to Carnegie Mellon University (CMU). The system was integrated into CMU's Scarab lunar rover. Scarab is a joint effort between CMU, Glenn's Space Flight Systems and Research and Technology Directorates, NASA's In-Situ Resource Utilization Project, and the NASA Ames Research Center to develop an Earth analog for a lunar rover. The Smart Power System is a stand in for more lunar friendly power systems, which might be based on radioisotope heat sources.

As described in a Pittsburgh Post-Gazette article, "The robotic rover, Scarab, is designed to drill into the ground and obtain core samples a meter long that it also can process and analyze. The eventual goal is finding hydrogen, and possibly water and other chemicals, that



Power supply; PWM, pulse-width modulation.

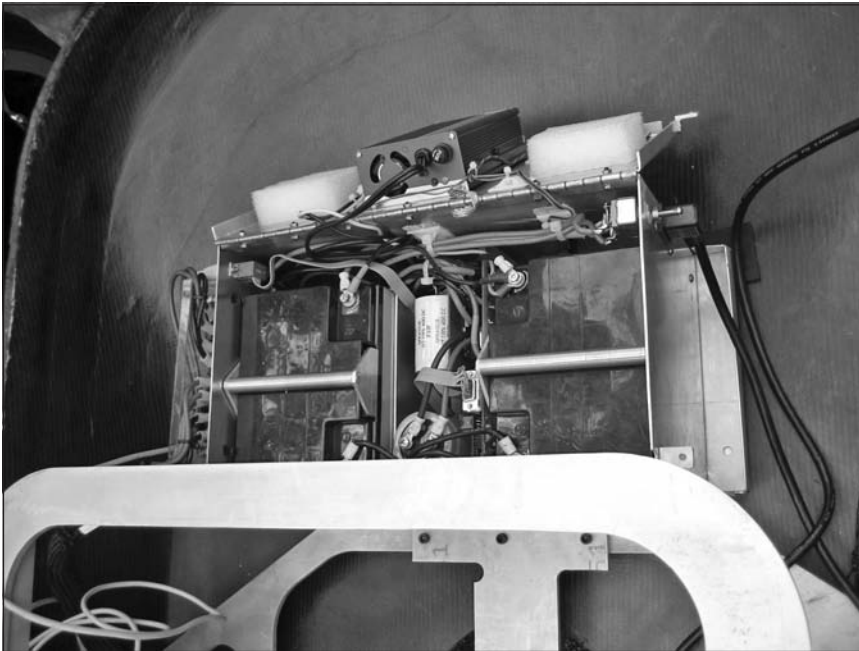
The Smart Power System integrates a battery bank, a charging system, and a power converter with electrical characteristics similar to that of Glenn's Stirling Radioisotope Generator (see the diagram). This system also incorporates a microprocessor-based instrumentation package that communicates with Scarab's central processing unit (CPU) through a serial data link. This system produces a nominal 28-V bus for the general power needs of the robot and a second programmable 720-W supply that can be adjusted by the rover for any voltage between 24 and 48 V. The Scarab rover (see the photograph) currently uses the programmable supply for the wheel drive motors. In addition to providing flexibility, the Smart Power System allows CMU to instantaneously monitor several power system variables during testing and operation. This functionality will allow power-consumption modeling for different mission objectives, which could provide invaluable information for a power-constrained mission such as a lunar exploration.



Scarab lunar rover.

can be mined on the moon to produce fuel, water and air essential for supporting lunar outposts” (ref. 1).

Glenn’s Optical Instrumentation and NDE Branch designed the Smart Power System, which is the only noncommercially available subsystem in Scarab (see the following photograph). The Smart Power System gives CMU the flexibility to try different actuators and instruments with varying power requirements. It also monitors the two power buses for voltage and current, calculates instantaneous power and power converter efficiency, and can be set to cut the programmable voltage output at a current level chosen by the Scarab CPU to prevent overload conditions. Thus, CMU has been able to monitor instantaneous power system variables while testing Scarab. The Smart Power System also can initiate communication with the CPU autonomously when an anomalous condition, such as low battery voltage or a current overload, occurs. For mission safety, if the Smart Power System were to fail, Scarab would not lose battery power and the battery voltage would appear on the programmable bus. A system such as this could eventually be extended to flight-level hardware, which would allow for a highly robust power system capable of a high level of autonomy, thus off-loading the spacecraft CPU and increasing performance and reliability.



Power system within Scarab.

Reference

1. Templeton, David: CMU Rolls Out Prototype for Robotic Moon Rover. Pittsburgh Post-Gazette, Sept. 21, 2007. <http://www.post-gazette.com/pg/07264/819398-85.stm>

Glenn Contacts:

Larry Greer, 216–433–8770,
Lawrence.C.Greer@nasa.gov
Mike Krasowski, 216–433–3729,
Michael.J.Krasowski@nasa.gov

Ohio Aerospace Institute (OAI) Contact:

Joe Flatico, 216–433–5053,
Joseph.M.Flatico@nasa.gov

ASRC Corporation Contact:

Nuha Nawash, 216–433–3146,
Nuha.S.Nawash@nasa.gov

Authors:

Lawrence C. Greer III,
Michael J. Krasowski, Joseph M. Flatico,
and Nuha S. Nawash

Headquarters Program Office:

Exploration Systems Mission Directorate

Programs/Projects:

In-Situ Resource Utilization

N-Channel Junction-Field-Effect-Transistor-Based Digital Logic Gate Structure Using Resistive Level Shifters and Configurable From High-Temperature Silicon Carbide Electronics Developed

At the NASA Glenn Research Center, a circuit topography was developed and used to create usable digital logic gates using N-channel (negatively doped) junction field effect transistors (JFETs) and load resistors, level shifting resistors, and supply voltages whose values are all based on the direct-current parameters of those JFETs. This method has direct application to the current state of the art in high-temperature (500 °C and higher) silicon carbide (SiC) device production. This work enables digital logic and state machine capabilities for systems operation in extremely hot environments like the surface of Venus, near hydrothermal vents, within nuclear reactors, in space (SiC is inherently radiation hardened), and within internal combustion engines. The basic structure of this innovation can be reconfigured into various analog circuit functions through the use of feedback structures.

The present state of the art in SiC component production allows for single to small-number component production of N-channel JFETs and epitaxial resistors on a single substrate. Other logic types require mixes of complementary P- (positively doped) and N-channel devices, or mixes of depletion and enhancement mode devices, and do not work at extreme temperatures. A circuit design was developed to allow logic gates to be developed using only epitaxial resistors and N-channel JFETs.

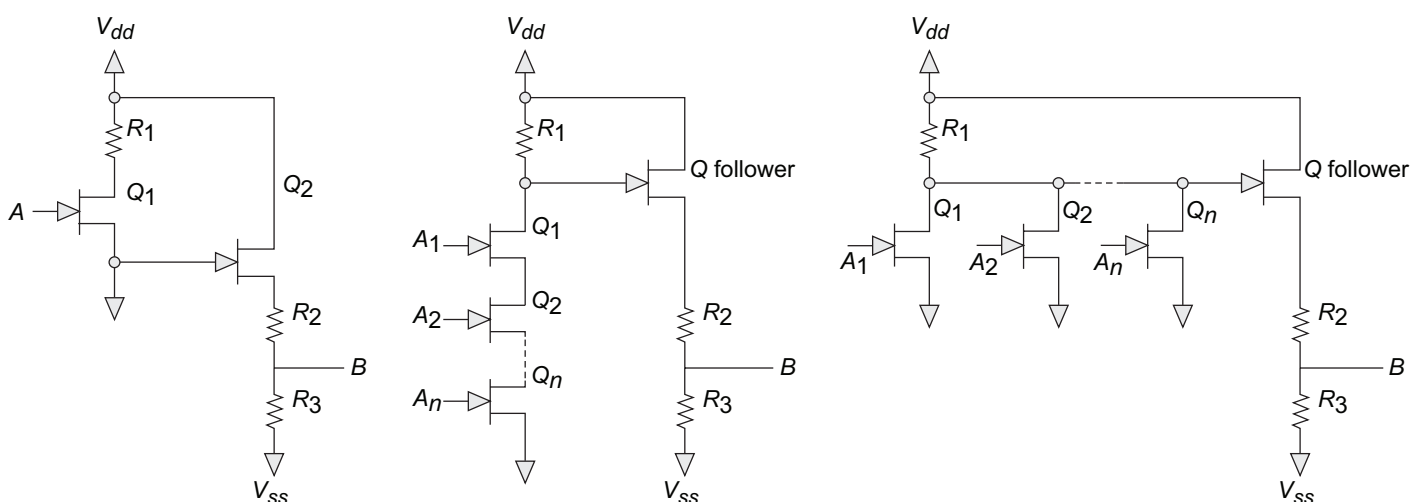
The circuit diagram on the left shows a simple inverter architecture. Here $R_1 = R_2 = R_3$, and this value is related to the characteristics of Q_1 and Q_2 . The power rails, V_{SS} and V_{DD} , are also chosen from JFET characteristics and

are equal in magnitude, differing only in polarity. Thus, with a logic 0, that is $\frac{1}{2} V_{SS}$, at point A , the output at point B is a logic 1, that is zero volts. With a logic 1, that is zero volts at point A , the output at point B is a logic 0, that is $\frac{1}{2} V_{SS}$.

If Q_1 is replaced with a series string of n FETs (see the center circuit diagram), the device becomes an n -input NAND gate. The output remains at logic 1 until every n input is at a logic 1, at which time it will go to a logic 0.

If Q_1 is replaced with a parallel string of m FETs (see the circuit diagram on the right), the device becomes an m -input NOR gate. The output will go to a logic 0 if any m input is at a logic 1.

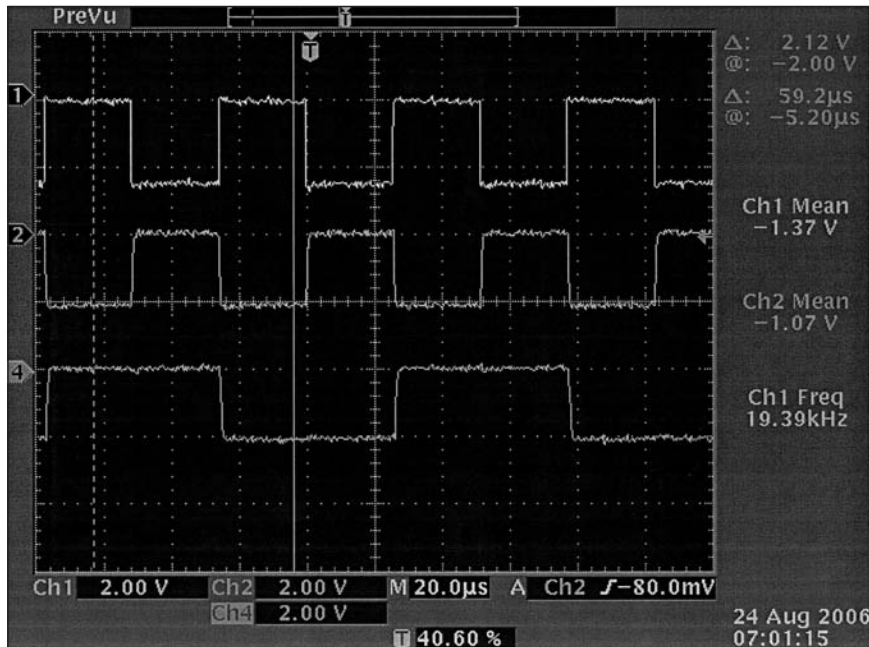
A divide-by-two logic circuit configured as an edge-triggered cross-coupled D flip flop was synthesized using this technique and configured using room-



Left: Basic inverter circuit, showing points A and B ; resistors R_1 , R_2 , and R_3 ; N-channel JFETs Q_1 and Q_2 ; and power rails V_{DD} and V_{SS} . Center: Basic NAND (not and) circuit. Right: Basic NOR (not or) circuit.

temperature JFETS and resistors. The final figure shows the input clock as the top trace with the bottom trace showing the output, which is one-half the frequency of the input. The center trace is the inversion of the clock input as created within the flip-flop structure.

This innovation—made from state-of-the-art, high-temperature SiC JFET devices and epitaxial resistors—allows for the configuration of combinatorial-, pulse-, and clock-mode digital logical functions. With proper feedback, it also allows for the configuration of linear and nonlinear analog building blocks.



Oscilloscope traces of divide-by-two circuits synthesized using the basic gates and built using room-temperature components. The top trace is the input clock, the middle trace is the inversion of the input, and the bottom trace is the output at one-half of the input frequency.

Glenn Contacts:

Michael J. Krasowski, 216-433-3729,
Michael.J.Krasowski@nasa.gov

Norman F. Prokop, 216-433-6718,
Norman.F.Prokop@nasa.gov

Authors:

Michael J. Krasowski and
Norman F. Prokop

LEW Number:

LEW-18256-1

Headquarters Program Office:

Aeronautics Research Mission Directorate

Programs/Projects:

Subsonic Fixed Wing Project, Integrated
Vehicle Health Management Program

Great Lakes Environmental Aerial Monitoring Team Developed and Tested Second-Generation Hyperspectral Instrument Suite on NASA Glenn's Learjet 25

The members of the Great Lakes Environmental Aerial Monitoring Team (GLEAM) have designed, developed, integrated, and flight tested a second-generation hyperspectral imager (HSI) for aerial water quality measurement. During 2007, the HSI worked with a suite of instruments to obtain the spectral signature data of algae in the western basin of Lake Erie and in Lake Huron's Saginaw Bay. The instrument suite consists of a point spectrometer designed by the NASA Glenn Research Center, the Glenn-designed and -built second-generation HSI, a commercial-off-the-shelf Global Positioning System (GPS) receiver and three-axis inclinometer sensor for aircraft absolute position and attitude, and a high-performance real-time data acquisition system and software. The newly designed and built HSI obtains spectrally and spatially resolved images of the lake in very narrow wavelength bands (or channels) of light (<2.5 nm wide). The wavelength span that the HSI covers is approximately 400 to 900 nm; therefore, approximately 200 wavelength channels of the lake's color information are simultaneously obtained for each lake image spatial pixel.

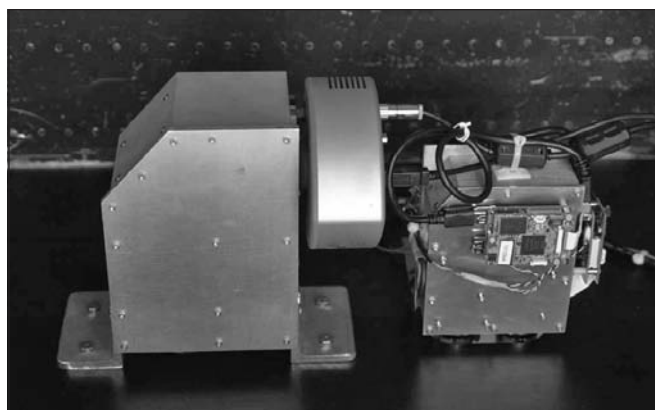
The photograph on the left shows the inside of the second-generation HSI. The internal optics of this imager were upgraded to increase the light throughput by $2\times$ ($f/2.0$ system) with superior imaging characteristics. In addition, a very sensitive, low-noise, thermoelectrically cooled, electron-multiplying charge-coupled device (EMCCD) camera sensor with $16\times$ more dynamic range was used to replace the much noisier and uncooled complementary metal oxide semiconductor (CMOS) imager in the first-generation unit. These changes resulted in a dramatic improvement in both the image quality and signal-to-noise ratio over the first-generation HSI. The point spectrometer significantly expands the capabilities of the system by providing highly accurate measurements of the incident solar spectrum as well as measurements of the atmos-

pheric water vapor content for quantifying the effect of the atmosphere on the measurements. This combined sensor suite will permit much more accurate and higher quality spectral radiometric measurements of the constituents of the Great Lakes as surveyed from the air. This increase in measurement accuracy will allow researchers to detect lower concentrations of pollutants or harmful algal blooms.

The entire suite of instruments weighs less than 10 lb and uses less than 100 W of power. The photograph on the right shows the HSI instrument suite as mounted inside the Lear 25 instrument section. The lenses point downward at the ground and are protected by a laser-grade optical window. The second-generation HSI takes advantage of a modular design permitting rapid changes to either the lenses or orientation of the EMCCD. The front lens can be changed to modify the field of view and resolution of the instrument through the focal length and magnification. In addition, the EMCCD can be changed



Second-generation HSI with the cover removed. The EMCCD camera sensor and final focusing lens assembly (not shown) mount on the bottom side of the instrument. For scale, the bolt holes in the background are located 1-in. (25.4-mm) apart.



Second-generation HSI (left) next to the smaller first-generation HSI (right). The two imagers are shown as installed in Glenn's Lear 25. They are aimed straight down through a window in the underside of the aircraft.

for a different type of camera if higher speed or greater light sensitivity is required. This makes the package very flexible in terms of the platform that it can be deployed on.

Bibliography

Hunt, Spencer: Tracking Erie's Deadly Algae—NASA's New Scanner Helps Keep an Eye on a Growing Problem. Columbus Dispatch, Sept. 25, 2007. http://www.dispatch.com/live/content/science/stories/2007/09/25/sci_Eriealgae.ART_ART_09-25-07_B4_7H7UMMK.html?sid=101

View HSI data on NASA's "Life on Earth" Web portal:

http://www.nasa.gov/vision/earth/lookingatearth/great_lakes_algae.html

Glenn contacts:

John D. Lekki, 216-433-5650,
John.D.Lekki@nasa.gov

Dr. Quang-Viet Nguyen, 216-433-3574,
Quang-Viet.Nguyen-1@nasa.gov

Authors:

John D. Lekki and Dr. Quang-Viet Nguyen

Programs/Projects:

Glenn Internal Research &
Development Funds

Instrument Developed for Indicating the Severity of Aircraft Icing and for Providing Cloud-Physics Measurements for Research

Science Engineering Associates, Inc., in conjunction with researchers at the NASA Glenn Research Center, has developed an instrument that will provide the flight deck with an indication of the severity of the icing conditions encountered and the type of icing environment. This instrument also can assist in cloud physics measurements that support ongoing aircraft-icing programs within NASA. Measurements from this instrument will help to characterize the severity of aircraft-icing conditions by quantifying the size of cloud water drops, cloud liquid water content, cloud ice water content, and cloud total water content.

As shown in this photograph, the instrument sensor head can be mounted on the outside of an aircraft and be positioned and oriented to intercept the ambient airflow. The sensor head contains four hot-wire elements in an open housing that is heated in a controlled manner to keep it free of ice. The hot-wire sensing elements have different shapes and sizes and, therefore, exhibit different measurement efficiencies with respect to droplet size and water phase (liquid, frozen, or mixed).

Three of the hot-wire sensing elements are oriented across the airflow to intercept incoming cloud water. For each of these elements, the liquid water content or total water content affects the power required to maintain a constant temperature in the presence of cloud water. Each of these three elements is considered to be subject to two forms of heat loss. The first form consists primarily of convective loss attributable to the flow of air past the element. This form is sometimes termed the "dry" loss because it excludes the cooling effect of the impinging water. The second form of heat loss is the cooling effect of impinging water. When the element intercepts liquid cloud water,



Instrument sensor head. Copyright Science Engineering Associates, Inc.; used with permission.

energy is lost from the element in heating the water from ambient temperature to the equilibrium temperature for evaporation, and further energy is lost as latent heat of vaporization. When the element intercepts cloud ice crystals, there is an additional loss consisting of the latent heat of fusion for melting the ice. In operation, each element is maintained at a temperature of 140 °C by a digital electronic feedback control subsystem. The power expended in maintaining this constant temperature is the measurement datum associated with the element.

The fourth hot-wire sensing element, referred to as the “reference element,” is oriented along the direction of airflow so that it does not intercept cloud water; but it is still subject to convective cooling. Like the other three elements, the reference element is maintained at constant temperature. For this element, the power needed to maintain the constant temperature is a measure of the dry heat loss and is thus termed the “dry” power. The cloud water content is estimated in a first-principles computation based on known relationships among the cloud water content, hot-wire power levels, dimensions of the sensor wires, ambient temperature, and true airspeed.

Measurement data acquired under known conditions in a wind tunnel can be used to calibrate an instrumentation system like the one in the following photograph, which is installed on a research aircraft to determine the median volume diameter of cloud water droplets, given the differences among the responses of the hotwire sensing elements. The system can discriminate between normal icing conditions, supercooled large-droplet conditions, and glaciated conditions (ice particles), providing the flight deck an indication of the severity of the environment that the aircraft is encountering.



Instrument sensor system. Copyright Science Engineering Associates, Inc.; used with permission.

Bibliography

Design and Initial Wind Tunnel Testing of a Prototype Icing Detector Having the Ability to Detect and Discriminate Normal LWC Icing Threats, Ice Crystal Threats and SLD Condition Threats. 2007 SAE Aircraft & Engine Icing International Conference, In-Flight Ice Detection Systems, oral presentation, Seville, Spain, Sept. 24 to 27, 2007.

Lilie, Lyle; Bouley, Dan; and Sivo, Chris: Instrument for Aircraft-Icing and Cloud-Physics Measurements—Data on Cloud Water Content Are Deduced From Hot-Wire Power A Levels. NASA Tech Briefs, vol. 30, no. 11, 2006. <http://www.techbriefs.com/content/view/823/34/>.

Glenn Contact:

Edward F. Emery, 216-433-5694,
Edward.F.Emery@nasa.gov

Science Engineering Associates, Inc., Contacts:

Lyle Lilie, 860-450-1717, lvlel@scieng.com

Dan Bouley, 860-450-1717,
danb@scieng.com

Chris Sivo, 860-450-1717,
chriss@scieng.com

Author:

Edward F. Emery

LEW Number:

LEW-18029-1

Headquarters Program Office:

NASA Small Business Innovation Research

Programs/Projects:

Aviation Safety Program

Invention Inquiries:

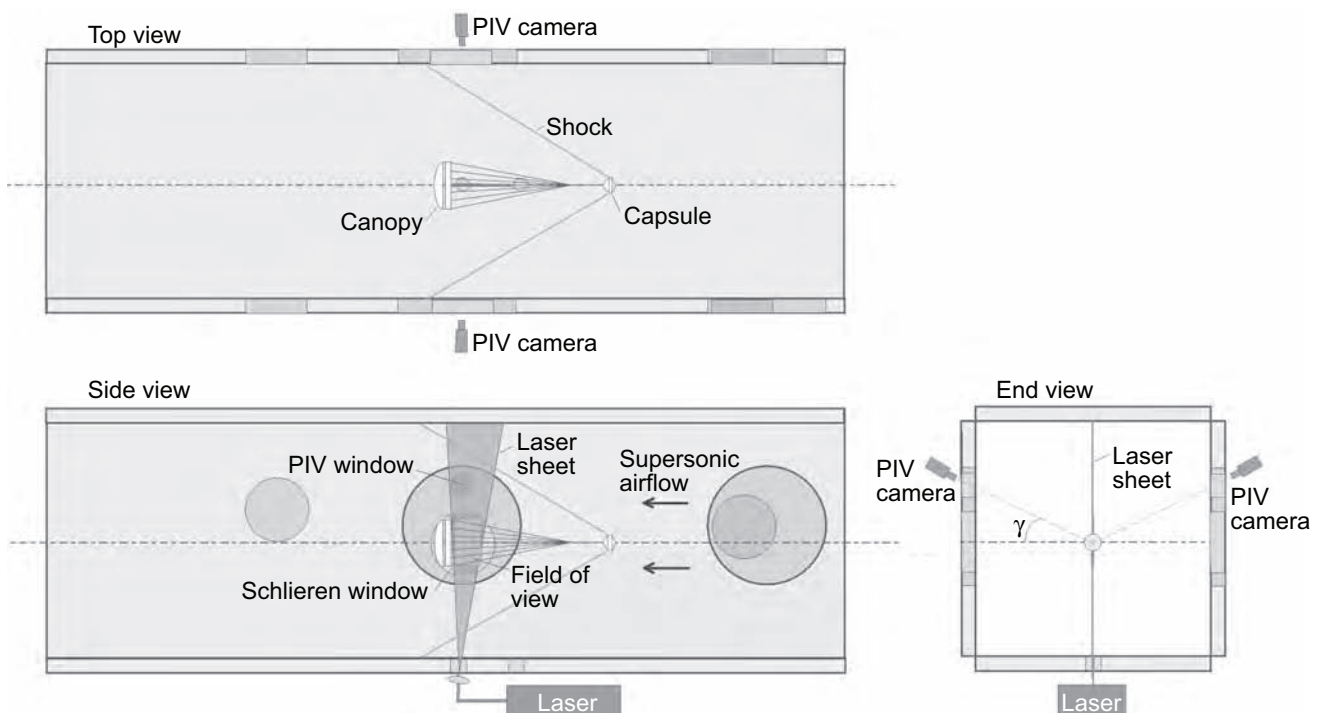
Inquiries concerning rights for the commercial use of this invention should be addressed to NASA Glenn Research Center, Innovative Partnerships Office, Attn: Steve Fedor, Mail Stop 4-8, 21000 Brookpark Road, Cleveland, OH 44135. Refer to LEW-18029-1.

Particle Image Velocimetry Capability Installed and Checked Out in NASA Glenn's 10- by 10-Foot Supersonic Wind Tunnel

A new stereo particle image velocimetry (stereo PIV) system has been installed and checked out at the NASA Glenn Research Center's 10- by 10-Foot Supersonic Wind Tunnel (10×10 SWT). The initial application of the system is in support of the upcoming Mars Science Laboratory (MSL) parachute test in the 10×10 SWT. The stereo PIV system provides nonintrusive, three-dimensional measurements of the canopy flow field and bow shock in the wake of the MSL capsule. The system includes a flow seeder installed upstream of the test section as well as a pulsed Nd:YAG laser and a pair of stereo PIV cameras installed at the test section. The PIV and seeder systems were designed in-house at Glenn by civil servant and contractor technicians and engineers.

Commercial smoke generators were used to seed the tunnel airflow with very small mineral oil smoke particles (0.2 to 0.3 μm). A chamber to house the smoke generators was assembled outside of the wind tunnel and connected to an existing 6-in. natural gas supply to the wind tunnel air heater, which is currently dormant. The gas supply line routed the smoke into the tunnel bellmouth area upstream of the test section and distributed the smoke particles through the air heater natural gas manifold and central array of 60 combustors.

The proposed stereo PIV setup for the upcoming MSL test is shown with and without the MSL hardware in the figures, on this page and the next page, respectively. This configuration was checked out during wind tunnel runs in May 2007. The pulsed Nd:YAG laser was mounted below the test section floor and generated a streamwise vertical laser sheet in the test section. Painting the test section ceiling flat black helped minimize unwanted reflections of the laser sheet. New 12-in.-diameter borosilicate crown glass windows were designed, fabricated, and installed adjacent to the existing 33-in. schlieren windows so that PIV data and schlieren data could be obtained during the same wind tunnel run. The PIV cameras were mounted just outside the new windows, one on either side of the test section.



Stereo PIV setup in the 10×10 test section to survey canopy flow in the wake of the MSL capsule.

During the tunnel checkout run, stereo PIV data were collected at the tunnel centerline. At the tunnel vertical and horizontal centerlines, the field of view of the stereo PIV system was 28 in. high by 18 in. wide. The PIV data were collected over Mach 2.0 to 2.6. Then, the processed data were used to compute the ensemble-averaged flow-field properties. The results showed that the relative turbulence intensity in the tunnel test section is less than 1 percent and that the flow angularity is less than 0.25°. Shocks emanating from the wind tunnel floor and ceiling plates are readily visible in the processed veloc-



Stereo PIV setup in the 10×10 test section (three-dimensional view).

ity fields, where the 5-m/sec change in flow velocity across the weak shocks is clearly visible in the u - and v -components of velocity. As mentioned before, this PIV system has been successfully checked out and is ready to support the planned MSL parachute tests in late 2007.

Find out more about Glenn's facilities:
<http://facilities.grc.nasa.gov>

Glenn Contacts:

Dr. Mark P. Wernet, 216-433-3752,
Mark.P.Wernet@nasa.gov

James W. Roeder, Jr., 216-433-5677,
James.W.Roeder@nasa.gov

Authors:

James W. Roeder, Jr., and
Dr. Mark P. Wernet

Headquarters Program Office:

Exploration Systems Mission Directorate

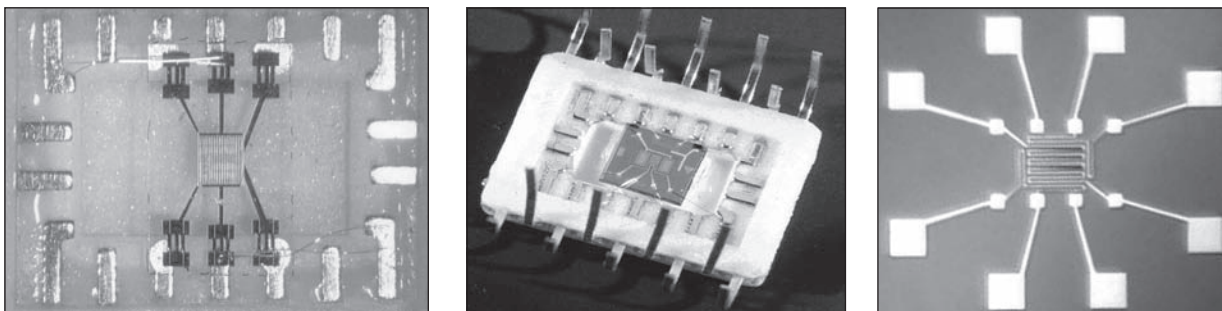
Programs/Projects:

Mars Science Laboratory—Entry, Descent
& Landing Program, Aeronautics Test
Program

Multiparameter Fire-Detection System Miniaturized and Tested for Possible Use on Crew Exploration Vehicle

Fire safety is an ongoing concern both on the ground and in aerospace applications. In particular, in environments such as the space shuttles, *International Space Station*, and the Crew Exploration Vehicle (CEV), early and accurate detection of a fire is a crucial safety issue given the closed environment and limited avenues of escape. Previous work led by NASA resulted in a low-false-alarm Multi-Parameter, MicroSensor-Based Fire Detection System (MMFDS). This system was evaluated at the Federal Aviation Administration for detecting fires in the cargo bay of aircraft. The MMFDS consistently detected fires with no false alarms. This core technology is now being transitioned from aeronautics applications to possible implementation on the CEV.

The basic approach behind this fire detection system is to combine a variety of sensors to interrogate the environment and identify the onset of a fire. The photographs on the next page show examples of sensors that have relevance to fire detection. These sensors are produced by microfabrication techniques for minimal size, weight, and power consumption. The parameters



Three example microsensors that can be used for fire detection. Left: Resistive nanocrystalline tin oxide sensor used for hydrocarbon or carbon monoxide detection. Center: Schottky diode and resistivity-based sensor for hydrogen/hydrocarbon detection. Right: Electrochemical cell that can be configured to measure a range of species including carbon dioxide.

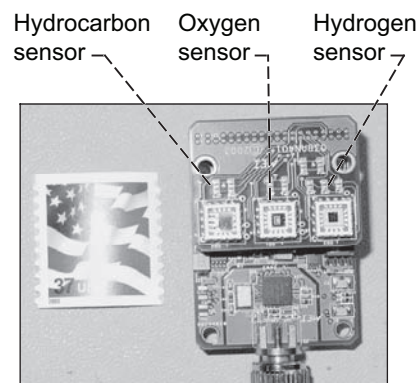
measured include carbon monoxide, carbon dioxide, hydrogen/hydrocarbons, humidity, and particulates. Together with support hardware and software, these sensors make a complete system to detect the onset of fires.

This year, activities centered on testing and miniaturizing the sensors for possible inclusion in CEV applications. This included life-time tests to determine the long-term reliability of the fire-detection system and evaluation of the system in several operational tests. One series of tests conducted at the NASA White Sands facility in conjunction with the NASA Johnson Space Center evaluated the system's ability to monitor the postfire environment and hardware for postfire cleanup. These tests, along with others planned to be conducted within the next year, will validate this multisensor approach to early fire detection, which includes both chemical sensors and particulate detection. In addition, the system is being integrated into the "lick and stick" hardware being developed for Crew Launch Vehicle (CLV) leak-detection applications (see the photograph to the right). The overall approach is to have a compact system that provides a range of measurement capabilities to enable reliable fire detection and monitoring of the postfire environment. This system can be wired or wireless to enhance deployment opportunities.

Overall, the CEV work represents a change for fire-detection technology in space applications. Traditional space systems just measured particulates to determine the presence of a fire. The new microsensor technology can measure not only particulates but also chemical species to fundamentally improve the reliability of fire detection and the safety of the crew in space exploration vehicles and habitats.

Glenn Contacts:

Gary Hunter, 216-433-6459, Gary.W.Hunter@nasa.gov
 Jennifer Xu, 216-433-6669, Jennifer.C.Xu@nasa.gov
 Paul Greenberg, 216-433-3621, Paul.S.Greenberg@nasa.gov
 Gary A. Ruff, 216-433-5697, Gary.A.Ruff@nasa.gov
 Larry K. Dungan, 281-483-3560, Larry.K.Dungan@nasa.gov



Prototype version of a "lick-and-stick" leak-detection system with hydrogen, hydrocarbon, and oxygen detection capabilities combined with supporting electronics. This basic system, being prepared for CLV applications, is also serving as a platform for a miniaturized, smart fire-detection system.

Authors:

Dr. Gary W. Hunter, Dr. Gary A. Ruff, and Dr. Jennifer C. Xu

Headquarters Program Office:

Constellation Project Office

Programs/Projects:

Exploration Technology Development Program, Fire Prevention, Detection and Suppression project

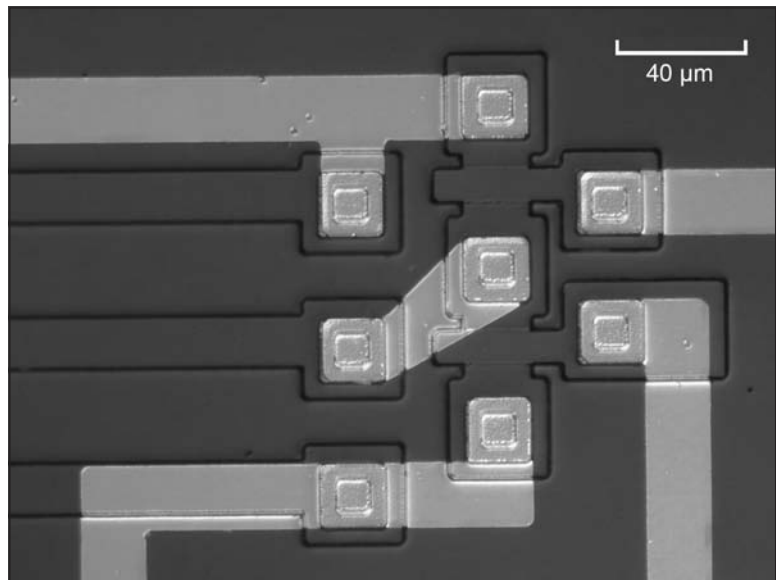
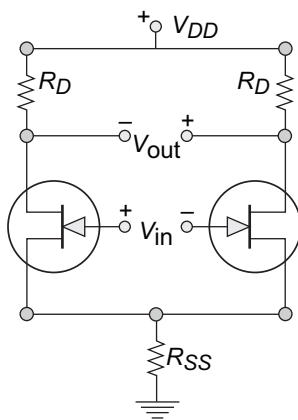
Silicon Carbide Integrated Circuit Fabricated and Electrically Operated for 2000 hr at 500 °C

High-temperature semiconductor transistor integrated circuit (IC) electronic chips capable of prolonged 500 °C operation would enable important advancements in the sensing and control of combustion in jet engines, making them cleaner, safer, and more fuel efficient. In addition, such chips would be keys to the long-term operation of scientific probes on or near the scorching 460 °C surface of Venus. Although there have been reports of short-term (less than 10 hr) semiconductor IC operation at 500 °C or above, much longer operating times are needed for these and other beneficial high-temperature electronics applications. Toward this end, the NASA Glenn Research Center has been pioneering silicon carbide (SiC) transistor IC electronics technology targeted for greatly prolonged operational durability at 500 °C. These efforts previously demonstrated important foundational building blocks for 500 °C durable ICs (including high-temperature metal-semiconductor contacts (ref. 1), packaging (ref. 2), and discrete transistors (ref. 3)) and a simple inverting amplifier stage made from discrete resistors and transistors connected together on a circuit board (ref. 4).

Building on this foundation, civil servants and Ohio Aerospace Institute (OAI) researchers at Glenn designed, fabricated, and electrically operated a differential-amplifier IC chip continuously at 500 °C for more than 2000 hr. This is the first semiconductor transistor IC to demonstrate stable continuous electrical operation in such a harsh high-temperature oxidizing air environment over such an extended period of time.

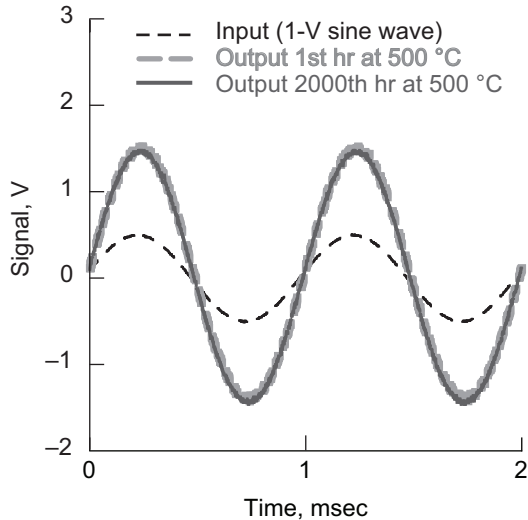
The differential-amplifier IC consisted of two transistors and three resistors integrated (i.e., interconnected to each other to form the circuit) over less than half a square millimeter of area of a single SiC chip. The circuit schematic diagram shows the differential amplifier, and the optical microscope photograph shows the differential amplifier on the surface of the SiC chip as it appeared prior to packaging.

The graph on the next page plots the voltage-versus-time waveforms (recorded on a digitizing oscilloscope) that verified proper operation of the differential-amplifier IC. The IC amplifies a 1-kHz sine wave input test signal with 1-V peak-to-peak amplitude (black signal in the graph) into a 3-V peak-to-peak amplitude sine wave output signal. The output signals recorded



Left: Silicon carbide (SiC) differential amplifier IC. Circuit power supply voltage, V_{DD} , 40 V; circuit resistors, $R_D = R_{SS} = 545 \Omega$. Right: The heart of the SiC differential-amplifier IC chip, showing the two 6H-SiC junction field effect transistors (on the right side) and part of the three 6H-SiC resistors (on the left side) that make up the IC.

from the 1st and 2000th hours of the 500 °C test also are shown. The fact that the 1- and 2000-hr output waveforms fall on top of each other demonstrates that no appreciable degradation of circuit functionality occurred despite prolonged operation in the harsh 500 °C ambient environment.



Voltage versus time waveforms recorded by a digitizing oscilloscope showing that the IC sitting in an oven at 500 °C amplifies a 1-V-amplitude sine wave input test signal into a 3-V-amplitude sine wave output wave at the start (1st hour) and end (2000th hour) of the harsh-environment durability test.

This demonstration of 500 °C transistor IC operational durability represents an important step toward significantly expanding the operational envelope of sensor signal-processing electronics for harsh environments. An important next step in the development of 500 °C IC technology is to greatly increase the single-chip transistor count, which in turn, would enable much greater 500 °C IC functionality beyond simple signal amplification.

References

1. Okojie, Robert S.: Thermally Stable Ohmic Contacts on Silicon Carbide Developed for High-Temperature Sensors and Electronics. Research & Technology 2000, NASA/TM—2001-210605, 2001, pp. 59–60. <http://www.grc.nasa.gov/WWW/RT2000/5000/5510okojie.html>
2. Chen, Liang-Yu: Packaging Technology Designed, Fabricated, and Assembled for High-Temperature SiC Microsystems. Research & Technology 2002, NASA/TM—2003-211990, 2003, pp. 69–70. <http://www.grc.nasa.gov/WWW/RT2002/5000/5510chen.html>
3. Neudeck, Philip G.: Packaged SiC Transistor Operated at 500 °C for 2000 hr in Oxidizing Air Ambient. Research & Technology 2005, NASA/TM—2006-214016, 2006, pp. 56–57. <http://www.grc.nasa.gov/WWW/RT/2005/RI/RIS-neudeck2.html>

4. Neudeck, Philip G.; and Chen, Liang-Yu: High-Temperature Amplifier Based on a Silicon Carbide Metal-Semiconductor Field Effect Transistor and Ceramic Packaging Designed, Fabricated, and Electrically Operated at 500 °C. Research & Technology 2006, NASA/TM—2007-214479, 2007, pp. 97–98. <http://www.grc.nasa.gov/WWW/RT/2006/RI/RIS-neudeck.html>

Find out more about silicon carbide electronics research at Glenn:

<http://www.grc.nasa.gov/WWW/SiC/>

Glenn Contacts:

Dr. Philip G. Neudeck, 216–433–8902,
Philip.G.Neudeck@nasa.gov

Dr. Glenn M. Beheim, 216–433–3847,
Glenn.M.Beheim@nasa.gov

Ohio Aerospace Institute (OAI) Contacts:

David J. Spry, 216–433–3361,
David.J.Spry@nasa.gov

Dr. Liang-Yu Chen, 216–433–6458,
Liangyu.Chen-1@nasa.gov

Authors:

Dr. Philip G. Neudeck

LEW Numbers:

LEW–17,717–1 and LEW 18,344–1

Headquarters Program Office:

Aeronautics Research Mission Directorate

Programs/Projects:

Integrated Vehicle Health Management Program, Subsonic Fixed Wing Project, Supersonics Project

Reliability of Silicon Carbide Pressure Transducers Evaluated at 600 °C

The growing demand for pressure measurements in high-temperature environments (>500 °C) has spurred the development of robust, reliable pressure sensors. As a result, research has focused on taking advantage of the superior thermomechanical properties of silicon carbide (SiC) semiconductors to develop micropressure sensors that would extend sensing capability to 600 °C and beyond. For space exploration, SiC pressure sensors could monitor conditions on Venus, where the pressure is as high as 90 bar, the temperature approaches 500 °C, and the atmosphere contains acidic clouds (ref. 1). For aeronautics, accurate measurement of pressure in the combustion sections of aeroengines could provide (1) improved fuel management efficiency, (2) improved validation of computer fluid dynamics codes used in designing and producing engines, and (3) monitoring of thermoacoustic instability in engine combustion chambers to prevent lean blowout or flameout—such instability can cause an engine to stall or can potentially damage critical engine components if not mitigated (ref. 2).

This article presents recent results of an evaluation of the long-term reliability of SiC pressure sensors operating at 600 °C at the NASA Glenn Research Center. The goal was to determine the optimum burn-in time to achieve stable operation and to identify new failure mechanisms induced by long-term operation at high temperature.

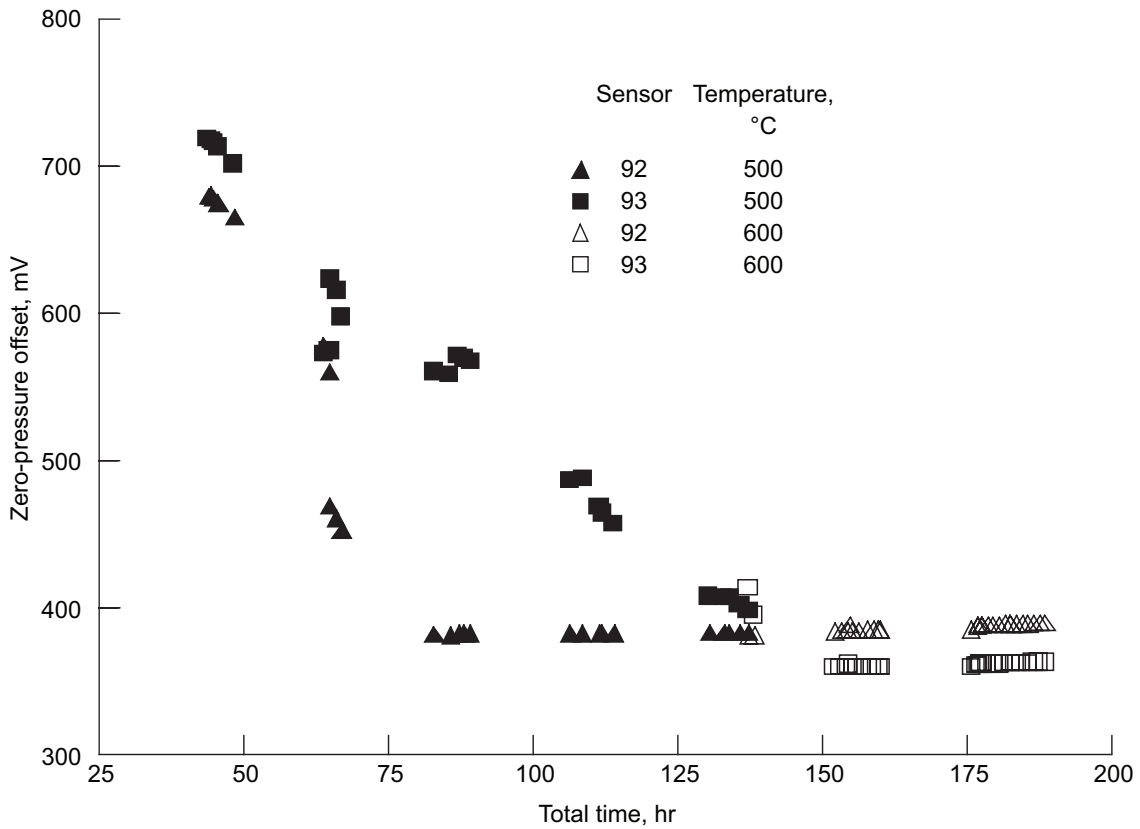
The photograph shows the SiC transducers in the test fixture where they were leak tested before placement in the oven. The bottom right inset shows the SiC sensor as it was attached to the aluminum nitride header. This part went into the fixture first. Pressure was initially applied to determine if any transducer was leaking. Any leaking transducer (see the bottom left inset) was replaced and sent for failure analysis.

During soak time at temperature, the performance characteristics of the transducers were recorded and analyzed. Initially, two SiC pressure transducers (92 and 93) were evaluated simultaneously as function of time, first at 500 °C and then at 600 °C, as shown in the top graph on the next page. Subsequent evaluations were performed at 600 °C.

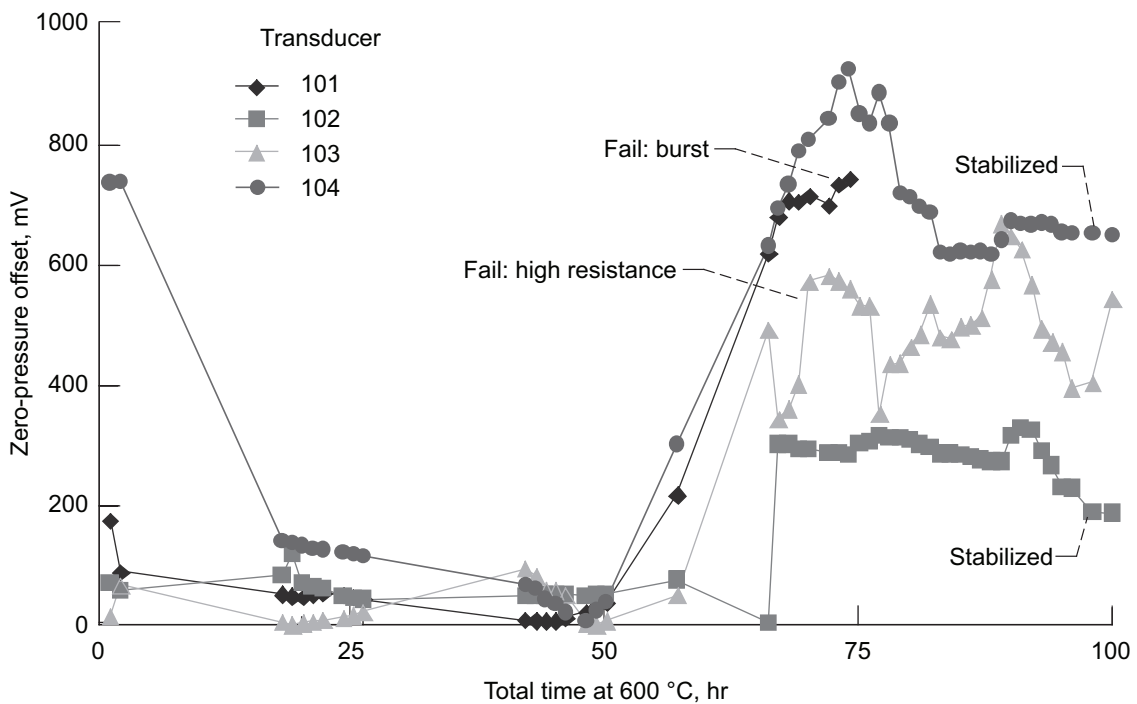
The bottom graph on the next page shows the results of transducers 101 to 104, evaluated for 100 hr. During the soak period, a leak was observed in transducer 101 and transducer 103 had a resistance value that was out of specification. Evaluation of these two transducers was aborted and they were sent for failure analysis. After 100 hr, transducers 102 and 104 were pressure tested at 600 °C and cooled to room temperature. The results are shown in the final graph.



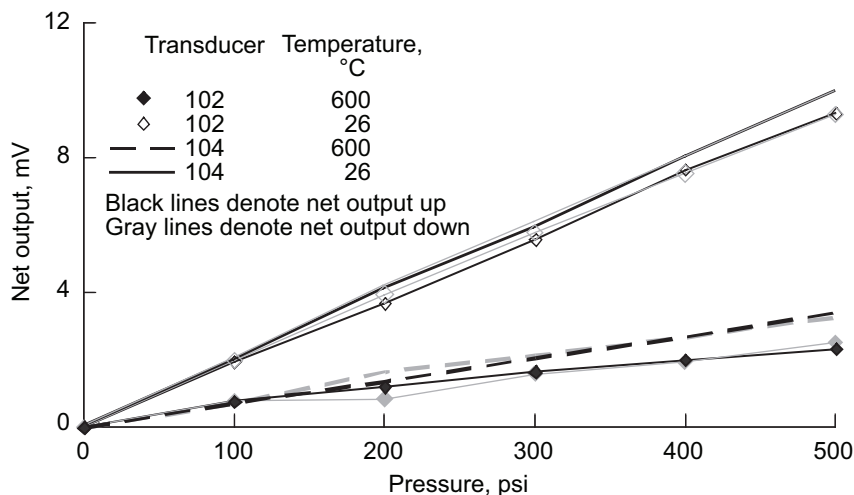
This test setup for the accelerated testing of SiC pressure transducers supports a maximum of four transducers. Bottom right inset: Transducer header with the SiC sensor element prior to insertion in the fixture. Bottom left inset: Example of a leak observed in a SiC pressure transducer prior to high-temperature soak. After the transducer was replaced, no leaks were observed. Leaks could be due to a burst sensor diaphragm or a crack in the aluminum nitride.



Zero-pressure offset voltage of transducers 92 and 93 during burn-in header at 500 and 600 °C. The initial soak at 500 °C was to avoid the possibility of transient thermal stress on the packaged sensor.



Zero-pressure offset voltage of transducers 101 to 104 during burn-in at 600 °C. Transducer 101 failed after developing a leak, and transducer 103 failed after the output resistance went out of specification. Transducers 102 and 104 began trending toward stability after 100 hr.



Net output voltage as function of pressure for transducers 102 and 104 after 100-hr burn-in at 600 °C and post-burn-in measurement at room temperature. After three cycles of testing at pressure and temperature, the transducers showed no discernable changes in performance.

Find out more about silicon carbide electronics research at Glenn:
<http://www.grc.nasa.gov/WWW/SiC/>

Glenn Contact:
Dr. Robert S. Okojie, 216-433-6522,
Robert.S.Okojie@nasa.gov

Author:
Dr. Robert S. Okojie

LEW Number:
LEW-17256-1

Headquarters Program Office:
Aeronautics Research Mission Directorate

Programs/Projects:
Subsonic Rotary Wing Project,
Supersonics Project

References

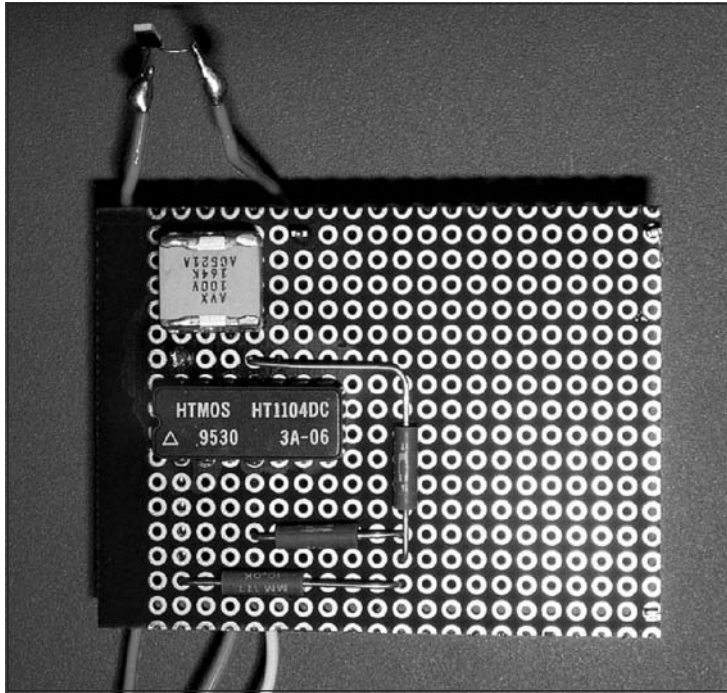
1. Venus. World Book at NASA. http://www.nasa.gov/worldbook/venus_worldbook.html
2. Lefebvre, Arthur Henry: Gas Turbine Combustion. 2nd ed., Taylor & Francis, Philadelphia, PA, 1999.

Temperature Sensor Developed for a Wide Range of Applications From Hot Jet Engine Environments to Cryogenic Space Missions

The implementation of a distributed control system in NASA subsonic fixed-wing and jet engine applications requires sensors and electronic interface circuitry that are located with monitoring and control transducers for engines and actuators, in hot environments where temperatures easily exceed 150 °C. In addition to meeting the operational requirements, placement of the electronics in the harsh temperature environment allows simpler signal multiplexing, improves system performance, and minimizes signal degradation. Similar situations arise for essential location of electronics in cold temperature environments, like the NASA James Webb Space Telescope and space-based infrared satellite systems. In both of these applications, electronics must be able to operate at cryogenic temperatures because of operational requirements and for low-noise capture and processing of very weak signals.

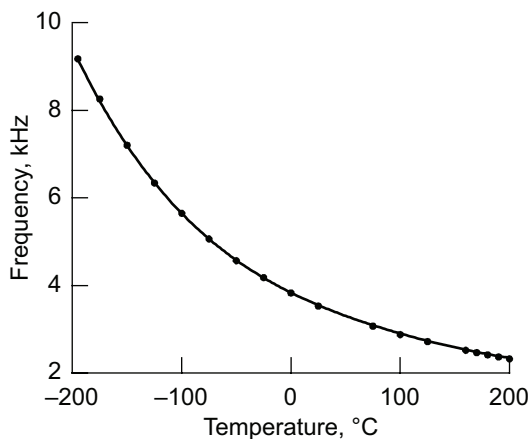
exploration missions, space qualification of flightlike hardware, and establishing the reliability of commercial-off-the-shelf electronics for space use. Results obtained on the developed and commercial parts under extreme temperatures and wide thermal cycling are used to establish safe operating areas and are disseminated to mission planners and system designers so that they can optimize circuit and system design and mitigate risks.

The Extreme Temperature Electronics Program at the NASA Glenn Research Center focuses on the development of electronic parts and circuits for space



Wide-range temperature sensor circuit.

A prototype temperature-sensing circuit was designed and assembled at Glenn using advanced electronic parts for operation in extreme temperature environments. The photograph shows the circuit board that was evaluated between -195 and 200 $^{\circ}\text{C}$. The circuit was built to sense temperature and to produce an output consisting of a stream of rectangular pulses whose frequency was a function of the sensed temperature. The output pulses can be fed into a data acquisition system; then a controller or a computer will give a direct readout of the temperature through the use of a look-up table, a built-in algorithm, or a mathematical model. A typical output response of the temperature-to-frequency conversion circuit is shown in the graph.



Output frequency versus sensed temperature.

Glenn's Extreme Temperature Electronics Program is supported by the NASA Electronic Parts and Packaging Program and the NASA Fundamental Aeronautics Program, Subsonic Fixed Wing Project, Distributed Engine Control Task. The research and development efforts are being performed in-house through collaboration with other Government agencies, industrial and aerospace companies, and academia. The program supports missions as well as technology development efforts at the NASA Johnson Space Center, NASA Goddard Space Flight Center, and Jet Propulsion Laboratory.

Find out more about the research of Glenn's Space Environmental Durability Branch:

<http://www.grc.nasa.gov/WWW/epbranch/ephome.htm>

Glenn Contacts:

Richard L. Patterson, 216-433-8166,
Richard.L.Patterson@nasa.gov

Dr. Ahmad Hammoud, 216-433-8511,
Ahmad.Hammoud@nasa.gov

Authors:

Richard L. Patterson and
Dr. Ahmad Hammoud

Headquarters Program Office:

Exploration Systems Mission Directorate,
Environmental Services Division;
Aeronautics Research Mission Directorate

Programs/Projects:

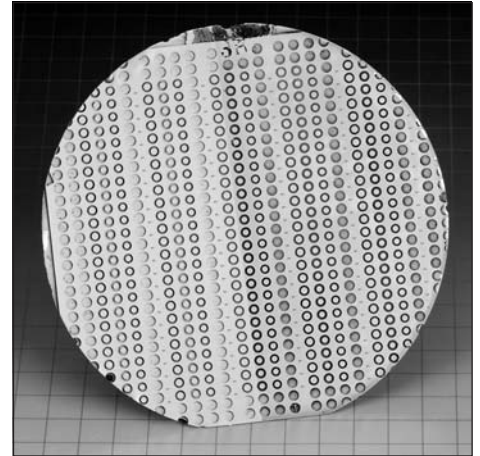
Lunar Landers, Mars Orbiters and Landers,
James Web Space Telescope, NASA
Electronic Parts and Packaging Program,
NASA Electronic Parts Assurance Group,
NASA Fundamental Aeronautics
Program, Subsonic Fixed Wing Project,
Distributed Engine Control Task

Microelectromechanical Systems Packaging Technique and Chip Fabrication Method Developed for High-Temperature, Harsh-Environment Silicon-Carbide Pressure Sensors

Because pressure sensors packaged by traditional means cannot operate above 400 °C, researchers at the NASA Glenn Research Center have developed a new packaging method and fabrication technique for producing silicon-carbide- (SiC-) based pressure sensors that can operate reliably in high temperatures and harsh environments. With no need for cooling, SiC-based pressure sensors produced using these techniques currently operate for 130 hr at 600 °C in air.



Dr. Robert Okojie examines SiC sensors fabricated in a SiC wafer.



Hundreds of SiC sensors fabricated in a SiC wafer prior to cutting the wafer into pieces and assembling.

These sensors were demonstrated in the Hi-Fly Project at the Johns Hopkins University Applied Physics Laboratory, where data indicated that the SiC sensor was operable and voltage output followed that of the benchmark transducer. This demonstration proved the value of inserting these sensors closer to the engine chamber to directly measure pressure fluctuations, which can be used to improve computational fluid dynamics codes.

The sensors were also tested in the United Technologies experimental test rig at Glenn. Glenn researchers detected 310-Hz thermoacoustic instability in a combustion test rig operating at 420 °C with accuracy comparable to that of a water-cooled piezoceramic pressure sensor.

This technology greatly improves pressure sensor reliability because it eliminates the failure-inducing thermomechanical stress that exists in traditionally packaged sensors. Data reliability is increased because these SiC pressure sensors can be located in closer proximity to the sensed environment than conventional silicon-based sensors can. The lower weight of these sensors, because of the elimination of water-cooling plumbing, makes these devices less complex and relatively inexpensive and it reduces the tear-down cycle for engine maintenance. This also leads to reduced engine weight and, hence, improved fuel efficiency.



Subassembled SiC MEMS-DCA pressure transducer. The pressure sensor is directly attached to the aluminum nitride (AlN) header. The AlN header has been brazed to the kovar metal tube. The subassembled part is then slid into a stainless steel package and clamped at the kovar. The SiC sensor and AlN header are not touching the stainless steel.

SiC sensor reliability problems at high temperatures due to poor packaging, coupled with inherently high SiC material and capital costs, have discouraged large-scale commercialization. As a result, the introduction of SiC devices into high-temperature environments was delayed. Along with its novel packaging technique, this technology's new fabrication process is solving those problems by incorporating multiple SiC sensor functions on a single wafer, significantly reducing manufacturing cost and time. In October 2007, the technology was licensed to Endevco Corporation, a Meggitt Group Company. Endevco is developing and marketing a high-temperature, media-isolated pressure sensor.

NASA plans to use this technology in aircraft engine performance diagnostics and active control strategies in NASA's Subsonics, Supersonics, and Hypersonics Projects as well as in future missions to Venus to measure atmospheric pressure. Additional pressure sensor opportunities include commercial and military aviation, oil and gas drilling, missiles and fuses, space exploration, land- and sea-based vehicles, and power generation. This technology could also enable integrated microsystems for real-time control of combustion to further improve aviation safety and combustion efficiency.

Glenn Contacts:

Kathleen K. Needham, 216-433-2802,
Kathleen.K.Needham@nasa.gov

Dr. Robert S. Okojie, 216-433-6522,
Robert.S.Okojie@nasa.gov

Authors:

Lee Ann Obringer and Dr. Robert S. Okojie

LEW Numbers:

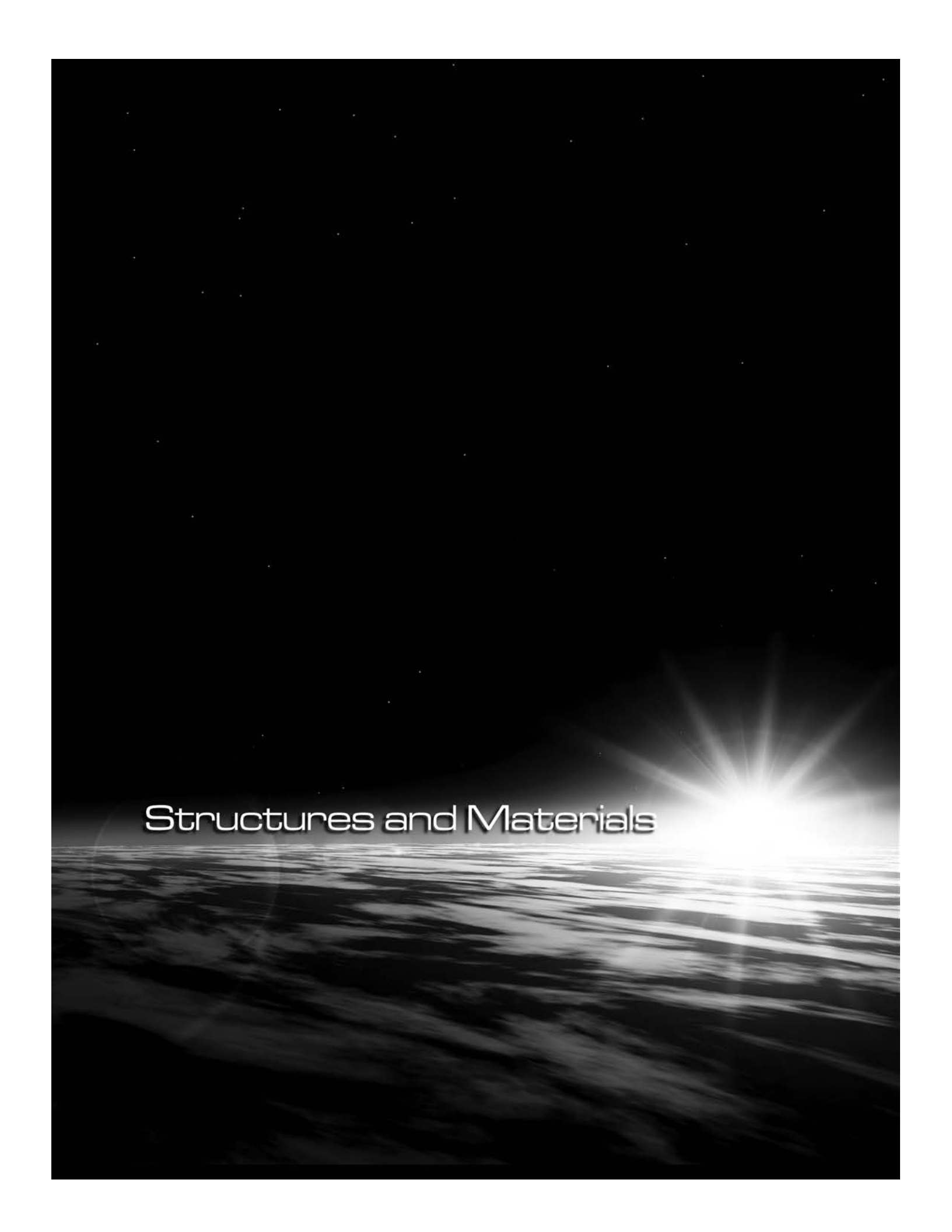
LEW-17170-1 and LEW-17256-1

Headquarters Program Office:

Aeronautical Research Mission Directorate

Programs/Projects:

Fundamental Aeronautics Program, Glenn Microsystems Initiative, Hi-Fly Project, Subsonics Project, Supersonics Project, Hypersonics Project, future missions to Venus to measure atmospheric pressure



Structures and Materials

Notch Fatigue Strength of a Powder Metallurgy Disk Superalloy Evaluated

New powder metallurgy (PM) disk superalloys, such as ME3 (ref. 1), low solvus, high refractory (LSHR) (ref. 2), and Alloy 10 (ref. 3), that have been developed in recent years enable rim temperatures in turbine disk applications to approach 700 °C. However, before these alloys can be utilized at 700 °C, their long-term durability must be ensured. One of the key requirements for disk rims is notch fatigue strength. This requirement is extremely important because of the blade attachment geometry at the disk rim. Furthermore, the imposition of a dwell at maximum load, associated with takeoff and landing, can compromise notch fatigue strength (ref. 1). For these reasons, a study was undertaken to assess the notch dwell fatigue strength of a modern PM disk alloy through spin pit evaluation of a prototypical disk. The first element was screening potential heat treatments with respect to notch fatigue strength at 704 °C, utilizing a conventional notch fatigue specimen with a stress concentration factor K_t of 2 and a 90-sec dwell at peak load. The results are reported here.

HEAT TREATMENTS FOR LSHR

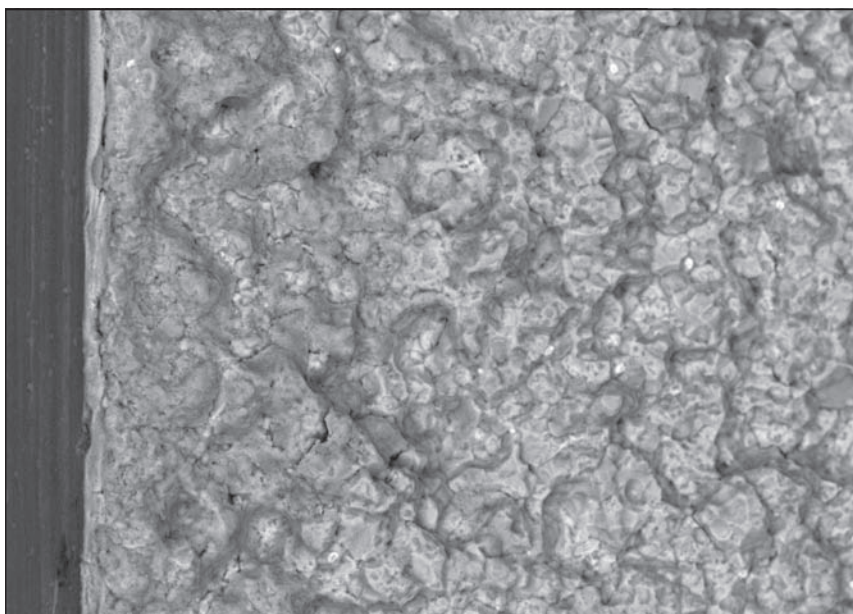
Code	Solution step, °C for 1.5 hr	Quench	Single-step age: 775 °C for 8 hr	Two-step age: 855 °C for 4 hr, then 775 °C for 8 hr
J1	1135	Oil	X	
J2	1135	Oil		X
E1	1135	Fan air	X	
E2	1135	Fan air		X
H1	1171	Fan air	X	
H2	1171	Fan air		X

The material selected for this program was LSHR, a third-generation PM superalloy developed by NASA, strengthened by about 60-percent gamma prime phase. Six commercially viable heat treatments, presented in the table, were evaluated in this program, producing a variety of microstructures. Each

heat-treatment option was designed to produce a different mix of tensile, creep, and crack-growth properties.

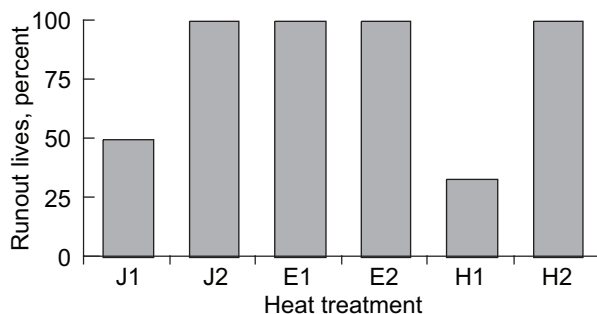
The notch dwell fatigue tests were run using a peak, net section stress of 793 MPa that was applied for 90 sec in each cycle. The selection of stress was aggressive but reasonable for a disk rim application. Because these tests were quite lengthy, the initial screening matrix called for testing up to six specimens from each heat-treatment lot to failure, or a 10,000-cycle runout condition, approximating the life requirement for turbine disks.

Notch dwell fatigue testing of the first 12 specimens, 2 from each heat treatment, produced very interesting results. Three of twelve failed in less than 1000 cycles, whereas all others reached the 10,000-cycle runout condition. Because of these results, the remaining 24 tests were run to 2000 cycles to accelerate data acquisition and enhance statistics on failure after less than 1000 cycles. The results of all 36 tests showed that the failures were bimodal, with 7 of 36 specimens failing in less than 1000 cycles and the remaining specimens reaching the desired runout lives. Preliminary examination of the failed specimens (see the photomicrograph) did not reveal anything unusual on the fracture surface; that is, no large pores or inclusions. In the bar chart on the next page, the fraction of specimens that failed is plotted as a function of heat treatment. As seen in this plot, all the low-life failures were with the J1 and H1 heat treatments. Although the J1 and H1 heat treatments are different in certain respects, they both produce microstructures with the best creep resistance and, therefore, are the most resistant to stress relaxation. This suggests that higher stress levels maintained during the dwell for J1 and H1 may have led to premature failure.



10 µm

Fracture surface of a notch fatigue specimen.



Notch dwell fatigue data for LSHR at 704 °C.

In conclusion, six potential heat-treatment options for a third-generation PM disk alloy, LSHR, were studied with respect to notch dwell fatigue strength at 704 °C. Initial results showed four of the six heat treatments would meet life targets for turbine disks with respect to notch dwell fatigue strength. The remaining two heat treatments, with lives less than 1000 cycles, would not meet requirements at 704 °C.

References

1. Gabb, Timothy P., et al.: Characterization of the Temperature Capabilities of Advanced Disk Alloy ME3. NASA/TM—2002-211796, 2002. <http://gltrs.grc.nasa.gov>
2. Gabb, Timothy P., et al.: Thermal and Mechanical Property Characterization of the Advanced Disk Alloy LSHR. NASA/TM—2005-213645, 2005. <http://gltrs.grc.nasa.gov>

3. Jain, Sushil K.: High HPR Core Materials (Area of Interest 4.0) Regional Engine Disk Process Development (Sub-AOI 4.2.4) Final Report. NASA Contract NAS3-27720, 1999. Available from NASA Center for Aerospace Information.

Find out more about the research of Glenn's Advanced Metallics Branch:
<http://www.grc.nasa.gov/WWW/AdvMet/webpage/>

Glenn Contacts:

John Gayda, 216-433-3273,
 John.Gayda-1@nasa.gov

Timothy P. Gabb, 216-433-3272,
 Timothy.P.Gabb@nasa.gov

Authors:

Dr. John Gayda, Dr. Timothy P. Gabb, and Jack Telesman

Headquarters Program Office:

Aeronautics Research Mission Directorate

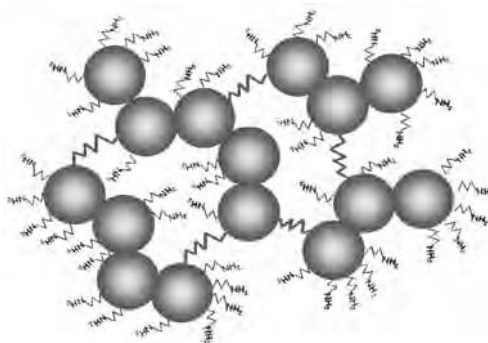
Programs/Projects:

Aviation Safety Program

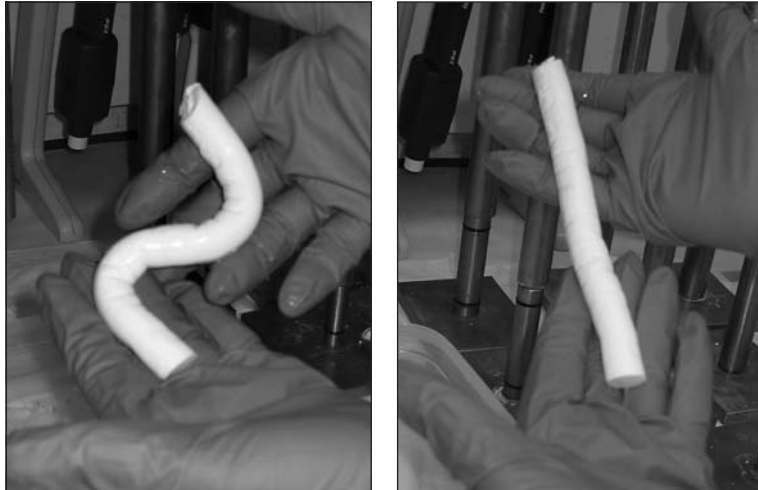
Flexible Cross-Linked Aerogels Developed

Silica aerogels with their low density and thermal conductivity are potential candidates for various thermal, optical, and acoustic applications for aerospace, including multipurpose structures for vehicles, spacesuits, and habitats. However, the use of aerogels has been restricted because of their inherent fragility, hygroscopic nature, and poor mechanical properties. Over the past 10 years, research in improving the physical and mechanical properties of silica aerogels has been under extensive investigation. The NASA Glenn Research Center has placed much emphasis in the last few years on incorporating a surface modifier such as amine or vinyl functional silica precursor into a silica-based aerogel, followed by crosslinking with an organic monomer including isocyanates, epoxies, or styrene (refs. 1 and 2). In these hybrid materials, results have shown that strength could be improved by a hundred times while only doubling the density over those of native aerogels, or non-cross-linked aerogels.

Although cross-linked aerogels are a great improvement over native silica aerogels, for many applications—insulation for space suits, for example—it is most desirable to have a more flexible material. Recently, Glenn developed



Cartoon showing how a flex-link additive (shown as the largest squiggly lines) is incorporated into Glenn-developed polymer cross-linked silica aerogels. This figure is shown in color in the online version of this article (<http://www.grc.nasa.gov/WWW/RT/2007/Str-Mat/02-RXP-nguyen.html>).



A porous gel with flex-link additive can be manipulated without breaking.

a more flexible and resilient polymer cross-linked aerogel by incorporating a flexible linking group (or flex-link) into the underlying silica structure along with the surface functional cross-linking groups as demonstrated in the diagram on the preceding page. Results so far indicate that with an increasing amount of the flex-link additive, gels are much less fragile and more flexible, as shown in these photographs.

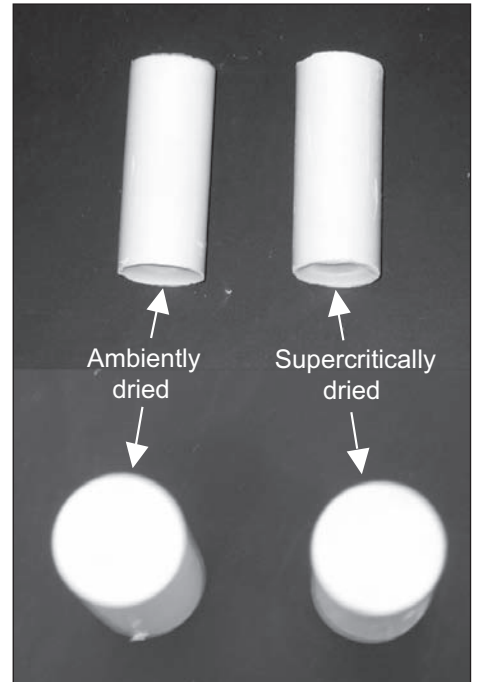
Typical aerogels require supercritical fluid extraction of the solvent in order to maintain the gel's porous network in the final product. Ambiently dried gels (xerogels) typically collapse and shrink, giving a much more dense material. However, it has been observed that, by adding a higher concentration of the flex-link additive, the gels could be air-dried at an ambient pressure without shrinkage. The photograph on the right shows two monoliths containing the additive, one air-dried and the other supercritically dried. Their sizes and densities are similar. Other properties are under investigation.

References

1. Meador, Mary Ann B., et al.: Cross-Linking Amine-Modified Silica Aerogels With Epoxies: Mechanically Strong Lightweight Porous Materials. *Chem. Mater.*, vol. 17, no. 5, 2005, pp. 1085–1098.
2. Capadona, Lynn A., et al.: Flexible, Low-Density Polymer Crosslinked Silica Aerogels. *Polymer*, vol. 47, no. 16, 2006, pp. 5754–5761.

Ohio Aerospace Institute (OAI) Contact:

Dr. Baochau N. Nguyen, 216–433–2738, Baochau.N.Nguyen@nasa.gov



Ambiently dried versus supercritically dried aerogel samples containing flex-link additive.

Glenn Contact:

Dr. Mary Ann Meador, 216–433–3221, Maryann.Meador@nasa.gov

Authors:

Dr. Baochau N. Nguyen,
Dr. Mary Ann Meador,
Stephanie L. Vivod, and Marissa Tousley

Headquarters Program Office:

Aeronautics Research Mission Directorate

Programs/Projects:

Fundamental Aeronautics Program,
Subsonic Fixed Wing Project, Subsonic
Rotary Wing Project

Manufacturing Process for Polymer Cross-Linked Aerogel Composites Developed

Polymer cross-linked silica aerogels developed at the NASA Glenn Research Center have shown promising enhancements of mechanical properties in comparison to pure silica aerogels without compromising density or thermal conductivity. Thus, these materials may be enabling for future space exploration missions. They may also advance aeropropulsion systems that demand lighter weight, robust, dual-purpose materials for acoustic or thermal insulation and for structural elements of habitats, rovers, astronaut suits, and cryotanks.

Incorporation of 3-aminopropyltriethoxysilane into the silicate sol-gel process provides functionality on the backbone of the silica aerogel that promotes grafting of various polymers (polyisocyanates, epoxides, etc.) into the structure. The intimate mixing of the polymer cross-links within the aerogel structure and the covalent bonding between the inorganic and organic phases are essential to controlling the material properties. Thus, processing variables are of central importance, and Glenn scientists have optimized many of these variables for producing the highest strength aerogels relative to bulk density using di-isocyanate as the cross-link (ref. 1). Glenn, however, does not have the facilities to scale up the aerogel process and investigate commercially viable manufacturing in their facility. Hence, they have joined forces with Aspen Aerogels to develop these processes.

Although monolithic aerogel materials are technically interesting, they are difficult to produce in large quantities using supercritical extraction processing methods if the gels are rigid. Fiber-reinforcement of the cross-linked aerogels is intended to make them flexible enough to be spiral wound during processing and is an important step toward establishing scaleup and viable commercial production. During the early part of this project, Aspen Aerogels worked with Glenn to reproduce certain optimum formulations of the cross-linked aerogels in fiber composites, benchmarking density, thermal conductivity, and mechanical compression. Measured properties of the composites all came within 10 percent of that previously reported for the monolithic materials. Some of these composites are pictured in the photograph.

The next steps for this project include substituting more environmentally friendly raw materials for safer large-scale manufacturing and developing a more streamlined process. The ultimate goal is to scale the process for

producing polymer cross-linked aerogels developed on the bench to a semi-pilot scale without sacrificing properties.

Reference

1. Meador, Mary Ann B.: Structure-Property Relationships in Porous 3D Nanostructures as a Function of Preparation Conditions: Isocyanate Cross-Linked Silica Aerogels. Chem. Mater., vol. 19, no. 9, 2007, pp. 2247–2260.

Find out more about the research of Glenn's Durability and Protective Coatings Branch:

<http://www.grc.nasa.gov/WWW/EDB/>

Glenn Contact:

Dr. Mary Ann Meador, 216–433–3221, Maryann.Meador@nasa.gov

Ohio Aerospace Institute (OAI) Contact:

Dr. Baochau Nguyen, 216–433–2738, Baochau.N.Nguyen@nasa.gov

Aspen Aerogels Contact:

Dr. George L. Gould, 508–691–1136, ggould@aerogel.com

Authors:

Dr. Mary Ann Meador and
Dr. George L. Gould

LEW Number:

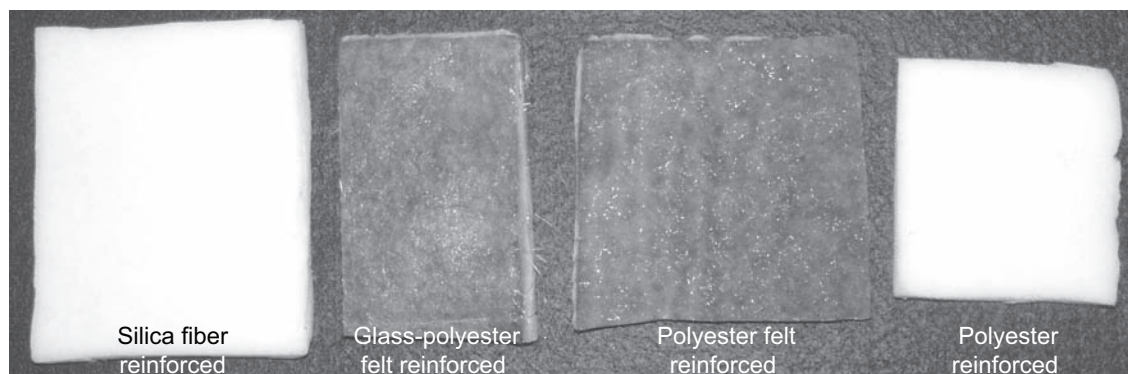
LEW–17,685

Headquarters Program Office:

Fundamental Aeronautics Program

Programs/Projects:

Subsonic Rotary Wing Project, Subsonic Fixed Wing Project



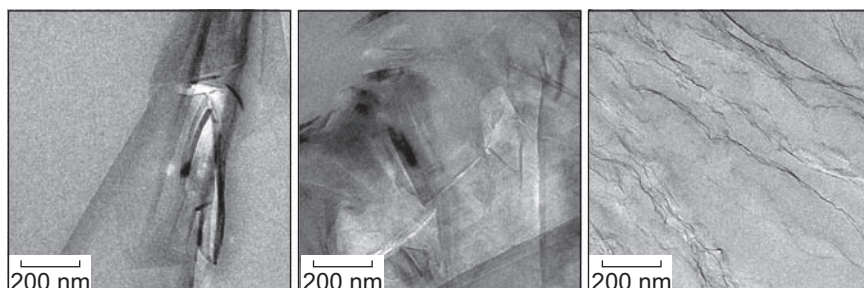
Polymer cross-linked aerogel composites made with four different fiber compositions. The aerogel component reproduces a formulation developed by Glenn with comparable density, mechanical properties, and thermal conductivities.

Physical Properties of Exfoliated Graphite Nanocomposites Tailored by Variation of Graphite Surface Functionality

The physical and transport properties of epoxy/graphite nanocomposites are highly dependent on the extent of graphite surface modification. Increased oxidation promotes bonding with the matrix polymer, but at the expense of conductivity. Therefore, it is critical that the polymer-graphite system is tailored to meet multiple property criteria. Three graphite samples with varying degrees of functionalization were used in this study.

In this work, graphite flakes were functionalized by three separate methods. The first was edge oxidation by intercalation of nitric acid and sulfuric acid into natural flake graphite, followed by rapid thermal treatment (EG, ref. 1). The second technique employed bonding an epoxy coating to the graphite surface (Adherent-TG679) via a coupling agent. The final method was chemical oxidation followed by thermal treatment to functionalize the graphene sheets (FGS). The details of this procedure are described elsewhere (ref. 2). In this case, the graphene layers lose their ordered stacking characteristics.

The transmission electron microscope (TEM) images illustrate that surface treatment had a large effect on the level of dispersion achieved in the epoxy matrix. The balance between particle size, dispersion, and oxygen content dictates a number of composite properties. High electrical conductivity is expected under the ideal condition of minimal oxidation and maximum dispersion. Unfortunately, a low degree of oxidation yields particle aggregation, necessitating high loading for conductivity. Furthermore, increased oxidation reduces conductivity, again requiring higher loadings for conductivity. The table summarizes electrical resistivity data.



TEM images of EG, Adherent-TG679, and FGS (left to right, respectively) in an epoxy matrix.

With all the modified graphite employed in this study, the functional groups introduced onto the graphene surface may react with the amine curing agent. This creates a strong bond between the matrix and filler, but it alters the resin stoichiometry, affecting the nanocomposite properties. Therefore, for the Adherent-TG679

Sample	Resistivity, $\Omega\text{-cm}$	Sample	Resistivity, $\Omega\text{-cm}$	Sample	Resistivity, $\Omega\text{-cm}$
EG		TG679		FGS	
0-wt% excess amine					
0-wt% graphite	Nonconductive	0-wt% graphite	Nonconductive	0-wt% graphite	Nonconductive
0.5-wt% EG	3.0×10^{10} (nonconductive)	0.5-wt% TG	1.3×10^7	0.5-wt% FGS	5.0×10^{10} (capacitive)
1.0-wt% EG	1.0×10^{10} (nonconductive)	1.0-wt% TG	8.8×10^5	1.0-wt% FGS	1.0×10^5
0-, 5-, or 10-wt% excess amine					
3.0-wt% EG/ 0-wt% excess amine	3.0×10^5	0.5-wt% TG/ 5-wt% excess amine	4.6×10^5	0.5-wt% FGS/ 5-wt% excess amine	7.0×10^{10} (capacitive)
		1.0-wt% TG/ 5-wt% excess amine	1.4×10^5	1.0-wt% FGS/ 5-wt% excess amine	5×10^9
		0.5-wt% TG/ 10-wt% excess amine	2.2×10^5	0.5-wt% FGS/ 10-wt% excess amine	8×10^9
		1.0-wt% TG/ 10-wt% excess amine	9.1×10^5	1.0-wt% FGS/ 10-wt% excess amine	1.0×10^5

and FGS samples, where functionalization was significant, nanocomposites containing increasing concentrations of amine curing agent were prepared. It is evident from the table that, within each stoichiometric ratio, increasing the graphite content reduced the nanocomposite resistivity. The EG samples contain poorly dispersed graphite; therefore, we see a decrease in resistivity as filler loading is increased. FGS was well dispersed, but heavily oxidized; therefore, these nanocomposites showed capacitive behavior until 1-wt% material was dispersed. The greatest improvement in conductivity was observed in the Adherent-TG679 samples, where oxidation and dispersion were intermediate in comparison to the other samples. Within these materials, the electrical resistivity was decreased by 5 orders of magnitude at a loading of 1 wt%. In addition, this loading did not affect the processing or mechanical properties of the Adherent-TG679 nanocomposites.

The toughness of the epoxy nanocomposites was given by the energy required to break the tensile specimens. This value was calculated by the area under the load displacement curve obtained from tensile tests. The load displacement curve approximates a stress-strain curve because the stress and strain values can be calculated from load-displacement data. The tensile test data from these materials demonstrated no change in toughness for the samples prepared with stoichiometric quantities of epoxy to amine. Within the 5-percent excess amine samples, there was up to a 37-percent increase in toughness, but the data were scattered and inconsistent. However, with the addition of 10-percent excess amine, there was significant bonding between the graphene sheets and the matrix, which consistently provided a threefold to fourfold increase in the energy needed to break the sample. Scanning electron microscope images of the fracture surfaces show no evidence of failure at the interface.

We have seen that two properties, toughness and conductivity, require graphite with very different surface characteristics. With regard to electrical conductivity, low oxidation and higher graphite loading provided better results. The opposite was true for mechanical properties. Understanding the level of oxidation present on the graphite, and working accordingly to strengthen the interface, can provide the best of both properties. For example, Adherent-TG679 with 1-wt% loading and 10-percent excess amine has greatly enhanced material toughness as well as very low resistivity.

This work was performed in collaboration with Professors Ilhan Aksay and Robert Prud'homme, as well as Dr. Douglas Adamson at Princeton University, supported from the NASA University Research, Engineering, and Technology Institute on BioInspired Materials under award NCC-1-02037. Epoxy-coated TG679 was provided by Adherent Technologies, Inc., funded by NASA Phase II Small Business Innovation Research.

References

1. Chen, Guohua, et al.: Preparation of Polystyrene/Graphite Nanosheet Composite. *Polymer*, vol. 44, no. 6, 2003, pp. 1781–1784.
2. Schniepp, Hannes C., et al.: Functionalized Single Graphene Sheets Derived From Splitting Graphite Oxide. *J. Phys. Chem. B*, vol. 110, no. 17, 2006, pp. 8535–8539.

Glenn Contact:

Sandi G. Miller, 216-433-8489,
Sandi.G.Miller@nasa.gov

Author:

Sandi G. Miller

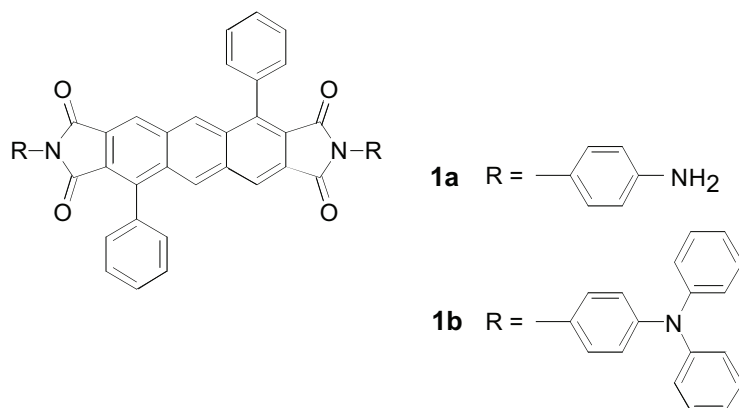
Headquarters Program Office:

Aeronautics Research Mission Directorate

Programs/Projects:

Subsonic Fixed Wing Project,
Supersonics Project

Fluorescent Dye Developed for the Detection of Nitroaromatic Compounds



Chemical structures of fluorescent sensors.

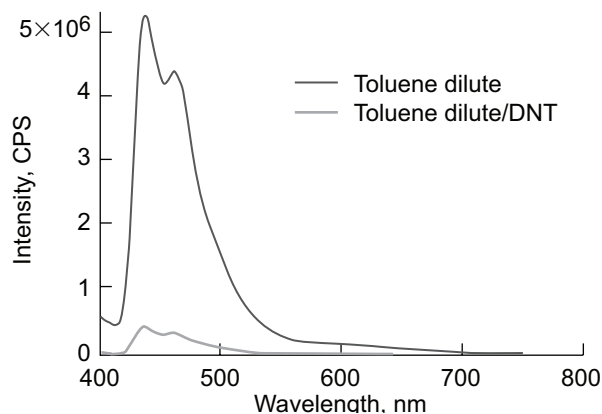
The detection of chemical and biological warfare agents and explosives is important for national defense and homeland security. Detection techniques for these threats must be simple and easy to use, accurate, and portable. A variety of techniques have been developed including spectroscopic, chromatographic, and electrochemical methods. Among these, fluorescence-based techniques are particularly attractive because they are easy to apply, have low detection limits, and the necessary instrumentation can be incorporated into a small package that has low power requirements.

Researchers in the Polymers Branch of the NASA Glenn Research Center have been developing fluorescent sensors for detecting chemical and biochemical species. The approach being explored by this team utilizes a molecule with a fluorescent core that is capped by different groups (R), whose structure can be changed to tailor the sensitivity of the dye to different chemical species (see the diagram). An earlier result from this effort was the development of an on-off fluorescent sensor (**1a**) for detecting chemical warfare agents, such as

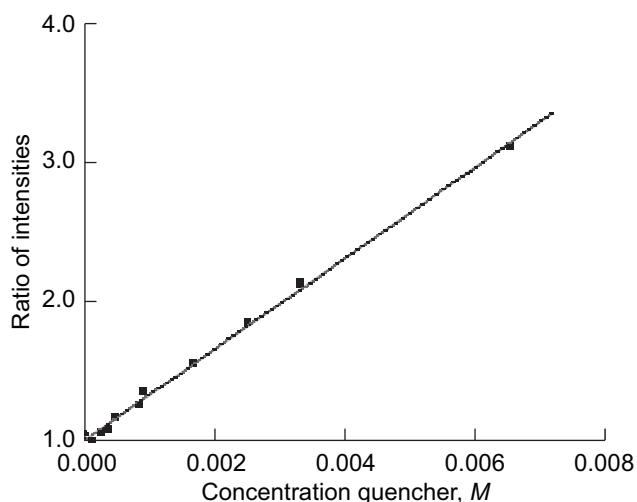
Sarin (ref. 1). Because of an efficient intramolecular excited-state electron transfer reaction, this dye molecule by itself does not fluoresce. However, when the electron transfer process is suppressed by the presence of certain analytes, including acids and analogues of Sarin, the dye molecule becomes fluorescent.

Recently, a new dye (**1b**) was prepared that can detect nitroaromatic compounds, such as 2,4-dinitrotoluene (DNT). Nitroaromatics, such as 2,4,6-trinitrotoluene (TNT) are frequently the major components of explosive devices. The fluorescence spectrum of **1b** in toluene is shown in the left graph. The addition of DNT quenches the fluorescence of **1b** and reduces the intensity of its fluorescence spectrum.

A Stern-Volmer plot for the quenching of the fluorescence of **1b** by DNT in toluene is shown in the right graph. The rate constant for the quenching, determined from the slope of this plot, was $1.02 \times 10^{11} \text{ M}^{-1} \text{ sec}^{-1}$, indicating that this is a highly efficient process. Further study of this system and its potential use in detecting other compounds used in explosives is underway.



The fluorescence spectrum of **1b** in toluene and in toluene containing DNT. The intensity of the fluorescence spectrum is reduced because of electron transfer quenching by DNT. CPS, counts per second.



Stern-Volmer plot of the effect of added concentrations of DNT on the fluorescence quantum yield of **1b** in toluene.

Reference

1. Ilhan, Faysal; Tyson, Daniel S.; Meador, Michael A.: Synthesis and Chemosensory Behavior of Anthracene Bisimide Derivatives. *Chem. Mater.*, vol. 16, 2004, pp. 2978–2980.

Glenn Contact:

Dr. Michael A. Meador, 216–433–9518, Michael.A.Meador@nasa.gov

Ohio Aerospace Institute (OAI) Contact:

Daniel S. Tyson, 216–433–3187, Daniel.S.Tyson@nasa.gov

Authors:

Dr. Michael A. Meador, Dr. Daniel S. Tyson, and Ashley Carbaugh

Headquarters Program Office:

Aeronautics Research Mission Directorate

Programs/Projects:

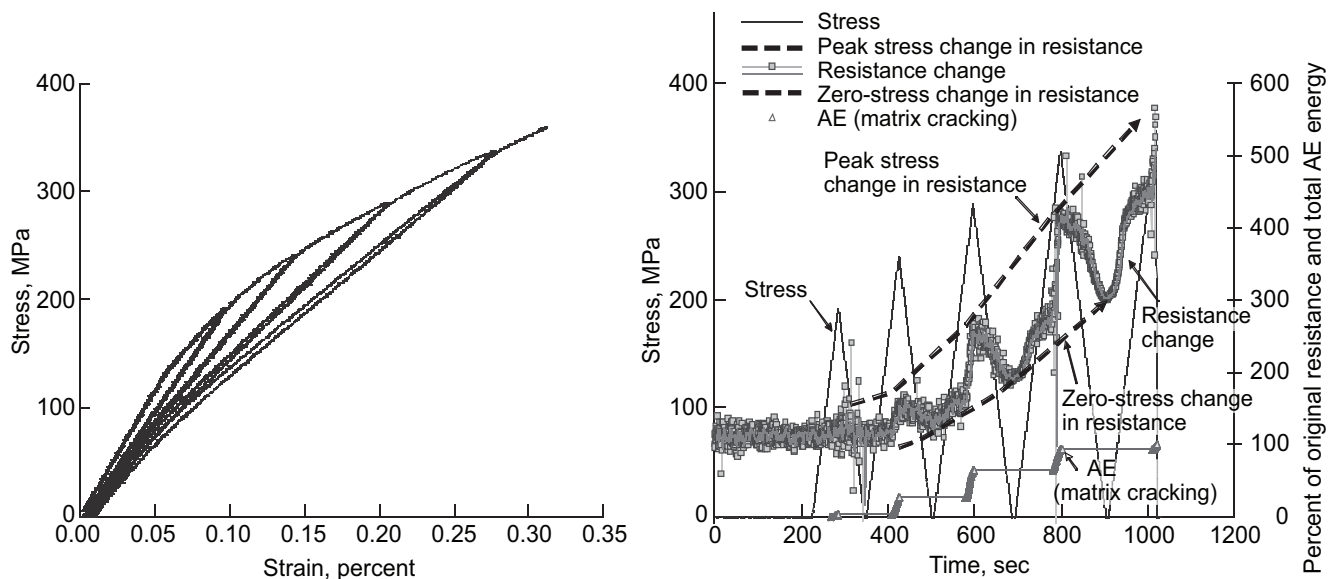
Subsonic Fixed Wing Project

Electrical Resistance Tested as a Nondestructive Evaluation Technique for Silicon Carbide/Silicon Carbide Composites

Ceramic matrix composites developed at the NASA Glenn Research Center are considered to be state-of-the-art structural materials for high-temperature (>1200 °C) oxidizing environments. They are now being pursued for turbine airfoil components in military and civilian aircraft and hold promise as future materials for NASA hypersonic and space applications. One of the key factors for implementing these materials is the ability to detect damage and predict useful life. Current nondestructive evaluation (NDE) techniques such as ultrasonic scanning, thermal diffusivity, or x ray are not sensitive to cracking that occurs transverse to the length of these types of composites. Unfortunately, this is often a mode of failure when these materials are loaded in tension. Therefore, a significant need is to develop NDE techniques that are sensitive to in-plane damage and that can be used to

quantify and feed models to predict the useful remaining life of components.

One technique being explored at the NASA Glenn Research Center that shows great promise is electrical resistance. Since the fibers and the matrix are both conductive, the composite as a whole is very sensitive, electrically, to changes in fiber type and matrix type and to damage that occurs during mechanical testing. The left graph shows a typical



Left: Stress-strain curve for a typical Sylramic-iBN reinforced slurry-cast melt-infiltrated composite. Right: The change in electrical resistance and accumulation of acoustic emission during the unload-reload test. This figure is shown in color in the online version of this article. (<http://www.grc.nasa.gov/WWW/RT/2007/Str-Mat/06-RXC-morscher.html>).

unload-reload tensile test to failure of a Sylramic-iBN fiber (Dow Corning, Midland, MI) reinforced slurry-cast melt-infiltrated composite (GE Power Systems Composites, Newark, DE) developed under NASA's Ultra-Efficient Engine Technology program. During this test, the specimen was monitored with both acoustic emission (AE) (ref. 1) and electrical resistance. The data for the stress, AE, and electrical resistance are shown in the right graph on the preceding page. It is clear that, as AE increases (a measure of matrix cracking), electrical resistance increases accordingly. In fact, resistance increases over 400 percent over the entire test, which shows how sensitive this technique is to damage accumulation. The "zero-stress change" in resistance also increases significantly, which bodes well for this technique to be used as an inspection technique, either onboard or between missions. Future plans include performing high-temperature tension tests to monitor the combined effects of stress and oxidation.

With these promising results, research is continuing to determine the effect of composite constituents and fiber architecture on resistance change. Early results show that resistance increases by several orders of magnitude for chemical-vapor-infiltrated matrix composites in comparison to melt-infiltrated matrix composites. This expands the potential for this technique to characterize the quality of ceramic matrix composite processing. The technique also should be able to evaluate complex shapes such as corners and curvature as well as mechanical joints. Finally, modeling efforts are underway to couple the electrical and mechanical properties of woven ceramic matrix composites based

on the fiber-architecture and composite constituents to aid the life modeling of these composite materials.

Reference

1. Morscher, Gregory N.: Stress-Dependent Matrix Cracking in 2D Woven SiC-Fiber Reinforced Melt-Infiltrated SiC Matrix Composites. *Comp. Sci. Technol.*, vol. 64, no. 9, 2004, pp. 1311–1319.

Glenn Contact:

Dr. Andrew J. Eckel, 216–433–8185,
Andrew.J.Eckel@nasa.gov

Ohio Aerospace Institute (OAI) Contact:

Dr. Gregory N. Morscher, 216–433–5512,
Gregory.N.Morscher@nasa.gov

Authors:

Dr. Gregory N. Morscher, Craig E. Smith,
and Dr. Zhenhai Xia

Headquarters Program Office:

Aeronautics Research Mission Directorate

Programs/Projects:

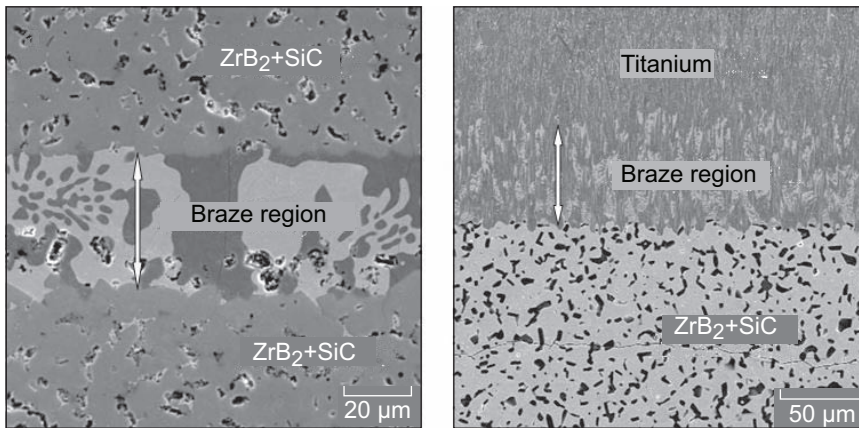
Hypersonics Project

Technology for Integrating Ultra-High-Temperature Ceramic Composites With Metallic Systems Developed

Refractory metal diborides have high melting points and good oxidation resistance in extreme environments, which allows them to operate at 2150 to 2770 K. Among these, zirconium diboride (ZrB_2) has a significantly lower density than the refractory metals based on tungsten and rhenium that are used in applications involving intense thermal loads. ZrB_2 -based ultra-high-temperature ceramic composites (UHTCC) have been considered for a wide variety of thermal protection system components of space vehicles reentering the Earth's atmosphere. These composites typically contain additives, such as silicon carbide (SiC) to improve oxidation resistance and strength, and carbon (C) to improve thermal stress resistance. Properties of ZrB_2 -based UHTCC can be modified by adding fibers of C and SiC as toughening and strengthening phases, respectively.

One area of special interest is the development of technologies for joining and attaching UHTCC to metallic components. Researchers at the Ohio Aerospace Institute, NASA Glenn Research Center, and University of Wisconsin-Stout have vacuum brazed ZrB_2 -based UHTCC to high-temperature metals and alloys such as titanium, copper-clad-molybdenum, and Inconel 625 superalloy by employing copper-silver-titanium brazes (liquidus temperature,

$T_L \sim 1073$ to 1173 K), nickel-base metallic glasses ($T_L \sim 1320$ K), and palladium-base brazes ($T_L \sim 1493$ to 1513 K). Three ZrB_2 -based UHTCCs were prepared by hot pressing: ZrB_2 -SCS9-SiC, ZrB_2 -SiC-C, and ZrB_2 -SiC. Both ZrB_2 -SiC and ZrB_2 -SiC-C achieved full densification during fabrication; however, ZrB_2 -SCS9-SiC contained residual porosity (~30 percent) and microcracks oriented perpendicular to the SCS9 fibers, which formed because of a large mismatch in the coefficients of thermal expansion of ZrB_2 and the SCS9 fiber. The joints were examined using optical and scanning electron microscopy coupled with energy-dispersive x-ray spectroscopy and by Knoop microhardness test.



Microstructure of joints fabricated with a 65wt%Pd-35wt%Co braze alloy in ZrB_2 -SiC composites and in a ZrB_2 -SiC and titanium system.

The joints were structurally sound and generally devoid of microcracks and shrinkage porosity, and the interfaces were well defined and sharply demarcated (see the photomicrographs). Compositional readjustments caused by the dissolution of the composite and metal substrates led to metallurgical bonding in composite-to-metal joints. Relatively high titanium concentrations were observed at the composite/braze interfaces in composite/titanium joints. Partial melting of the Inconel 625 substrate in contact with palladium-base brazes during joining at 1493 to 1513 K led to considerable chemical attack of the SCS9 fibers in the ZrB_2 -SiC-C composites. In the UHTCC joints made using the nickel-base metallic glass braze, chemical compatibility was ensured because both the braze and the UHTCC contained boron and silicon. However, some microcracking occurred in the joint region because of embrittlement when an amorphous nickel-braze with relatively large amounts of boron (3.1 wt%) and chromium (~6.5 wt%) was used. No such cracks formed in chromium-free, low-boron metallic glass-braze alloys. Preliminary results showed that metallurgically sound joints could be created using all of the selected braze alloys; however, the highest use-temperatures and good oxidation resistance of palladium-base brazes makes them the most promising for further investigation.

The distribution of Knoop microhardness across the joints (see the graph) depended on the substrate and the braze alloy. For a given system, Knoop microhardness profiles were reproducible and consistent with the expected behavior. The fully dense ZrB_2 -SiC composites displayed higher hardness than the braze region in the ZrB_2 -SiC-based joints. However, the ZrB_2 -SCS9-SiC and ZrB_2 -SiC-C composite regions displayed lower hardness than the braze region (in spite of the presence of hard SiC and ZrB_2). This occurred because of extensive microcracking and incomplete densification (~30-percent residual porosity) in ZrB_2 -SCS9-SiC, and interfacial weakening caused by the presence of carbon in the fully dense ZrB_2 -SiC-C composite.

Bibliography

Singh, M.; and Asthana, R.: Joining of Zirconium Diboride-Based Ultra High-Temperature Ceramic Composites Using Metallic Glass Interlayers. *Mater. Sci. Eng. A*, vols. 460–461, 2007, pp. 153–162.

Glenn Contact:

Dr. Andrew J. Eckel, 216–433–8185,
Andrew.J.Eckel@nasa.gov

Ohio Aerospace Institute (OAI) Contact:

Dr. Mrityunjay Singh, 216–433–8883,
Mrityunjay.Singh-1@nasa.gov

Authors:

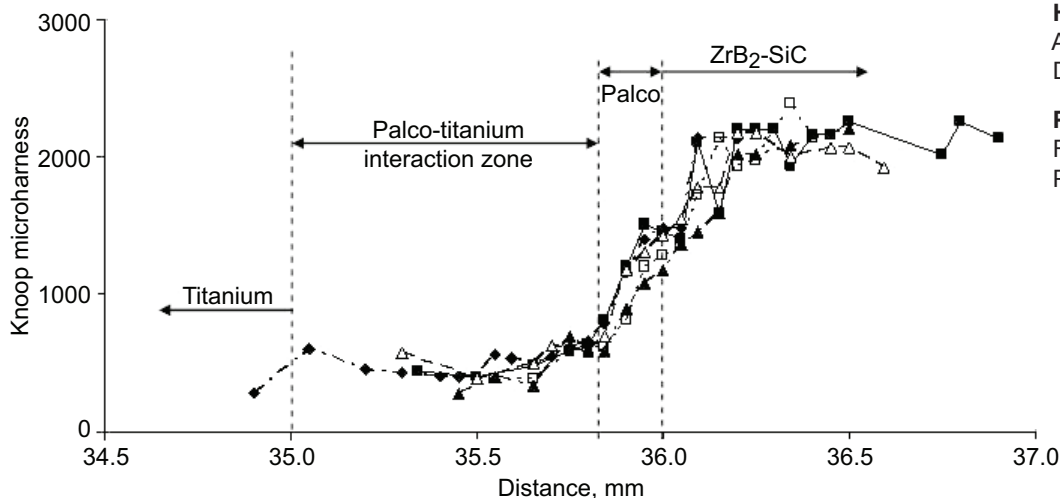
Dr. Mrityunjay Singh and Dr. Rajiv Asthana

Headquarters Program Office:

Aeronautics Research Mission
Directorate

Programs/Projects:

Fundamental Aeronautics
Program, Hypersonics Project



Knoop microhardness profiles across the joint interface in ZrB_2 -SiC/Palco/titanium system. The symbols represent multiple scans across the joint.

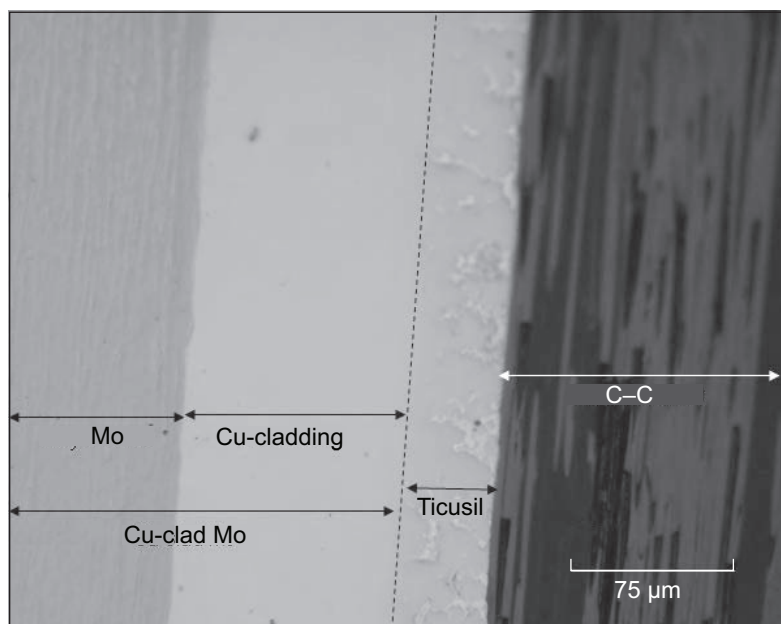
Joining of Carbon-Carbon Composites to Metals Demonstrated for Thermal Management Applications

Carbon-carbon (C–C) composites are used in a number of aerospace and ground-based applications, such as the nose cone and leading edges of the space shuttle, rocket nozzles, exit cones, heat shield, and aircraft braking systems. A number of applications of C–C require the composite to be integrated (joined or attached) to metals or other substrates. One particular area of current interest is the utilization of C–C composites in thermal management applications. A number of such applications utilize copper-clad molybdenum (Cu-clad Mo) because of its tailorable thermal conductivity and thermal expansion properties. However, the high density of Cu-clad Mo (e.g., 9.7 g/cm³) has limited its use in lightweight heat-rejection systems. C–C composites containing high-conductivity carbon fibers provide excellent heat dissipation and low expansion properties at considerably reduced weight. Acting in combination, Cu-clad Mo and C–C can provide excellent heat dissipation and some weight advantage over the heavier Cu-clad Mo. By controlling the clad layer thickness in Cu-clad-Mo, the coefficient of thermal expansion (CTE) mismatch between C–C and Cu-clad Mo can be designed to minimize residual stresses during joining and service while maintaining acceptable levels of thermal conductivity needed for thermal management applications.

Researchers from the Ohio Aerospace Institute, ASRC Aerospace Corporation, NASA Glenn Research Center, and University of Wisconsin-Stout have brazed chemical-vapor-infiltrated (CVI) C–C composites (P–120 fibers) and resin-derived C–C composites (T–300 fiber) to Cu-clad Mo (Cu-Mo-Cu layer thickness ratio: 13%-74%-13%) using five commercial copper-silver (Cu-Ag)

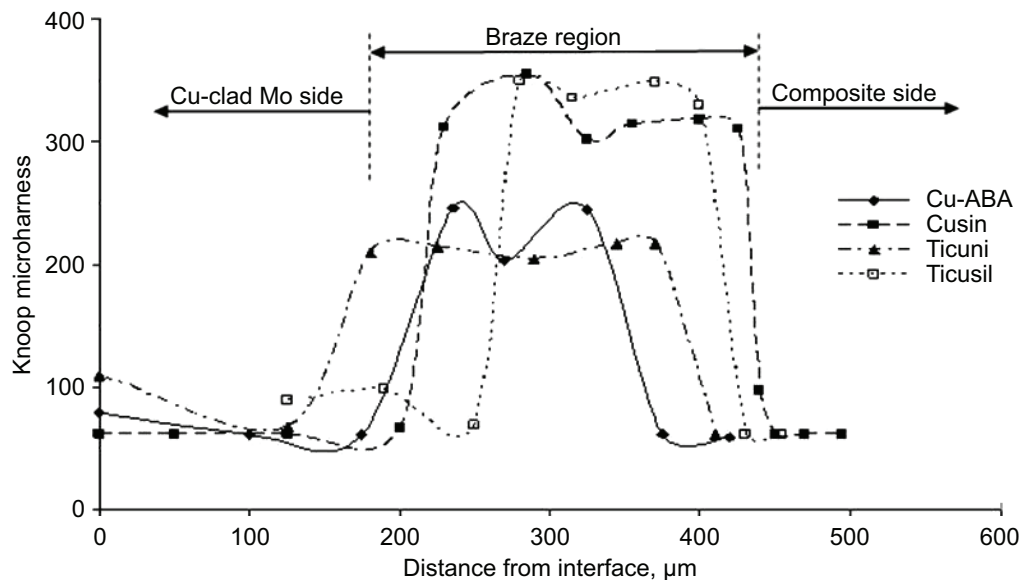
active braze alloys with good thermal conductivity and ductility: Cu-ABA, Ticuni, Ticusil, Cusil-ABA, and Cusin-1 ABA.¹ The presence of Cu as a cladding on Mo and as an alloying additive in brazes ensures chemical compatibility and enhanced ductility at the joint interfaces. The joints were vacuum brazed under a load of 0.30 to 0.4 N at 15 to 20 °C above the braze liquidus (~10⁻⁶-torr vacuum, 5-min soak). Joints were characterized using optical and scanning electron microscopy, energy dispersive x-ray spectroscopy, and Knoop microhardness measurements across the joint.

The joints displayed intimate physical contact and were free of structural imperfections such as interfacial microvoids, shrinkage porosity, and microcracking (see the photograph). Extensive braze infiltration of interfiber regions in the CVI C–C composites occurred regardless of the carbon fiber orientation at the mating surface. Titanium- (Ti-) bearing braze alloys displayed good spreading on C–C, with Ticusil (4.5-wt% Ti) exhibiting better coverage than Cusil-ABA (1.75-wt% Ti). Some dissolution and interdiffusion of elements across the joint were observed. In particular, the joint interfaces were enriched in Ti, which is consistent with the high chemical affinity of Ti toward C and the large negative change in the Gibb's free energy for TiC formation via $Ti + C \rightarrow TiC$ ($\Delta G = -171.18$ kJ at 1123 K). The Cu cladding on Mo did not melt at the joining temperatures (~1050 to 1100 K), which were below the melting point of Cu (1357 K); however, some dissolution of Cu occurred in the braze. In joints made using resin-derived C–C composites, there was evidence of some cracking within the C–C composite owing to the low interlaminar shear strength of the composite. The Knoop microhardness



Substrates and braze region in C–C/Ticusil/Cu-clad-Mo system.

¹From Morgan Advanced Ceramics, Hayward, CA. The braze compositions (in wt%) are Cu-ABA (92.75Cu-3Si-2Al-2.25Ti), Ticuni (70Ti-15Cu-15Ni), Ticusil (68.8Ag-26.7Cu-4.5Ti), Cusil-ABA (63Ag-35.25Cu-1.75Ti), and Cusin-1 ABA (63Ag-34.25Cu-1Sn-1.75Ti).



Knoop microhardness profiles across the joint in C–C/Cu-clad-Mo joints made using different brazes.

profiles (see the graph) displayed gradients in the joint region with an abrupt rise in hardness in the vicinity of the braze region and a sharp decline in the adjoining Cu-clad Mo and C–C regions.

Bibliography

Singh, M.; Asthana, R.; and Shpargel, T.P.: Brazing of Carbon-Carbon Composites to Cu-Clad Molybdenum for Thermal Management Applications. *Mater. Sci. Eng. A*, vols. 452–453A, 2007, pp. 699–704.

Glenn Contact:

Dr. Andrew J. Eckel, 216–433–8185, Andrew.J.Eckel@nasa.gov

Ohio Aerospace Institute (OAI) Contact:

Dr. Mrityunjay Singh, 216–433–8883,
Mrityunjay.Singh-1@nasa.gov

Authors:

Dr. Mrityunjay Singh, Tarah P. Shpargel,
and Dr. Rajiv Asthana

Headquarters Program Office:

Aeronautics Research Mission Directorate

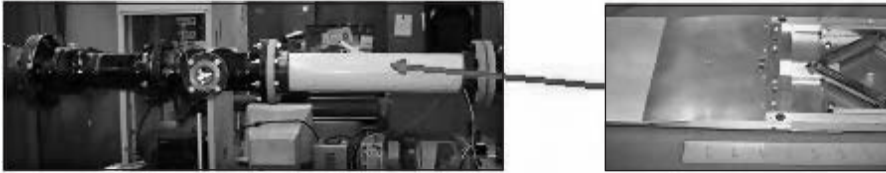
Programs/Projects:

Fundamental Aeronautics Program,
Subsonic Fixed Wing Project

Nickel-Titanium-Platinum High-Temperature Shape-Memory-Alloy Viability Established Through Wind Tunnel Testing of a High-Speed Adaptive Inlet

The development of adaptive structures that would allow aircraft to perform new missions or to perform current missions more effectively has long been a goal of the aeronautics industry. One of the components identified as benefiting greatly from adaptive technology is high-speed inlets, which if capable of changing geometry or cross-sectional area during flight, would result in improved performance at all points along the flight envelope from slow subsonic to supersonic cruise. However, the limiting factor to developing adaptive inlets has been the availability of extremely compact, yet high force actuators that could be integrated into the structure. Conversely, this would be an ideal application for shape memory alloys, but materials capable of operating

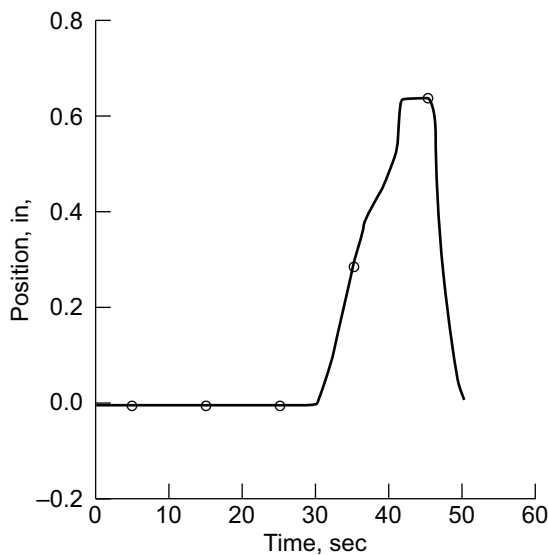
at the high temperatures encountered during supersonic flight, approaching 200 °C at Mach 2.0, are not commercially available. Thus, this is an ideal application for the family of high-temperature shape memory alloys (HTSMAs) recently developed at the NASA Glenn Research Center (ref. 1).



Version-1 inlet compression ramp model, which can be actuated with a NiTiPt HTSMA, prior to installation in the Princeton subsonic/supersonic wind tunnel (shown on the left side of the figure).

Through collaboration with Continuum Dynamics, Inc. (CDI, Ewing, New Jersey), a nickel-titanium-platinum (NiTiPt) HTSMA was incorporated into a series of increasingly more sophisticated subscale components, demonstrating the capability of these new shape memory alloys to actuate the movement of a compression ramp within a high-speed inlet. The Ni-50Ti-20Pt (at.%) HTSMA was developed and processed into wire form by Glenn. (Detailed characterization of alloys similar to that used in the demonstration can be found in ref. 2.) The NiTiPt alloy wire was then integrated into a series of demonstration components by CDI (supported through a combination of NASA Small Business Innovation Research and CDI Internal Research & Development funding). The initial tabletop demonstrator was capable of ramp movement through combined translation and rotation, changing both the capture area and flow angle for the inlet. After the conceptual design was demonstrated, a pair of subscale systems capable of ramp translation through force applied by the HTSMA were developed and tested in the supersonic wind tunnel at Princeton University.

The Version-1 inlet compression ramp, shown in the photographs, was successfully tested at flow speeds up to Mach 0.7, which resulted in dynamic pressures equivalent to those found at altitudes of 40,000 to 50,000 ft at supersonic conditions. The displacement-time response of this ramp under



The displacement-time response of the Version-1 inlet compression ramp while acting against dynamic pressure equivalent to that encountered under supersonic conditions.

high subsonic conditions is shown in the graph. More recently, a Version-2 inlet compression ramp was successfully tested up to Mach 1.0. Additional details on the design and testing of the supersonic inlet ramp actuator can be found in reference 3.

These tests indicated that the NiTiPt HTSMA was capable of generating the forces necessary to actuate the compression ramp under high dynamic pressures and was more than capable of operating in the high-temperature environments encountered at supersonic speeds. Thus, through a combination of new functional materials and appropriate designs, adaptive structures for aeronautic applications are coming closer to reality. Future research, if funding is made available, would include testing of a more sophisticated Version-3 inlet ramp capable of both translation and rotation at supersonic speeds.

References

1. Noebe, R., et al.: Wire Drawing and Postprocessing Procedures Developed for a New NiTiPt High-Temperature Shape-Memory Alloy. Research & Technology 2005, NASA/TM—2006-214016, 2006, pp. 138–139. <http://www.grc.nasa.gov/WWW/RT/2005/RX/RX29T-noebe1.html>
2. Noebe, Ronald, et al.: Properties and Potential of Two (Ni,Pt)Ti Alloys for Use as High-Temperature Actuator Materials. Proceedings of SPIE Smart Structures and Materials 2005: Active Materials: Behavior and Mechanics, vol. 5761, 2005, pp. 364–375.
3. Quackenbush, Todd R., et al.: Development and Test of an HTSMA Supersonic Inlet Ramp Actuator (Future of SMA). Proceedings of the 15th SPIE Smart Structures/NDE Annual International Symposium, vol. 6930, 2008, paper 6930–25.

Find out more about this research:**Glenn's Advanced Metallics Branch:**

<http://www.grc.nasa.gov/WWW/5000/MaterialsStructures/metallics/>

Continuum Dynamics, Inc. (outside site):

<http://www.continuum-dynamics.com/>

Glenn Contact:

Dr. Ronald D. Noebe, 216-433-2093, Ronald.D.Noebe@nasa.gov

Authors:

Dr. Ronald D. Noebe and
Dr. Todd Quackenbush

Headquarters Program Office:

Aeronautics Research Mission Directorate

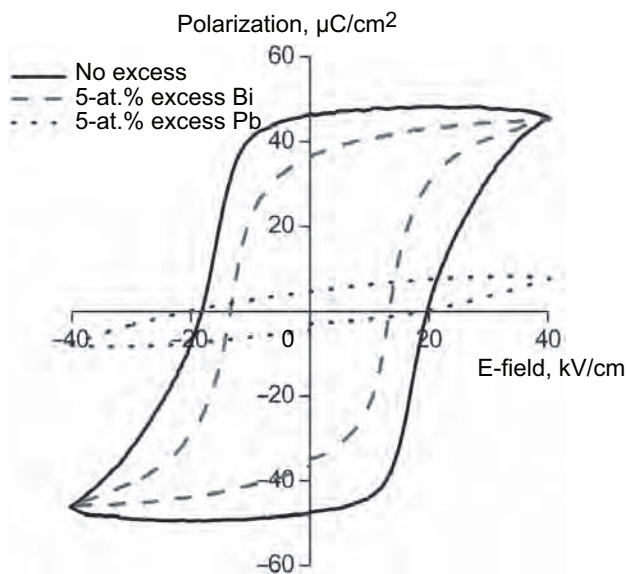
Programs/Projects:

Supersonics Project, Small Business
Innovation Research

High-Temperature Piezoelectric Material Developed

There are a plethora of aeronautic and aerospace applications that benefit from piezoelectric materials that can operate at high temperatures. In air-breathing engines, piezoelectric actuators can be used for active combustion control for fuel modulation to mitigate thermoacoustic instabilities and/or gas flow control to improve mixing characteristics by pulsed injection of air to reduce nitrogen oxide (NO_x) emissions and improve efficiency. Piezoelectric actuators can be used as synthetic jets for active flow control to mitigate the boundary layer separation on the blade surface, to reduce tip losses, and to help to control noise. Applied to turbomachinery, they can reduce blade vibration, which in turn, reduces stress, increases safety margins, and extends life. NASA space and science missions utilize a variety of piezoelectric materials for instruments and actuators. The actuators are, for the most part, restricted because of limitations on high-temperature operating conditions. The most

commonly used PZT (lead zirconium titanate) family of piezoelectric ceramics has a low Curie temperature ($T_C \sim 350^\circ\text{C}$ for Navy Type II), above which piezoelectric activity is absent. The upper-use temperature of PZT-based piezoelectric ceramics is further limited to less than 180°C because of the increased conductivity of these dielectric materials. Two main challenges in producing high-temperature piezoelectrics are (1) to increase T_C without an increase in loss tangent ($\tan \delta$) as a function of temperature and (2) demonstrate high piezoelectric activity.



Hysteresis loops for $\text{BiScO}_3\text{-PbTiO}_3$ with 0-at.% excess, 5-at.% excess Pb, and 5-at.% excess Bi.

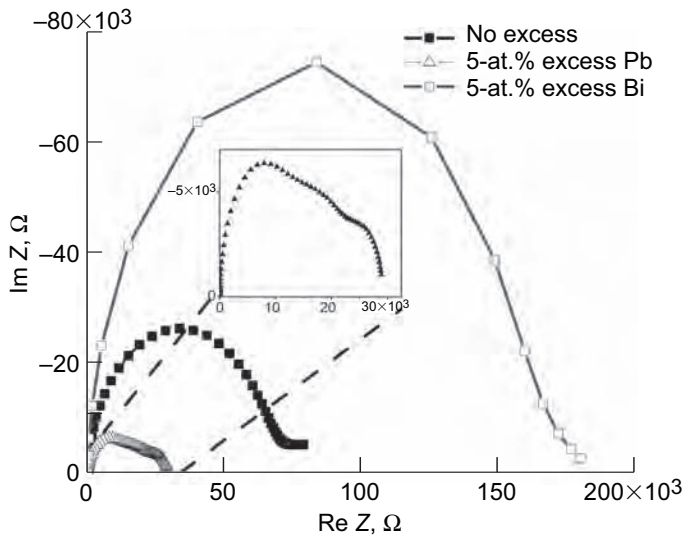
A variety of $(1-x)\text{BiScO}_3\text{-(}x\text{)PbTiO}_3$ (BS-PT) compositions have been developed at the NASA Glenn Research Center to show large electromechanical activity and thus a superior material for piezoelectric actuators and sensors. This includes the promising high-temperature piezoelectric candidate $0.63\text{BiScO}_3\text{-}0.37\text{PbTiO}_3$ (63BS-37PT), which is near its morphotropic phase boundary ($x = 0.64$). T_C for this composition is greater than 400°C .

The greatest challenge in developing high-temperature piezoelectrics for actuators is to sustain the insulating ability of the ceramics. Effects of excess lead (Pb) and bismuth (Bi) on dielectric, ferroelectric, and piezoelectric properties

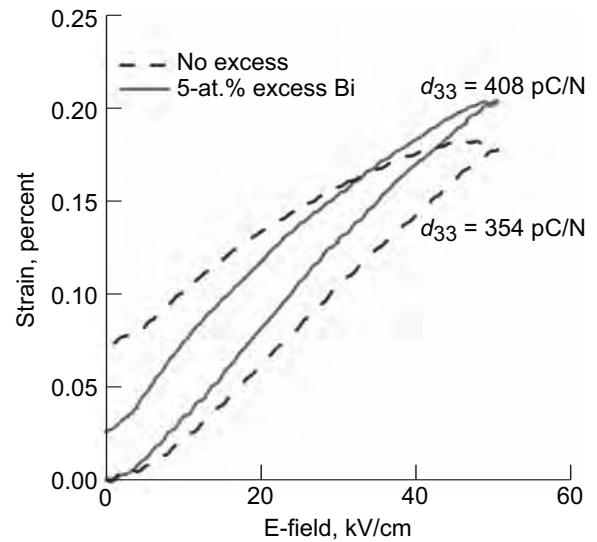
and microstructure have been investigated. Excess Pb addition decreased the resistivity because of the grain boundary contribution to the conductivity at elevated temperatures, coupled with an order-of-magnitude decrease in grain size. The resulting ceramics could not be poled because of their decreased resistivity (see the graph on the preceding page).

A new method of processing was developed for grain boundary engineering using excess Bi^{3+} , and the piezoelectric material response was investigated using impedance spectroscopy to sort out the grain boundary and grain interior contributions at elevated temperatures (see the next graph). The grain-boundary-engineered $63\text{BiScO}_3\text{-}0.37\text{PbTiO}_3$ piezoelectric of excess Bi increased the resistivity significantly and improved the poling conditions, resulting in an increase in the piezoelectric coefficient d_{33} from 354 to 408 pC/N

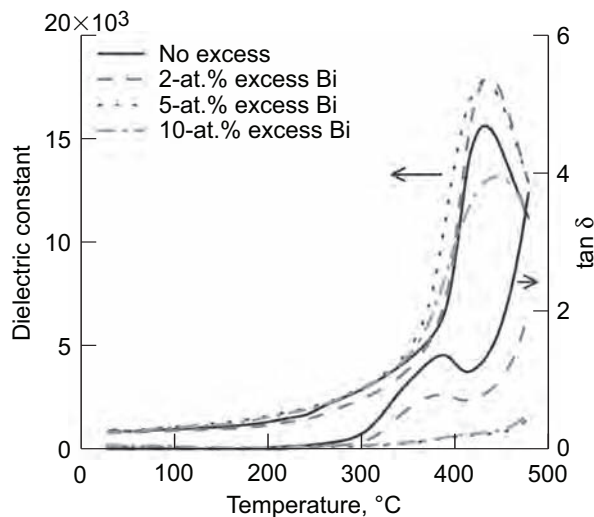
(picocoulombs/Newton) (see the graph on the left). The loss tangent decreased more than one order of magnitude at elevated temperatures ($>300\text{ }^\circ\text{C}$) (see the bottom graph). No grain boundary contribution to the conductivity was observed despite a significant increase in the grain boundary area. This research provides a pathway to obtain piezoelectric ceramics with low losses at elevated temperatures and improved ferroelectric characteristics, and thus will enable high-temperature actuators for aerospace applications.



Impedance (Z) results of $\text{BiScO}_3\text{-PbTiO}_3$ with 0-at.% excess, 5%-at. excess Pb, and 5-at.% excess Bi measured from 1 Hz to 1 MHz at $325\text{ }^\circ\text{C}$.



Unipolar field-induced strain for $\text{BiScO}_3\text{-PbTiO}_3$ with 0-at.% excess and 5-at.% excess Bi.



Loss tangent (at 10 kHz) as a function of temperature for compositions with 0-, 2-, 5-, and 10-at.% excess Bi.

Glenn Contacts:

Dr. Andrew J. Eckel, 216-433-8185,
Andrew.J.Eckel@nasa.gov

Dr. Frederick W. Dynys, 216-433-2404,
Frederick.W.Dynys@nasa.gov

Case Western Reserve University

Contact:

Dr. Ali Sayir, 216-433-6254,
Ali.Sayir-1@nasa.gov

Authors:

Dr. Ali Sayir and Dr. Alp Sehirlioglu

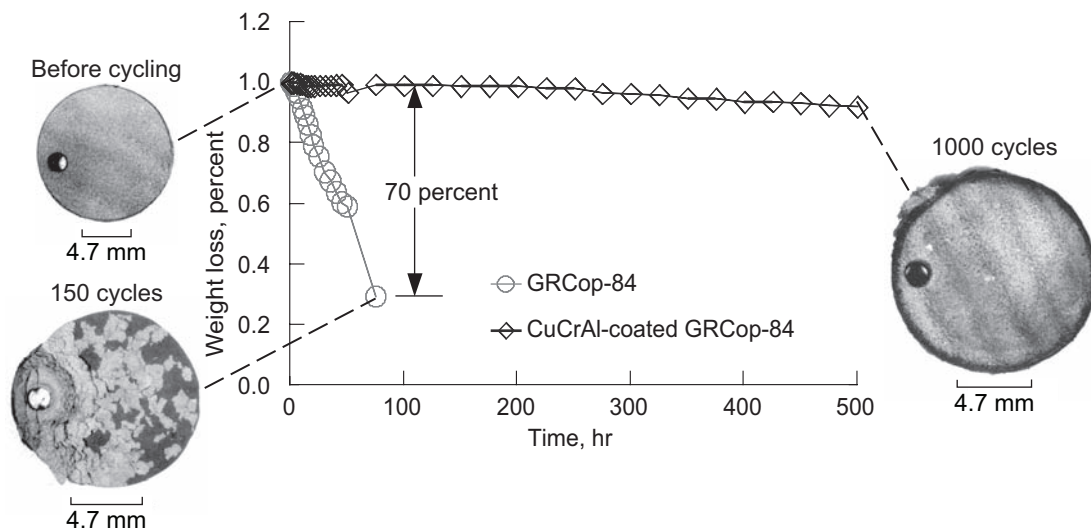
Headquarters Program Office:

Aeronautics Research Mission Directorate

Programs/Projects:

Supersonics Project, Air Force Office of Scientific Research

Glenn-Developed Copper-Chromium-Aluminum Coatings Evaluated for Reusable Launch Vehicles



CuCrAl-coated GRCop-84 test coupons lasted 500 hr at 973 K with about a 10-percent loss in weight because of the oxidation of the uncoated edges. The coating itself was intact and showed no microstructural or visual deterioration. In contrast, the uncoated specimen lost 70 percent of its original weight after 75 hr. The insets show photographs of the tested and untested specimens.

Advanced copper alloy combustion liners and nozzles made of GRCop-84 (Cu-8at.%Cr-4at.%Nb)¹ are being considered for use in NASA's next generation of reusable launch vehicles. However, copper alloys are susceptible to environmental attack by hydrogen and oxygen in the combustion gases, which reduces life, increases the cost of vehicle operation, and reduces engine efficiency. The NASA Glenn Research Center has successfully developed several overlay coating technologies for protecting GRCop-84 substrates from environmental attack. As part of this technology development program, new thermal CuCrAl coatings² were developed and evaluated in qualification tests.

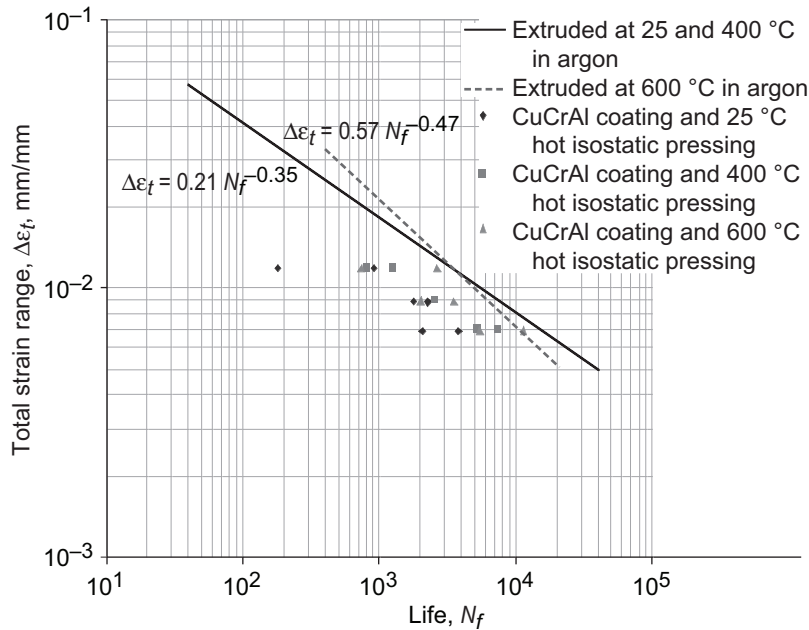
Atomized CuCrAl powders were sprayed on GRCop-84 specimens at room temperature by the cold-spray deposition process at ASB, Inc., under contract. The specimens were hot isostatically pressed prior to testing. Microstructural assessment of the coating quality and low-cycle fatigue and cyclic oxidation tests were conducted at the NASA Glenn Research Center. The microstructural observations revealed that the coatings were generally dense. Thermal cyclic oxidation tests conducted between 773 and 1073 K revealed that the CuCrAl-coated GRCop-84 performed exceedingly well in comparison to the uncoated specimens. For example, the coated specimen lasted up to 1000 cycles, corresponding to a cumulative time of 500 hr at 973 K, where the specimen was maintained for 30 min at temperature followed by a 5-min natural cool down (see the preceding figure). In comparison, the uncoated

GRCop-84 lasted for 150 cycles, corresponding to a cumulative time of 75 hr and a loss of about 70 percent of its original weight.

Several important points may be noted. First, the CuCrAl-coated GRCop-84 specimens lasted more than twice the expected design life of an advanced reusable launch vehicle. Second, these results revealed that coating GRCop-84 liners with the new CuCrAl coatings is expected to permit their use at temperatures 200 to 300 K above that of uncoated GRCop-84 liners. Third, the coating was intact and bonded to the substrate even after 40 thermal cycles at 1073 K, which is relatively high for a copper alloy. Fourth, the low-cycle fatigue lives of the CuCrAl-coated and uncoated specimens were comparable within a factor of 2 to 3 with no evidence of coating debonding (see the graph on the next page).

¹Cu, copper; Cr, chromium; Nb, niobium.

²Al, aluminum.



Comparison of the low-cycle fatigue lives of CuCrAl-coated and uncoated GRCop-84 specimens between 298 and 873 K. The results reveal that the fatigue lives for the coated specimens are comparable with those for the uncoated specimens within experimental scatter. $\Delta\epsilon_t$ is the total strain range.

The new CuCrAl coatings show great promise as protective coatings for copper alloy liners. Future studies would include conducting tests under high heat fluxes in a hydrogen-oxygen combustion flame.

Find out more about the research of Glenn's Durability and Protective Coatings Branch:

<http://www.grc.nasa.gov/WWW/EDB/>

Glenn Contacts:

Dr. Sai V. Raj, 216-433-8195,

Sai.V.Raj@nasa.gov

Dr. Bradley A. Lerch, 216-433-5522,

Bradley.A.Lerch@nasa.gov

Authors:

Dr. Sai V. Raj, Dr. Bradley A. Lerch, and

Dr. Jegan Karthikeyan

LEW Number:

LEW 17,521-1

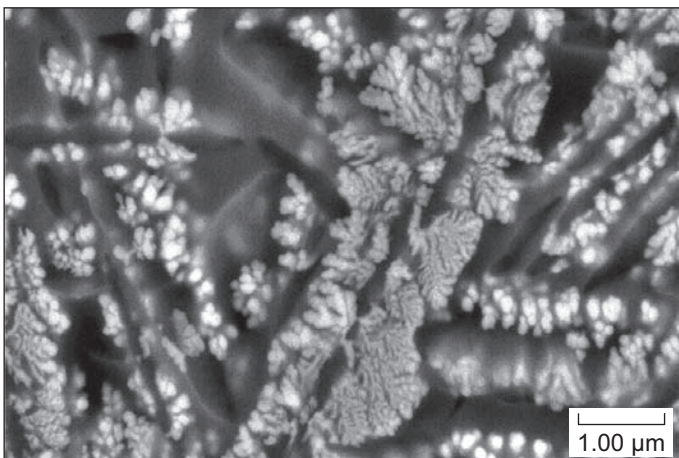
Headquarters Program Office:

Exploration Systems Mission Directorate

Programs/Projects:

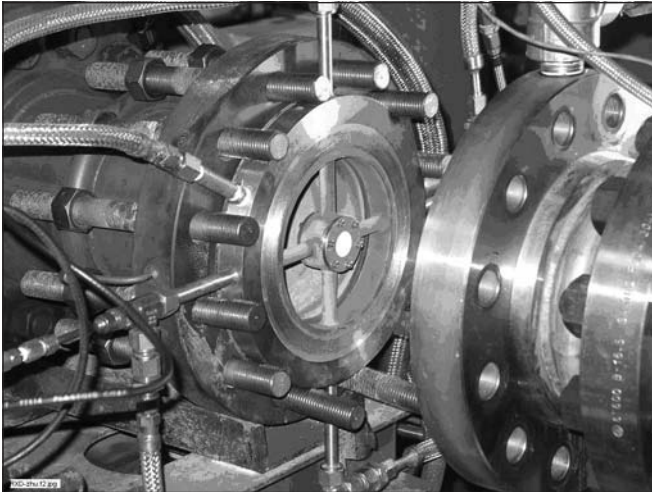
Constellation Systems, Hypersonics Project

Nanocomposite Environmental Barrier Coatings Evaluated for High-Temperature Combustion Environment Stability



Microstructure of an advanced $HfO_2-Al_2O_3-RE$ aluminosilicate nanocomposite coating.

Advanced multicomponent environmental barrier coatings (EBCs) were developed for lightweight SiC/SiC ceramic-matrix-composite and monolithic silicon nitride (Si_3N_4) turbine engine component applications by extending the component temperature capability and long-term durability in oxidizing and water-vapor-containing combustion environments (refs. 1 and 2). The coating systems demonstrated improved phase stability, lower thermal conductivity, and improved sintering and thermal stress resistance under simulated engine heat-flux and thermal cycling conditions, largely because of their defect-clustering structures, which were



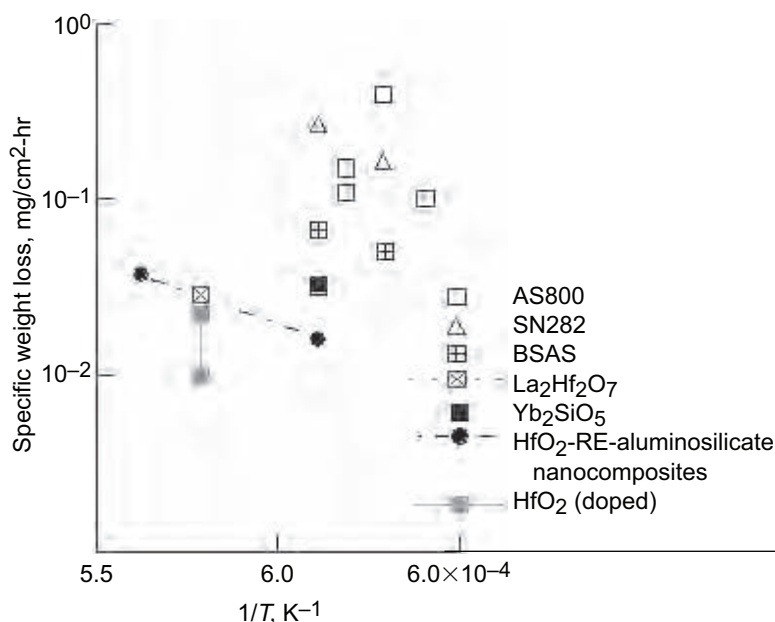
High-pressure burner rig setup for ceramic coating and substrate specimen stability evaluations at high temperatures in 6 atm.

designed to promote the creation of thermodynamically stable oxide defect clusters and/or nanophases within the coating systems. In particular, low-thermal-expansion, multicomponent hafnium oxide–aluminum oxide–rare earth- ($\text{HfO}_2\text{-Al}_2\text{O}_3\text{-RE-}$) doped aluminosilicate nanocomposite EBC systems were recently developed at the NASA Glenn Research Center for thin turbine airfoil EBC applications, aiming at a design for significantly improved long-term stability and durability performance.

The advanced coatings were evaluated for high-temperature combustion environmental stability in high-pressure burner rig simulated engine environments. The scanning electron microscope image on the preceding page

shows the microstructure of the advanced $\text{HfO}_2\text{-Al}_2\text{O}_3\text{-RE}$ silicate composite coating processed using a plasma spray and subsequent reactive synthesis approach. The photograph shows the coating specimen stability testing setup in the high-pressure burner rig for the simulated combustion stability evaluations at high temperatures.

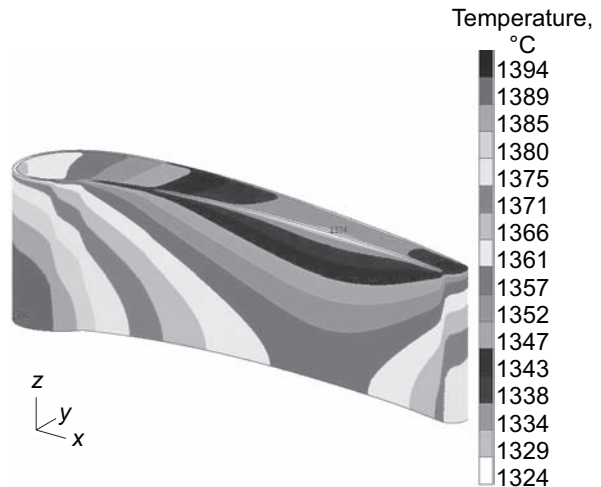
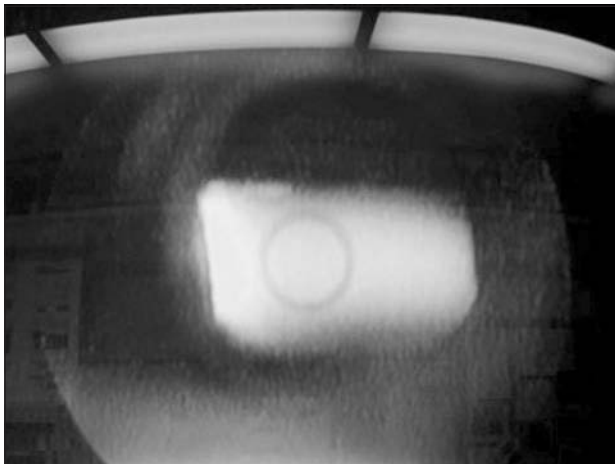
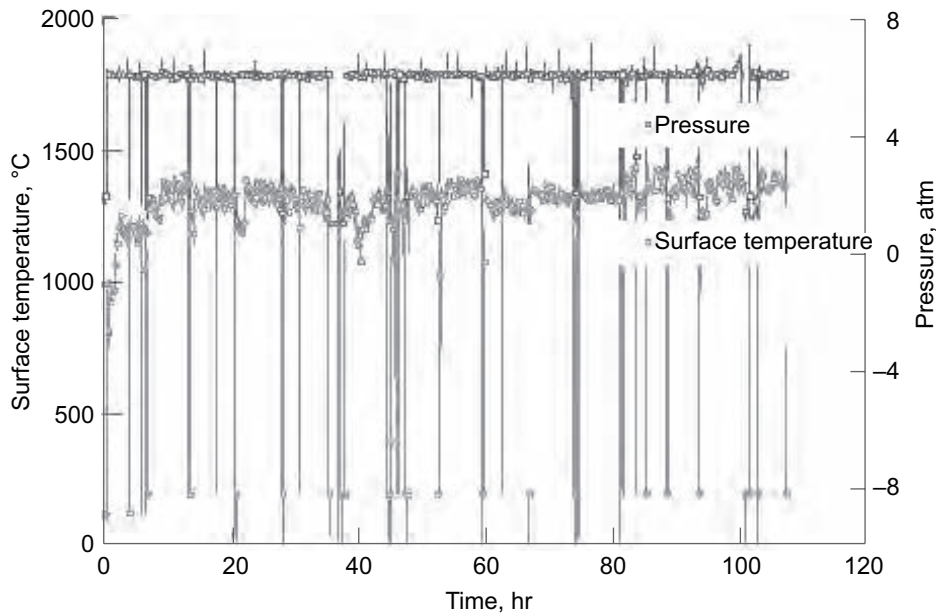
The graph shows the water vapor stability results of the $\text{HfO}_2\text{-Al}_2\text{O}_3\text{-RE}$ silicate composite coatings in the high-pressure burner rig simulated 6-atm combustion gas environments, as measured by the specific weight loss at temperatures up to 2740 °F (1504 °C). In comparison to other selected ceramic coatings and the substrate materials (in particular, Si_3N_4 AS800 and SN282), the nanocomposite coatings were among those with the best combustion water-vapor recession resistance at high temperature, indicating the excellent combustion environment stability. In addition, the nanocomposite coating structures are expected to improve the coating mechanical properties, especially for the thin coating configuration required by highly loaded turbine airfoil applications.



High-temperature stability of ceramic coating and component substrate materials determined by the high-pressure burner rig. The nanocomposite coating showed excellent combustion gas environment stability.

The coating stability and durability validations also were conducted on three coated silicon-based ceramic vanes in the high-pressure burner rig at 2500 °F (1371 °C) for 100 hr, also in 6 atm. As shown in the figure on the next page, the maximum temperatures were approximately 2541 °F (1394 °C) on the coated vane leading edges of the components, as predicted by finite element modeling based on the temperature measurements in the vane midsection.

In summary, multicomponent $\text{HfO}_2\text{-RE}$ aluminosilicate nanocomposite coatings were synthesized, and the coating cyclic durability and combustion gas water vapor stability were demonstrated in simulated engine environments. Further coating system development is planned for improving the coating and component system durability under simulated engine environment and stress conditions.



Top: Temperature profile of the coated ceramic vane testing in the high-pressure burner rig for the coating system validation. Bottom left: A coated ceramic vane under testing in the high-pressure burner rig. The circle in the picture shows the pyrometer temperature measurement location. Bottom right: Modeled temperature distribution: maximum temperature 1394 °C (2541 °F). This figure is shown in color in the online version of this article, (<http://www.grc.nasa.gov/WWW/RT/2007/Str-Mat/12-RXD-zhu.html>).

References

1. Zhu, Dongming; and Miller, Robert A.: Multifunctionally Graded Environmental Barrier Coatings for Si-Based Ceramic Components. U.S. Patent Application 11/510,573, Aug. 28, 2006.
2. Zhu, Dongming; Fox, Dennis S.; and Pastel, Robert T.: High Pressure Burner Rig Testing of Advanced Environmental Barrier Coatings for Si₃N₄ Turbine Components. The 31st International Cocoa Beach Conference & Exposition on Advanced Ceramics & Composites, Daytona Beach, FL, 2007.

Find out more about the research of Glenn’s Durability and Protective Coatings Branch:

<http://www.grc.nasa.gov/WWW/EDB/>

Glenn Contact:

Dr. Dongming Zhu, 216-433-5422,
Dongming.Zhu@nasa.gov

Authors:

Dr. Dongming Zhu, Robert T. Pastel,
Dennis S. Fox, Dr. Louis J. Ghosn,
Dr. Robert A. Miller, and Dr. James L. Smialek

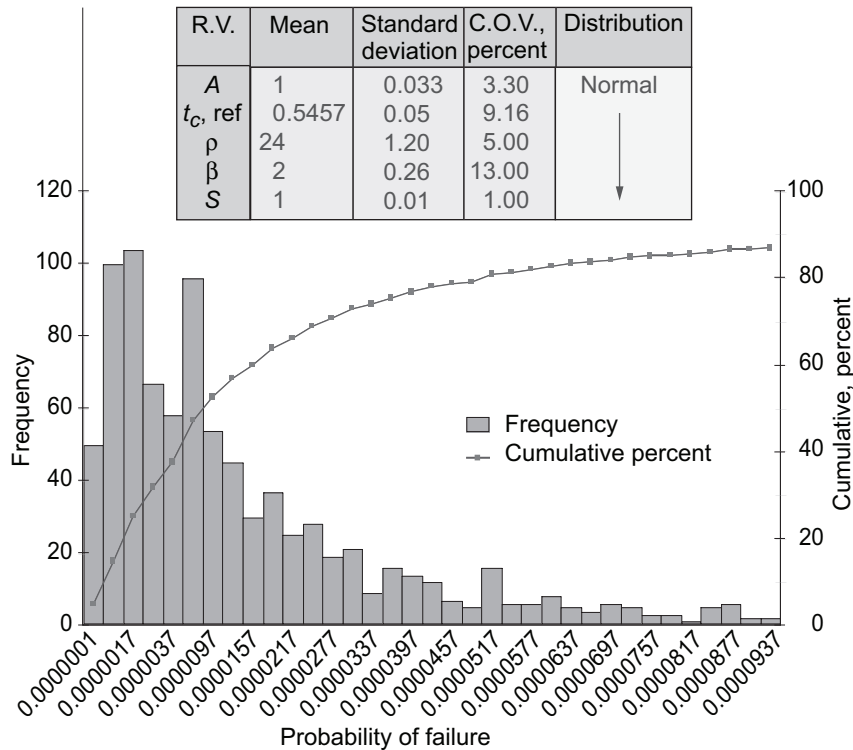
Headquarters Program Office:

Aeronautics Research Mission Directorate

Programs/Projects:

Supersonics Project

Stress Rupture Life Models and Reliability Measures Established for Composite Overwrapped Pressure Vessels



Probability-of-failure histogram constructed from 1000 Monte Carlo simulations for a typical composite overwrapped pressure vessel using the Phoenix model of conditional probability of failure for the Kevlar overwrap. R.V., random variables; C.O.V., coefficient of variation; A, random variable to track variability in the burst strength of orbiter vessels; $t_{c, \text{ref}}$, characteristic time scale for burst strength; ρ , model parameter—power law exponent; β , model parameter—lifetime scatter factor; S, random variable to track variability in Lawrence Livermore data.

Composite overwrapped pressure vessels (COPVs) are often used for storing pressurant gases onboard spacecraft such as the *International Space Station* and orbiter. Because overwraps are subjected to sustained loads for long periods, stress rupture failure is a major concern. It is therefore important to ascertain the reliability of these vessels by analysis, since the testing of each flight design cannot be completed on a practical time scale.

The work reported here was sponsored by the NASA Engineering Safety Center (refs. 1 and 2). This article discusses how reliability measures for COPVs can be established. These are currently used as the basis for certifying the continued flight rationale for the aging COPVs on the orbiter. Reference 3 gives the complete details of the models.

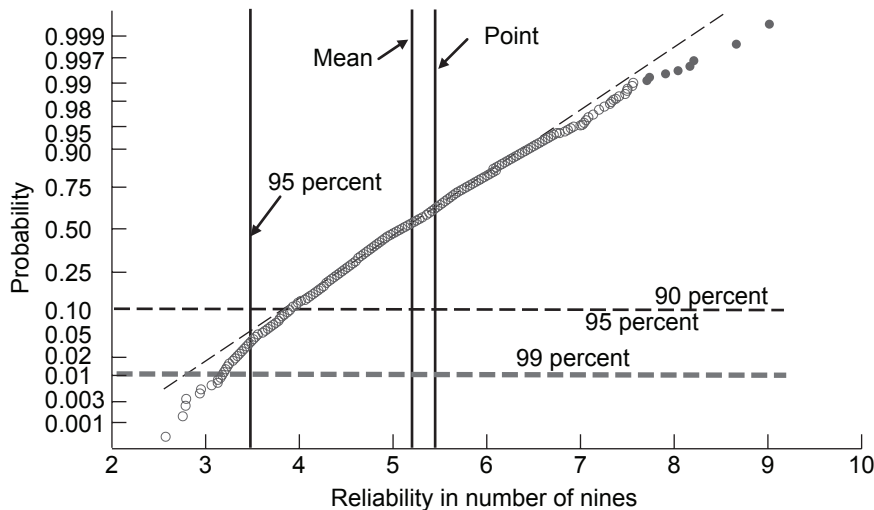
The reliability of COPVs is computed by the following equation of Phoenix (refs. 1 to 3),

$$P(t, \sigma) = 1 - \exp \left[- \left\{ \left(\frac{t}{t_{c, \text{ref}}} \right) \left(\frac{\sigma_{\text{op}}}{\sigma_{\text{burst}}} \right)^{\rho} \right\}^{\beta} \right]$$

where $P(t, \sigma)$ represents the probability of failure at time t , the quantity $(\sigma_{\text{op}}/\sigma_{\text{burst}})$ is the ratio of fiber stress at operating pressure to fiber stress at burst pressure (called the fiber stress ratio), t is time, $t_{c, \text{ref}}$ is a reference time, ρ is the power law exponent, and β is the Weibull shape parameter for lifetime.

The value for σ_{burst} is determined from the flight COPV burst test data. The parameters $t_{c, \text{ref}}$, ρ , and β are determined based on Lawrence Livermore National Laboratory's Kevlar/epoxy COPV stress rupture test data. Because of the limited amount of data, especially at lower stress ratios, all these parameters must be considered to have uncertainties with the respective probabilistic distributions associated with these parameters. One can compute reliability on the basis of nominal values for these parameters and establish the so-called point estimate for the reliability. To account for uncertainties associated with the parameters, one must adopt a probabilistic approach to compute mean values of the reliability integrating over the parameter uncertainty distributions. Similarly, one can calculate lower confidence bounds on the reliability estimate at some confidence such as 90 or 95 percent. The appropriate reliability measure to use in certification of flight worthiness of a specific COPV is often decided by the appropriate program office, such as the Orbiter Program Office.

A typical uncertainty distribution on failure probability, based on 1000 Monte Carlo simulations, is shown in the bar chart. Here the values assumed are $t_{c, \text{ref}} = 0.5457$, $\rho = 24$, and $\beta = 1.97$. The uncertainty distributions for these parameters are taken as normal for all the variables with coefficients of variation representative of the Lawrence Livermore data sample sizes. The figure on the next page shows a normal probability plot of



Normal probability plot of reliability in terms of number of nines ($= -\log_{10}$, probability of failure) for a typical COPV.

reliability where the x-axis shows reliability in “number of nines” for each Monte Carlo simulation. The mean probability of survival for this simulation is 0.999993, whereas the 95-percent confidence value is 0.9998. A point estimate based on deterministic analysis indicates that the probability of survival is 0.999996.

It is clear from these simulations that, although a high reliability (five nines) is shown based on deterministic point estimates, when all the uncertainties are considered, the reliability suffers significantly, resulting in a loss of two nines.

References

1. Orbiter Kevlar/Epoxy Composite Overwrapped Pressure Vessel for Flight Rationale, Technical Assessment Report. NASA Engineering and Safety Center Report RP-07-34, version 1.0, Apr. 12, 2007. Available from the NASA Engineering and Safety Center.

2. Shelf Life Phenomenon and Stress Rupture Life of Carbon/Epoxy Composite Overwrapped Pressure Vessels (COPVs). NASA Engineering and Safety Center Report RP-06-83, version 2.0, Sept. 14, 2006. Available from the NASA Engineering and Safety Center.

3. Murthy, Pappu L.N., et al.: Stress Rupture Life Reliability Measures for Composite Overwrapped Pressure Vessels. NASA/TM-2007-214848, 2007. <http://gltrs.grc.nasa.gov>

Glenn Contacts:

Dr. Pappu L.N. Murthy, 216-433-3332, Pappu.L.Murthy@nasa.gov

Dr. John C. Thesken, 216-433-3012, John.C.Thesken@nasa.gov

Cornell University Contact:

Prof. S. Leigh Phoenix, 607-255-8818, slpb@cornell.edu

Jet Propulsion Laboratory (JPL) Contact:

Dr. Lorie Grimes-Ledesma, 818-393-3592, Lorie.R.Grimes-Ledesma@jpl.nasa.gov

Authors:

Dr. Pappu L.N. Murthy, Dr. John C. Thesken, Prof. S. Leigh Phoenix, and Dr. Lorie Grimes-Ledesma

Headquarters Program Office:

NASA Engineering Safety Center

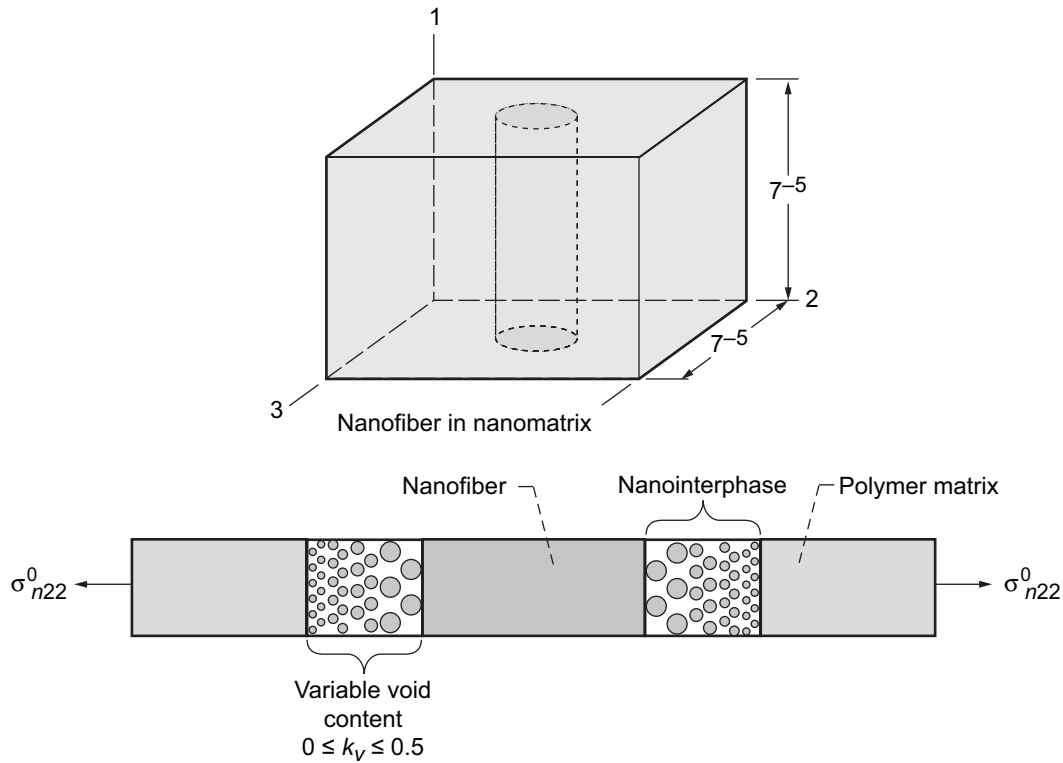
Programs/Projects:

Orbiter Program Office

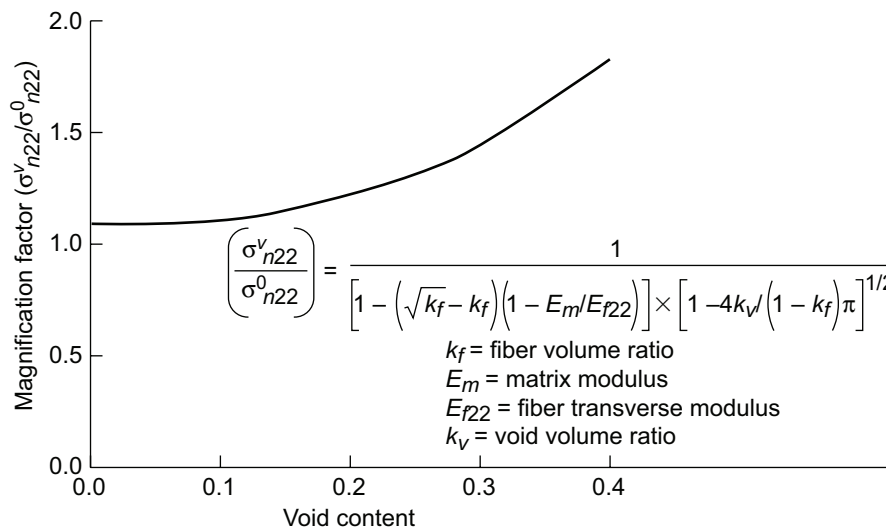
Probabilistic Simulation for Nanocomposite Characterization Developed and Included in the Computer Code ICAN/JAVA

A unique mechanistic method has been developed at the NASA Glenn Research Center to probabilistically simulate five uniaxial strengths and the six moduli of a mono-nanofiber uniaxial composite. A nanocomposite property simulation cannot produce fiber alignment with uniform dispersion. The fibers are aligned only for predicting “point” through-the-thickness properties. The fuzziness of the nanofibers can be simulated by estimating the angle of single fibers through the thickness of a nanopoly, which is shown schematically in the diagram on the next page. The simulation requires 18 constituent properties for the fiber and 12 for the matrix, the fabrication processes, and the loading conditions.

This paragraph describes the interphase and how it is modeled. The diagram shows a vertical section (upper part of the diagram) with a unit thickness equal to that of the nanocomposite and containing a single fiber. As seen in the slice (lower part of the diagram), the fiber interphase is represented by a series of progressively larger volume voids starting with the smallest near the matrix



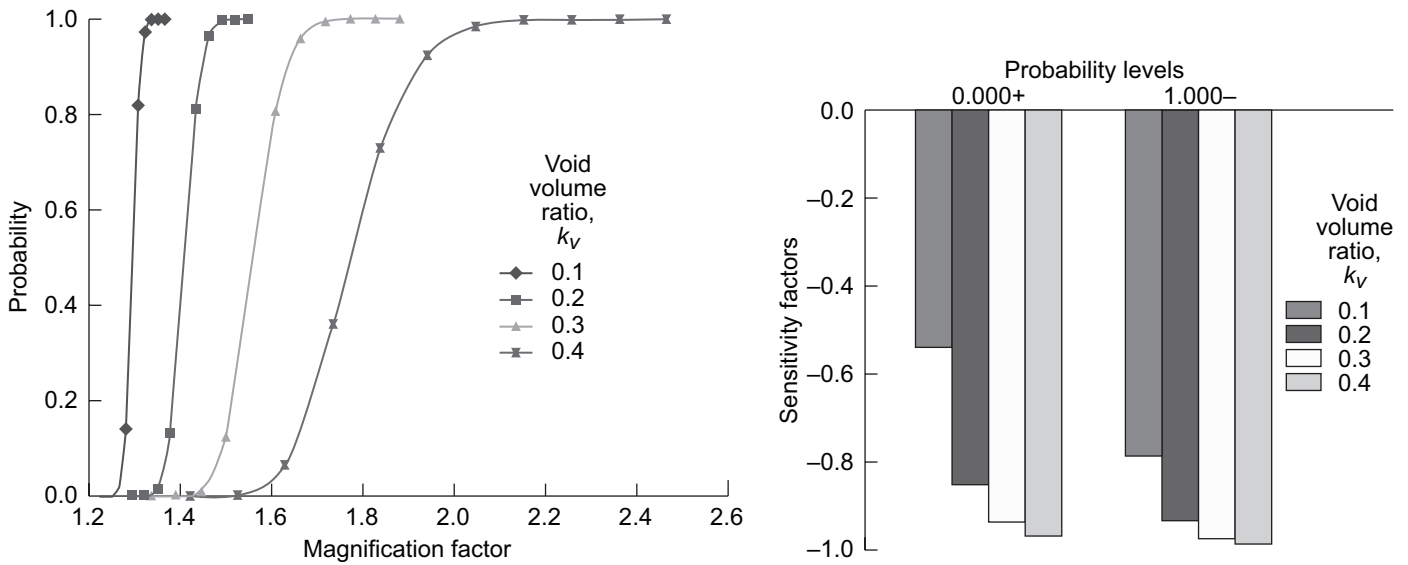
Vertical section of a composite nanocell through the nanofiber center. Dimensions are given in nano-inches.



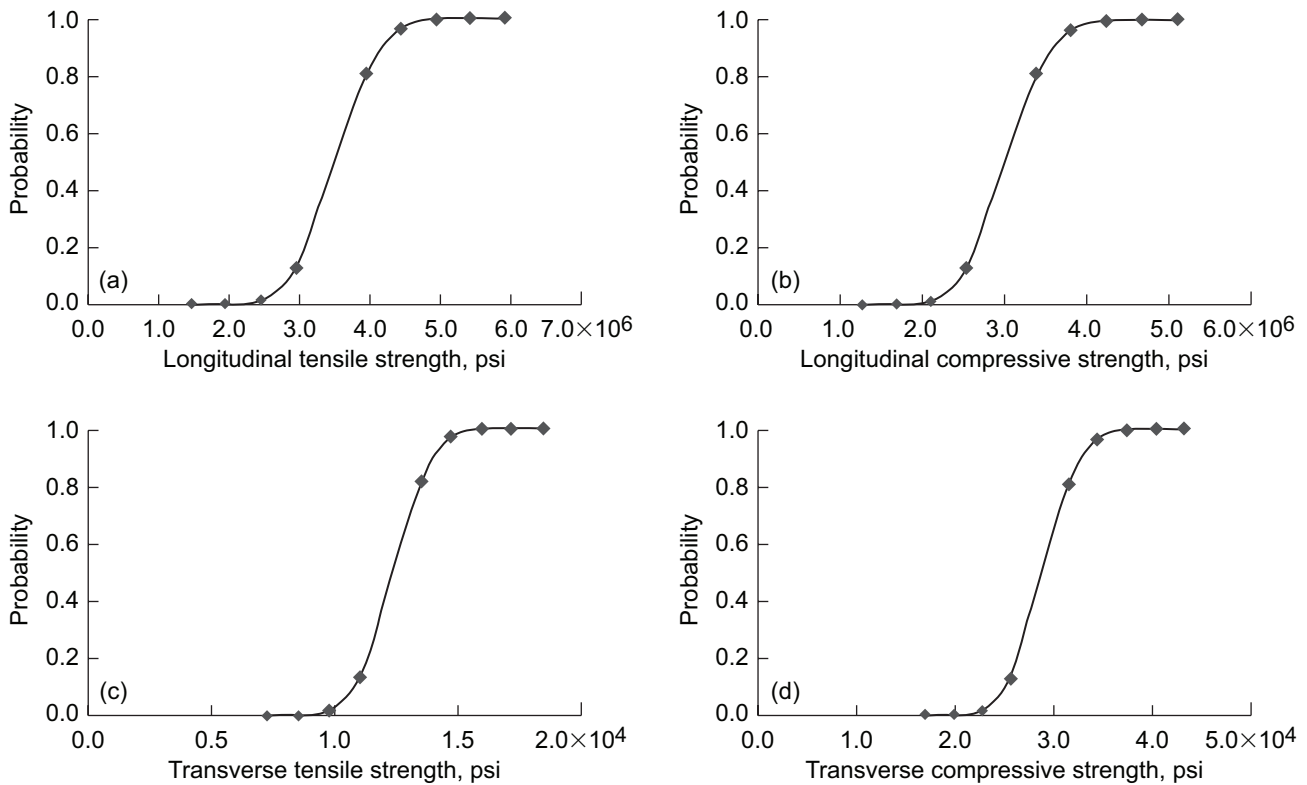
Nanocomposite magnification factor; σ_{n22}^v indicates tensile stress in the presence of voids; σ_{n22}^0 indicates tensile stress with no voids.

interface and ending with the largest in the fiber interface. The stress in the matrix will be magnified because of the voids. This is shown in this graph for a nanocomposite with a 0.05 fiber volume ratio and a void volume ratio that varies from 0.05 to 0.4. Note that, in the lower part of the diagram, the matrix is continuous even though it is filled with progressively larger voids; otherwise, the stresses would not be continuous in the matrix. To fill up a conventional ply with a thickness of 0.005 in. and a width of 1 in., one would need about 1×10^6 nanofibers, a very

large number indeed. The magnification factor of the effect of the voids in the interphase is shown in the graph on the preceding page. This factor increases from about 1.1 to about 2. This simulation shows that the maximum void effect will be nearest to the fiber interface.



Left: Probabilistic magnification factor of voids in the interphase. Right: Effect of void sensitivities on the interphase magnification factor.



Probabilistically plotted nano-uniaxial strength.

The probabilistic void magnification factor is shown in the top left graph. It can be seen that the larger the void content, the greater the deviation. The leftmost curve represents the data closest to the matrix interphase interface, and the rightmost curve represents the data closest to the fiber interphase interface. The respective scatter varies from about 0.1 for the curve closest to the matrix to about 1 for the curve closest to the fiber. The corresponding

sensitivities are shown in the bar chart, which shows that the void sensitivities on the magnification factor are large. The probabilistic void effects on the uniaxial strengths are plotted in the bottom figure. The various parts in the figure show the

spread in the longitudinal tensile strength, longitudinal compressive strength, transverse tensile strength, and transverse compressive strength. The distribution for the two longitudinal strengths is relatively large, varying about 500 ksi (from 150 to 650 ksi) for tensile strength and about 360 ksi (from 140 to 500 ksi) for compressive strength.

This unique probabilistic theory for predicting the properties of nanocomposites is based on composite micromechanics with progressive substructuring down to a nanoscale slice of a nanofiber, where all the governing equations are formulated. The equations and theoretical development have been programmed into the computer code Integrated Composite Analyzer Recoded in Java (ICAN/JAVA). The characterization included two fabrication parameters, five nano-uniaxial strengths, and all the constitutive nanocomposite properties.

Glenn Contact:

Christos C. Chamis, 216-433-3252,
Christos.C.Chamis@nasa.gov

Authors:

Dr. Christos C. Chamis and
Rula M. Coroneos

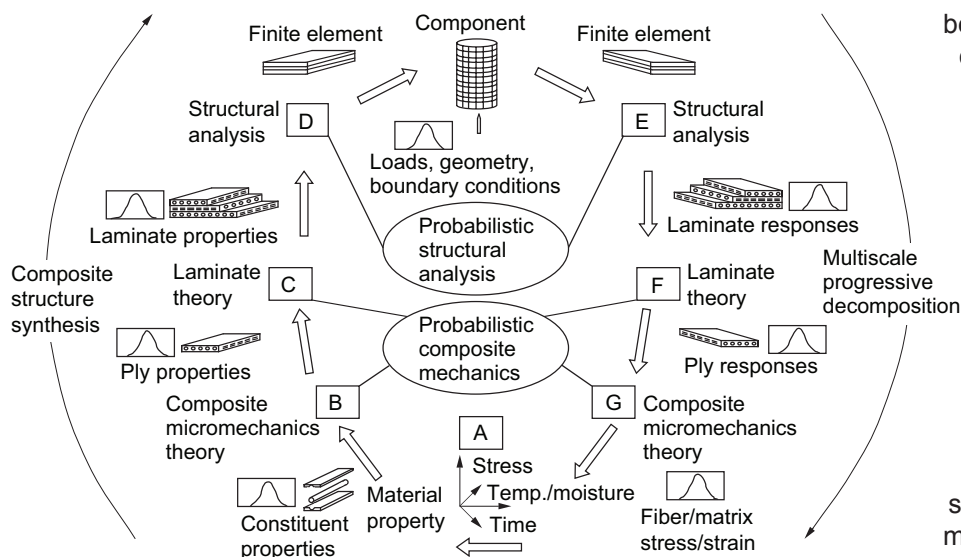
Headquarters Program Office:

Aeronautics Research Mission Directorate

Programs/Projects:

Glenn Technology Development and Tools

Formal Methodology Developed for Probabilistically Evaluating the Design of Composite Structures

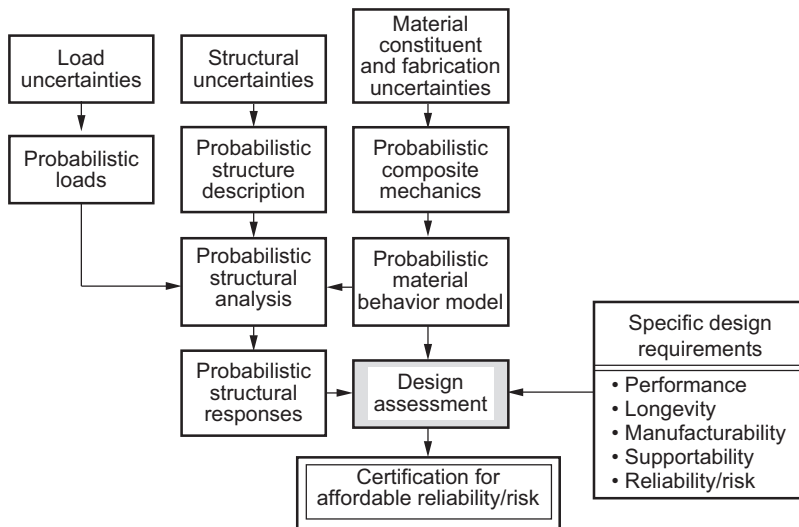


Concept for the probabilistic assessment of composite structures.

Composite materials are widely used in modern structures for high performance and reliability. However, because these structures usually operate in hostile and random service environments, it is difficult to predict their structural performance. In addition, experiments show that the composite structural

behavior exhibits wide scatter because of inherent uncertainties in the design variables. The design variables, known as primitive variables, include the fiber and matrix material properties at the constituent level, fiber and void volume ratios, ply misalignment, ply thickness, the fabrication process, the random structure size, boundary conditions, loadings, and the environment.

The scatter (results between the lowest and highest values) in structural behavior cannot be computationally simulated by traditional deterministic methods, which use a safety factor to account for uncertain (scattered) structural behavior. Thus, these methods cannot determine the structural reliability of a composite structure. A probabilistic design methodology is needed to do that accurately.



Probabilistic design assessment of composite structures.

MATERIAL PROPERTIES AT THE CONSTITUENT LEVEL
FOR SKIN AND STRINGERS

[Assumed uncertainty scatter, ± 5 percent from mean.]

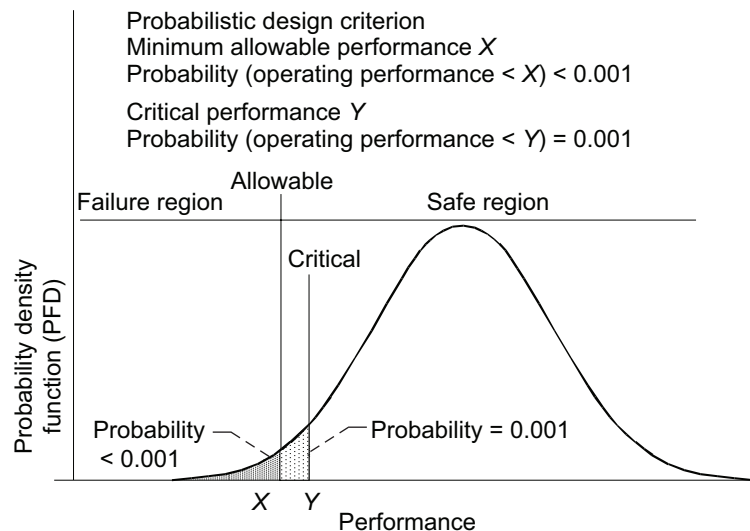
Property		Assumed distribution type	Mean ^a
Definition	Symbol, units of measure		
Fiber properties			
Moduli, normal	E_{f1} , Mpsi	Normal	31.0
	E_{f2} , Mpsi	Normal	2.0
Moduli, shear	G_{f1} , Mpsi	Normal	2.0
	G_{f2} , Mpsi	Normal	1.0
Poisson's ratio	ν_{f12}	Normal	0.2
	ν_{f23}	Normal	0.25
Coefficients of thermal expansion	α_{f1} , ppm/ $^{\circ}$ F	Normal	-0.55
	α_{f2} , ppm/ $^{\circ}$ F	Normal	5.6
Density	ρ_f , lb/in. ³	Normal	0.063
Number of fibers	N_f	Constant	10 000
Fiber diameter	d_f , in.	Normal	0.0003
Heat capacity	C_f , Btu/in. $^{\circ}$ F	Normal	0.17
Heat conductivities	K_{f1} , Btu-in./hr in. ² - $^{\circ}$ F	Normal	580
	K_{f2} , Btu-in./hr in. ² - $^{\circ}$ F	Normal	58
	K_{f3} , Btu-in./hr in. ² - $^{\circ}$ F	Normal	58
Fiber tensile stress	S_{fT} , ksi	Weibull	400
Fiber compressive stress	S_{fC} , ksi	Weibull	400
Matrix properties			
Modulus, normal	E_m , Mpsi	Normal	0.5
Modulus, shear	G_m , Mpsi	Normal	0.185
Poisson's ratio	ν_m	Normal	0.35
Thermal expansion coefficient	α_m , ppm/ $^{\circ}$ F	Normal	42.8
Density	ρ_m , lb/in. ³	Normal	0.0443
Heat capacity	C_m , Btu/in. $^{\circ}$ F	Normal	0.25
Heat conductivity	K_m , Btu-in./hr in. ² - $^{\circ}$ F	Normal	1.25
Tensile strength	S_{mT} , ksi	Weibull	15
Compressive strength	S_{mC} , ksi	Weibull	35
Shear strength	S_{mS} , ksi	Weibull	13
Moisture expansion	β_m , (in./in.)/1% moisture	Normal	0.004
Moisture diffusivity	D_m , in. ² /sec	Normal	0.002

^aTypical values for graphite-fiber/epoxy-matrix composites at 0.6 fiber volume ratio.

The NASA Glenn Research Center has developed a formal methodology to efficiently and accurately quantify the scatter in the composite structural response and to evaluate composite structural design, while accounting for the uncertainties at all composite scale levels (constituent, ply, laminate, and structure), as in the diagram on the preceding page. This methodology, which integrates microcomposite and macrocomposite mechanics and laminate theories, finite element methods, and probability algorithms, was implemented through the Integrated Probabilistic Assessment of Composite Structures (IPACS) computer code (see the flow diagram to the left), which in essence describes a multifunctional, multiscale design.

IPACS is used to evaluate composite structures probabilistically for all types of structural performance factors, such as instability, clearance, damage initiation, delamination, microbuckling, fiber crushing, and resonance damage (multiscale). Since IPACS uses a special probability algorithm—the fast probability integrator, instead of the conventional Monte Carlo simulation—an enormous amount of computational time can be saved (multifunctional). Therefore, a probabilistic composite structural analysis, which cannot be done traditionally, becomes desirable especially for large structures with many uncertain variables. The typical case analyzed herein demonstrates IPACS for the probabilistic evaluation of composite structures and illustrates the formal multiscale, multifunctional design evaluation methodology.

In the structural design of a composite, uncertainties can originate at different scale levels. At the constituent level, the material properties for the fiber and matrix are the major sources of uncertainties. Typical values are listed in the table. At all stages of the fabrication process, the fabrication variables—such as fiber volume ratio, void volume ratio,



Safe and failure regions in a probability space.

ply misalignment, and ply thickness—show considerable scatter. At the structure level, variation of the geometry during the assembly stage, uncertain boundary conditions, and random thermal-mechanical loads contribute significantly to the scatter in the composite structural response.

A typical design criterion can be stated as follows: “The probability of a failure event should be less than an acceptable value, say 10^{-3} .” A failure event occurs when the structural response is greater than the allowable response. This probability is defined as the failure probability. The allowable response divides the possible response domain into safe and failure regions as shown in the preceding graph. The predicted failure probability is the area under the probability density function in the failure region. The critical response (see the graph) is determined by IPACS such that the probability of a response exceeding this critical value is in the safe region. When the critical response falls within the safe region, the design is acceptable. When the critical response falls within the failure region, the design is unacceptable, and a redesign is needed. Sample probabilistic design criteria for the various failure modes follow:

- (1) Instability—The probability that the buckling load is smaller than the design load should be less than 10^{-3} .
- (2) Clearance—The probability that the nodal displacement is greater than the allowable tolerance should be less than 10^{-3} .
- (3) Resonance avoidance—The probability that the natural frequency is greater than its upper bound should be less than 10^{-3} .
- (4) Delamination—The probability of delamination should be less than 10^{-3} .

Bibliography

Chamis, Christos, C.: Probabilistic Design of Composite Structures. NASA/TM—2006-214660, 2006. <http://gltrs.grc.nasa.gov>

Glenn Contact:

Dr. Christos C. Chamis, 216-433-3252, Christos.C.Chamis@nasa.gov

Author:

Dr. Christos C. Chamis

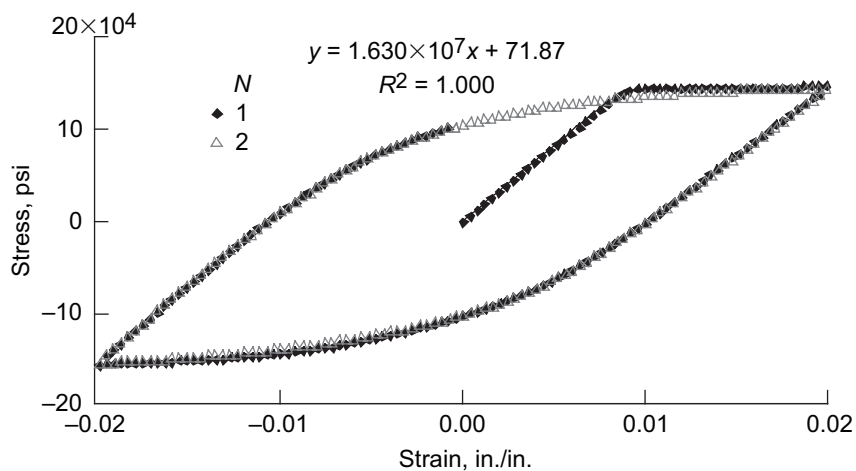
Headquarters Program Office:

Aeronautics Research Mission Directorate

Programs/Projects:

Glenn's Technology Development and Tools

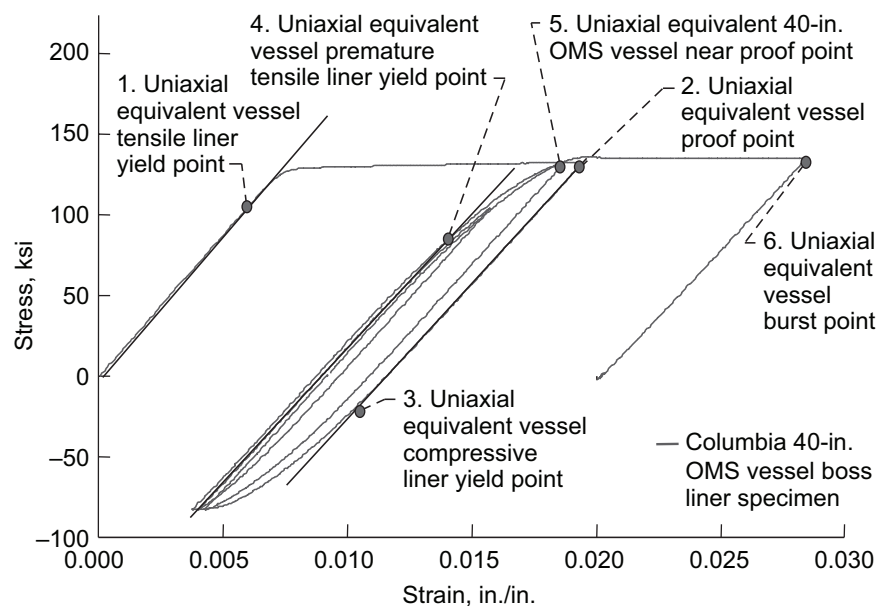
Bauschinger Effect on Mechanical Response of Composite Overwrapped Pressure Vessels Investigated



Fully reversed stress-strain response of Ti-6-4 mill-annealed from an extruded bar, demonstrating the Bauschinger effect: cycles 1 and 2 (Bradley A. Lerch, private communication).

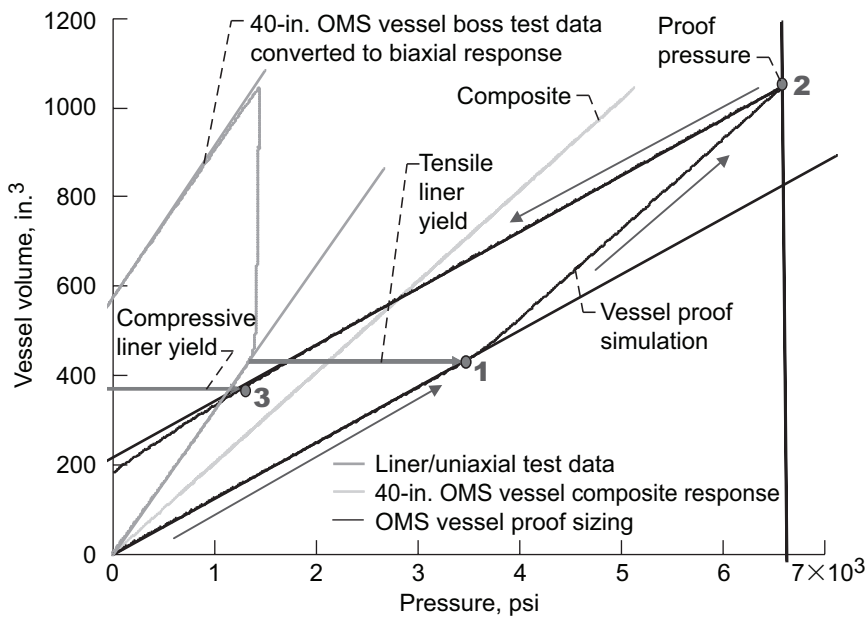
Predicting the mechanical response of the composite overwrapped pressure vessels for the space shuttle requires an accurate constitutive representation of the annealed Ti-6-4 alloy liner materials. Early structural analyses have assumed an elastic-perfectly-plastic response, which does not capture the Bauschinger stress-strain response that occurs during load reversals that exceed yield stress. This was demonstrated in load-reversal studies conducted on specimens excised from plaques cut from the boss region of the Orbital Maneuvering System (OMS) 40-in.-diameter spherical vessel and milled flat to meet ASTM requirements (ref. 1). Except for possible forging-induced variations, this material was deemed to closely resemble the state of the membrane liner material prior to autofrettage and subsequent operation loads.

The Bauschinger effect is observed in annealed Ti 6-4 materials as evidenced by cyclic stress-strain curves similar to those found in the open literature (see the top graph) and the present testing of uniaxial specimens harvested from the Columbia OMS vessel boss material. The uniaxial tests performed on the boss material were designed to closely mimic the vessel load reversals induced by autofrettage (proof sizing), a leak test, and recent vessel tests made by the White Sands Test Facility to near proof and burst (see the bottom graph). The uniaxial specimen was subjected to plastic work equivalent to the amount of plastic work predicted to occur during the biaxial loading of the liner.

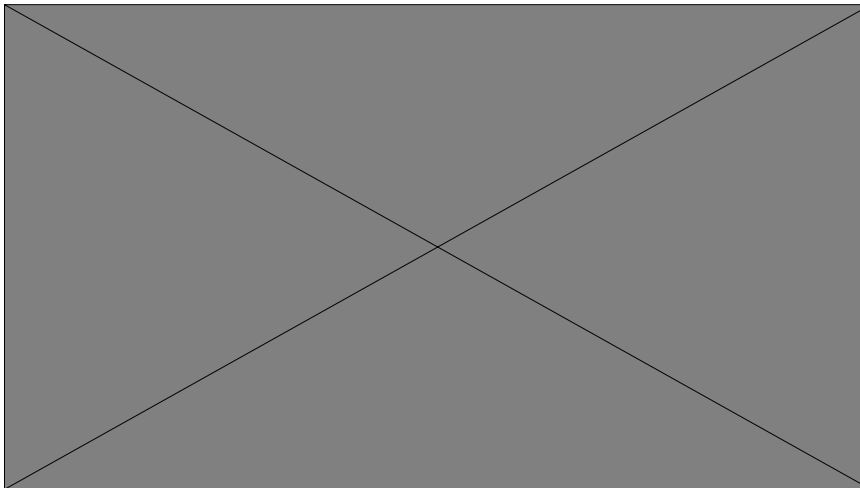


Uniaxial load cycle applied to a boss liner specimen to simulate 40-in. OMS vessel test load reversals (ref. 2).

Conversely, the acquired uniaxial test data have been transformed to estimate the biaxial liner response and have been used to simulate the volume-pressure vessel response. The top graph on the next page illustrates an application of the constitutive data to simulate



The Bauschinger effect can cause the vessel liner to yield in compression during unloading from proof sizing. Dots 1, 2, and 3 refer to the bottom graph on the preceding page—uniaxial load cycle.



Full-scale 40-in. vessel test by the NASA White Sands Test Facility. The Bauschinger effect explains premature tensile yielding of the 40-in. OMS vessel liner in the near proof test. Dot 4 refers to the bottom graph on the preceding page—uniaxial load cycle.

References

- Standard Test Methods for Tension Testing of Metallic Materials. Book of Standards, Volume 03.01, ASTM E8/E8M-8, ASTM International, West Conshohocken, PA, 2003.
- Salem, Jonathan A., et al.: Strength, Fatigue, and Fracture Toughness of Ti-6AL-4V Liner From a Composite Over-Wrapped Pressure Vessel. NASA/TM-2008-215147, 2008. <http://gltrs.grc.nasa.gov>

Glenn Contacts:

John C. Thesken, 216-433-3012,
John.C.Thesken@nasa.gov

Jon Salem, 216-433-3313,
Jonathan.A.Salem@nasa.gov

Brad Lerch, 216-433-5522,
Bradley.A.Lerch@nasa.gov

Jim Sutter, 216-433-3226,
James.K.Sutter@nasa.gov

NASA Kennedy Contact:

Richard W. Russell, 321-861-8618,
Richard.W.Russell@nasa.gov

Authors:

Dr. John C. Thesken,
Dr. Jonathan A. Salem,
Dr. Bradley A. Lerch, Dr. James K. Sutter,
and Richard W. Russell

Headquarters Program Office:

Shuttle Program Office

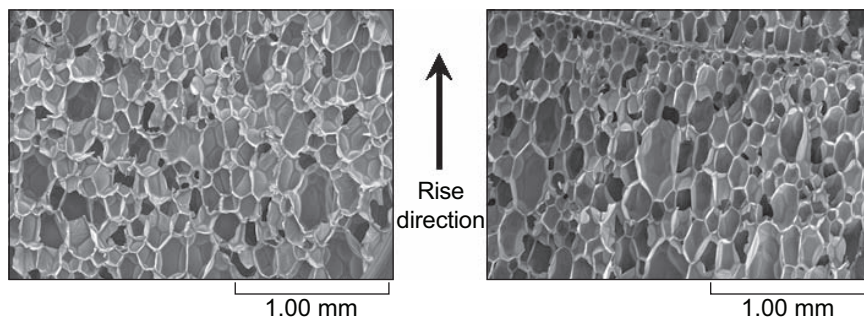
Programs/Projects:

Orbiter Project Office

autofrettage, a leak test, and near-proof-loading cycles. The volume-pressure simulation indicates that the liner becomes nonlinear and yields during unloading from the autofrettage pressure. The final graph, from data measured during subsequent loadings, shows that the characteristics of the near-proof simulation are similar to the actual measured response of a 40-in. OMS vessel and predicts liner yielding at less than the leak test pressure of 5400 psi. The Bauschinger effect offers an explanation for the early onset of liner yielding observed in the near-proof test of the 40-in. OMS vessel.

Micromechanics Model Developed for External Tank Spray-On Foam Insulation

The catastrophic loss of the Space Shuttle Columbia has spawned numerous engineering and scientific studies focused on improving the engineering infrastructure for the spray-on foam insulation of the space shuttle's external tank. Among these many studies are efforts to improve the ability to quantify the stress and strain states in the foam applications during the space shuttle's ascent to space in order to obtain a better understanding of the mechanisms that result in foam shedding and debris liberation.



Space shuttle foams. Left: BX-265. Right: NCFI24-124.

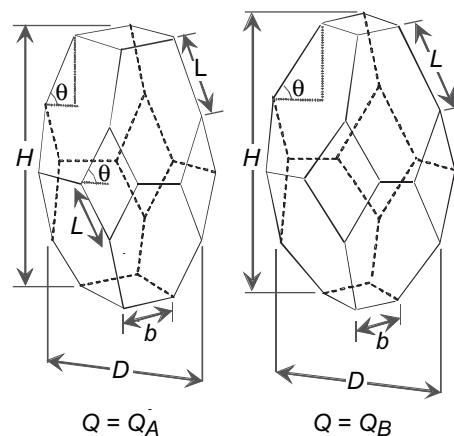
Because of the foaming and rising process, the foam microstructure is elongated in the rise direction (see the photomicrographs) and, as a result, the foam is stronger and stiffer in this direction. The stiffness ratio (which is the ratio of the rise direction modulus to the normal-to-rise direction modulus, as well as the ratio of the strengths) depends strongly on the amount of elongation of the microstructure and the shape of the representative repeating unit cell.

Researchers in the Mechanics and Lifting Branch of NASA Glenn Research Center's Structures and Materials Division have developed a micromechanics model for foams using an elongated tetrakaidecahedron (Kelvin model) as the repeating unit cell (see the sketches and ref. 1). Since the cell faces are very thin relative to the cell edges, the model neglects the contribution of the cell faces and it lumps all the solid matter into the edges. The cell edges are assumed to possess axial, bending, and torsional rigidity. The micromechanics model yields algebraic expressions for the foam elastic constants and strength in the principal material directions in terms of the microstructural dimensions H , D , L , b , and θ (defined in the figure on the right); the edge cross-section properties; and the strength and stiffness of the solid material.

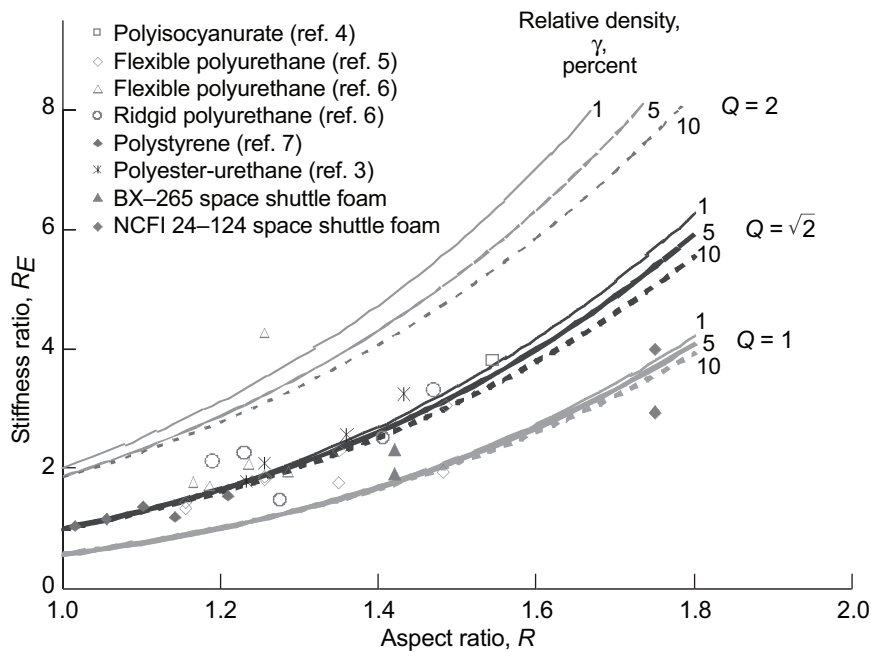
The size and shape of an elongated tetrakaidecahedron is uniquely defined by specifying the value of three of the microstructural dimensions, since the dimensions are related by $H = 4L \sin \theta$ and $D = 2L \cos \theta + \sqrt{2}b$. The shape is defined by the aspect ratio, $R = H/D$, and the parameter $Q = b/(L \cos \theta)$. The effect of the aspect ratio on the shape is fairly obvious. The effect of the value of Q on the unit cell shape is illustrated in the sketches, where the two tetrakaidecahedrons are drawn to have the same aspect ratio, but their Q values are such that $Q_A > Q_B$. Our micromechanics model was developed using an elongated Kelvin model with the most general geometric description, one that

requires specifying the values of three of the microstructural dimensions. Previous models were developed that required the values of only two dimensions (refs. 2 and 3) by placing the undue restriction on the foam microstructure that $Q = \sqrt{2}$. Thus, our micromechanics model is applicable to a wider range of foams.

In the graph on the next page, the stiffness ratio is plotted versus the cell aspect ratio for various values of Q . The experimental results reported by a number of previous researchers are also included. Most of the foams fall along the curves where $Q = \sqrt{2}$. However, some of the foams deviate considerably from these curves, most notably the shuttle foams BX-265 and NCFI24-124. Previously, these deviations were explained as experimental scatter. We may now explain this behavior as being attributed to a foam microstructure where $Q \neq \sqrt{2}$.



Two elongated tetrakaidecahedron (Kelvin) unit cells illustrating the key microstructural dimensions. Both unit cells have the same cell dimensions, H and D , but different values of Q ($Q_A > Q_B$).



Stiffness ratio versus cell aspect ratio for various Q values and relative densities. This figure is shown in color in the online version of this article (<http://www.grc.nasa.gov/WWW/RT/2007/Str-Mat/17-RXL-sullivan.html>).

5. Hilyard, N.C. (ed.): *Mechanics of Cellular Plastics*. Appl. Sci., London, 1982.
6. Huber, A.T.; and Gibson, L.J.: *Anisotropy of Foams*. J. Mater. Sci., vol. 23, no. 8, 1988, pp. 3031–3040.
7. Mehta, B.S.; and Colombo, E.A.: *Mechanical Properties of Foamed Thermoplastics*. J. Cell. Plast., vol. 12, no. 1, 1976, pp. 59–66.

Glenn Contacts:

Dr. Roy M. Sullivan, 216–433–3249,
Roy.M.Sullivan@nasa.gov

Dr. Bradley A. Lerch, 216–433–5522,
Bradley.A.Lerch@nasa.gov

Authors:

Dr. Roy M. Sullivan, Dr. Louis J. Ghosn,
and Dr. Bradley A. Lerch

Headquarters Program Office:

Space Shuttle Program

Programs/Projects:

External Tank Project

With the present model, the stresses in the foam cell edges, on the microscale, can be easily resolved from the global stresses in the foam insulation. This will help us to understand the mechanisms responsible for foam shedding and debris liberation during the space shuttle ascent.

References

1. Sullivan, Roy M.; Ghosn, Louis J.; and Lerch, Bradley A.: *An Elongated Tetraikadehedron Model for Open-Cell Foams*. NASA/TM—2007-214931, 2007. <http://gltrs.grc.nasa.gov>
2. Dementev, A.G.; and Tarakanov, O.G.: *Model Analysis of the Cellular Structure of Plastic Foams of the Polyurethane Type*. Mekh. Polim., no. 5, 1970, pp. 859–865.
3. Gong, L.; Kyriakides, S.; and Jang, W.-Y.: *Compressive Response of Open-Cell Foams. Part I: Morphology and Elastic Properties*. Int. J. Solids Struct., vol. 42, nos. 5–6, 2005, pp. 1355–1379.
4. Gupta, S., et al.: *Final Year Project, Cambridge University Engineering Department, Cambridge, UK, 1986*. (Obtained from Gibson, Lorna J.; and Ashby, Michael F.: *Cellular Solids: Structure and Properties*, second ed., Cambridge University Press, Cambridge, UK, 1997, fig. 6.21, p. 265.)

Structural Benchmark Testing Completed for Ares I-X Upper Stage Simulator Segment Joints



Artist's depiction of the Ares I launch vehicle moments after liftoff. Inset shows a photograph of the Pathfinder I fabrication trial, a prototype USS structural shell segment.

The NASA Glenn Research Center is developing, designing, and building an Upper Stage Simulator (USS) for the NASA Constellation Program's first test flight, the Ares I-X (see the preceding figure). The purpose of this unmanned Ascent Development Flight Test is to test the solid rocket motor First Stage, vehicle flight controllability, and environment characterization. For a description of the Ares I mission and purpose, see reference 1. Success relies on the USS to not only accurately represent the second-stage geometry and mass properties, but to also react favorably to the static and dynamic structural load environment to which it will be subjected. The importance of the latter was

reflected in the project's test and verification effort requirement to experimentally validate several key analytical structural properties through in-house subelement testing at Glenn's Structural Benchmark Test Facility.

For simple, low-cost fabrication, the USS is being fabricated from short, easily transported circular shell segments of common design (see the inset). The segments will be assembled end-to-end at the NASA Kennedy Space Center using many threaded fasteners. These connect mating internal circumferential flanges in adjacent segments and form a "segment joint." The discontinuities in the shell structure consequent to this configuration result in variable stiffness and strength throughout the stage length. This is not intrinsic to the actual second stage and has been the subject of much detailed analysis. To verify analytical values for segment joint stresses, deflections, stiffness, and strength, Glenn researchers fabricated several jointlike subelements of varying circumferential span using flight production practices. These test articles were carefully instrumented with strain gauges, load cells, and displacement transducers (see the photograph on the next page) and were placed under monotonic and cyclic tension and compression loads in a 100,000-lb-capacity biaxial load frame at the Structural Benchmark Test Facility. The measured responses of the subelements were scrutinized and compared with the predicted values; all critical structural properties were successfully verified within pre-established margins. The now-completed segment joint testing was an early success for the USS team.



Segment joint stiffness test article mounted in Glenn's Structural Benchmark Test Facility in-plane biaxial load frame gets a final checkout of instrumentation before load testing begins.

Benchmark testing was performed by the Mechanics and Life Prediction Branch of Glenn's Structures and Materials Division. The ongoing Ares I-X USS work is managed by the Launch Systems Project Office of the Space Flight Systems Directorate in support of NASA's Exploration Systems Mission Directorate, Constellation Systems Program, Ares I/Crew Launch Vehicle Project.

Reference

1. NASA FY 2008 Budget Estimates.
http://www.nasa.gov/pdf/168652main_NASA_FY08_Budget_Request.pdf

Find out more about this research:

Glenn's Launch Systems Project Office:

<http://spaceflight systems.grc.nasa.gov/LaunchSystems/>

Glenn's Space Flight Systems Directorate:

<http://spaceflight systems.grc.nasa.gov>

Glenn's Structures and Materials Division:

<http://www.grc.nasa.gov/WWW/5000/MaterialsStructures/>

Glenn's Life Prediction Branch:

<http://www.grc.nasa.gov/WWW/LPB/>

NASA Glenn Research Center:

<http://www.nasa.gov/glenn/>

Glenn Contacts:

David L. Krause, 216-433-5465,
David.L.Krause@nasa.gov

Frank J. Ritzert, 216-433-8199,
Frank.J.Ritzert@nasa.gov

William K. Thompson, 216-433-2638,
William.K.Thompson@nasa.gov

University of Toledo Contact:

Ralph J. Pawlik, 216-433-8563,
Ralph.J.Pawlik@nasa.gov

Authors:

David L. Krause, Ralph J. Pawlik,
Frank J. Ritzert, and William K. Thompson

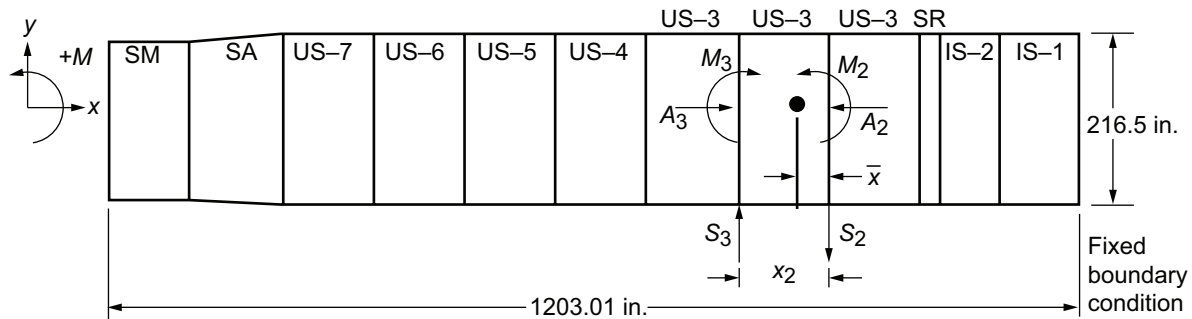
Headquarters Program Office:

Exploration Systems Mission Directorate

Programs/Projects:

Constellation Systems Program,
Ares I/Crew Launch Vehicle Project

Effects of Cracks and Residual Stresses at the Toe of the Ares I-X Upper Stage Simulator Shell-to-Flange Weld Quantified Using Probabilistic Approaches and the NASGRO Crack-Growth Code



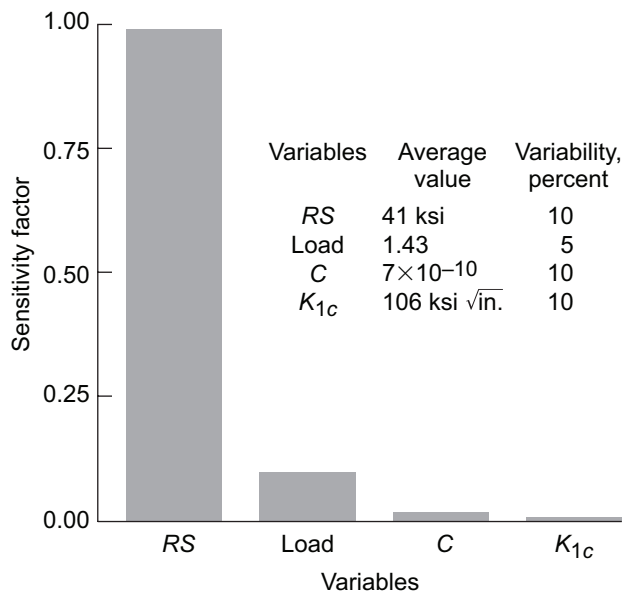
Ares I-X USS primary structural components. SM, Service Module; SA, Spacecraft Adaptor; US, Upper Stage segment; IS, Interstage segment; SR, Separation Ring; M, applied moment; A, axial force; S, shear force; X, segment length.

The primary structures of the Ares I-X Upper Stage Simulator (USS) space vehicle (see the sketch) are constructed of welded mild steel plates, which caused some concern that welding flaws could cause structural failure. It was considered critical to quantify the impact of uncertainties in residual stress, material porosity, applied loads, and material and crack-growth properties on the reliability of the welds during the Ares I-X preflight and flight. A criterion was established—an existing maximum size crack at the weld toe must be smaller than the maximum allowable flaw size—to estimate the reliability of the welds. Consequently, researchers at the NASA Glenn Research Center developed a spectrum of maximum allowable flaw sizes for different combinations of the listed variables through probabilistic crack-growth analyses using the ANSYS finite element analysis code with the NASGRO crack-growth code, in conjunction with the NESSUS probabilistic analysis code.

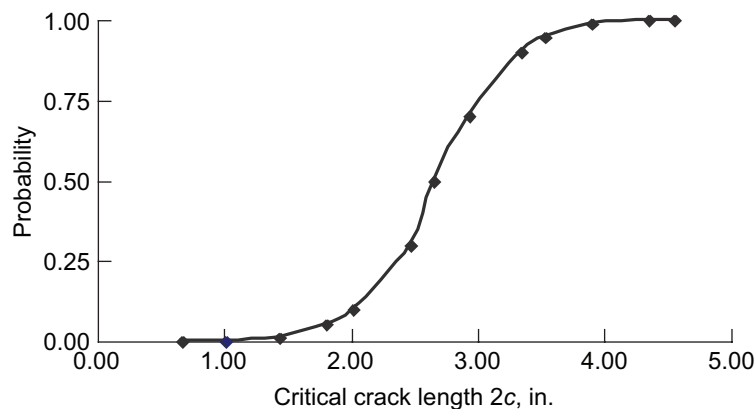
Several factors can complicate the prediction of structural reliability in the presence of welding flaws: (1) the locations, sizes, and orientations of flaws are unknown, (2) the fidelity of the crack-growth modeling is uncertain, and (3) the residual stress field produced by the welding process is not well characterized. To account for these “uncertainties in the uncertainties,” N&R Engineering conducted a series of analyses at Glenn that contained different assumptions to gain confidence in the results. The purpose was to estimate the critical flaw size—the largest allowable crack size that will permit four load or flight schedules (including handling, rollout, preflight, launch, and flight) before the crack becomes unstable (uncontrolled crack growth) or reaches the flow stress limit,¹ depending on the selected criteria. In other words, after reaching the critical crack (flaw) size, the component will be able to sustain four more load schedules before the crack either becomes unstable or the flow stress is exceeded. Four loading schedules are used instead of one to handle the uncertainties and provide a margin of operational safety.

¹“Flow stress limit” represents the average of the material’s yield strength and ultimate strength.

The global model was too coarse to accurately determine peak stress levels. Hence, a 12°-sector fine-mesh submodel was created to substantially increase fidelity in the region of the peak stress identified by the global model analysis. Initial probabilistic analyses revealed that stresses were much more sensitive to the applied load uncertainties than to uncertainties in Young’s modulus and Poisson’s ratio. Hence, subsequent analyses focused on the uncertainties in the applied loads, residual stress *RS*, fracture toughness, and crack-growth-rate constant. Later sensitivity results showed that residual stress is the dominant variable when the flow stress is not exceeded (see the bar chart on the next page) during crack propagation.



Variable sensitivities for crack size “2c”—flow stress not exceeded (probability level 0.0001). RS, residual stress; C, crack growth rate constant; K_{1c} , fracture toughness.



Probabilistic crack size “2c” results—flow stress not exceeded. Cumulative distribution function (CDF) of critical flaw length “2c” for a surface crack SC17 (RS = 41 ksi); mean, 2.56 in.; standard deviation, 0.53.

Glenn Contact:

Dr. Shantaram S. Pai, 216–433–3255,
Shantaram.S.Pai@nasa.gov

N&R Engineering Contact:

Peter A. Hoge, 440–845–7020

Authors:

Dr. Vinod K. Nagpal, Dr. Bhogilal M. Patel,
and Peter A. Hoge

Headquarters Program Office:

Exploration Systems Mission Directorate

Programs/Projects:

Ares I–X

Representative results show that the mean values of the critical flaw size were 2.56 in. long (see the line graph) along the surface and 0.416 in. deep through the 0.5-in. shell thickness for the 41-ksi RS case. Because these values are well beyond the minimum flaw detection criteria in welding inspection, these flaw sizes should be easily detectable by nondestructive evaluation or even by visual inspection. Note that these specific crack dimensions should not be used as the permissible crack sizes for welding inspection.

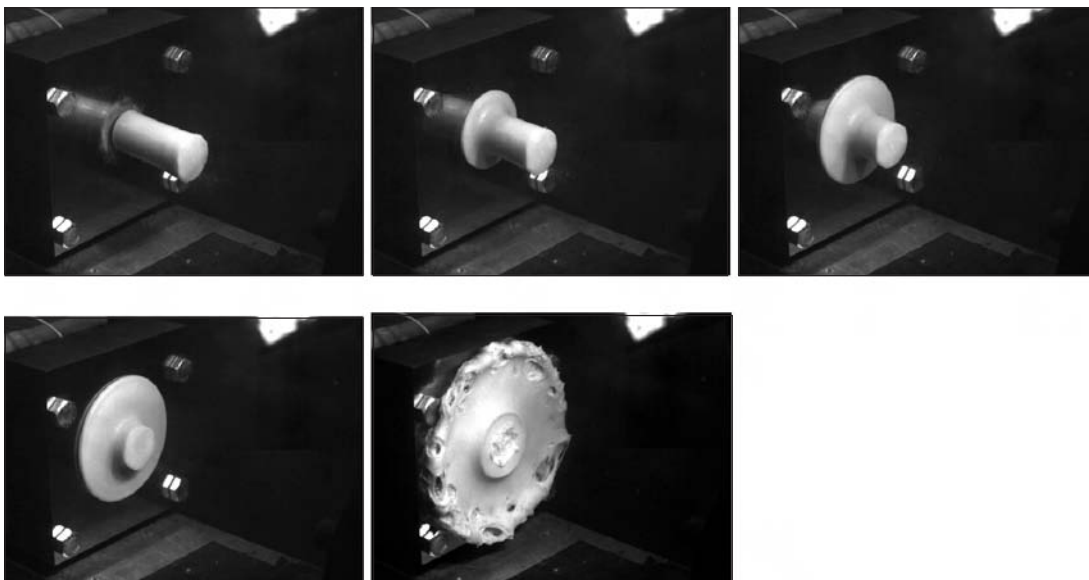
Pressure Measured in Ballistic Impact Testing of Simulated Birds

Bird strike at launch presents a potential danger to current and future space vehicles. Work is underway to study artificial bird simulators made of gelatin, phenolic microballoons, and water for use in impact testing of space structures. It has been shown, both theoretically and experimentally, that when a relatively soft, porous cylinder impacts a rigid object, the pressure at the interface consists of an initial short-duration spike, followed by a longer duration region with lower amplitude. The duration of the initial pressure response depends on both the geometry and material properties of the projectile, but it is typically measured in tens of microseconds, with a short rise time. Measuring this initial response accurately requires instrumentation with a high-frequency response and, for digital data acquisition, high sampling rates. In the present study, a series of tests was conducted to investigate this initial pressure region and whether or not commonly available instrumentation can be used to measure it.

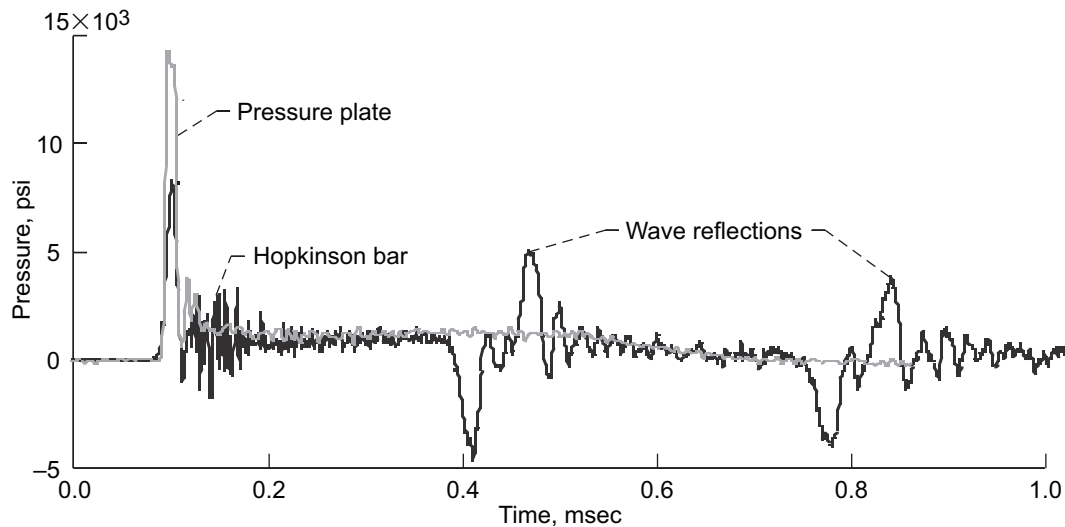
The pressure response of right circular gelatin cylinders was measured during impact tests on two instrumentation systems, a piezoelectric pressure sensor and a long bar instrumented with strain gauges, commonly known as a Hopkinson bar. The pressure sensor was flush mounted according to the manufacturer's specifications in the center of a hardened steel plate measuring 6- by 6- by 2-in. thick that was mounted on a massive support structure. The Hopkinson bar was Al 6061-T6 with a diameter of 1.25 in. and a length of 36 in. Four sets of strain gauges were mounted along the length of the bar. The projectiles were cylindrical with a nominal length of 2.4 in., a diameter of 1.25 in., and a mass of 46.6 g. Actual specific gravity of the specimens averaged 0.94. This series of photographs is from an impact test using the pressure sensor. The graph on the next page compares typical responses from the pressure sensor and the Hopkinson bar.

In all cases, the maximum pressure measured by the pressure sensor was significantly greater than that measured by the Hopkinson bar. However, in the steady flow region, both transducers showed similar results. The likely explanation for the difference in the peak pressure region is that the pressure sensor, which was located at the center of the impacting cylinder, measures a local pressure, whereas the Hopkinson bar measures an averaged strain over the whole area. As soon as impact occurs, release waves in the impacting cylinder begin to reduce the strain at the plane of impact, which reduces the average strain across the face. After the initial spike, however, the flow becomes uniform and both transducers show similar results.

For the type of projectile that is currently being considered for use as a substitute bird, the pressure sensor used in this study appears to be appropriate for measuring local pressures. The frequency response is adequate to measure the



Impact of a gelatin cylinder on a pressure sensor mounted at the center of a plate.



Pressure measurements from a 365-ft/sec test on a pressure plate and a 371-ft/sec test on a Hopkinson bar.

anticipated pressures, especially for larger projectiles, which will likely be used. On the basis of these results, future work will likely involve instrumentation systems based on a piezoelectric pressure sensor.

Glenn Contacts:

Dr. J. Michael Pereira, 216-433-6738; J.M.Pereira@nasa.gov
Duane M. Revilock, 216-433-3186, Duane.M.Revilock@nasa.gov

Authors:

Dr. J. Michael Pereira and
Duane M. Revilock

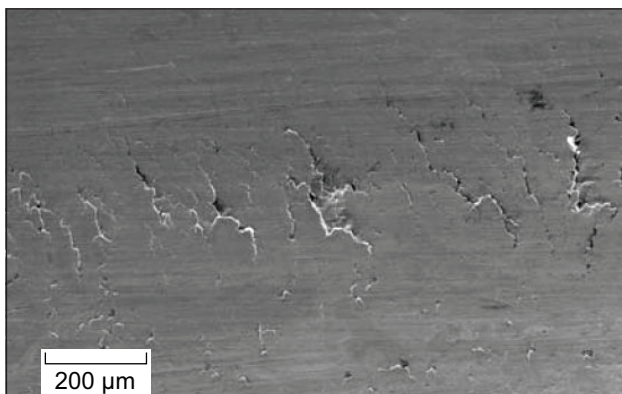
Headquarters Program Office:

Exploration Systems Mission Directorate

Programs/Projects:

Crew Exploration Vehicle

Probabilistic Analysis Conducted of Space Shuttle Body Flap Actuator Ball Bearings

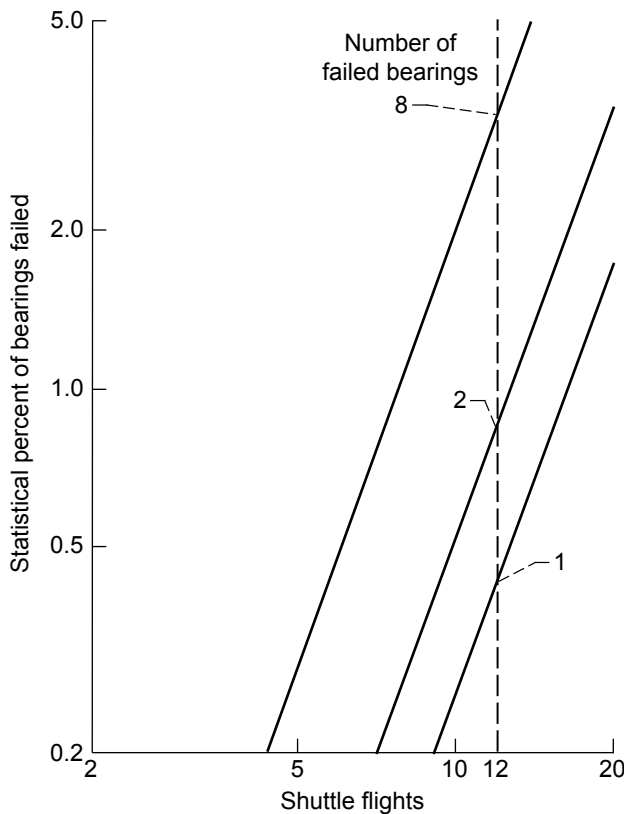


Scanning electron microscope view of wear band of shuttle body flap actuator bearing inner race after 20 flights.

A probabilistic analysis, using the two-parameter Weibull-Johnson method, was performed on experimental life test data from space shuttle actuator bearings. Experiments were performed on a test rig under simulated conditions to determine the life and failure mechanism of the grease-lubricated bearings that support the input shaft of the space shuttle body flap actuators. The failure mechanism was wear (see the photograph), which can cause loss of bearing preload. These tests established life and reliability data for both flight and ground operation of the shuttle.

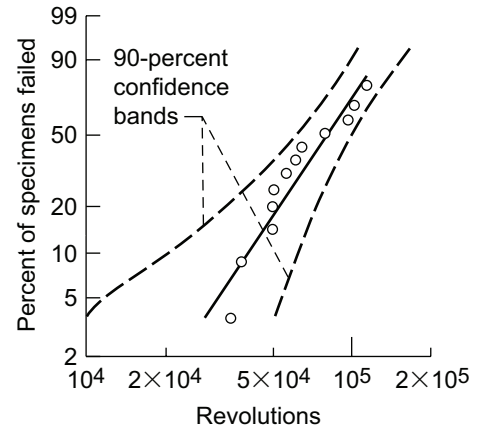
Test data were used to estimate failure rate and reliability as a function of the number of shuttle missions flown. Weibull analysis (shown in the graph on the right) was performed on the test data. This analysis established a reliability level of 96.9 percent for a life of 12 missions for the four actuators on one shuttle, each of which has a two-bearing shaft assembly.

The following graph shows the predicted failure rate for one, two, and all eight bearings on a shuttle as a function of the number of flights. A probabilistic system analysis for four shuttles, each of which has four actuators, predicts a single bearing failure in one actuator of one shuttle after 22 flights (a total of 88 flights for a four-shuttle fleet). This prediction is comparable with actual shuttle flight history in which a single actuator bearing was found to have failed by wear at 20 flights.



Estimated life and reliability of input shaft bearings as a function of shuttle flights.

After the onset of severe wear, these bearings would no longer be fit for their intended use. However, the gradual onset of this failure mode indicates that imminent seizure is unlikely. Thus, bearing failure should not cause a failure of the actuator that would endanger the space shuttle as long as a reasonable inspection schedule is followed.



Weibull plot of bearing fatigue tests at 24 °C, 16- to 24-kN load, and 50- to 80-rpm speed.

Bibliography

Oswald, Fred B., et al.: Probabilistic Analysis of Space Shuttle Body Flap Actuator Ball Bearings. NASA/TM—2008-215057, 2008. <http://gltrs.grc.nasa.gov>

Find out more about the research of Glenn’s Mechanical Component Branch:

<http://www.grc.nasa.gov/WWW/5900/5950/>

Glenn Contacts:

Fred B. Oswald, 216–433–3957, Fred.B.Oswald@nasa.gov

James J. Zakrajsek, 216–433–3968, James.J.Zakrajsek@nasa.gov

Erwin V. Zaretsky, 216–433–3241, Erwin.V.Zaretsky@nasa.gov

Authors:

Fred B. Oswald, Timothy R. Jett, Roamer E. Predmore, and Erwin V. Zaretsky

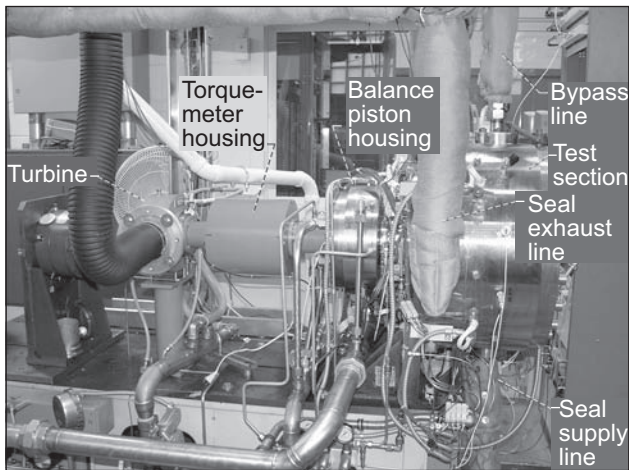
Headquarters Program Office:

Aeronautics Research Mission Directorate

Programs/Projects:

Fundamental Aeronautics Program, Subsonic Rotary Wing Project, Advanced Mechanisms and Tribology Technologies for Durable Lightweight Actuation and Mechanical Power Transmission Systems

Fatigue Crack Growth Behavior Evaluated for Grainex Mar-M 247 Used in NASA's High-Temperature, High-Speed Turbine Seal Test Rig



Glenn's High-Temperature, High-Speed Turbine Seal Test Facility.

The fatigue crack growth (FCG) behavior of Grainex Mar-M 247, a high-temperature nickel-based superalloy, was evaluated for the High-Temperature, High-Speed Turbine Seal Test Facility at the NASA Glenn Research Center (see the photograph). The facility tests current and advanced air-to-air seals, such as labyrinth, brush, and finger seals. These seals are used to control secondary airflows in the compressor and turbine sections of jet engines. The Grainex Mar-M 247 superalloy is currently used for the disk that serves as the running surface for seal tests in the facility. Because of extreme seal test conditions of temperature, pressure, and surface speeds, surface cracks may develop over time in the disk bolt holes. The current research—a collaboration of researchers from the U.S. Army Research Laboratory, Glenn, and Case Western Reserve University—resulted in a nondestructive eddy-current inspection interval to preclude catastrophic disk failure.

To simulate FCG behavior in the disk bolt holes, surface-flawed, or K_b , specimens were fabricated by Low Stress Grind, Inc., (Cincinnati, OH) from a sacrificial test disk and tested at Glenn's Fatigue and Fracture Labs at a test temperature of 650 °C. The half-disk-shaped flaws were electrodischarged machined into one side of the K_b specimen rectangular gauge section and were instrumented. Experimental FCG versus cycle data were obtained using the direct-current electrical potential difference method (ref. 1). The FCG rate was calculated per ASTM E-647. Finally, the stress intensity range was calculated using equations developed for a semielliptical surface crack by Newman and Raju (ref. 2). Data from two tests were combined after statistical tests determined similarity in their regressions. Then, the data were fitted to a Paris-type relationship:

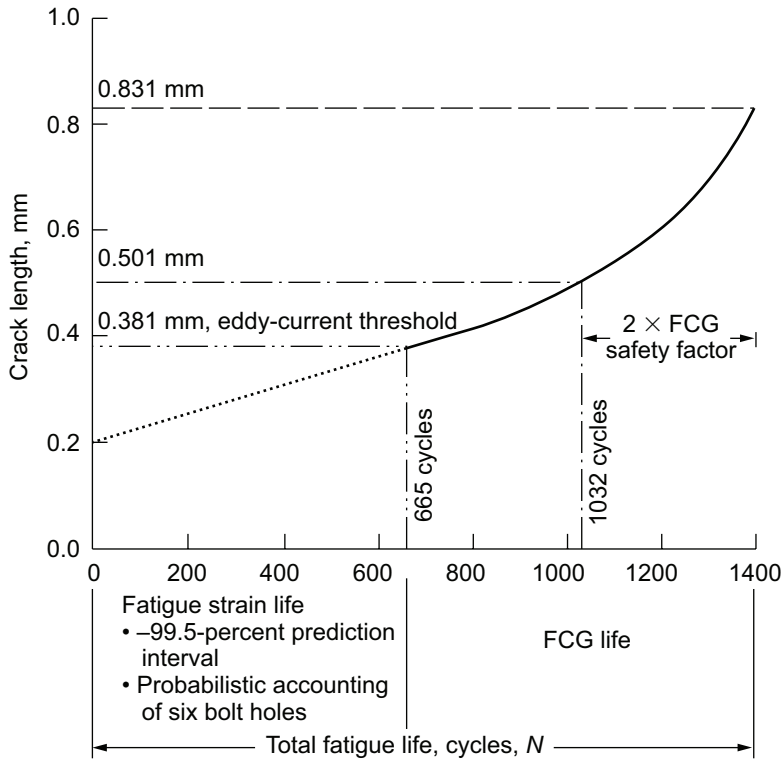
$$da/dN = C(\Delta K)^m$$

¹ K_{IC} is the critical fracture toughness (mode I) in megapascals times square root of meters.

where da/dN is the FCG rate (mm/cycle), C is the coefficient (mm/cycle)/(MPa \sqrt{m}) ^{m} , ΔK is the stress intensity range (MPa \sqrt{m}), and m is the exponent.

Small crack growth behavior was observed at low ΔK values. This may be due to the relatively large grain size (1.6 mm) of Grainex Mar-M 247. Also, calculated initial and final plastic zone sizes were found to be smaller than the material grain size. Finally, linear-elastic fracture mechanics criteria may have been exceeded because of the lack of available material for a proper K_{IC} test specimen.¹ From an engineering assessment, a safety factor of 2 was used to predict FCG life. However, the data agreed with literature in that the FCG rate increased with increasing temperature. A conservative K_{IC} range of 40 MPa \sqrt{m} was used to iteratively calculate the fatigue cycles to failure.

The FCG life of the Grainex Mar-M 247 material was found to be 367 cycles at a crack depth of 0.501 mm using a factor of 2 on life at maximum operating conditions. Combining this result with previous fatigue strain-life experimental work (ref. 3) gave a total fatigue life of 1032 cycles at a crack depth of 0.501 mm. Eddy-current inspections of the disk bolt holes are suggested starting at 665 cycles since eddy-current thresholds are currently at 0.381 mm (see the graph on the next page). Inspection intervals are recommended every 50 cycles at maximum operating conditions.



Total fatigue life of Grainex Mar-M 247 at maximum operating conditions for Glenn's turbine seal test facility.

References

1. Gangloff, R.P.: Electric Potential Monitoring of Crack Formation and Subcritical Growth From Small Defects. *Fatigue Eng. Mater. Struct.*, vol. 4, no. 1, 1981, pp. 15–33.

2. Newman, J.C., Jr.: and Raju, I.S.: Stress-Intensity Factor Equations for Cracks in Three-Dimensional Finite Bodies. *Fracture Mechanics: 14th Symposium, Volume I: Theory and Analysis*, ASTM STP-791. J.C. Lewis and G. Sines, eds., ASTM International, Philadelphia, PA, 1983, pp. 238–265.

3. Delgado, Irebert R., et al.: Strain-Life Assessment of Grainex Mar-M 247 for NASA's Turbine Seal Test Facility. *J. Eng. Gas Turbines Power*, vol. 127, no. 3, 2005, pp. 615–620.

Find out more about Glenn's turbine seal research:

<http://www.grc.nasa.gov/WWW/TurbineSeal/>

U.S. Army Research Laboratory at Glenn Contact:

Irebert Delgado, 216-433-3935, Irebert.R.Delgado@nasa.gov

Author:

Irebert R. Delgado

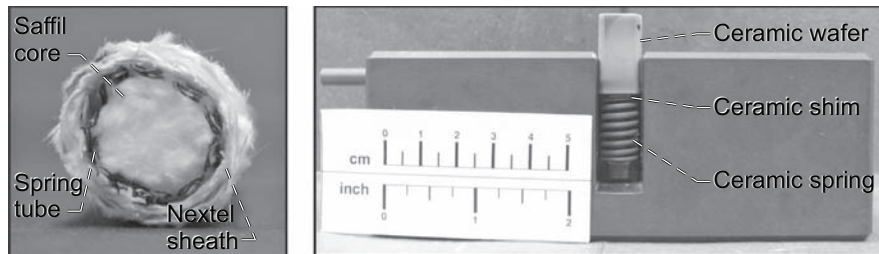
Headquarters Program Office:

Aeronautics Research Mission Directorate

Programs/Projects:

Fundamental Aeronautics Program, Subsonic Fixed Wing Project

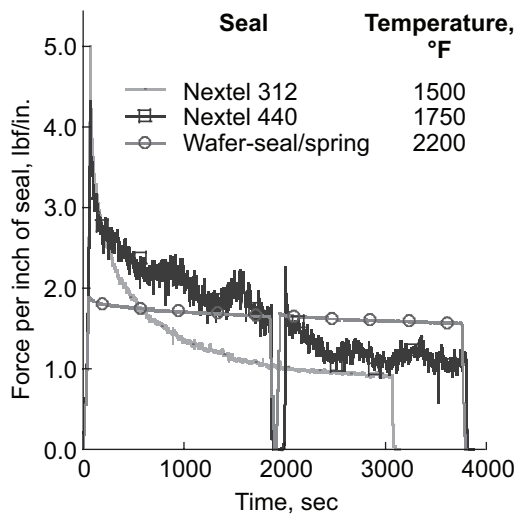
High-Temperature Seals Evaluated for Hypersonic Airframe Applications



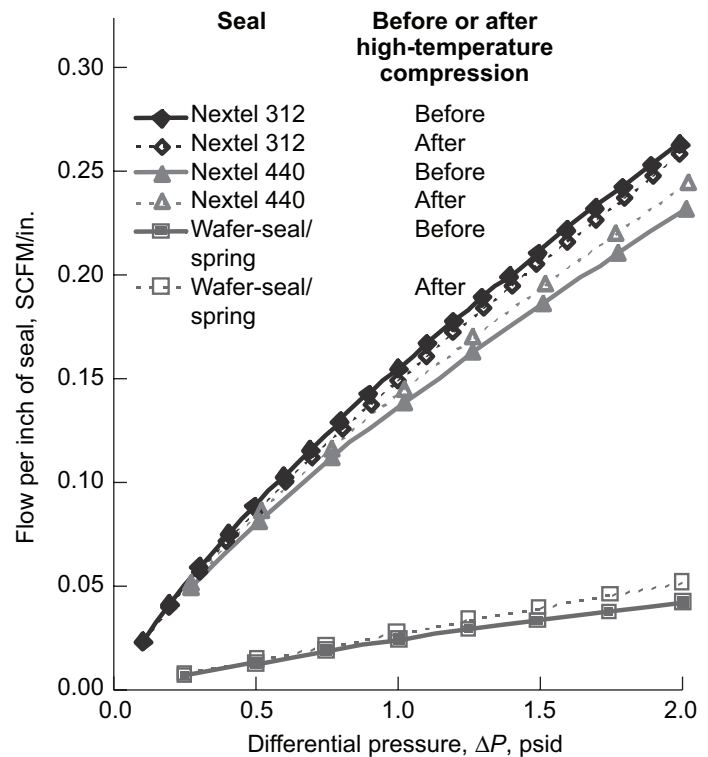
Left: Example of spring-tube thermal barrier. Right: Example of ceramic wafer/spring sealing system.

To support development of an advanced hypersonic vehicle, researchers at the NASA Glenn Research Center conducted critical-function performance tests on seal candidates for high-temperature airframe and control surface

applications. Both spring-tube thermal barriers and ceramic wafer seals (see the photographs) were considered as prime candidates for several key locations on this vehicle. To determine the suitability of these seals, researchers performed high-temperature compression tests to assess seal resiliency and room-temperature leakage tests to evaluate flow-blocking ability before and after compression testing. The tests were conducted in state-of-the-art test rigs at Glenn.



Load relaxation for several high-temperature airframe seal candidates.



Seal leakage (in standard cubic feet per minute per inch) against a carbon/carbon ceramic matrix composite surface before and after high-temperature compression testing for several high-temperature airframe seal candidates.

The graph on the left displays the load relaxation of the seal candidates as a function of time. During these tests, the seals were compressed at high temperatures for about 1 hr, and the amount of load on the seals was monitored. This characteristic can indicate the ability of the seal to effectively track any changes in the gap between the surfaces it is meant to seal. As shown in the graph, a thermal barrier composed of a René 41 spring tube filled with Saffil insulation and overbraided with a Nextel 312 sheath retained approximately 20 percent of its initial load capacity after 3000 sec at 1500 °F. By comparison, a Nextel 440 thermal barrier with René 41 spring tubes and Saffil retained about 30-percent load capacity, but this was at a higher temperature (1750 °F) for a total of 3600 sec. The silicon nitride wafer seal/compression spring system displayed the best load performance at temperatures as high as 2200 °F, retaining nearly 83-percent load capacity after 3600 sec.

The graph on the right shows a representative plot of seal leakage against a carbon-carbon ceramic matrix composite surface before and after high-temperature compression testing. For all seal candidates evaluated, no significant degradation in leakage resistance was noted after high-temperature compression testing, indicating that the seals maintained sealing capability. In addition, the wafer seals exhibited room-temperature leakage values that were only one-fifth of those for the spring-tube rope seals, again illustrating the performance benefits of this seal system for demanding applications.

Through this research, engineers were able to determine the feasibility of using these seal types in several critical locations on the airframes and

control surfaces of hypersonic demonstrator vehicles.

Find out more about the research of Glenn's Mechanical Components Branch:

<http://www.grc.nasa.gov/WWW/5900/5950/>

University of Toledo Contact:

Jeffrey J. DeMange, 216-433-3568,
Jeffrey.J.Demange@nasa.gov

Glenn Contacts:

Patrick H. Dunlap, Jr., 216-433-3017,
Patrick.H.Dunlap@nasa.gov

Dr. Bruce M. Steinetz, 216-433-3302,
Bruce.M.Steinetz@nasa.gov

Authors:

Jeffrey J. DeMange, Patrick H. Dunlap, Jr.,
and Dr. Bruce M. Steinetz

Headquarters Program Office:

Hypersonics Space Act Agreement with
Lockheed Martin

Programs/Projects:

Hypersonics Project

Low-Noise Formate Spiral-Bevel Gears Evaluated

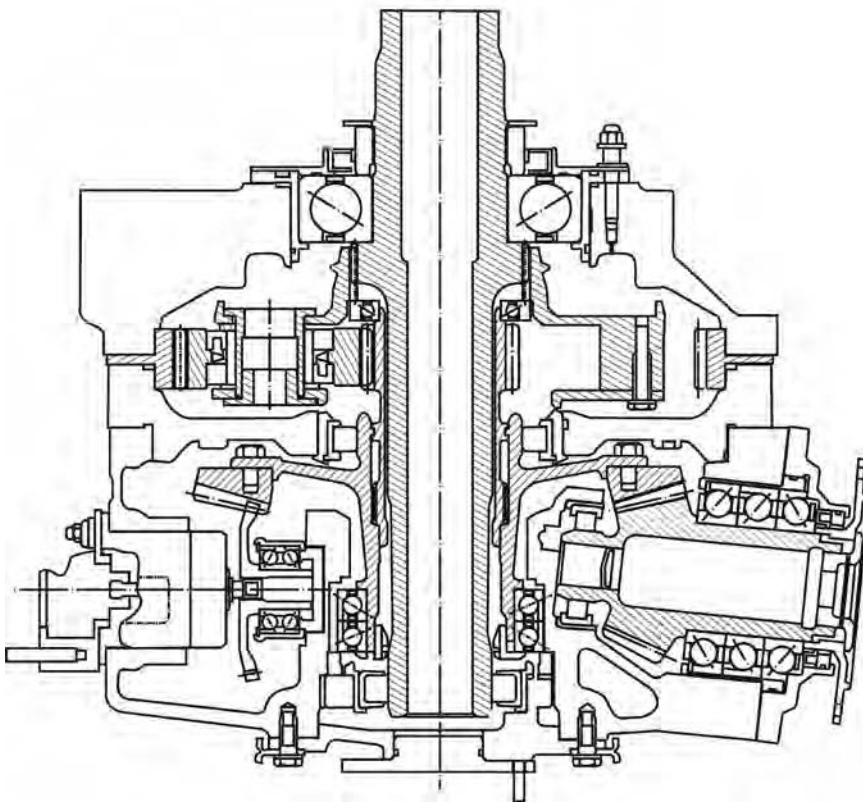
Spiral-bevel gears are used extensively in rotorcraft applications to transfer power and motion through nonparallel shafts. These gears are a main source of vibration and noise in gearboxes, which leads to noise in cabin interiors. Also, higher strength and lower weight are required to meet the needs of future aircraft. Previous studies on gears with tooth fillet and root modifications to increase strength have been reported as well as gears with tooth surfaces designed to reduce transmission errors. The results from these tests (ref. 1) showed a significant decrease in spiral-bevel gear noise, vibration, and tooth fillet stress. The spiral-bevel gears were manufactured using a face-milling process, the current standard for this type of gearing. The gear material was carburized, and the final manufacturing process was grinding to produce extremely high-precision tooth surfaces. In the face-milling process, a circular cutter (or grinding wheel) is designed and set into position relative to the gear blank to cut the correct spiral and pressure angles at a specific point on the tooth. The cutter then sweeps out the tooth form as it rotates about its axis. The relative motion between the cutter and the gear blank results in a time-consuming, costly process, but it is required to produce accurate teeth.

An alternative manufacturing approach is the Formate process. Similar to the face-milling process, the cutter (or grinding wheel) is positioned relative to the gear blank so that the correct spiral and pressure angles will be produced. The gear blank, however, is held stationary, and a tooth slot is form-cut by

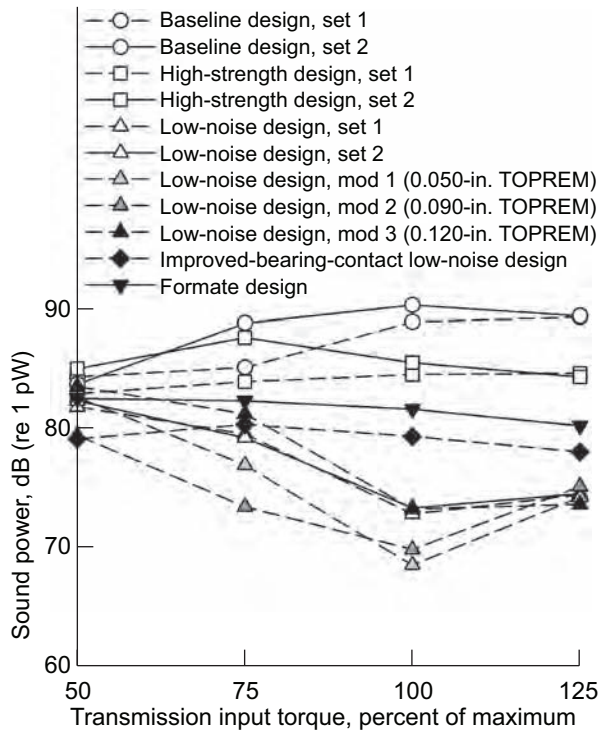
in-feeding the cutter without relative motion between the cutter and gear blank. This subtle difference substantially reduces the time and cost needed for manufacture.

In a cooperative project with Bell Helicopter and the University of Illinois at Chicago, a Formate spiral-bevel gear design along with a special generated pinion matched for low noise were evaluated. Experimental tests were performed on the OH-58D helicopter main-rotor transmission in the 500-hp Helicopter Transmission Test Stand at the NASA Glenn Research Center. The low-noise Formate spiral-bevel gear design was compared with the baseline OH-58D spiral-bevel gear design, and previous low-noise designs. Noise, vibration, and tooth strain tests were performed.

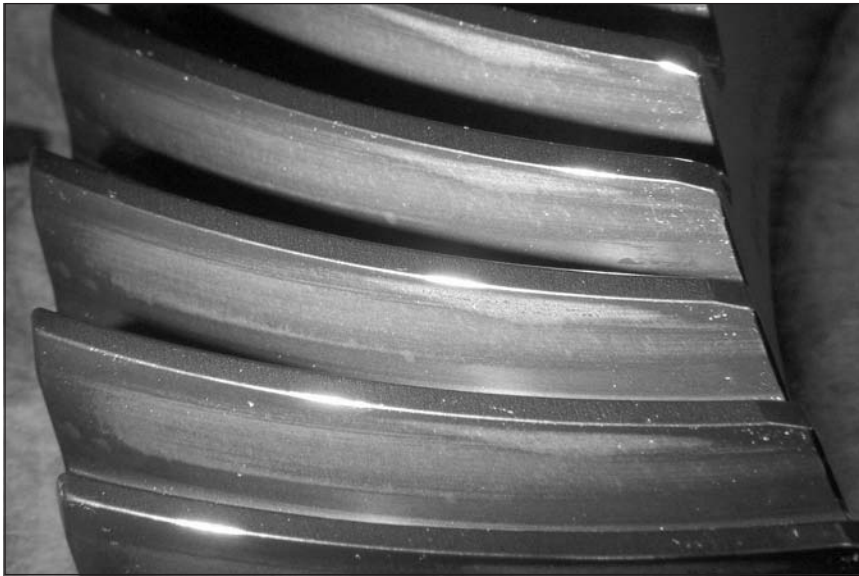
The Formate design showed a decrease in noise and vibration in comparison to the baseline OH-58D design, and it was similar to that of the previously tested improved-bearing-contact low-noise design. The pinion tooth stresses for the Formate design were significantly lower than for the baseline OH-58D design. Also similar to that of the improved-bearing-contact low-noise design, the maximum stresses of the Formate design shifted toward the heel, instead of the center of the face width as for the baseline, high-strength, and previously tested low-noise designs. Thus, the Formate design showed good promise for application in rotorcraft drive systems because of its lower noise, vibration, stress, and cost. For more details, see references 2 and 3.



OH-58D helicopter main-rotor transmission used in evaluation studies.



Comparison of noise of various gear designs, showing sound power¹ at spiral-bevel mesh frequencies. TOPREM is the decrease in the pressure angle at the tip of the grinding wheel used on the pinion during final machining.²



Formate spiral-bevel gear after noise, vibration, and strain evaluations. Tests resulted in normal contact patterns and no detrimental edge contact conditions.

References

- Lewicki, David G.; and Woods, Ron L.: Evaluation of Low-Noise, Improved-Bearing-Contact Spiral Bevel Gears. NASA/TM—2003-212353 (ARL—TR—2970), 2003. <http://gltrs.grc.nasa.gov>
- Lewicki, David G., et al.: Evaluation of a Low-Noise Formate Spiral-Bevel Gear Set. NASA/TM—2007-215032 (ARL—TR—4125 and ASME Paper DETC2007—34656), 2007. <http://gltrs.grc.nasa.gov>
- Lewicki, D.G., et al.: Evaluation of a Low-Noise Formate Spiral-Bevel Gear Set. Gear Technology, The Journal of Gear Manufacturing, vol. 25, no. 1, 2008, pp. 46–58.

Find out more about the research of Glenn's Mechanical Components Branch:

<http://www.grc.nasa.gov/WWW/5900/5950/>

U.S. Army Research Laboratory at Glenn Contact:

Dr. David G. Lewicki, 216–433–3970, David.G.Lewicki@nasa.gov

Glenn Contact:

James J. Zakrajsek, 216–433–3968, James.J.Zakrajsek@nasa.gov

Author:

Dr. David G. Lewicki

Headquarters Program Office:

Aeronautics Research Mission Directorate

Programs/Projects:

Fundamental Aeronautics Program,
Subsonic Rotary Wing Project

¹The sound power P is presented in the decibel scale, where $1 \text{ dB} = 10 \times \log(P/P_2)$, where $P_2 = 1 \text{ pW} = 1 \times 10^{-12} \text{ W}$.

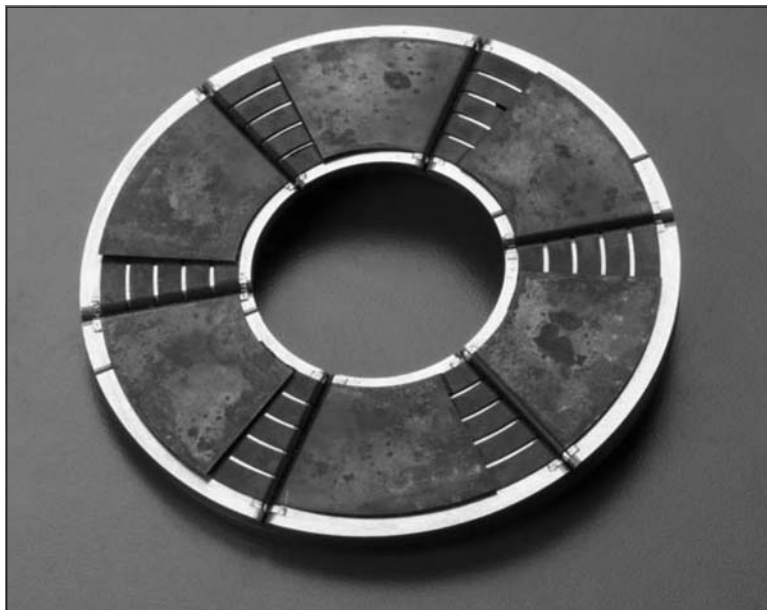
²This decrease in pressure angle causes more stock to be removed in the flank portion of the tooth to prevent interference with the top of the gear member during operation. The 0.050-, 0.090-, and 0.120-in. designations refer to the depth of modification along the blade cutting edge.

Design, Fabrication, and Performance of Open-Source Foil Bearings Demonstrated

Compliant foil bearing technology enables oil-free rotor support in high-speed turbomachinery, requiring only the process gas as a lubricant. A current NASA initiative assessing advanced rotorcraft propulsion systems envisions oil-free bearings in turboshaft engines to reduce engine weight. Since a single lubrication system is often used for both engine bearings and transmission gears, removing engine bearing lubrication requirements permits drive systems to run with optimized gear oil, allowing increased loading and power density.

Although foil bearing technology has made significant advances in recent years, industry adoption of the technology has been hindered by a perception of risk in the design and fabrication of bearings with adequate performance. Past applications have employed custom-designed bearings in small volumes, and few bearing suppliers exist. To make the technology more accessible and stimulate adoption, researchers at the NASA Glenn Research Center demonstrated and reported the design and fabrication processes required for foil bearings. Both journal and thrust bearings (see the photographs) were developed as part of this effort.

An exhaustive search of the open literature, and specifically expired patents, was performed to identify design features and geometries that are in the public domain and fully nonproprietary. Although modern, protected designs have demonstrated superior load capacity and damping to those now in the public domain, Glenn researchers demonstrated bearing performance levels acceptable for rotorcraft applications using the older designs. Furthermore, the demonstration bearings were operated at temperatures up to 540 °C and exposed to thousands of start-stop cycles.



Open-source foil thrust bearing.



Open-source foil journal bearing.

Although the reported details of the design and manufacturing process have been directed at industry, performance testing of these bearings has generated data needed for current numerical modeling efforts within academia. The ability to publish experimentally measured foil bearing data with corresponding detailed bearing geometry has until recently been hampered by the lack of available nonproprietary bearings with useful performance. This work has produced much-needed data to help validate current modeling codes.

Advanced rotorcraft propulsion architectures, as well as other turbomachinery serving NASA's power and propulsion systems, can achieve significant weight savings and performance increases by incorporating foil bearing shaft supports. The demonstration of bearing design, fabrication, and performance testing has increased development activities in industry and modeling activities in academia to further develop the technology base needed to integrate foil bearings into those systems.

Find out more about Glenn's Oil-Free Turbomachinery Program:

<http://www.grc.nasa.gov/WWW/Oilfree/>

Glenn Contact:

Dr. Christopher DellaCorte, 216-433-6056, Christopher.DellaCorte@nasa.gov

U.S. Army Research Laboratory at Glenn Contact:

Dr. Brian D. Dykas, 216-433-6058, Brian.D.Dykas@nasa.gov

Authors:

Dr. Christopher DellaCorte and
Dr. Brian D. Dykas

Headquarters Program Office:

Aeronautics Research Mission Directorate

Programs/Projects:

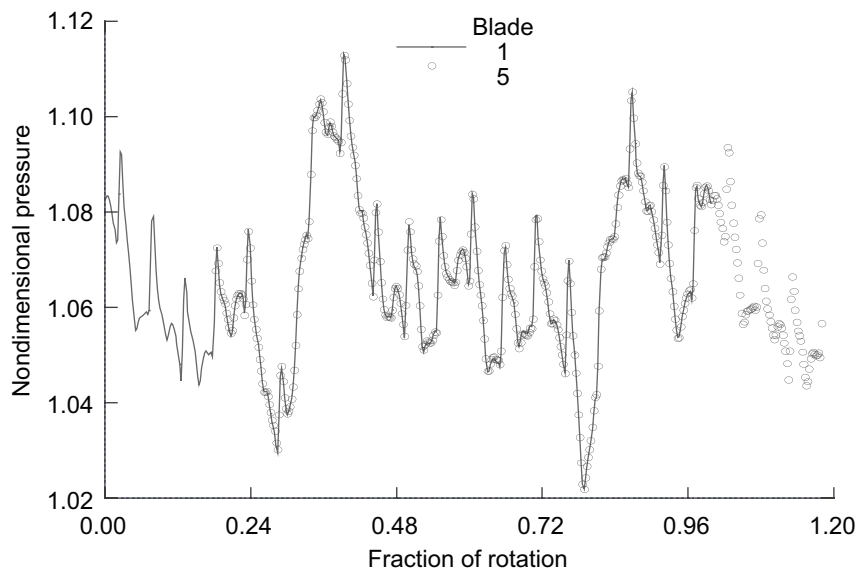
Subsonic Rotary Wing Project, Drive System

Full-Rotor Aeroelastic Analysis Capability Developed and Tested

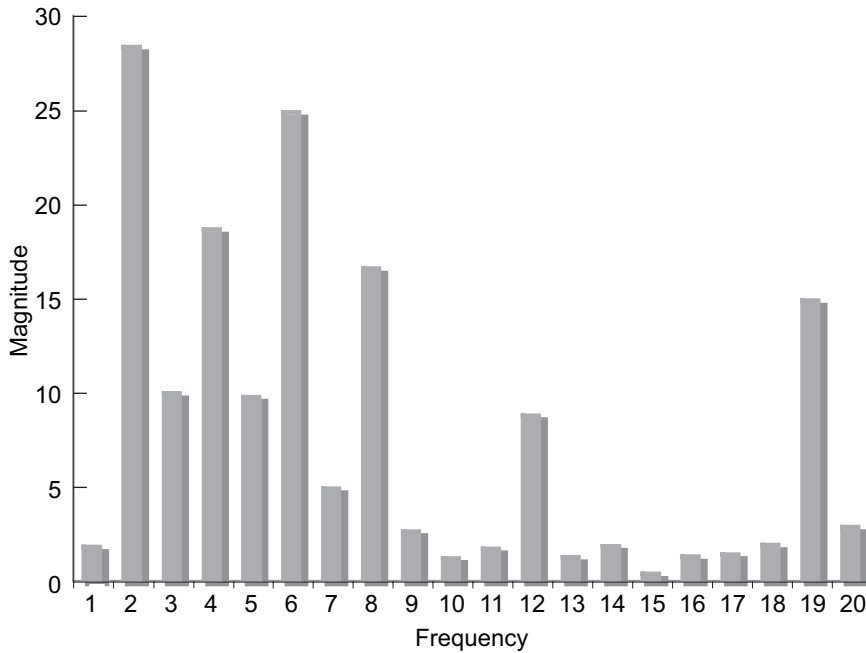
Failures in fan, compressor, and turbine blades can be caused by high-cycle fatigue due to forced-response aeroelastic vibrations. Such damaging aeroelastic vibrations can occur when an external unsteady aerodynamic excitation has a frequency that is nearly equal to a natural frequency of the blade and excites a structural vibration in the corresponding structural mode. A typical forced-response calculation models a single representative blade and a single representative blade passage. For more detailed aeroelastic analysis, it is sometimes necessary to model all blades in a blade row. Such a detailed analysis may be used when a fan stage operates with an incoming flow that includes a low-order inlet distortion. A full-rotor analysis is required to model such distortions when the fan stage includes an inlet guide vane in order to enable the accurate calculation of the unsteady aerodynamic forcing function on each blade. Also, such a detailed analysis enables the modeling of unsteady flow phenomena that are aperiodic, and thus cannot be modeled using the phase-lag or time-shift periodic boundary conditions used with a simplified single-passage analysis.

As part of the current work at the NASA Glenn Research Center, an aeroelastic analysis capability was developed with Glenn's TURBO-AE code (Reynolds-Averaged Navier-Stokes aeroelastic code) that includes calculating and recording the time history of surface pressure on all blades in a blade row. After this, Fourier analysis of the time history is used to identify forcing functions for various excitation sources and engine orders, and the forced-response vibration amplitude is calculated for each blade. A typical full-rotor analysis with the TURBO code requires the subdivision of the computational mesh into blocks for parallel computations on a computer cluster. Accordingly, the aeroelastic analysis capability also includes a step to correctly combine and merge the unsteady pressure information from various blocks to recover the time history of pressure excitation on each blade.

This new capability was verified and tested on an engine company fan configuration for which forced-response data had been previously acquired in a rig test. Calculations were made at a resonance crossing where the frequency of the forcing function excitation nearly coincided with a blade natural frequency. The line graph shows the computed time history of pressure at a representative point near the leading edge, at midspan on blades 1 and 5. The results demonstrate that the



Unsteady pressure plot showing the periodicity of the flow across blades 1 and 5.



Frequency components of the response shown in the line graph.

phase difference between blades is correctly modeled, and they show the strong 2/rev (engine order 2) excitation with other frequency components. The bar chart shows the harmonic components of the unsteady pressure with a prominent second harmonic (corresponding to the 2/rev) forcing function and other excitations including those from the inlet guide vane wakes. The dynamic response (vibratory displacements, stresses, and strains) was calculated by combining the unsteady aerodynamic forces with a finite-element structural dynamics model. This work enables a detailed forced-response calculation for more accurate estimation of the blade fatigue life.

The research work described here was performed jointly under a cooperative agreement between NASA and the University of Toledo. It was supported by the Subsonic Fixed Wing Project and the Integrated Inlet-Fan Simulation Project, Dr. John Lytle, Manager.

Glenn Contact:

Dr. Milind A. Bakhle, 216-433-6037,
Milind.A.Bakhle@nasa.gov

University of Toledo Contact:

Dr. T.S.R. Reddy, 216-433-6083,
Tondapu.S.Reddy@nasa.gov

Authors:

Dr. T.S.R. Reddy and Dr. Milind A. Bakhle

Headquarters Program Office:

Aeronautics Research Mission Directorate

Programs/Projects:

Fundamental Aeronautics Program,
Subsonic Fixed Wing Project,
Integrated-Inlet Simulation Project

Ultra-High-Power, Lightweight Cryogenic Motor Developed and Operated in Liquid Nitrogen

In fiscal year 2007, researchers at the NASA Glenn Research Center operated a switched-reluctance motor in liquid nitrogen (LN₂) with a power density as high as that reported for any motor or generator. The high performance stems from the low resistivity of copper (Cu) at LN₂ temperature (about one-seventh of room temperature) and from the geometry of the windings—the combination of which permits steady-state root-mean-square current density up to 7000 A/cm², about 10 times that possible in coils cooled by natural convection at room temperature. The joule heating in the coils is conducted to the end turns for rejection to the LN₂ bath. Minimal heat rejection occurs in the motor slots, preserving that region for conductor layers. In the end turns, the conductor layers are spaced to form a heat-exchanger-like structure that permits nucleate boiling over a large surface area.

The motor, described in reference 1, has 12 stator poles and 8 rotor poles, a 10-cm-diameter rotor, and a 5.08-cm axial stack of commercial 6-mil iron-cobalt high-strength laminations on both the rotor and stator. The motor pole laminations operate far into magnetic saturation, but the back iron does not. Commercial six-switch inverters, adapted to operate as asymmetrical bridges, provided up to 100-A current into each parallel section. The currents were controlled by a mixed digital/analog hysteresis controller that produced as close to a square-wave as the available voltage, inductance, back electromotive force, and switching rate would allow.

To save on power electronics, only 2 of the 12 coils were energized for the high-power tests. Test times at highest power were typically limited to 5 sec (too short to reach thermal steady state) because of the limited supply of LN₂ in the experimental Dewar. Tests showed that a single isolated coil in LN₂ can sustain currents as high as used in the motor, but it must still be shown that such currents are sustainable in the confines of the motor. The phases of switched reluctance motors are known to be independent if the back iron does not saturate, so performance measured with only two energized poles can be projected to 12, with appropriate allowance for drag.

If thermal steady state is achieved in longer tests, the specific power of this switched-reluctance motor would equal or exceed the specific power of any other tested electric machine known to us. Our highest projected power to date was 141 kW at 20,000 rpm in the 8.1-kg-EM motor.¹ This gives a specific power of 17.4 kW/kg-EM, about twice that of the best published room-temperature switched-reluctance motor and 49-percent higher than we reported a year ago for this motor (ref. 1). If a 60-percent increase in mass to 13.0 kg for the balance of the motor is assumed, the specific power would be 10.8 kW/kg, similar to the 10-kW/kg capability reported in reference 2 for a nonsuperconducting 1-MW exciter operating near LH₂ temperature.

¹EM denotes electromagnetic mass, mass of coils, and laminations.

References

1. Brown, Gerald V., et al.: Specific Power of Cryogenic Motor Increased 50 Percent. Research & Technology 2006, NASA/TM—2007-214479, 2007, pp. 281–282. <http://www.grc.nasa.gov/WWW/RT/2006/RX/RX51S-brown.html>
2. Oberly, C.E.: Lightweight Superconducting Generators for Mobile Military Platforms. Power Engineering Society General Meeting, IEEE, June 2006.

Glenn Contacts:

Gerald V. Brown, 216–433–6047,
Gerald.V.Brown@nasa.gov

Timothy P. Dever, 216–433–2384,
Timothy.P.Dever@nasa.gov

Jeffrey J. Trudell, 216–433–5303,
Jeffrey.J.Trudell@nasa.gov

Analex Corporation Contact:

Ralph H. Jansen, 216–433–6038,
Ralph.H.Jansen@nasa.gov

Authors:

Dr. Gerald V. Brown, Ralph H. Jansen,
Timothy P. Dever, Dr. Aleksandr S. Nagorny,
and Jeffrey J. Trudell

Headquarters Program Office:

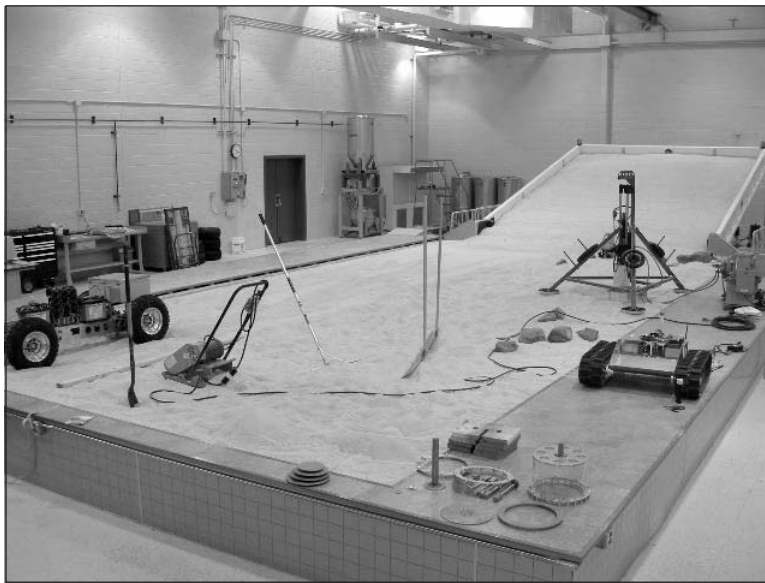
Aeronautics Research Mission Directorate

Programs/Projects:

Propulsion and Power, Vehicle Systems
Program, Revolutionary Aeropropulsion
Concepts, Alternate Energy Foundation
Technologies, Subsonic Propulsion

Simulated Lunar Operations Facility Designed and Built for Lunar Vehicle Research

In fiscal year 2007, the Surface Mobility Team designed and built the Simulated Lunar Operations (SLOPE) facility at the NASA Glenn Research Center. With NASA's goal to return to the Moon by 2020 and to occupy a Moon base continuously, lunar rovers of all sizes and capabilities will be required for transporting people, equipment, and regolith. These rovers must be able to traverse the widely varied lunar terrain, ranging from hard-packed to powdery surfaces and from level areas to the steep-sloped walls of huge craters. Therefore, the science of terramechanics (the interactions of machines and soils) as applied to the Moon is being explored at Glenn. Our plans include (1) helping determine whether future lunar vehicles will utilize wheels or tracks or something else altogether, (2) developing the sciences that will determine the geometry of the wheels, tracks, and tread patterns, (3) developing instrumentation and experimental methods to characterize the lunar terrain, and (4) developing vehicle traction test methodologies. A new facility and specialized test equipment were required for these efforts.



SLOPE facility overview.

The SLOPE facility is a unique indoor, climate-controlled, confined terrain of lunar simulant for conducting traction and other terrain-characterizing testing that relate to future lunar vehicles. SLOPE has a large level area measuring 11.9 m (39 ft) long and 6.0 m (19 ft 8 in.) wide. This area is currently filled to a depth of 0.3 m (12 in.) with a commercially available grade of sand that has shear characteristics similar to lunar regolith. The level area has boxed-in platforms that form a 1.2-m- (4-ft-) wide border along both long lengths, and these double as ventilation ducts. High-efficiency particulate air (HEPA) filter blowers at the end of each platform draw air from the over-terrain vents to help control the airborne silica dust that is raised when the sand is disturbed.

Joined to the end of the level bed is an additional testing area that can be tilted to any angle to simulate a crater wall for rover climb testing. The tilt bed portion is 4.7 m (15 ft, 5 in.) wide and 6.1 m (20 ft) long; there is an additional 0.6 m (2 ft) of level transitional area. The tilt bed is a steel structure that is lifted with two pairs of hydraulic rams to angles of up to 45°, although crater walls are not expected to exceed 30°.



SLOPE tilt bed.

A motor-driven radio-controlled test vehicle was designed and built in-house as a scientifically scaled version of the Apollo-era Lunar Roving Vehicle. The new test vehicle is used with a draw-bar cable-pull tester specially designed at Glenn to conduct traction testing. The soil strength is measured by a Glenn-specified instrument called a Bevameter (named in honor of Dr. Bekker who led the NASA terramechanics work during the Apollo program). In general, testing of new concepts for lunar wheel and track geometries in the SLOPE facility, both on the level and inclined areas, will provide invaluable test data that will support NASA's lunar terramechanics research and its new exploration mission needs.

**U.S. Army Research Laboratory at
Glenn Contact:**

Dr. Timothy Krantz, 216-433-3580,
Timothy.L.Krantz@nasa.gov

Glenn Contacts:

Jim Zakrajsek, 216-433-3968,
James.J.Zakrajsek@nasa.gov

Dr. Phil Abel, 216-433-6063,
Phillip.B.Abel@nasa.gov

Vivake Asnani, 216-433-3992,
Vivake.Asnani@nasa.gov

Author:

Steven W. Bauman

Headquarters Program Office:

Exploration Systems Mission Directorate

Programs/Projects:

Human and Robotics Systems

INDEX OF AUTHORS AND CONTACTS

Both authors and contacts are listed in this index. Articles start on the page numbers following the names.

A		D			
Abdul-Aziz, Dr. Ali	105, 107	Dalton, Penni J.	41	Gould, Dr. George L.	133
Abel, Dr. Phillip B.	176	de Groh, Kim K.	56	Graham, Scott R.	23
Adamovsky, Dr. Grigory	104	DeCastro, Jonathan A.	100	Green, Robert D.	88
Addy, Harold E. (Gene), Jr.	16	DeLaat, John C.	94	Greenberg, Paul S.	118
Ajmani, Dr. Kumud	29	Delgado, Irebert R.	167	Greer, Lawrence C., III	110
Anderson, Eric E.	84	DellaCorte, Dr. Christopher	172	Grimes-Ledesma, Dr. Lorie	149
Asnani, Vivake	176	DeMange, Jeffrey J.	168	Guynn, Mark D.	20
Asthana, Dr. Rajiv	138, 140	Denissen, Nicholas A.	13	Gyekenyesi, Dr. Andrew L.	105
		Dever, Timothy P.	175		
		Dippold, Vance F., III	9	H	
B		Dougherty, Kevin T.	102	Hall, Charles S.	66
Baaklini, Dr. George Y.	105	Dungan, Larry K.	118	Hall, Nancy Rabel	90
Bakhle, Dr. Milind A.	173	Dunlap, Patrick H., Jr.	168	Haller, William J.	20
Baldwin, Dr. Richard S.	34, 35	Dykas, Dr. Brian D.	172	Hammoud, Dr. Ahmad	124
Banks, Bruce A.	56, 59	Dynys, Dr. Frederick W.	143	Handler, Louis M.	66
Barlow, Karen L.	76	Dyson, Dr. Rodger W.	44	Heidmann, Dr. James D.	18
Bauman, Steven W.	176			Heikkinen, Bonnie	13
Beach, Duane E.	52	E		Herlacher, Michael D.	32
Beheim, Dr. Glenn M.	120	Easton, John W.	84	Hoberecht, Mark A.	37
Bencic, Timothy J.	109	Eckel, Dr. Andrew J.	137, 138, 140, 143	Hoge, Peter A.	162
Bennett, William R.	34, 35	Eichenberg, Dennis. J.	54	Horsham, Gary A.	34
Benson, Scott W.	25, 27	Emery, Edward F.	115	Hunter, Dr. Gary W.	118
Berger, Lauren A.	56	Engblom, Dr. William	13		
Berton, Jeffrey J.	20			I	
Bhatt, Dr. Ramakrishna T.	107	F		Ishac, Joseph A.	72
Bohman, Donna Y.	88	Fincannon, H. James	38		
Bouley, Dan	115	Fischer, Dr. David G.	78, 79	J	
Breisacher, Kevin J.	29	Fisher, Kenneth L.	20	Jansen, Ralph H.	175
Brinker, Dr. David J.	17	Flatico, Joseph M.	110	Jaworske, Dr. Donald A.	52
Briones, Janette C.	66	Follo, Jeffrey C.	32	Jett, Timothy R.	165
Brown, Dr. Gerald V.	175	Force, Dale A.	68	Jordan, Prof. Jacqueline	78
Bugga, Dr. Ratnakumar V.	34	Fox, Dennis S.	146	Juhasz, Dr. Albert J.	46
Bunnell, Charles T.	88	Frate, David T.	23		
Burke, Kenneth A.	36, 37	Freeman, Dr. Jon C.	69	K	
Button, Robert M.	43			Kacpura, Thomas J.	66
		G		Kamhawi, Dr. Hani	24
C		Gabb, Dr. Timothy P.	130	Karthikeyan, Dr. Jegan	145
Carbaugh, Ashley	136	Gaier, Dr. James R.	58	Kleinhenz, Dr. Julie E.	83
Cardin, Joseph	22	Gayda, Dr. John	130	Kobayashi, Takahisa	96
Chamis, Dr. Christos C.	150, 153	Geng, Steven M.	47	Kohout, Lisa L.	38
Chen, Dr. Liang-Yu	120	Georgiadis, Dr. Nicholas J.	13	Kojima, Dr. Jun	4
Chevalier, Christine T.	70	Ghosn, Dr. Louis J.	146, 158	Kopasakis, George	97
Colozza, Anthony J.	36	Goldstein, Dr. Marvin E.	2	Kory, Dr. Carol L.	70
Coroneos, Rula M.	150	Golliher, Eric L.	87	Krantz, Dr. Timothy	176
		Gonzalez, Marcelo C.	43	Krasowski, Michael J.	110, 112

Krause, David L.	160	O		Saunders, John D.	14
Kremic, Tibor	22	Obringer, Lee Ann	126	Sayir, Dr. Ali	143
L		Okojie, Dr. Robert S.	122, 126	Schreiber, Jeffrey G.	49
Landis, Dr. Geoffrey A.	53	Oriti, Salvatore M.	49	Sehirlioglu, Dr. Alp	143
Lankford, Dr. Dennis	13	Oswald, Fred B.	165	Shaltens, Richard K.	50
LaPointe, Dr. Michael R.	22	P		Shpargel, Tarah P.	140
Lee, Dr. Chi-Ming	8	Pai, Dr. Shantaram S.	162	Simon, Donald L.	96
Lee, Dr. Richard Q.	64	Palaszewski, Bryan A.	6	Simons, Dr. Rainee N.	68, 71
Leib, Dr. Stewart J.	2	Parsons-Wingerter, Dr. Patricia	81	Singh, Dr. Mrityunjay	138, 140
Lekki, John D.	105, 114	Pastel, Robert T.	146	Sivo, Chris	115
Lerch, Dr. Bradley A.	145, 156, 158	Patel, Dr. Bhogilal M.	162	Slywczak, Richard A.	72
Lewicki, Dr. David G.	170	Patterson, Michael J.	25, 27	Smart, Dr. Marshall C.	34
Lilie, Lyle	115	Patterson, Richard L.	124	Smialek, Dr. James L.	146
Litt, Jonathan S.	99, 100	Pawlik, Ralph J.	160	Smith, Craig E.	137
Long-Davis, Mary Jo	9	Paxson, Dr. Daniel E.	94, 102	Sowers, T. Shane	99
M		Pencil, Eric J.	22	Spry, David J.	120
Mackey, Jeffrey R.	90	Pereira, Dr. J. Michael	164	Steinetz, Dr. Bruce M.	168
Manzella, Dr. David H.	24	Pham, Nang T.	23	Struk, Dr. Peter M.	84
Manzo, Michelle A.	38, 41	Phoenix, Prof. S. Leigh	149	Suh, Joo	13
Mason, Lee S.	47	Plachta, David W.	28	Sullivan, Dr. Roy M.	158
McCarthy, Catherine E.	56	Potapczuk, Dr. Mark G.	16	Surgenor, Angela D.	8
McQuillen, John B.	76	Power, Dr. Greg	13	Sutter, Dr. James K.	156
Meador, Dr. Mary Ann	58, 131, 133	Predmore, Roamer E.	165	T	
Meador, Dr. Michael A.	136	Prokop, Norman F.	112	Telesman, Jack	130
Meyer, Michael L.	31	Q		Tewari, Dr. Surendra N.	107
Miller, Dr. Robert A.	146	Quackenbush, Dr. Todd	141	Thesken, Dr. John C.	149, 156
Miller, Sandi G.	134	R		Thompson, William K.	160
Miller, Sharon K.	59	Raj, Dr. Sai V.	145	Thurman, Douglas R.	20
Miller, Thomas B.	39	Reddy, Dr. T.S.R.	173	Tomsik, Thomas M.	8
Miranda, Dr. Félix A.	62	Reehorst, Andrew L.	17	Tornabene, Robert T.	23
Morscher, Dr. Gregory N.	137	Reid, Concha M.	34, 39	Tousley, Marissa	131
Motil, Susan M.	28	Reinhart, Richard C.	66	Towne, Dr. Charles E.	13
Mueller, Dr. Carl H.	62	Revilock, Duane M.	164	Trudell, Jeffrey J.	175
Murthy, Dr. Pappu L.N.	149	Ritzert, Frank J.	160	Tyson, Dr. Daniel S.	136
N		Robbins, Neal R.	71	V	
Nagorny, Dr. Aleksandr S.	175	Roberts, Lily M.	56	Vaden, Karl R.	32, 69, 70
Nagpal, Dr. Vinod K.	162	Roeder, James W., Jr.	117	Van Dresar, Dr. Neil T.	31
Nawash, Nuha S.	110	Rucker, Rochelle N.	56	Vickerman, Mary B.	81
Needham, Kathleen K.	126	Ruff, Dr. Gary A.	118	Vivod, Stephanie L.	131
Nelson, Dr. Chris	13	Russell, Richard W.	156	W	
Nessel, James A.	62, 64	S		Wagner, James D.	32
Neudeck, Dr. Philip G.	120	Sacksteder, Dr. Kurt R.	83	Wernet, Dr. Mark P.	117
Nguyen, Dr. Baochau N.	131, 133	Salem, Dr. Jonathan A.	156	Wilson, Dr. Jeffrey D.	70, 71
Nguyen, Dr. Quang-Viet	4, 114	Sanders, Bobby W.	14	Wintucky, Edwin G.	69
Niederhaus, Dr. Charles E.	90	Sanzi, James L.	52	Woike, Mark R.	109
Noebe, Dr. Ronald D.	141	Sarkisov, Dr. Sergey S.	104	Wong, Wayne A.	50

X

Xia, Dr. Zhenhai	137
Xu, Dr. Jennifer C.	118

Y

Yen, (Judy) Chia	8
Yoder, Dr. Dennis A.	13

Z

Zakany, James S.	23
Zakrajsek, James J.	165, 170, 176
Zaretsky, Erwin V.	165
Zhu, Dr. Dongming	146
Zimmerli, Dr. Gregory A.	31, 32, 79
Zoeckler, Joseph G.	23

REPORT DOCUMENTATION PAGE			Form Approved OMB No. 0704-0188		
<p>The public reporting burden for this collection of information is estimated to average 1 hour per response, including the time for reviewing instructions, searching existing data sources, gathering and maintaining the data needed, and completing and reviewing the collection of information. Send comments regarding this burden estimate or any other aspect of this collection of information, including suggestions for reducing this burden, to Department of Defense, Washington Headquarters Services, Directorate for Information Operations and Reports (0704-0188), 1215 Jefferson Davis Highway, Suite 1204, Arlington, VA 22202-4302. Respondents should be aware that notwithstanding any other provision of law, no person shall be subject to any penalty for failing to comply with a collection of information if it does not display a currently valid OMB control number.</p> <p>PLEASE DO NOT RETURN YOUR FORM TO THE ABOVE ADDRESS.</p>					
1. REPORT DATE (DD-MM-YYYY) 01-06-2008		2. REPORT TYPE Technical Memorandum		3. DATES COVERED (From - To)	
4. TITLE AND SUBTITLE Research & Technology 2007			5a. CONTRACT NUMBER		
			5b. GRANT NUMBER		
			5c. PROGRAM ELEMENT NUMBER		
6. AUTHOR(S) Riddlebaugh, Stephen, M., editor(s)			5d. PROJECT NUMBER		
			5e. TASK NUMBER		
			5f. WORK UNIT NUMBER WBS-None		
7. PERFORMING ORGANIZATION NAME(S) AND ADDRESS(ES) National Aeronautics and Space Administration John H. Glenn Research Center at Lewis Field Cleveland, Ohio 44135-3191			8. PERFORMING ORGANIZATION REPORT NUMBER E-16282		
9. SPONSORING/MONITORING AGENCY NAME(S) AND ADDRESS(ES) National Aeronautics and Space Administration Washington, DC 20546-0001			10. SPONSORING/MONITORS ACRONYM(S) NASA		
			11. SPONSORING/MONITORING REPORT NUMBER NASA/TM-2008-215054		
12. DISTRIBUTION/AVAILABILITY STATEMENT Unclassified-Unlimited Subject Categories: 01 and 31 Available electronically at http://gltrs.grc.nasa.gov This publication is available from the NASA Center for AeroSpace Information, 301-621-0390					
13. SUPPLEMENTARY NOTES This document is available online (http://www.grc.nasa.gov/WWW/RT/). For more information, visit Glenn's Web site at http://www.nasa.gov/glenn . For publicly available reports, visit the Glenn Technical Report Server at http://gltrs.grc.nasa.gov .					
14. ABSTRACT The NASA Glenn Research Center is pushing the envelope of research and technology in aeronautics, space exploration, science, and space operations. Our research in aeropropulsion, structures and materials, and instrumentation and controls is enabling next-generation transportation systems that are faster, more environmentally friendly, more fuel efficient, and safer. Our research and development of space flight systems is enabling advanced power, propulsion, communications, and human health systems that will advance the exploration of our solar system. This report selectively summarizes NASA Glenn Research Center's research and technology accomplishments for fiscal year 2007. Comprising 104 short articles submitted by the staff scientists and engineers, the report is organized into six major sections: Aeropropulsion, Power and Space Propulsion, Communications, Space Processes and Experiments, Instrumentation and Controls, and Structures and Materials. It is not intended to be a comprehensive summary of all the research and technology work done over the past fiscal year; most of the work is reported in Glenn-published technical reports, journal articles, and presentations. For each article in this report, a Glenn contact person has been identified, and where possible, a reference document is listed so that additional information can be easily obtained.					
15. SUBJECT TERMS Aeronautics; Aerospace engineering; Space flight; Space power; Materials; Structures; Electronics; Space experiments; Space communications; Instrumentation; Controls					
16. SECURITY CLASSIFICATION OF:			17. LIMITATION OF ABSTRACT UU	18. NUMBER OF PAGES 190	19a. NAME OF RESPONSIBLE PERSON STI Help Desk (email: help@sti.nasa.gov)
a. REPORT U	b. ABSTRACT U	c. THIS PAGE U			19b. TELEPHONE NUMBER (include area code) 301-621-0390



National Aeronautics and Space Administration

Glenn Research Center at Lewis Field
Cleveland, OH

Plum Brook Station
Sandusky, OH

www.nasa.gov